NUMERICAL SIMULATION OF WIND LOAD EFFECTS ON LOW RISE BUILDINGS

A THESIS SUBMITTED IN PARTIAL FULFILLMENT OF THE REQUIREMENT FOR THE AWARD OF THE DEGREE OF

MASTER OF TECHNOLOGY

(STRUCTURAL ENGINEERING)

TO

DELHI TECHNOLOGICAL UNIVERSITY

SUBMITTED BY

ANIRUDH KHATRI

ROLL NO.:2K20/STE/02

UNDER THE GUIDANCE OF

DR. RITU RAJ

ASSISTANT PROFESSOR

DELHI TECHNOLOGICAL UNIVERSITY

DEPARTMENT OF CIVIL ENGINEERING

DELHI TECHNOLOGICAL UNIVERSITY

BAWANA ROAD, DELHI-110042

DELHI TECHNOLOGICAL UNIVERSITY

(Formerly Delhi college of Engineering)

Shahbad Daulatpur, Baawana Road,

Delhi-110042

STUDENT'S DECLARATION

I, **Anirudh Khatri,** hereby certify that the work which is being presented in this thesis entitled **"Numerical simulation of wind load effects on low rise buildings"** is submitted in the partial fulfilment of the requirement for degree of **Master of Technology (structural engineering)** in Department of Civil Engineering at **Delhi Technological University** is an authentic record of my own work carried out under the supervision of **Asst. Prof. Ritu Raj.** The matter presented in this thesis has not been submitted in any other University/Institute for the award of Master of Technology Degree. Also, it has not been directly copied from any source without giving its proper reference.

Signature of Student

This is to certify that the above statement made by the candidate is correct to the best of my knowledge.

DELHI TECHNOLOGICAL UNIVERSITY

(Formerly Delhi college of Engineering)

Shahbad Daulatpur, Baawana Road,

Delhi-110042

CERTIFICATE

This is to certify that this thesis report entitled, **“Numerical simulation of wind load effects on low rise buildings”** being submitted by **Anirudh Khatri (Roll No. 2K20/STE/02)** at Delhi Technological University, Delhi for the award of the Degree of Master of Technology as per academic curriculum. It is a record of bonafide research work carried out by the student under my supervision and guidance, towards partial fulfilment of the requirement for the award of Master of Technology degree in Computational Design. The work is original as it has not been submitted earlier in part or full for any purpose before.

Ritu Raj

Dr. Ritu Raj

Assistant Professor

Civil Engineering Department

Delhi Technological University

Delhi-110042

ACKNOWLEDGEMENTS

This research work is the final output of my two years master's degree in Structural Engineering at the Delhi Technological University (DTU), New Delhi, India. I would therefore like to express my very great appreciation to the staff of Delhi Technological University (DTU) for their steadfast academic and administrative support, without which this work would not have been successful.

I wish to express my deepest gratitude to my research supervisor, Prof, Dr. Ritu Raj, Assistant Professor in the Department of Civil Engineering, Delhi Technological University, Delhi for their invaluable guidance, enduring patience, and nurturing support throughout this research without which successful completion would not have been possible. The knowledge and wisdom I have gained from them will forever guide me in education and life.

I extend my appreciation to my family members for their incessant encouragement and support to complete this course. I am also very much thankful to the wonderful moments and experiences shared with all the friends that I met throughout this study programme. These acknowledgements would be incomplete without mentioning the almighty for bringing this day in my life.

ANIRUDH KHATRI

ABSTRACT

Wind load plays a governing role in the designing of the roof in the coastal and hilly regions. The shape and angle of roof slope are key parameters while designing the structure for such loads. The present study demonstrates the variation of pressure due to wind loads on the pitched roof of a low rising building with different roof angles. The main parameters determining the pressure distribution over the building due to wind loads are length, height, span and roof angle.

Most research work have already been performed for the wind load calculations for different type of roofs in respect to different standards and conditions only for standard building shapes. However, this study solely focuses on pitched type roof with complete opening. The interference effect on low-rise structures is not given proper attention despite different

The study constitutes of interference effect of different structures due to corresponding building's location in a controlled system performed in ANSYS CFD simulations. Many studies on roofed structures have been performed in the past. However, interference effect with respect to different roof angles for different rotational arrangements of the structure were not observed in these studies. A *k*–*ε* model is used for the pressure distribution on the roof of the building model.

The simulation was performed in ANSYS CFD with different roof slopes (α) i.e, 10°,20°,30° and for different angles of rotations(Θ) i.e, 0°,30°,45°,60°,90° and for different spacing between the adjacent structures being different ratios of width of the building (B) i.e, 0B, B/2, 3B/2, 2B. Pressure Coefficient (C_p) have been calculated and different contour profiles are represented as results on the roof surfaces.

TABLE OF CONTENTS

LIST OF FIGURES

LIST OF TABLES

INTRODUCTION

1.1 GENERAL

Construction of a safe building structure in hilly and coastal terrains is a skill intensive and tedious process due to the presence of extreme wind speeds and unstable terrain. Additionally, such areas are prone to wind storms, cyclones, etc which cause potential damage of failure to the built-up building structures. Low-rise structures have an extensive usage in residential, commercial, public and private offices, industries and other functions (Singh and Roy 2021). Due to a widespread global usage of low-rise buildings, a comprehensive aerodynamic analysis of such buildings has gained a keen attention of research scholars of the world (Guirguisa et al. 2007, Huang et al. 2014, Richards and Norris 2015, Chen et al. 2018, Akon and Kopp 2018). Several research studies have been carried out on the low-rise building structures across the globe. It has been observed that the most affected part of the building structure due to heavy wind loads are the rooftops. Therefore, they suffer from an extensive damage, making them significantly vulnerable to the uplift action caused by vigorous wind forces (Zahrai 2014, Singh and Kumar 2019, Roy et al. 2017). It has also been observed that the shape of the rooftops significantly affects the surrounding wind environment (Van Hooff and Blocken 2010, Tominaga and Blocken 2015, Shen et al. 2016). Additionally, factors like velocity of wind, geometry of structures, type of roof and their roof angle and aerodynamics of flow around the building etc are also necessary to undergo a seamless and accurate analysis of a building structure in hilly and coastal areas. Designing a structure resilient to extreme wind loads in hilly or coastal areas will be hugely beneficial for the inhabitants of such areas by providing them a safer building structure. Moreover, it will also prevent the potential economic damage caused by cyclones, hurricanes, etc. The flow pressure induced on these structures may either increase or decrease depending on the spacing between them, their orientation with respect to wind direction. This effect is known as Interference Effect.

1.2 TYPES OF ROOFS

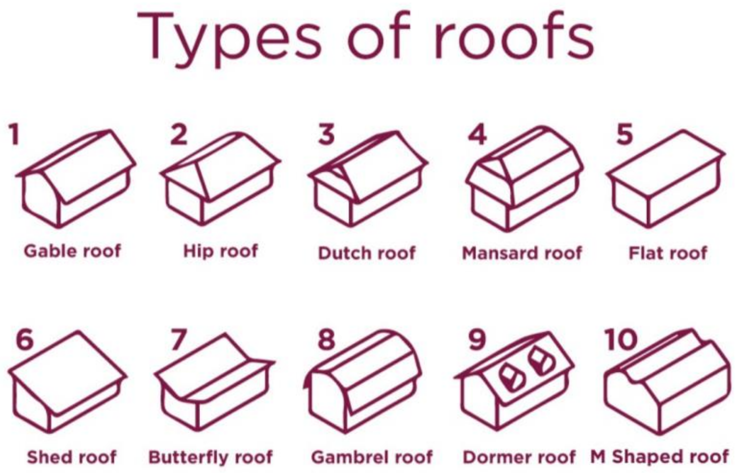

Fig.1 – Types of roofs

There are several types of roofs used in low rising buildings, named as gable roof, hip roof, Dutch roof, Mansard roof, Flat roof, shed roof, butterfly roof, Dormer roof, M shaped roof etc. In this study, the simulations are performed on pitched gable roof for different slope angles.

1.3 TYPES OF STRUCTURES

On the basis of height of a structure, a building can be broadly classified into two types i.e., the low-rise structures and the high-rise structures. A low-rise structure, possess a height of 20m, on the other hand, a high-rise structure has a height of 50m or more above ethe mean ground. Also, structures with a height between 20, to 50m are termed as mid-rise buildings.

On the basis of a type of a structure, the load calculations and design method vary. Generally, high rise buildings are exposed to higher lateral wind loads on their vertical faces, especially at higher storeys, leading to extreme pressure and high wind forces, However, the low-rise structures are projected well within the earth's atmospheric surface layer where wind flow is difficult to quantify.

1.4 WIND AND ITS EFFECT ON BUILDINGS

The relative motion of air to the Earth is known as wind. This is driven by thermal and pressure conditions prevailing in the atmosphere. The heat form solar energy in the atmosphere results in the pressure differences in the different regions of the Earth's surface. Meteorology, is the study of wind flow pattern which is a combination of Earth's rotation on its axis and the air flow around the atmosphere. The wind flows along the surface and interacts with different structures and obstacles. The faces and different section of structures or buildings are subjected to different varying loads due to these wind forces. This plays an important role in the atmospheric pressure conditions and is vital for environmental sustainability.

There have been many structural disasters in the recent years due to strong winds, as can be seen in the following images, the elevated houses are damaged due to the wind during Hurricane Katrina, 2005 (FEMA 549), severely damaging the roof framings and the end of gable roof. (Fig 1.1).

Fig 2 - Structural damage to elevated houses due to the wind during Hurricane Katrina, 2005 (FEMA 549)

Fig 3 – Damage to building curtain walls during F1/F2 Fort Worth Tornado (2000)

Hence, the wind load calculations are essential for a safer design and economical design of a building structure. These calculations are performed by the virtue of a wind tunnel testing. This method consumes alot of time and is rigorous and expensive as well. Also, such facilities are not very commonly available to carry out the experimentations.

CFD (Computational Fluid dynamics) , is a technique used to estimate wind loads by using numerical solutions for wind pressure in which a model if the structure is subjected to wind flow profile in an artificially built wind tunnel domain , In the current study , a such domain is used to determine the influence of wind on the roofs. The time averaged Reynold's Navier strokes (RANS) equations fo continuity momentum was investigated in this work by using the Ansys CFX solver with usual k - ε turbulence model. It follows the boundary conditions for the most natural situation.

1.5 BOUNDARY LAYER FORMATION

In the case of an ideal fluid, the fluid molecules can smoothly travel along the surfaces of the immersed bodies without losing any velocity from their free stream velocity. However, when real fluids are considered, the fluid molecules exhibit adhesion to the surface and tend to stick to the surface, thereby causing the contact layer to attain zero relative velocity. Due to the Brownian Motion between the fluid particles, the contact layer molecules retard the momentum of the immediate upper layer. The same effect carries on and on until the free stream velocity is attained by a layer. In this way, the immersed body retard the flow in its vicinity. To overcome this retardation, the fluid also imparts momentum on the body and therefore, exerts forces on the body, which is known as viscous drag. The complete zone of retarded flow is known as the boundary layer. The boundary layer is called a laminar boundary layer if the momentum exchange between the layers is only due to the Brownian motion. This is observed only in cases of low flow velocity and near the leading edges of the immersed bodies. As the distances from the leading edges increase and the flow velocity increase, the boundary layer does not remain stable and turbulent eddies start forming. This boundary layer is called the turbulent boundary layer. It is thicker than the laminar boundary layer and results in higher viscous drag.

1.6 BOUNDARY LAYER SEPARATION, WAKE FORMATION AND VORTEX SHEDDING

Bodies present inside a flow field are generally classified into two categories, viz. streamlined body, and bluff body. A bluff body separates the flow occurring over its surface. On the other hand, a streamlined body does not allow flow separation from its surface. Most buildings behave as bluff bodies immersed in air flow. A perfectly streamlined body in wind flow is not practically possible. However, aerofoil-type structures closely resemble a streamlined body due to the presence of streamlined surfaces above which, the boundary layer thickness is very small. The region of flow which is disturbed due to the presence of the body is called the wake region. This wake is narrower in the case of a streamlined body (Fig. 1.6) due to small boundary layer thickness leading to easier reattachment of flow. In the case of bluff bodies (Fig. 1.7), this reattachment is not easy due to the development of a thin region having high shear and vorticity [1].

These 8 shear layers move as concentrated vortices along the surface of the bluff body and dissipate by losing their energy gradually. This phenomenon is known as vortex shedding. The pattern and efficiency of vortex shedding depend upon the geometry of the bluff body.

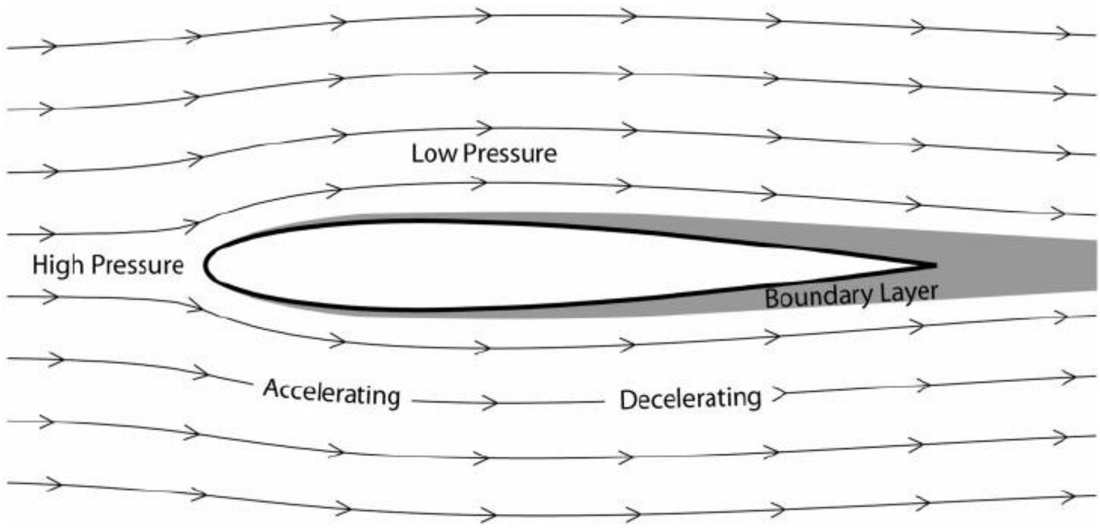

Fig 4 Flow around a streamlined body

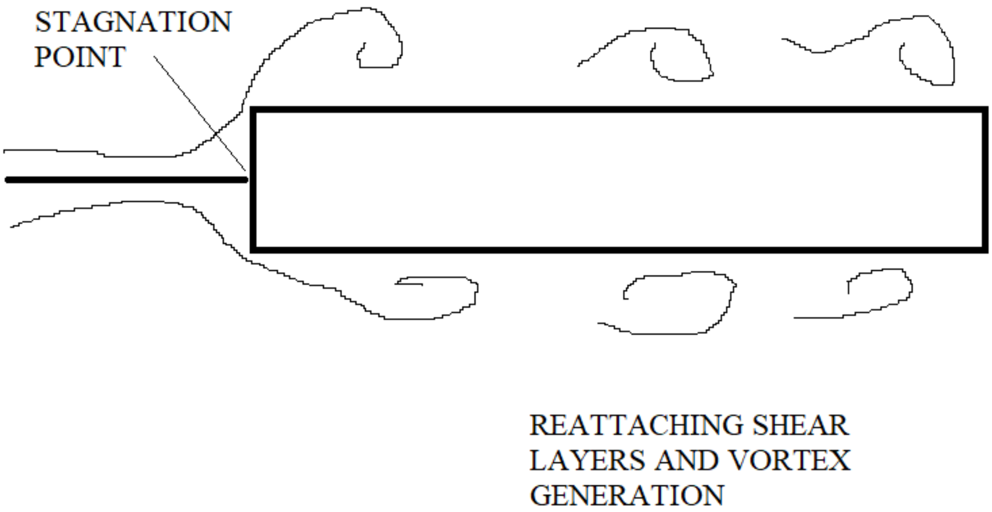

Fig 5 Flow around a bluff body

1.7 DETERMINATION OF WIND LOADS

Wind load calculations can be performed using codes, experimentally or by virtue of different software. As per codes, wind loads can only be calculated for basic shapes only. Two methods are used to calculate wind loads as per IS:875 (part 3) – 2015 as (i) pressure coefficient method and (ii) force coefficients method.

The design load on a structure is given by:

F = A x P……………………………………………………………......… (1.1)

Where,

F = wind force

P = wind pressure acting uniformly on area A, given by

$P = C_p \times P_d$ ……………………………………………………….…..….... (1.2)

Where, Cp = pressure coefficient, given in code

Pd = design wind pressure given by

Pd = Kd Ka Kc pz …………………………………………………………..…(1.3)

pz = wind pressure at height z given by

pz = 0.5 x ρ x Vz 2 ……………………………………………………..…. (1.4)

Vz = design wind speed at height z

ρ = density of air = 1.2 N-Sec2 / m4

Cp for the building with opening is given by-

Cp = Cpe - Cpi …………………………………………………….…... (1.5)

Where,

Cpe = external pressure coefficient,

Cpi = internal pressure coefficient.

Therefore, $P = (Cpe - Cpi). Pd^2$ ……………………...………………………….

(1.6)

As per IS: 875 (part-3) -2015 design wind speed, Vz is the function of basic wind speed Vb and It can be mathematically expressed as follows:

Vz = Vb x k1 x k2 x k3 x k4 ………………………………………………...(1.7)

Where,

Vb = basic wind speed

k1 = probability factor (risk coefficient)

k2 = terrain roughness and height factor

k3 = topography factor and,

k4 = importance factor for the cyclonic region

If the force coefficient method is used, the total wind load (F) on that particular building or structure is given by-

F = Cf Ae Pd ……………………………………………………………... (1.8)

Where,

Cf = The value of force coefficients applies to a building or structure as a whole

Ae = effective frontal area of the building or structure, and

Pd = design wind pressure

1.8 WIND PROFILE

Wind profiles are the plots of the flow velocity of wind over a surface of a body obstructing the free stream flow of wind. It gives the variation of wind velocities with height. For CFD study of wind loads, accurate numerical modeling of the wind profile is necessary to minimize errors. The commonly adopted wind profiles are power law, uniform flow profile, logarithmic flow profile, etc. The power law is given by

$$u_z = u_{ref} \times \left(\frac{\mathrm{z}}{\mathrm{zref}}\right)^{\alpha}$$

Where u_z is the wind velocity at height z, u_{ref} is the wind velocity at a reference height of z_{ref}, and α is the power law exponent and its value is different for different terrain conditions. For open terrain conditions, α is usually taken to be equal to 0.143.

Logarithmic law is also used in some cases, to model the wind velocity profile and is given by

$$u_z = u_* \; k \times \ln\left(\frac{z}{z0}\right)$$

where u* is the friction velocity, k is the Von Kármán constant (k ≈ 0.41), z0 is called roughness length, and is a characteristic of the terrain. For open flat terrain, z_0 is in the range of 0.001 m - 0.005 m and for dense urban areas, it can go as high as 5 m.

The logarithmic wind profile matches more closely for modeling wind speeds for lower 10 to 20 m heights and the power law produces a better profile for structures having over 100 m heights. In the intermediate zones, both power law and logarithmic law may be used for modeling the wind profile.

1.9 NEED OF THE STUDY

From the arguments stated above, the need to calculate the wind pressure on the low-rise building is required in the most efficient way with respect to time and cost. CFD simulations provide more understandable and conclusive results in contrast with other methods. The CFD simulations uses real-life like conditions for wind , and thus produces timely efficient and accurate results , thus to save time and costs as compared to wind tunnel method.

1.10 AIM OF THE STUDY

This study focuses at calculation of wind pressure on theow-rise structures mainly on the pitched roof. Wind pressure values on the roof are affected due to the interference of the adjacent buildings, this information is not available in the code of practices.

The study also projects light on the method of calculation by CFD simulations which is time and cost effective and provides information thoroughly on the different conditions.

1.11 OBJECTIVES

The objectives of the study are defined as follows:

1. To evaluate the coefficient of pressure on pitched slope roof.
2. To evaluate the coefficient of pressure on pitched roof with different roof angle.
3. To investigate the inference effect when multiple buildings are placed at different spacing.
4. To study variation of pressure coefficient distribution at various wind direction angles (0° to 90°)

2 LITERATURE REVIEW

2.1 GENERAL

R P Hoxey et al., (1993) The distribution of pressure over a building is governed by the shape of building. The basic building forms are four primary shapes being the height, span, length and pitch roof. Design codes do not properly conclude for the effect of building geometry though the influence of these parameters are difficult to track.

Stathopoulos et al. (1994) Have studied the effect of a tall nearby building on the wind loading of low buildings and also carried out wind tunnel tests to examine the effect of the location of trees in the vicinity of a low-rise building. Significant changes in wind pressures were observed.

Prem Krishna (1995) The lateral strength of buildings in areas other than the high seismic zones is mainly governed by wind loads and this aspect is more evident in zones of severe wind such as coastal regions, open terrains and summit of hills.

Y. L. Xu et al., (1997) The peak suction of the roof varies according to the pitch angle of the roof, 30-degree roof suffered the most suction on this case. For 15-degree and 20-degree roofs, the peak suction on gable roofs is higher than that of hip roofs.

S. Ahmad et al., (2001) They studied interference effects on wind load for hip roofs by conducting wind tunnel tests. Significant enhancements and shielding effects were observed for different configurations.

J.D. Ginger et al., (2003) A significant increase in the magnitude of the negative pressure coefficients on the leeward roof and wall, with an increase in aspect ratio, for oblique approach winds. These large suction pressures also generate large design wind load effects on the frames near the gable-end. Major standards severely underestimate the critical bending moments, and the effective pressure coefficients producing those bending moments, especially on the leeward roof slope.

P. A. Blackmore et al., (2006) Have performed wind flow experiments on real low-rise buildings of different shapes and side ratios, concluded that small changes in edges, shapes and direction of walls largely impact the wind flow.

Tecle et al. (2015) Have studied the Opening and Compartmentalization Effects of Internal Pressure in Low-Rise Buildings with Gable and Hip Roofs.

Y. Ozmen et al., (2016) The maximum values in the turbulence profiles occur in the mixing layer between the free Recirculation regions is much stronger and spreads up to the roof ridge with increasing roof stream flow and recirculation regions due to large velocity gradients.

Astha Verma et al., (2017) Pattern of wind pressure distribution on all in-between domes is identical and values of pressure and suction almost equal, irrespective of the number of domes. Maximum suction occurs near the peak in case of all the domes. Values of maximum suction on windward and leeward domes are almost equal, and are greater than those on in-between domes. Windward edges of all the domes are subjected to pressure, with small portion and value on windward dome as compared to all other domes.

Neelam Rani et al.,(2017) Here results in the form of contours and cross sectional variation of mean wind pressure coefficients. Mean wind pressure coefficients are evaluated from the measured values of pressures for seven wind incidence angles. Pressure coefficients are obtained for upper and lower roof surfaces separately.

Jagbir Singh et al., (2019) Roof shape and slope are both important parameters for the safety of a structure, especially when facing wind loads. When wind pressure coefficients from building models with openings were compared with pressure coefficients from building models without openings, it was found that the pressure coefficients for building models without openings are almost twice or three times that of the pressure coefficients for models with openings.

Mallick et al., (2019) Have worked on high rise buildings of various shapes like L, T, Z, C, E, +, N, Y, etc. by using experimental as well as numerical studies. It has been found that different plan shapes result into an altogether different wind pressure pattern.

Singh Jagbir et al., (2019) Have concluded that hexagonal shape has lower pressure coefficients than pentagonal roof surface, and this is due to better distribution of forces which further is cause of more faces.

J. Singh et al., (2019) Have worked on CFD simulation on wind effects over Pyramidal Roofs and have studied the effect of wind direction and roof slope for single and double storied pyramidal roof buildings.

Juliya Mironova (2020) the pressure affects not only neighboring high-rises, but also it has an impact on low-rise existing ones.

Prasenjit Sanyal et al., (2020) result shows variability of wind load and pressure due to change in the building side ratio.

Suman Kumar Laha et al., (2020) the simulation has been carried out by fixing the inclination angle of the panel at 25 through ANSYS Fluent software. The maximum stress which has been found here is 4196.4 Pa at 260 km/h wind speed when the maximum structural deformation has also been noticed.

Prasenjit Sanyal et al., (2021) They worked on high rise buildings of Y-shape by using experimental as well as numerical studies. It has been found that different plan shapes result into an altogether different wind pressure pattern.

3. EXPERIMENTAL SETUP

3.1 GENERAL

An experimental study is conducted through ANSYS CFX by simulation of different conditions for the different orientation of the roof. The wind pressure on the surface of the roof is determined and wind flow characteristics are obtained. Meshing conditions, model dimensions and detailed model description is further discussed in this chapter.

3.2 VALIDATION MODEL

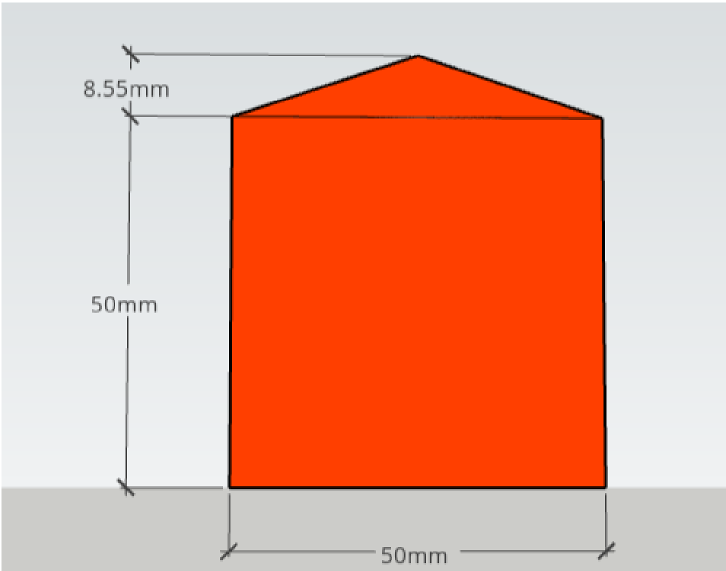

Fig 6- Elevation of the model

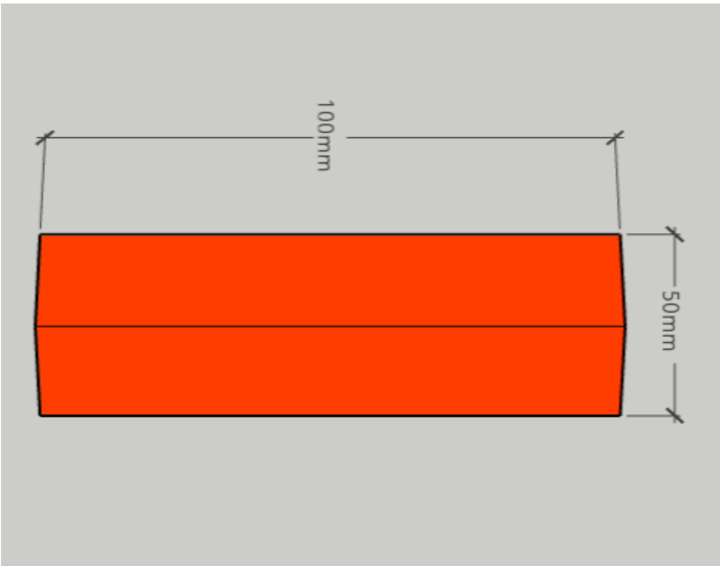

Fig 7 Plan of the model

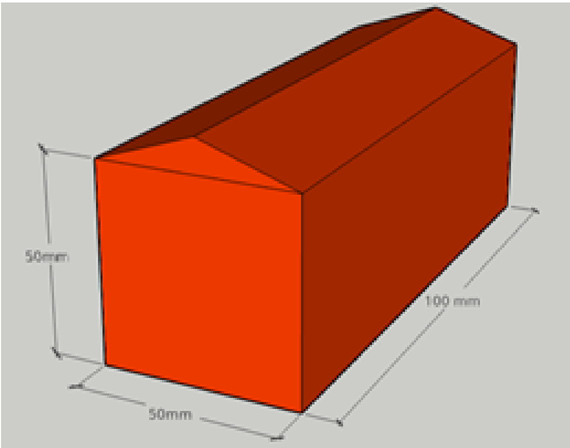

Fig 8- Isometric view of the model

For the validation of correct conditions adopted in ANSYS CFX and correct dimensions of the wind tunnel, a solid model of pitched roof is taken of the following dimensions.

Height (H) = 58.55mm, Width (W) = 50mm and Length (L) = 100mm.

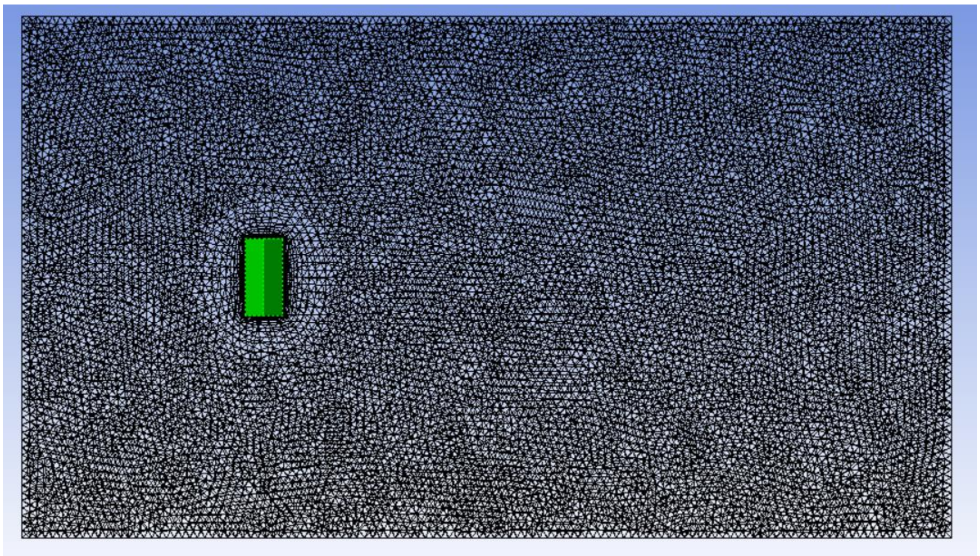

Fig 9- Plan of Domain Mesh

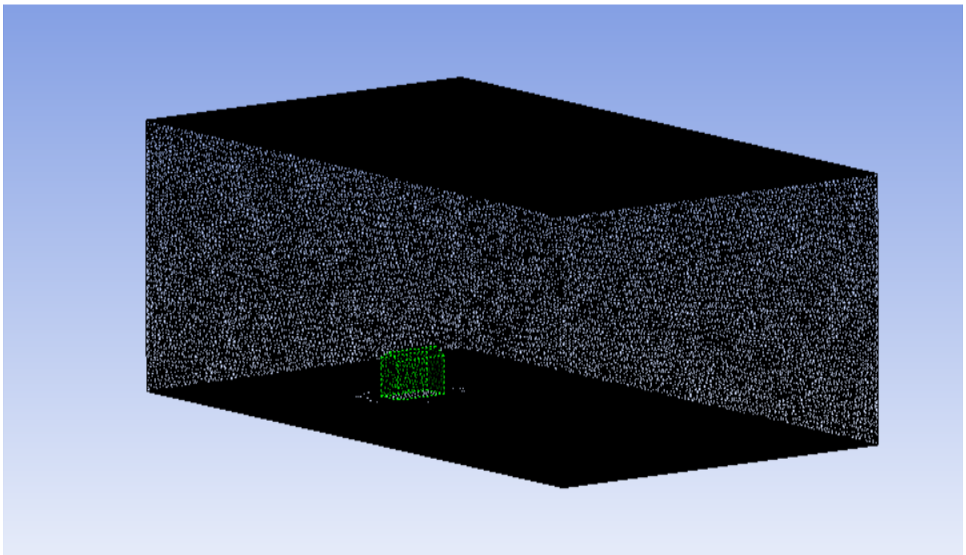

Fig 10 – Isometric view of domain mesh

A domain is adopted for simulation having distance of inlet and outlet equal to 5 times total height and 15 times total height respectively. The side aspect ratio and top clearance are also taken as 5 times total height. These dimensions produced the closest result to that of other dimensions adopted. The dimensions adopted are through the guidelines of Prasenjit Sanyal et al (2020). The length scale is taken as 1/100. The domain so produced possess enough space to account for any vortices and the outlet is distant enough to avoid backflow of wind. Meshing of the domain is done by tetrahedral elements. Mesh size is taken as 10mm and volume mesh size is taken as 0.01m. Hence nodes produced with these dimensions for the model are 1,40,991 with 7,36,659 elements. Finer meshing near the model and bottom wall is performed through inflation so the ends of the base and domain possess uniform meshing throughout the model. Furthermore, different face sizing is provided to the model for meshing to get finer mesh for the model than that the entire domain, solely to obtain more accurate results.

Boundary conditions and flow condition are as follows, the side walls of the domain are free slip walls and other walls as model and domain roof and bottom walls are no slip walls. An inlet velocity of 10m/s is implied and towards the outlet, average static relative pressure of 0 Pa is applied. With the boundary conditions so provided, the domain is similar to that of wind tunnel environment used by Dalui (2008) and Mukherjee et al. (2014).

3.3 VALIDATION ANALYSIS

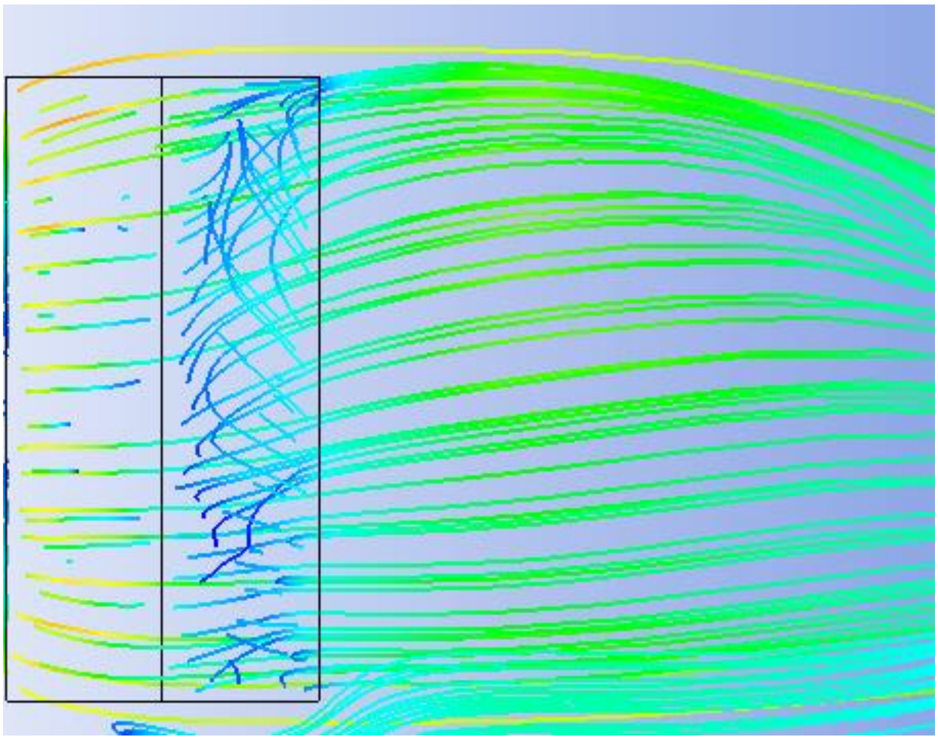

Fig11 -Top view of streamlines for roof

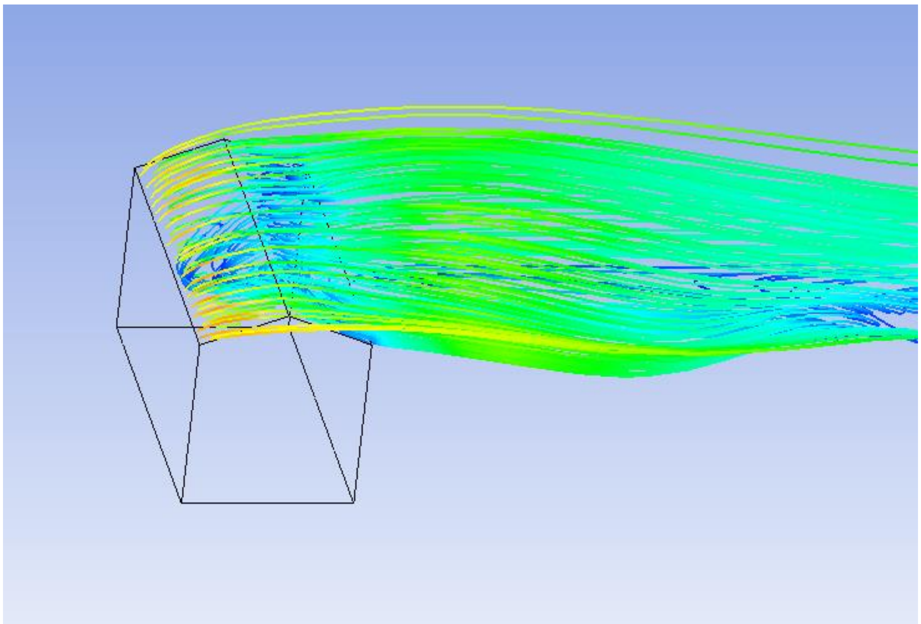

Fig 12- Isometric view of streamlines for roof

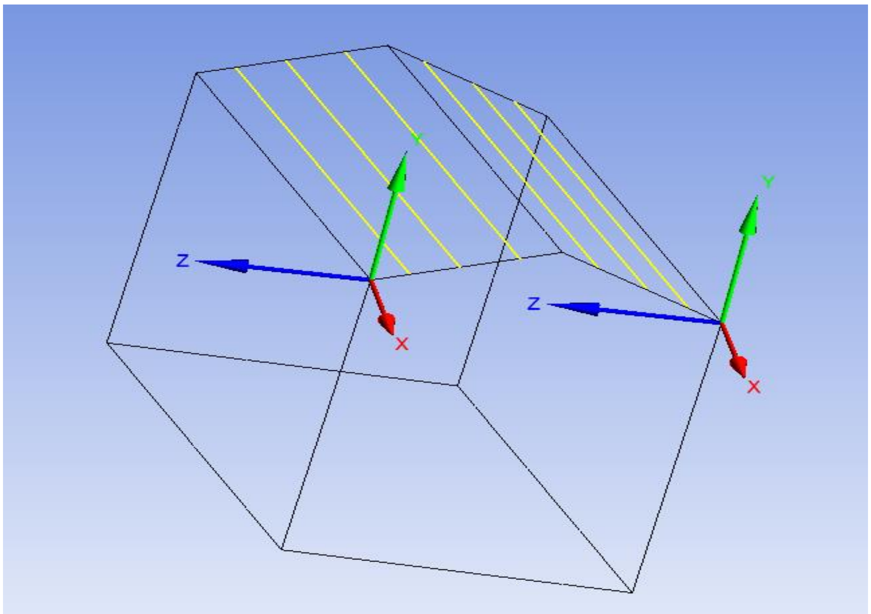

Fig 13 - projected lines on roof

The reference lines are projected on the roof top to of the roof of the structure at equidistant spaces. On these lines, several reference points are taken, pressure is calculated on these points to account for cumulative pressure calculations. Cp is then calculated by pressure values. This value is then compared to the codal provisions given in IS 875 (Part 3). The experimental value shows slight error of 5.86% from the values provided in the code. These domain conditions are kept same for further calculation of the structures for isolated and interference of several other structures.

Wind Angle (Ө°)	**C_{pe} for Surface from CFD Simulation**		**Average Value of C_{pe} for Roof from CFD Simulation**	**Average C_{pe} for Roof as per IS 875 (Part 3)**	**Average % Error**
	Roof A	Roof B			
0	**-0.94**	**-0.543**	**-0.741**	**-0.7**	**5.86%**

Table 1 – Validation of simulated structure

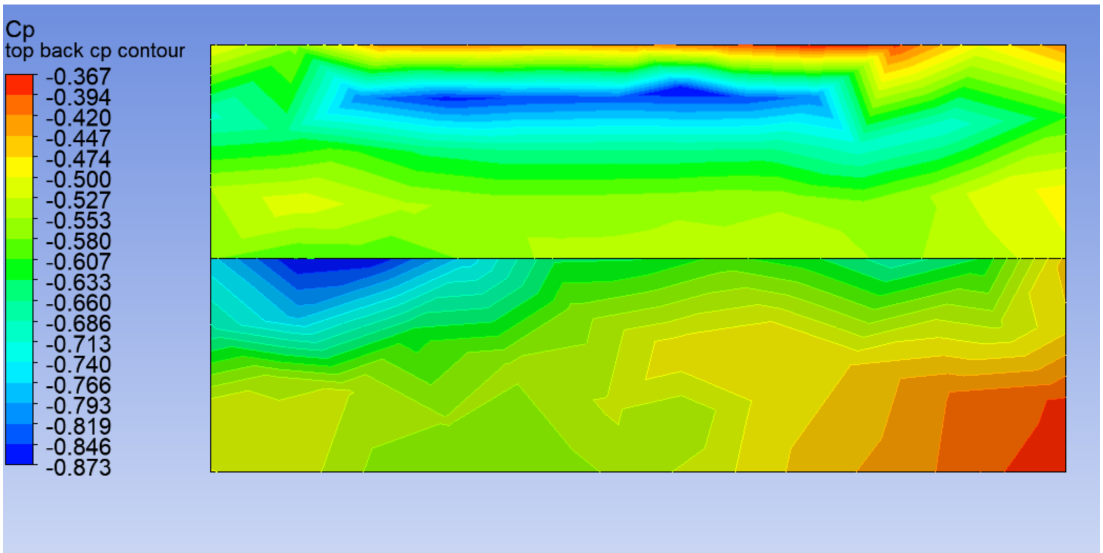

Fig 14 – C_p values for gable roof

3.4 ISOLATED MODEL

The domain and boundary conditions are further used to establish results for the concerned isolated model described below, the model is used to establish relations between C_p on the internal side as well as the external side of the roof, named as C_{pe} (for external side) and C_{pi} (for internal side).

The isolated model is a pitched roof, supported on 6 columns, having width and height of 50mm respectively and length of 100mm. The pitch angle (α) is varied for 3 concerned models as 10°, 20° and 30°

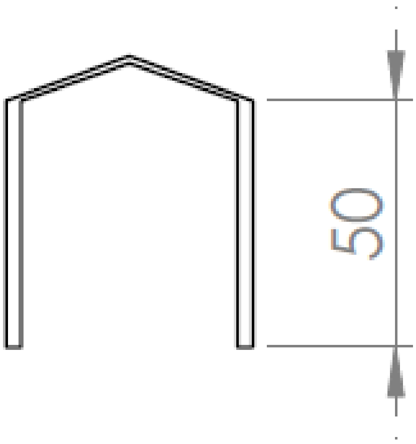

Fig 15 – elevation of model

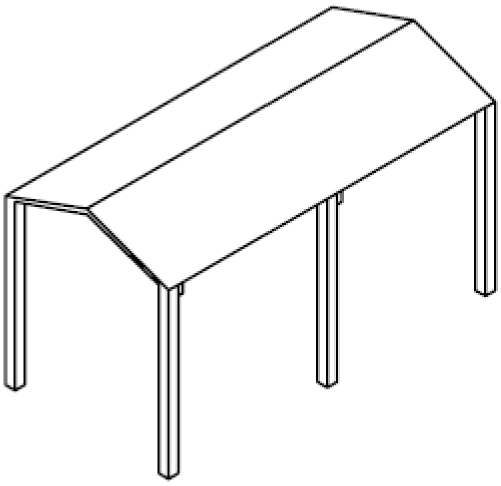

Fig 16 – Isometric view of model

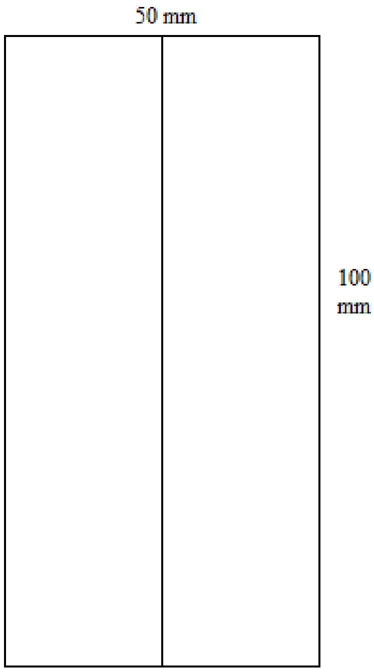

Fig 17 - Plan of the model

The isolated model is then simulated for same wind and boundary conditions as that of validated model domain and contour profiles for the same are produced to obtain pressure coefficients.

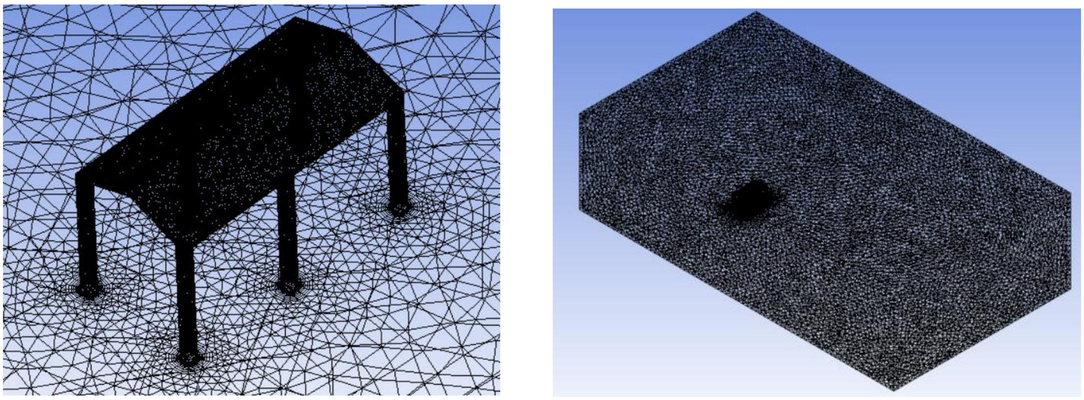

Fig 18 – domain mesh of isolated structure

The pressure calculations are perfomed for 4 rotations of the wind angle i.e, 0° , 30° ,60° and 90°. Contour profiles for internal and external presuure coefficient are as follows .

3.5 PRESSURE COEFFICIENTS OF ISOLATED STRUCTURE

3.5.1 Isolated structure 10°

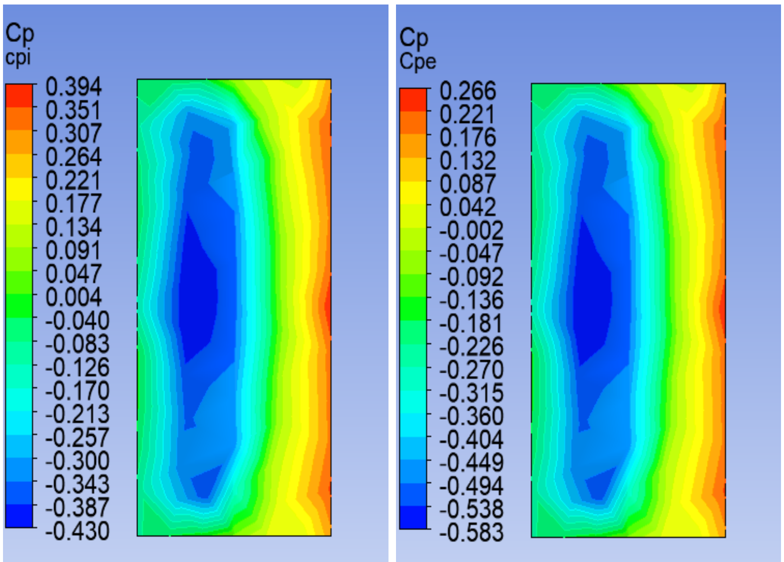

Fig 19 – C_{pe} and C_{pi} for 0° incidence angle

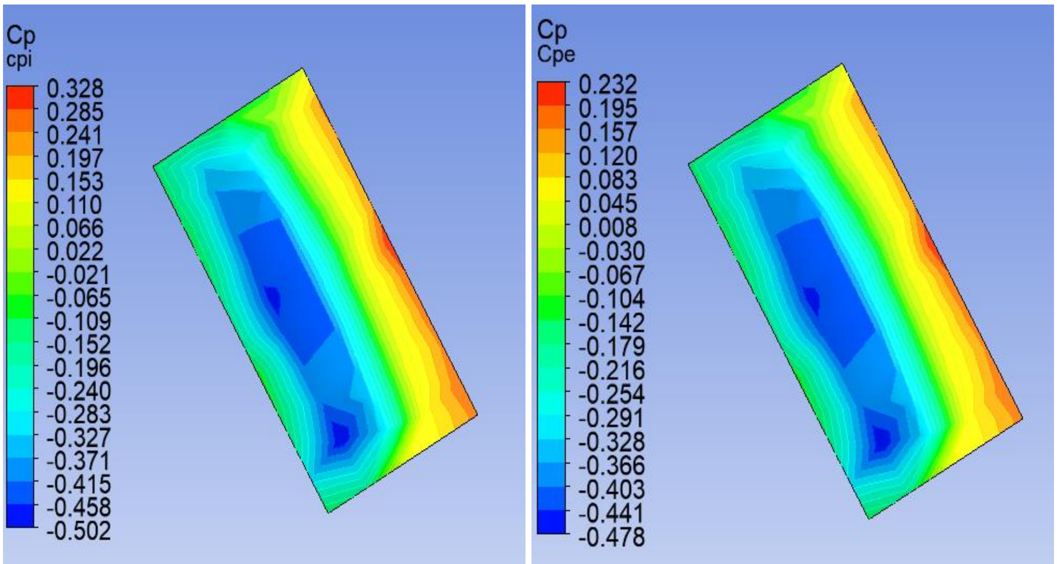

Fig 20 – C_{pe} and C_{pi} for 30° incidence angle

For a 0° and 30° incidence angle , the C_{pe} and C_{pi} are depicted in the figure 19 and 20 which are coefficient of external and internal pressure respectively. The Cpe is negative for most of the part in the figure, this is due to the eddies formed at the leeward side causing increased suction, which was result of the sharp edges of the roof top. The C_{pi} for both angles remained a uniform nature , with an average of positive value. This is due to the no resistance shown by the colum supports .

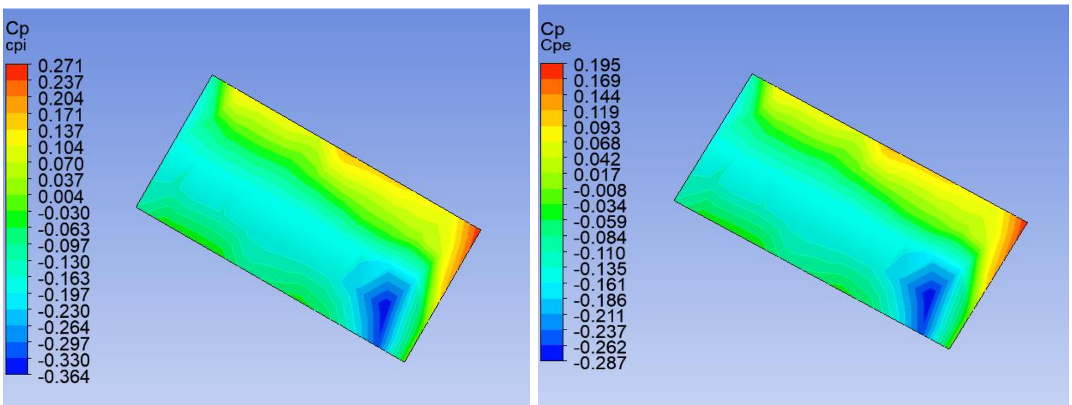

Fig 21 – C_{pe} and C_{pi} for 60° incidence angle

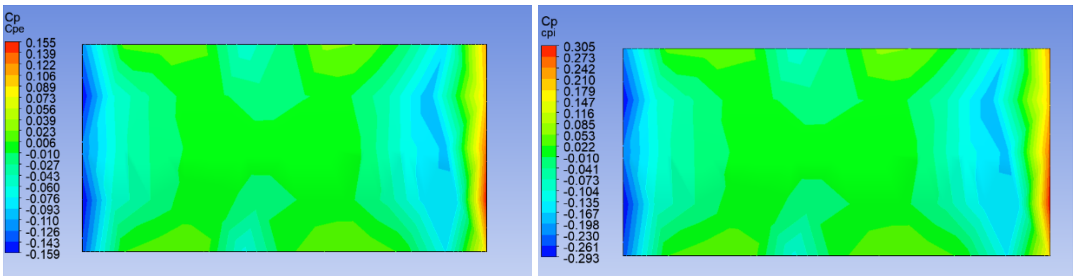

Fig 22 – C_{pe} and C_{pi} for 90° incidence angle

3.5.2 Isolated structure 20°

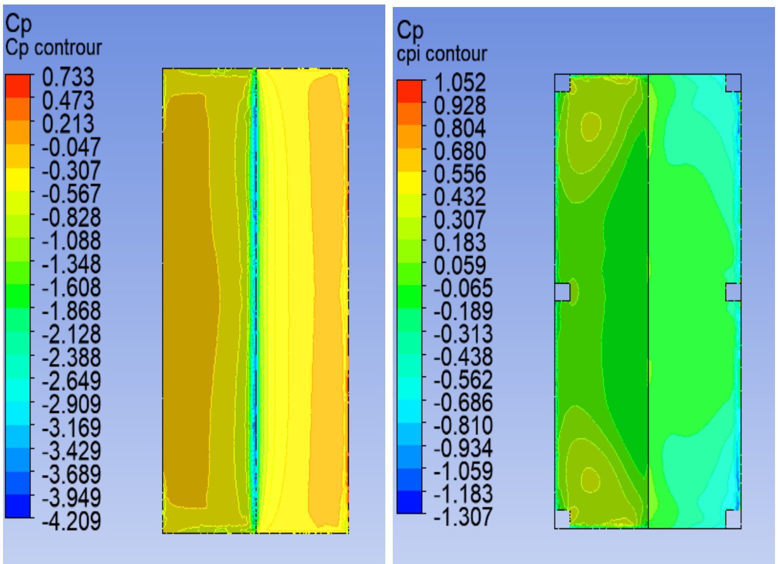

Fig 23 – C_{pe} and C_{pi} for 0° incidence angle

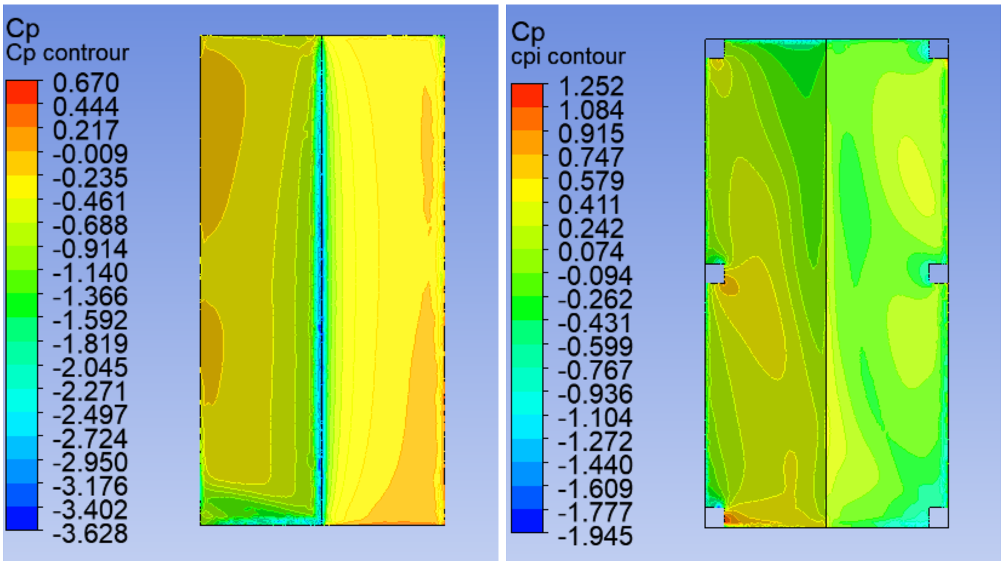

Fig 24 – C_{pe} and C_{pi} for 30° incidence angle

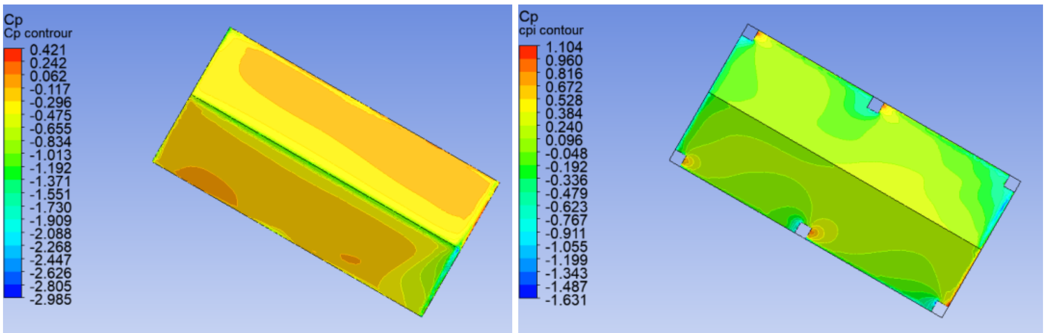

Fig 25 – C_{pe} and C_{pi} for 60° incidence angle

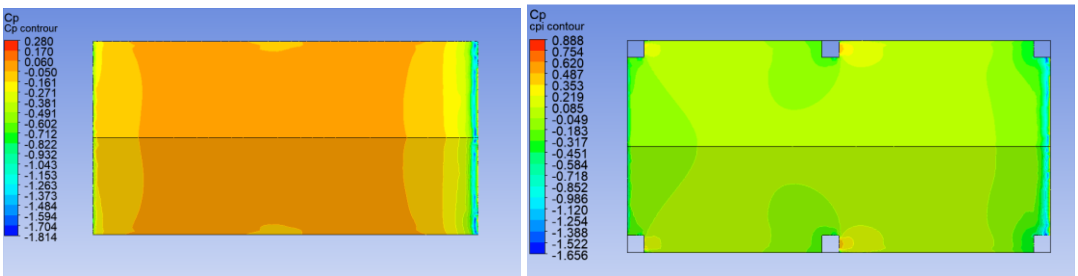

Fig 26 – C_{pe} and C_{pi} for 90° incidence angle

3.5.3 Isolated structure 30°

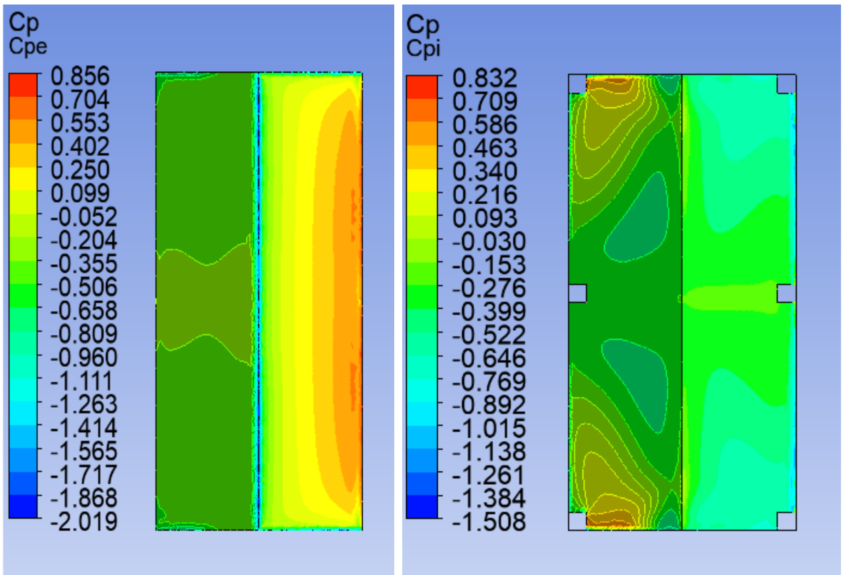

Fig 27 – C_{pe} and C_{pi} for 0° incidence angle

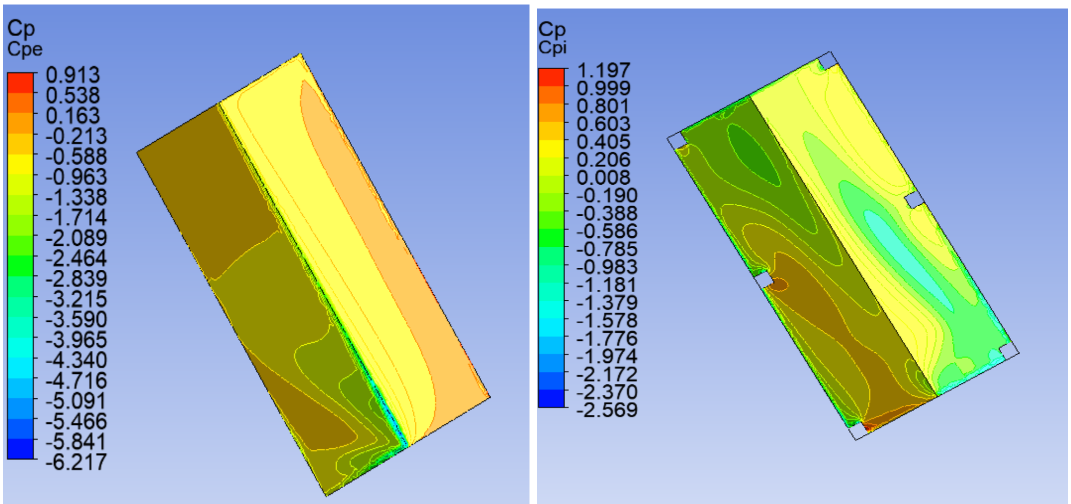

Fig 28 – C_{pe} and C_{pi} for 30° incidence angle

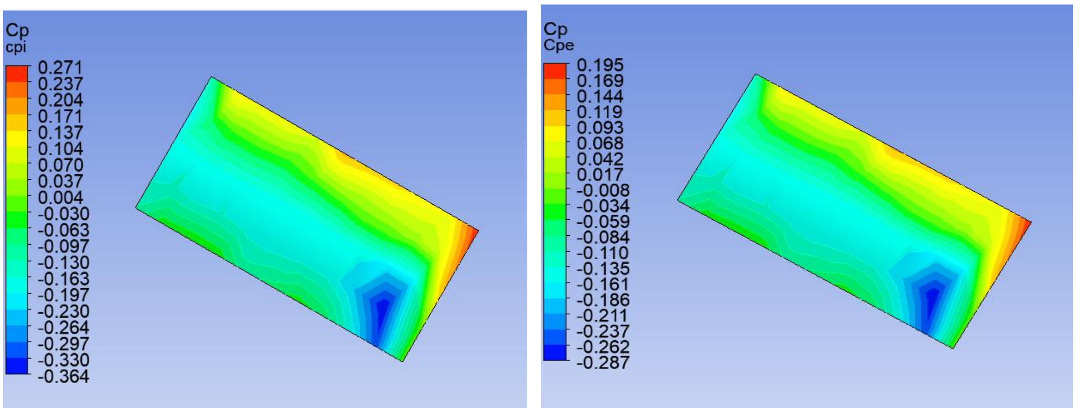

Fig 29 – C_{pe} and C_{pi} for 60° incidence angle

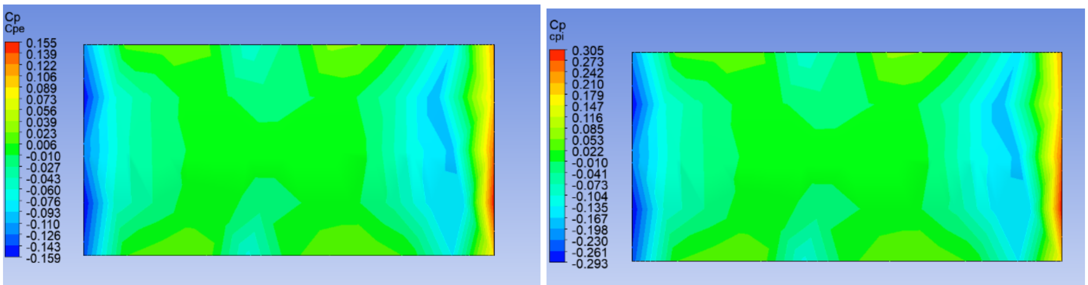

Fig 30 – C_{pe} and C_{pi} for 90° incidence angle

The C_p contours in Fig 21 – 30 are obtained corresposnding to the wind incidence for Pitched roof of 20° and 30° respectievely for different roations as 0° - 90°. The scenarios depict the building's orientation of sides facing towards the inlet and outlet of the domain. For both wind incidences, the contour variation for C_{pe} of roofs shows negative values thoroughout the roof surface.

Due to the bluff body nature of the pitched roof and the splitting of the wind streamline at the rooftoop , the $C_{pe(avg)}$ value for the external faces remained a higher value.

The values of C_{pi} are having smaller magnitudes and are causing suction for 90° wind incidence, since the wind has least interaction with the surface of the roof and most portion passes away showing least to none resistance for this rotation in all 3 cases.

The pressure coefficient values significantly decresed as building was rotated from 0° to 90°. Showing a regular pattern for the coefficients. However , as the angle of pitch incresed , this trend did not sustain and average pressure coefficient values showed significant dialation for the intermediate rotation values.

Significantly , for 30° pitch angle , the internal pressure coefficient attained a positive nature , this is due to more horizontal effect on the roof directly affecting the nature of building interaction with wind , which resulted in more pressure on the roof surface.

3.6 RELATION BETWEEN PRESSURE COEFFICENT AND PITCH ANGLE

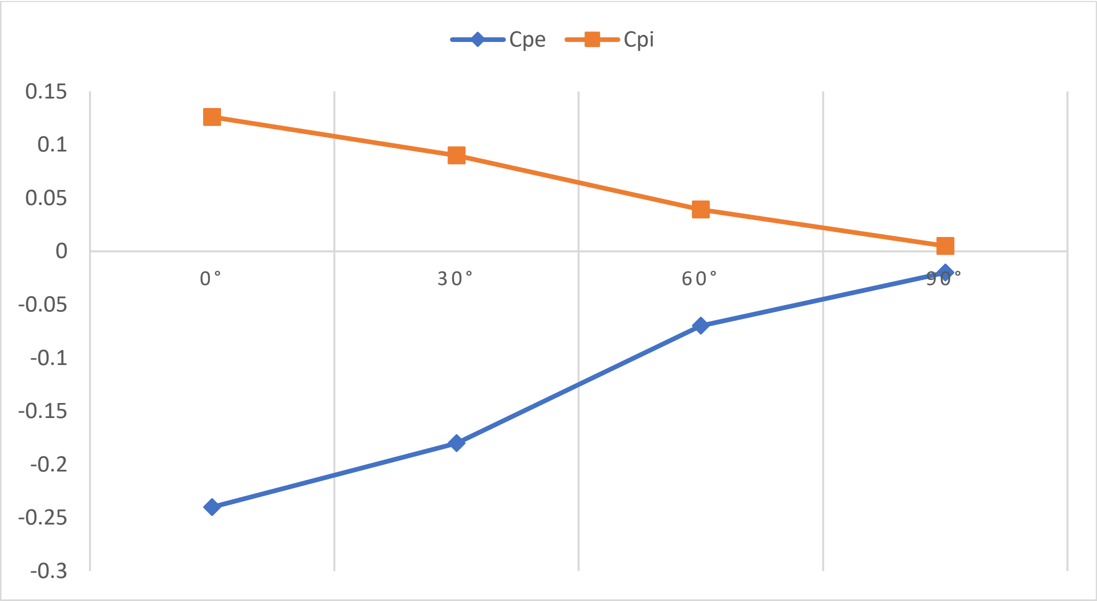

Fig 31 - Coefficient of Pressure (Cpe and Cpi) v/s Wind Incidence Angle (Ɵ°)

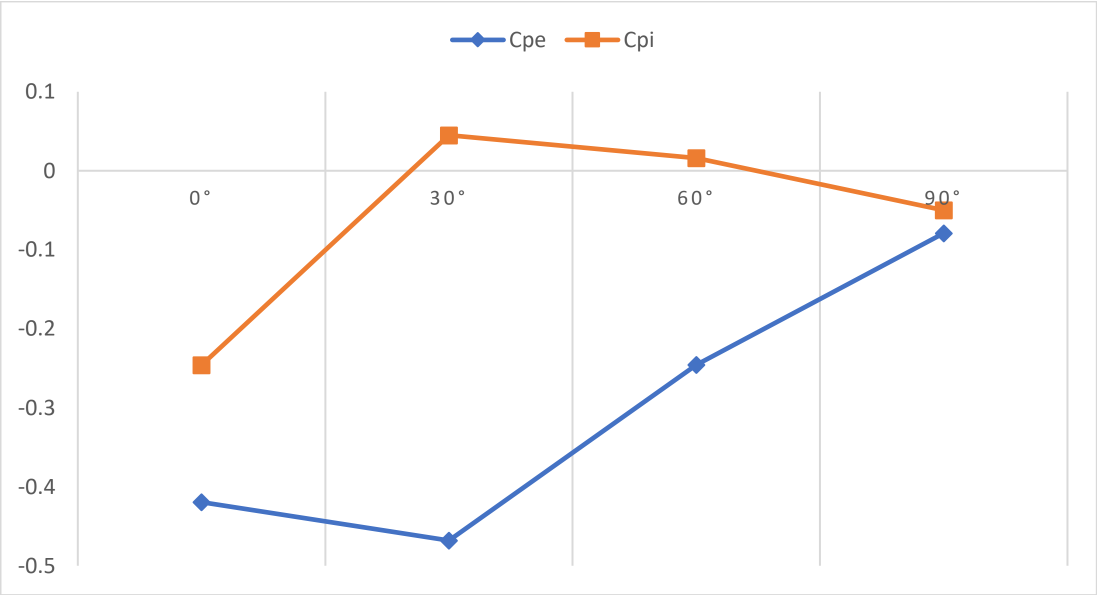

Fig 32 - Coefficient of Pressure (Cpe and Cpi) v/s Wind Incidence Angle (Ɵ°)

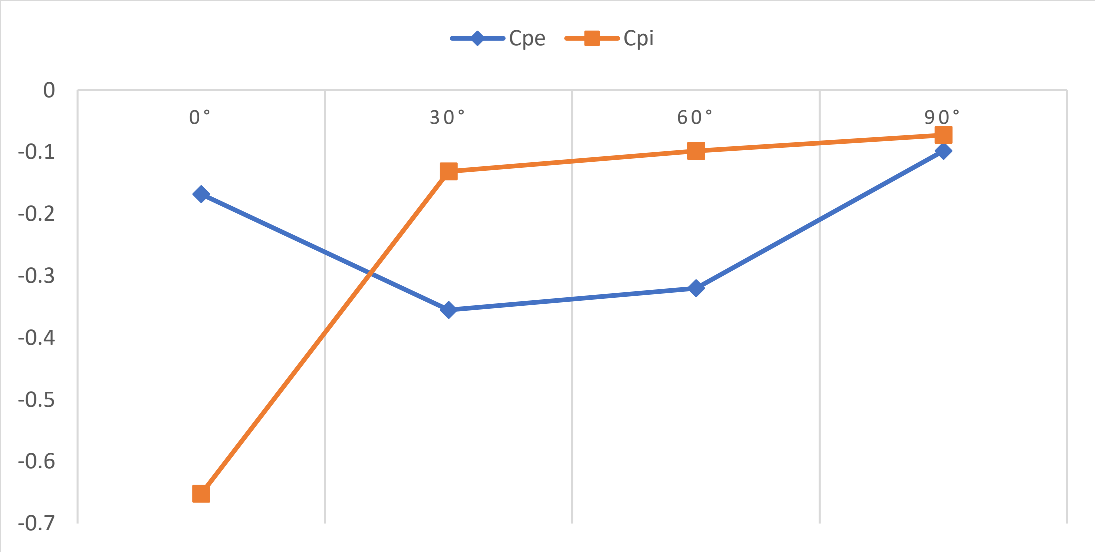

Fig 33 - Coefficient of Pressure (Cpe and Cpi) v/s Wind Incidence Angle (ϴ°)

The graphs represent the values of average coefficient of external as well as internal pressure for each building. A linear trend for the coefficient values can be observed in the case of 10° pitch angle for both the coefficients. Internal pressure coefficient for 20° pitch angle, turned from negative to positive from 30 degrees of rotation and further showed no prominent change, this is due to more surface area of wall internally has wind effect rather with zero rotation.

3.7 INTERFERENCE MODEL

The interefernce model is crated by placing the isolated structure in-line with respect to the other. The isolated structures are places at distance of 0,0.5,1,1.5 and 2 times the width. The coefficients of pressure are measured on each structure and respective contour profiles are plotted.

3.7.1 INTERFERENCE MODELS FOR DIFFERENT SPACING

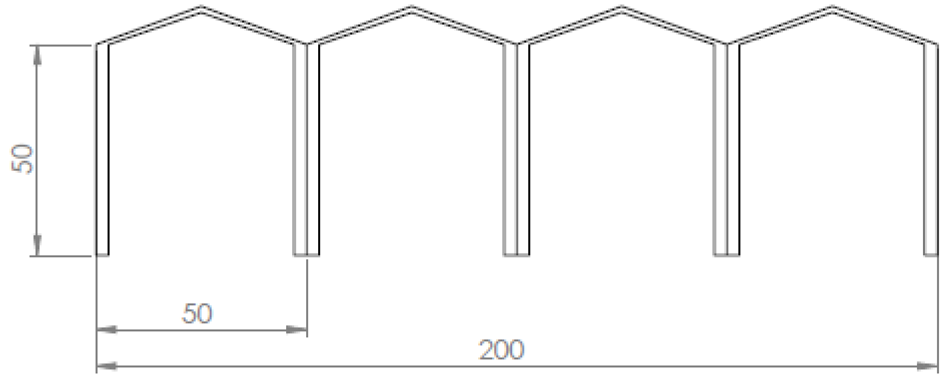

Fig 34 – Elevation of interference model for 0 spacing

Fig 35 – Plan of interference model for 0.5 b spacing

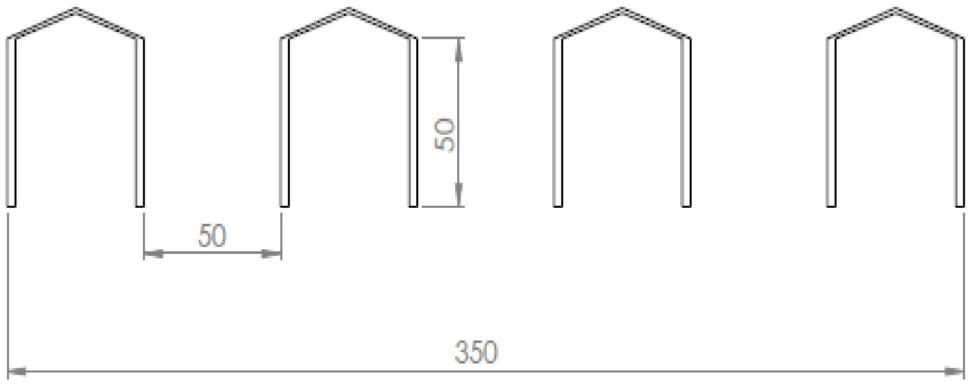

Fig 36 – Elevation of interference model for b spacing

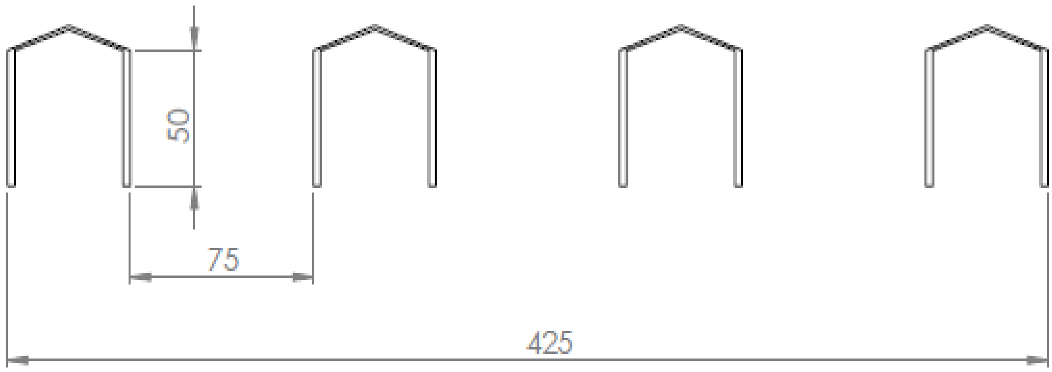

Fig 37 – Elevation of interference model for 1.5 b spacing

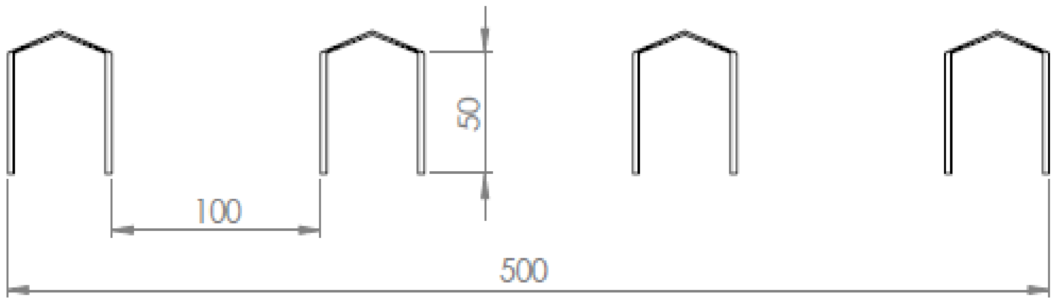

Fig 38 – Elevation of interference model for 2 b spacing

4. INTERFERENCE STUDY ON PITCHED ROOF

The wind flow is influenced by the structures in their vicinity. However, if other structures are also present in the vicinity of the model, the wind flow is affected due to the combined presence of the structures. This effect is known as the Interference effect. In the present study, the structure over which measurements are being made is called as Instrumented model and the structure which is interfering with the wind flow is known as Interfering Model. The effect on the instrumented model can be of two natures, i.e., either the wind load on the instrumented model due to the presence of interfering model will enhance or will get reduced. The former is known as the wind load enhancement effect and the latter is known as the shielding effect. The effect which will dominate depends upon the relative placement and orientation of the structures with the wind flow direction.

The contours and respective pressure coefficient values are plotted below for each rotation below, the windward side is represented by face a and leeward side is represented by face b, also depicted in the images connected with the respective graphs. The pressure values denote the average pressure coefficient values as mentioned, the average values are obtained by the same method as discussed in chapter 3 used for the validation model domain.

4.1 PRESSURE CONTOURS OF MODELS

4.1.1 Pitch Angle 10° and Spacing 0B

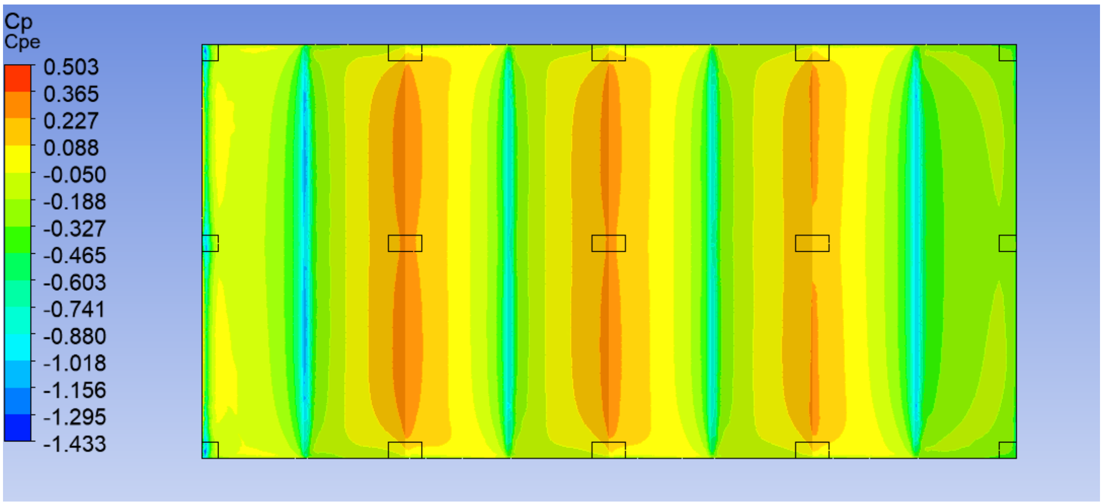

Fig 39 - External Pressure Coefficient at Wind Direction 0^0

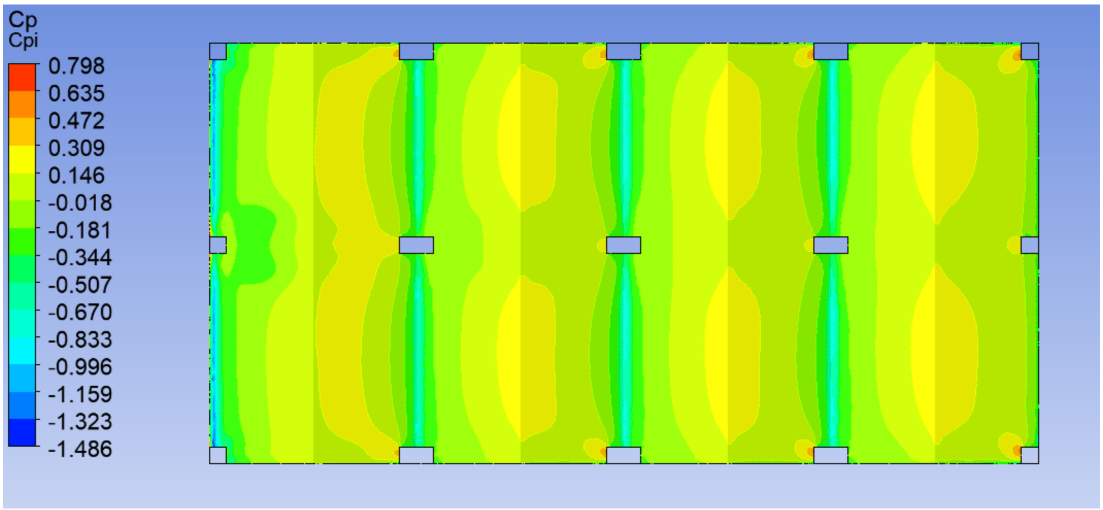

Fig 40 - Internal Pressure Coefficient at Wind Direction 0^0

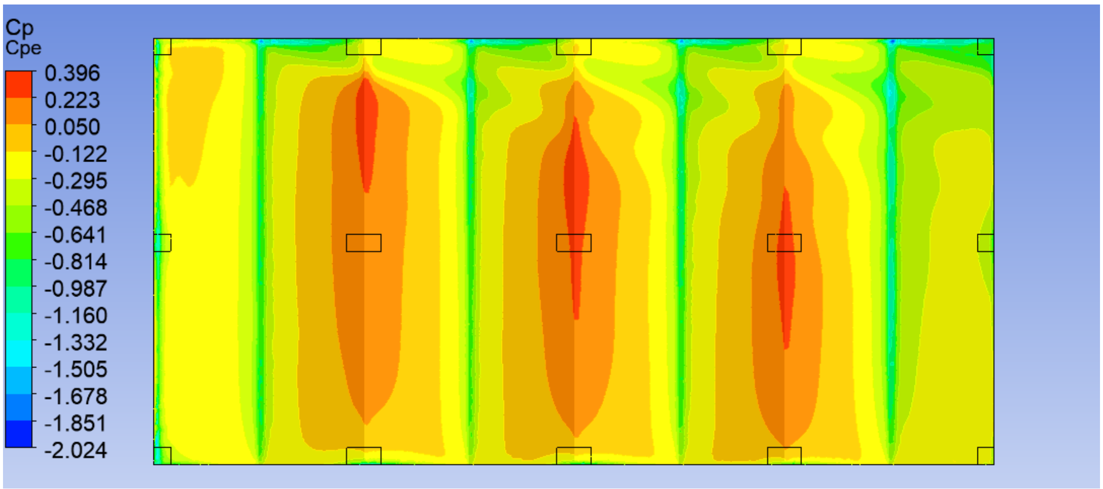

Fig 41 – External Pressure Coefficient at Wind Direction 30°

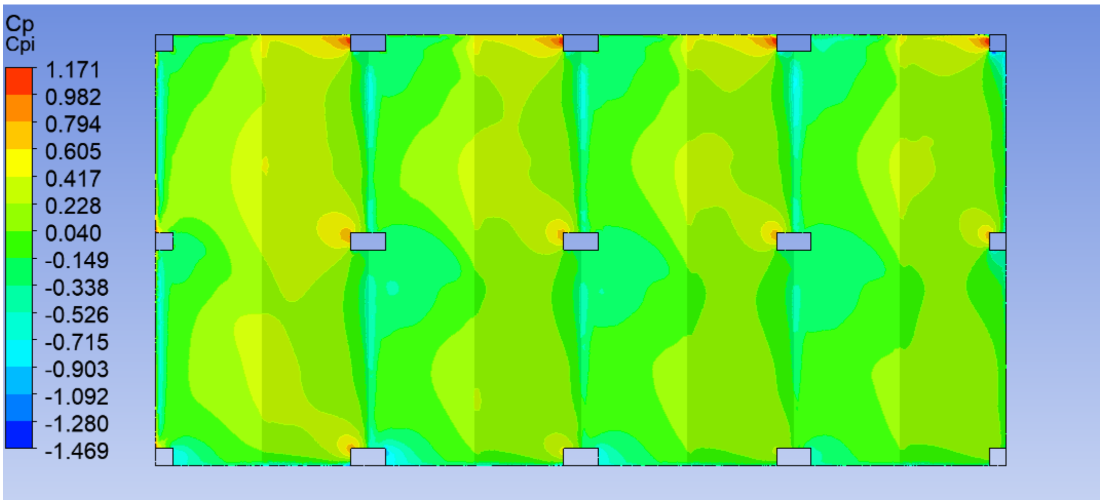

Fig 42 – Internal Pressure Coefficient at Wind Direction 30^0

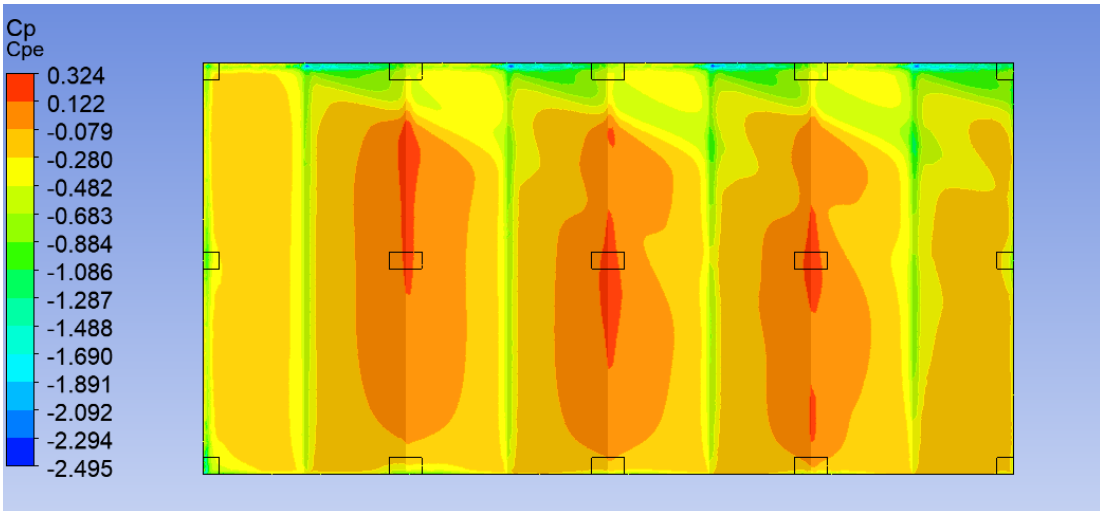

Fig 43 - External Pressure Coefficient at Wind Direction 45^0

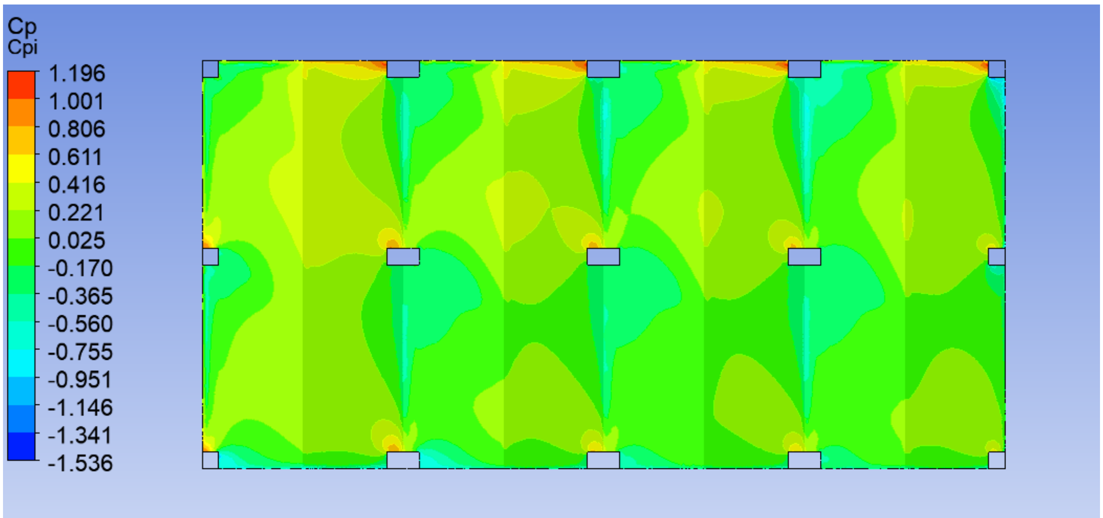

Fig 44 - Internal Pressure Coefficient at Wind Direction 45^0

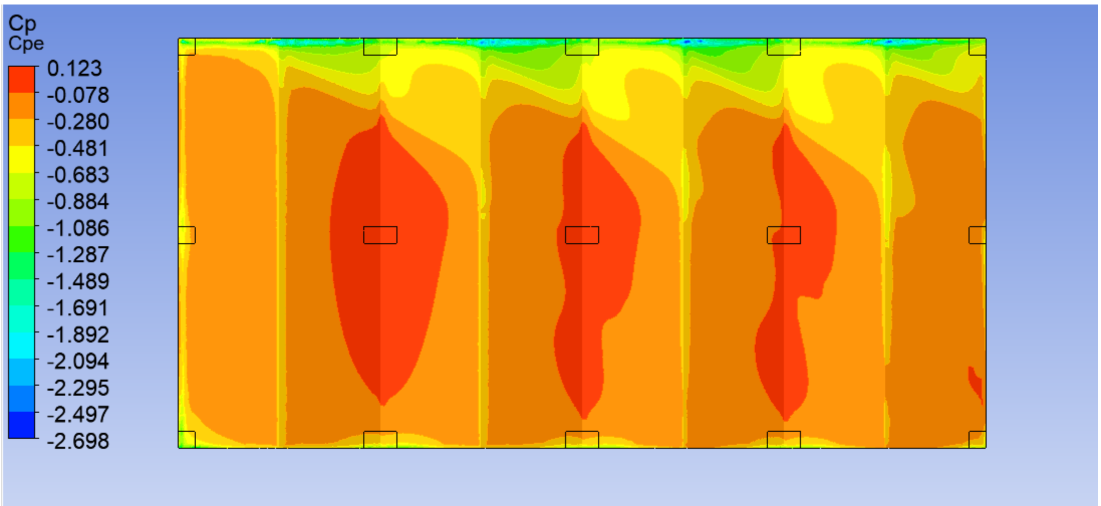

Fig 45 - External Pressure Coefficient at Wind Direction 60^0

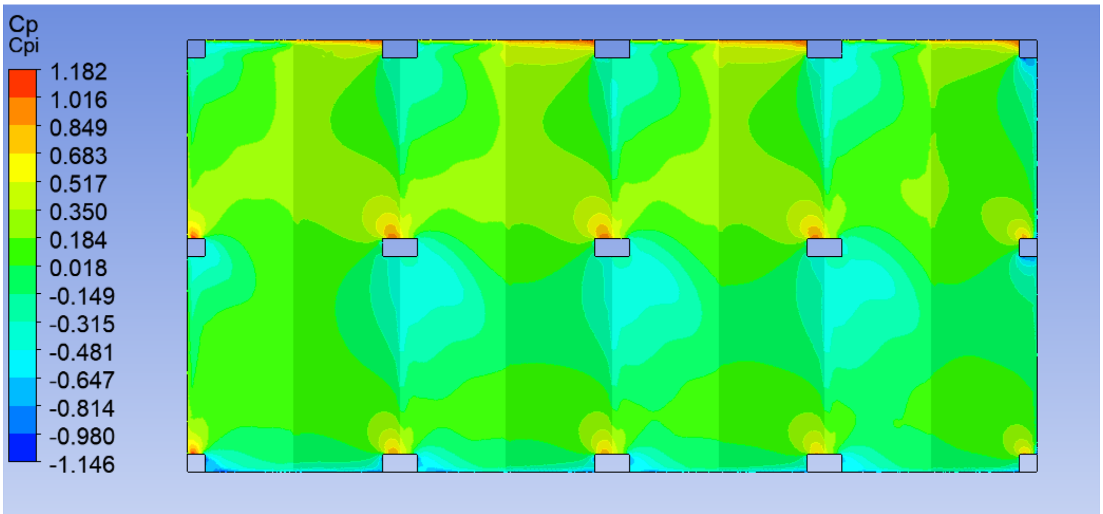

Fig 46 - Internal Pressure Coefficient at Wind Direction $60^{\ 0}$

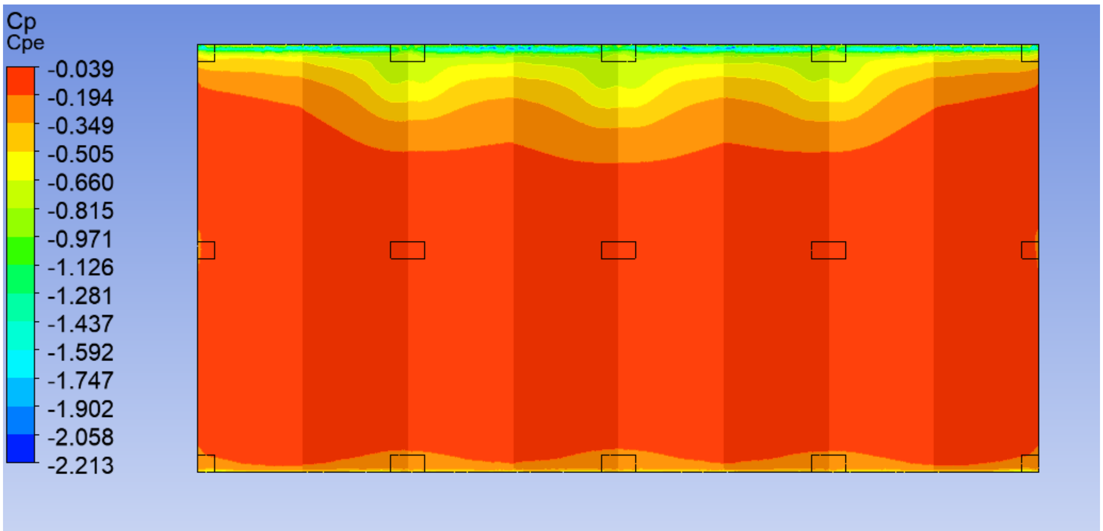

Fig 47 - External Pressure Coefficient at Wind Direction 90^0

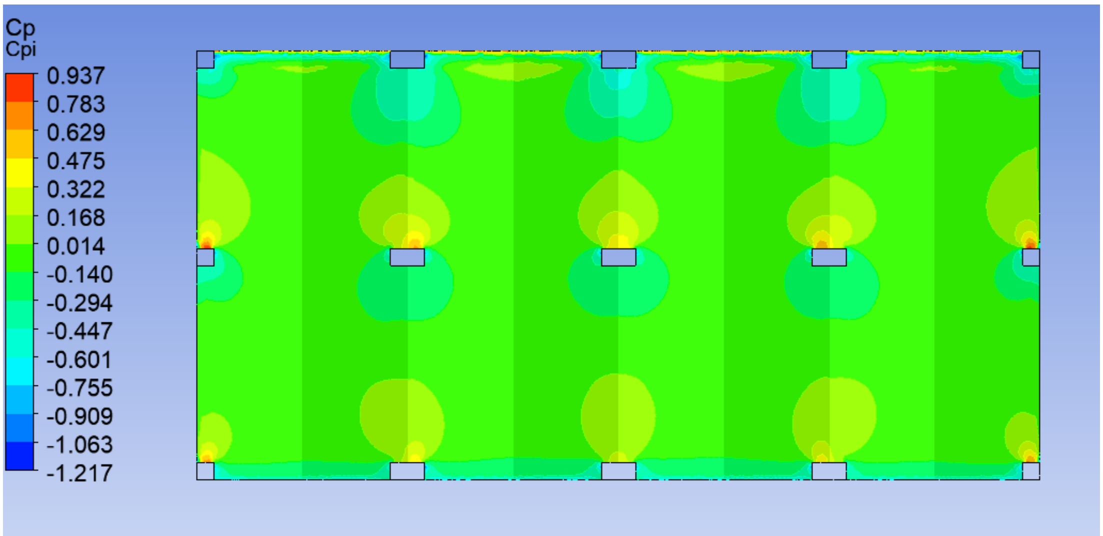

Fig 48 - Internal Pressure Coefficient at Wind Direction 90^0

4.1.2 Pitch Angle 10° and Spacing B/2

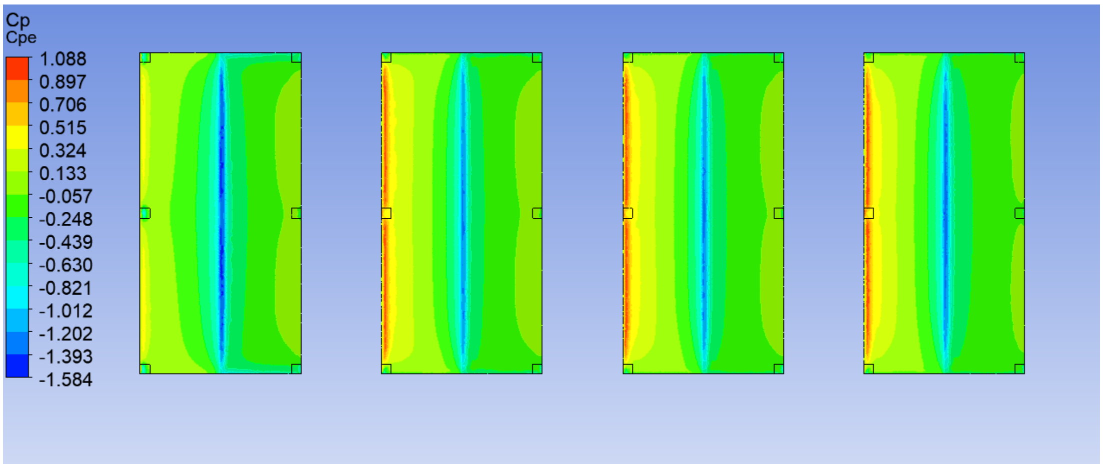

Fig 49 - External Pressure Coefficient at Wind Direction 0^0

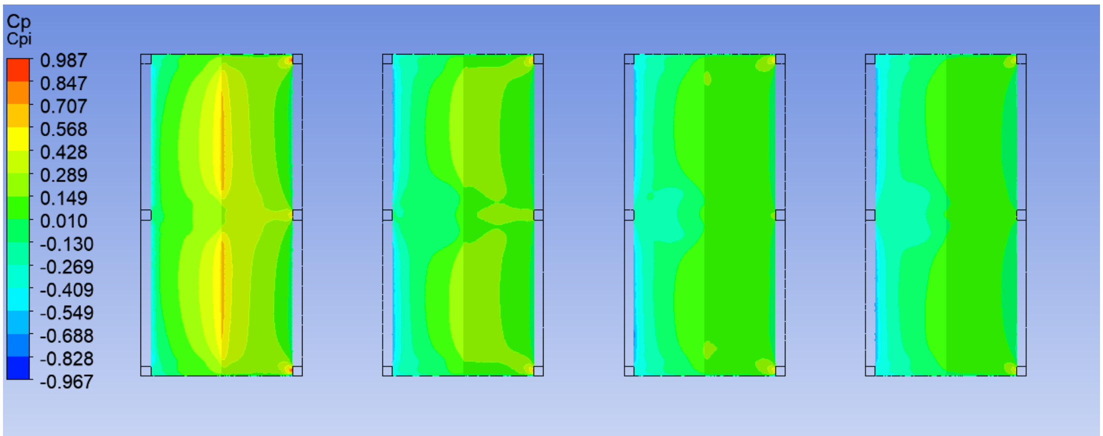

Fig 50 – Internal Pressure Coefficient at Wind Direction 0^0

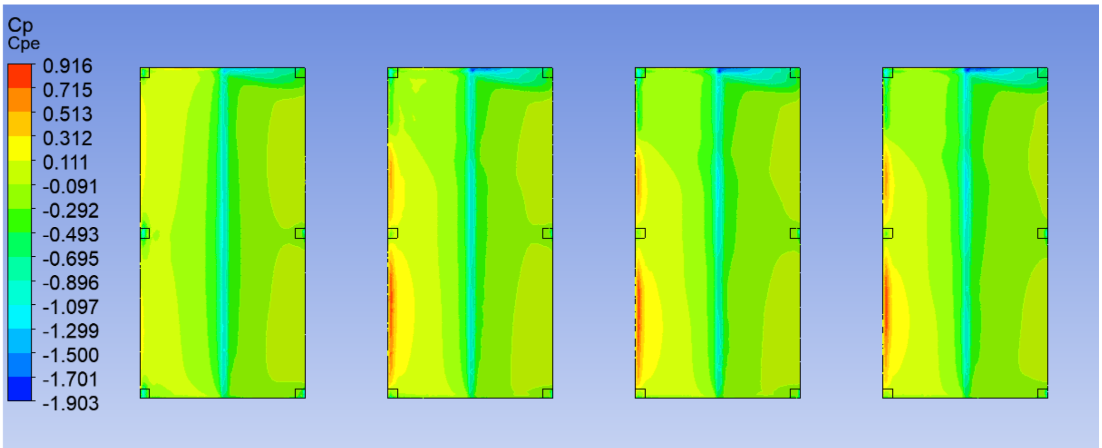

Fig 51 - External Pressure Coefficient at Wind Direction 30^0

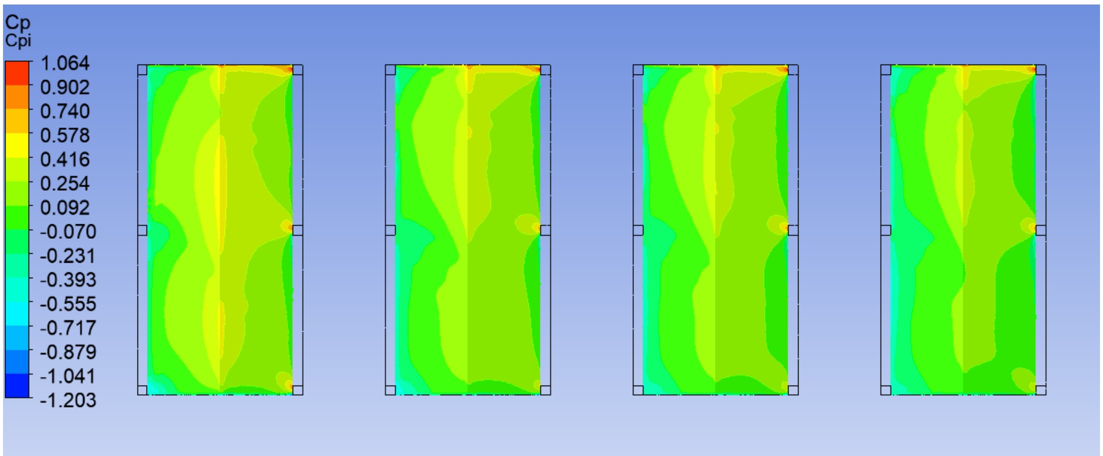

Fig 52 – Internal Pressure Coefficient at Wind Direction 30^0

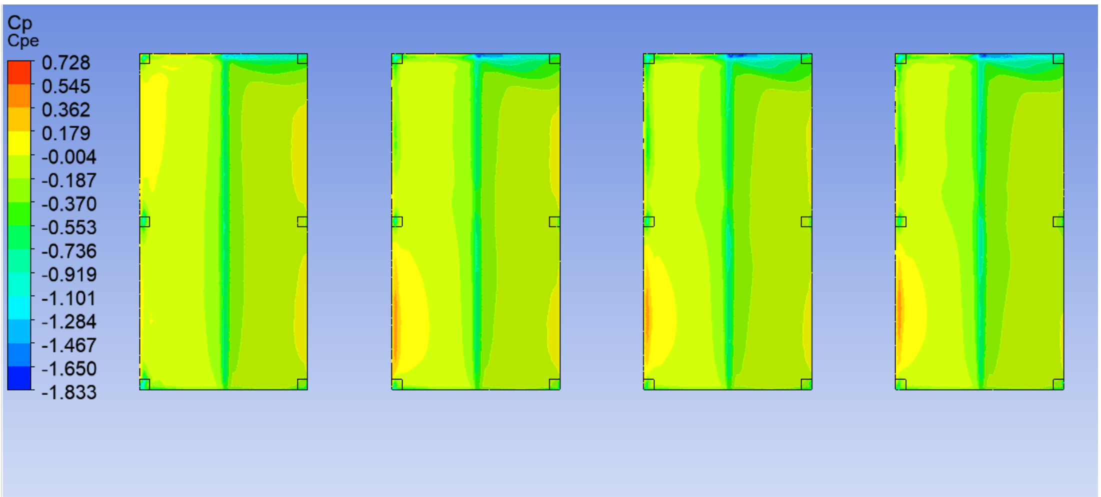

Fig 53 - External Pressure Coefficient at Wind Direction 45^0

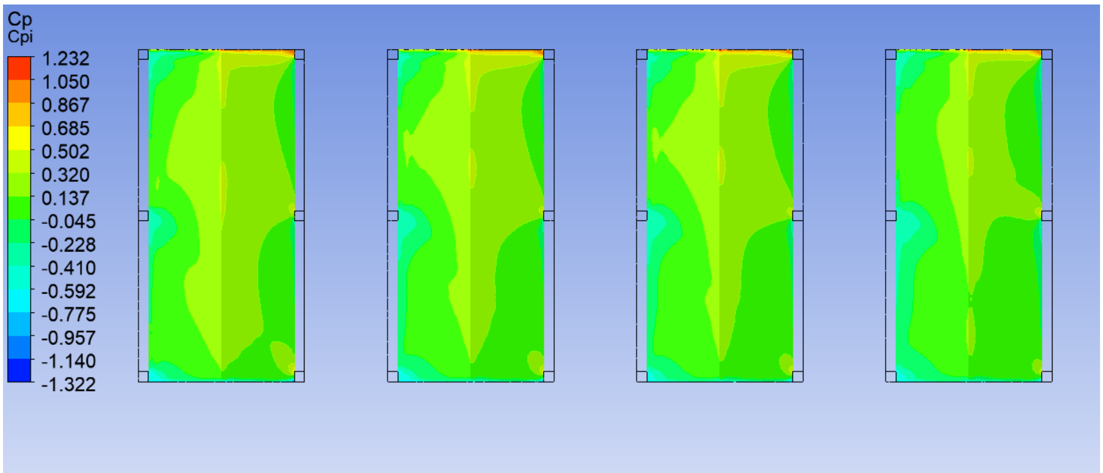

Fig 54 – Internal Pressure Coefficient at Wind Direction 45^0

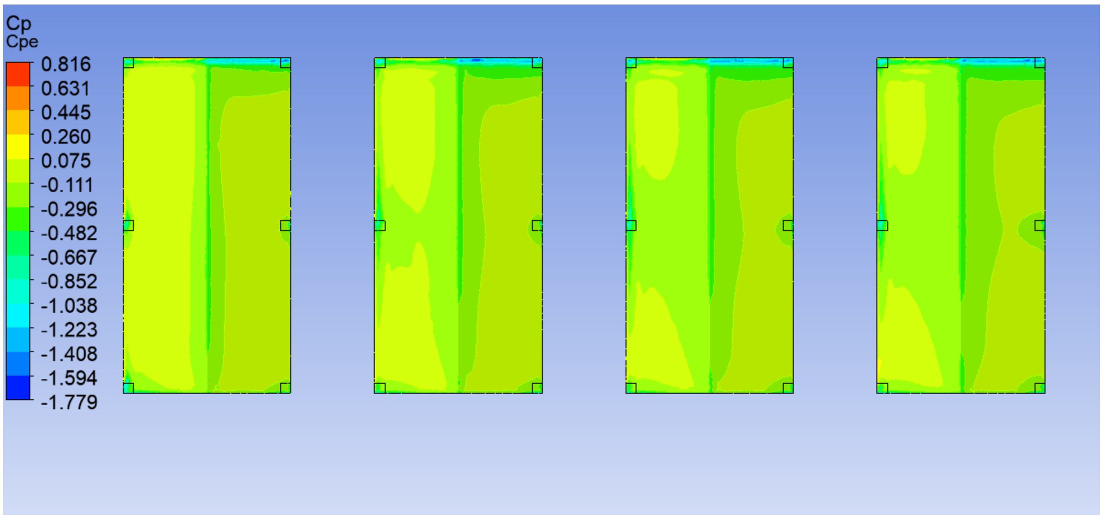

Fig 55 - External Pressure Coefficient at Wind Direction 60^0

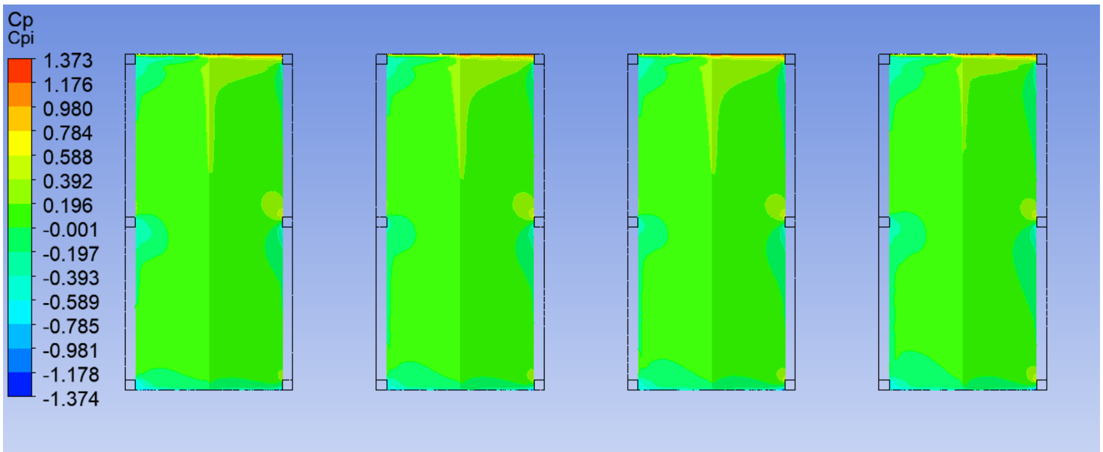

Fig 56 – Internal Pressure Coefficient at Wind Direction 60^0

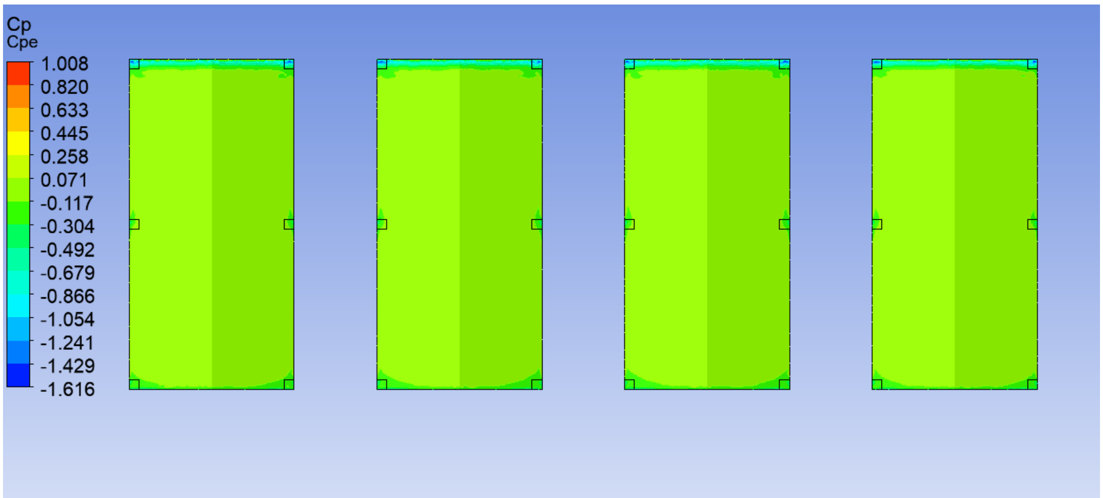

Fig 57 - External Pressure Coefficient at Wind Direction 90^0

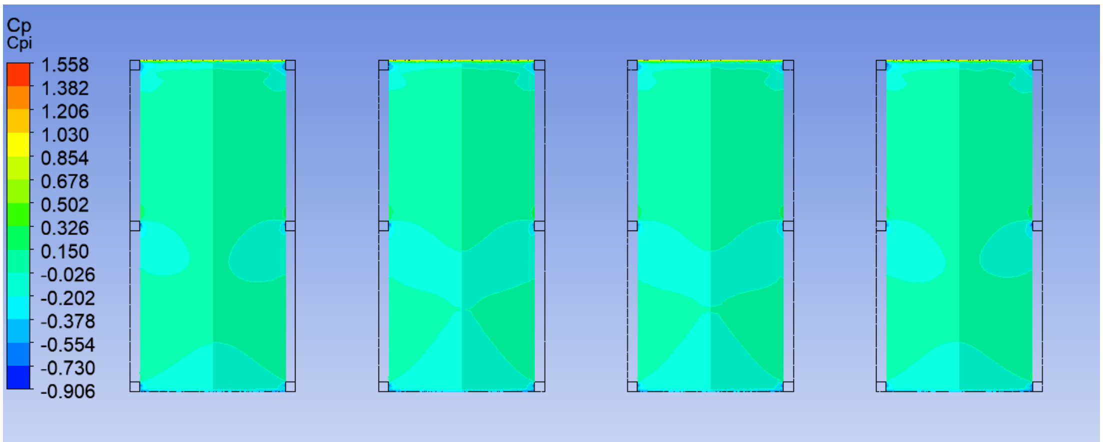

Fig 58 – Internal Pressure Coefficient at Wind Direction 90^0

4.1.3 Pitch Angle 10° and Spacing B

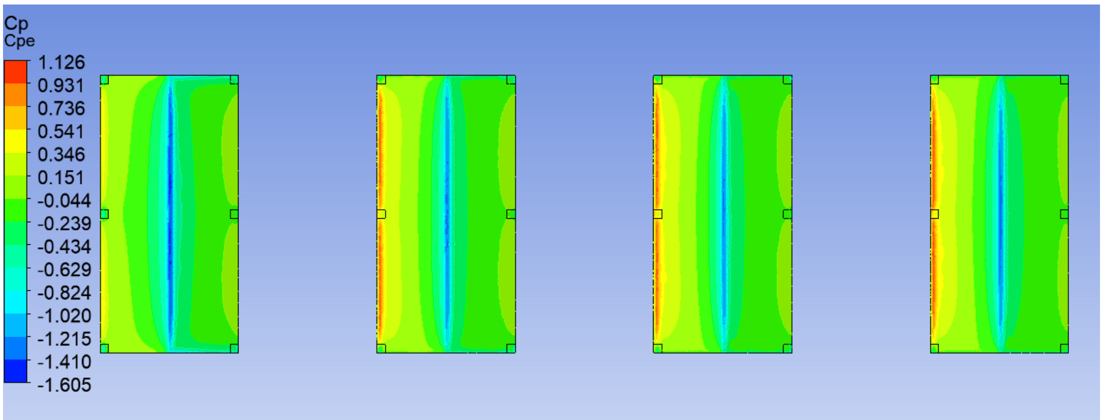

Fig 59 - External Pressure Coefficient at Wind Direction 0^0

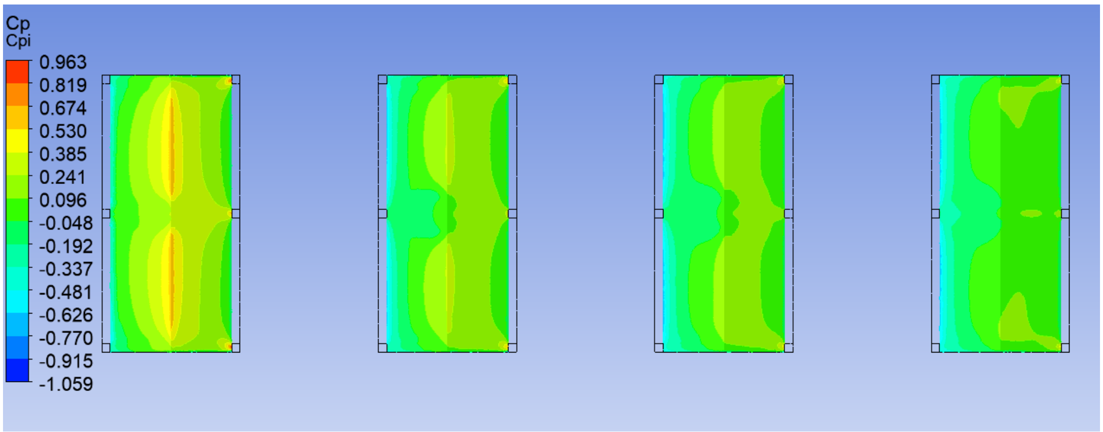

Fig 60 – Internal Pressure Coefficient at Wind Direction 0^0

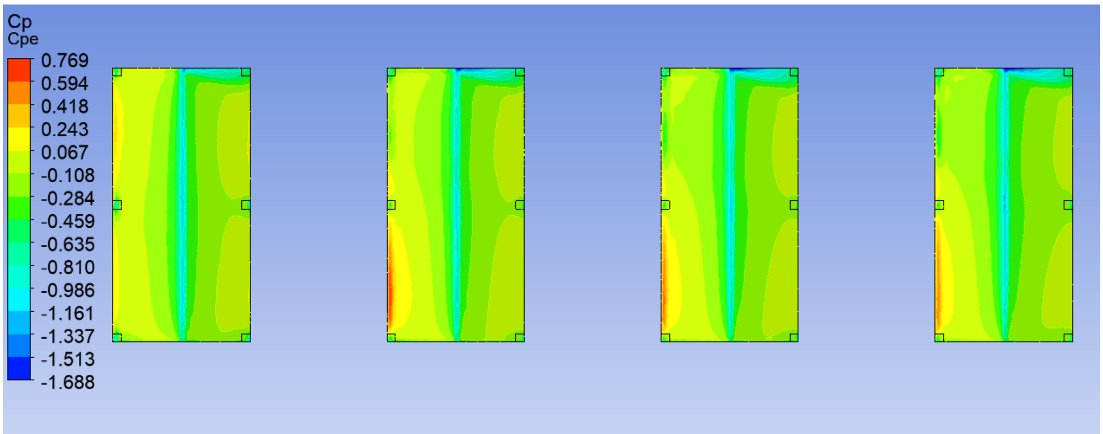

Fig 61 - External Pressure Coefficient at Wind Direction 30^0

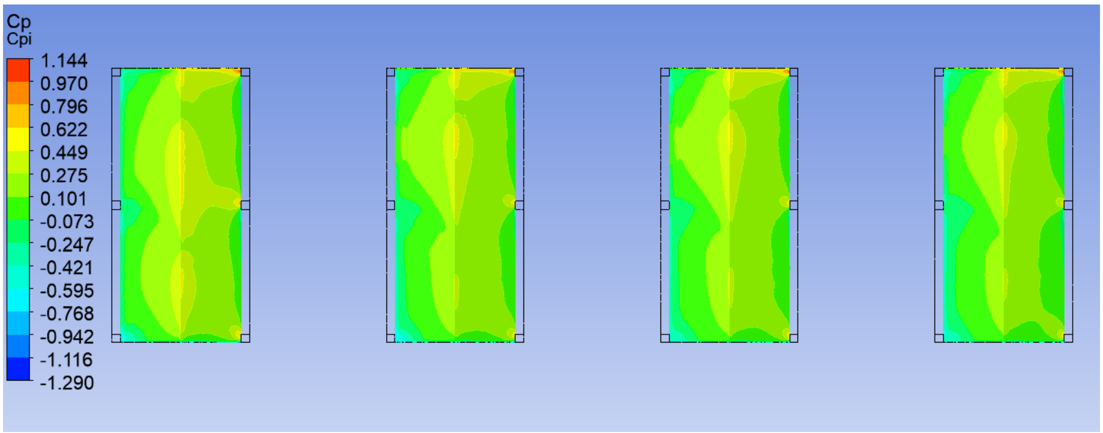

Fig 62 – Internal Pressure Coefficient at Wind Direction 30^0

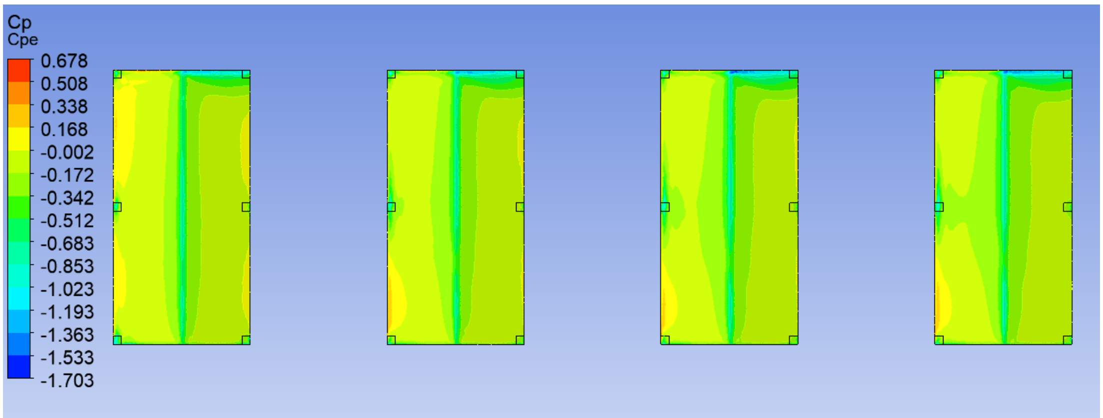

Fig 63 - External Pressure Coefficient at Wind Direction 45^0

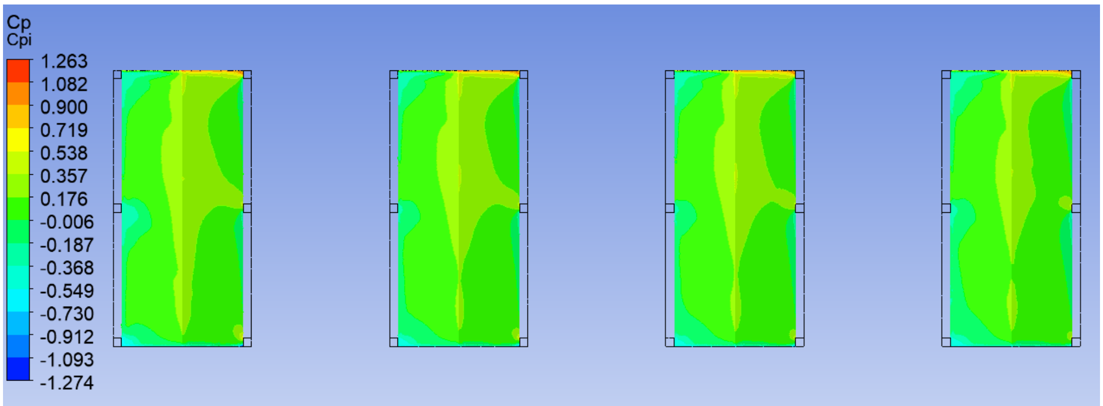

Fig 64 – Internal Pressure Coefficient at Wind Direction 45^0

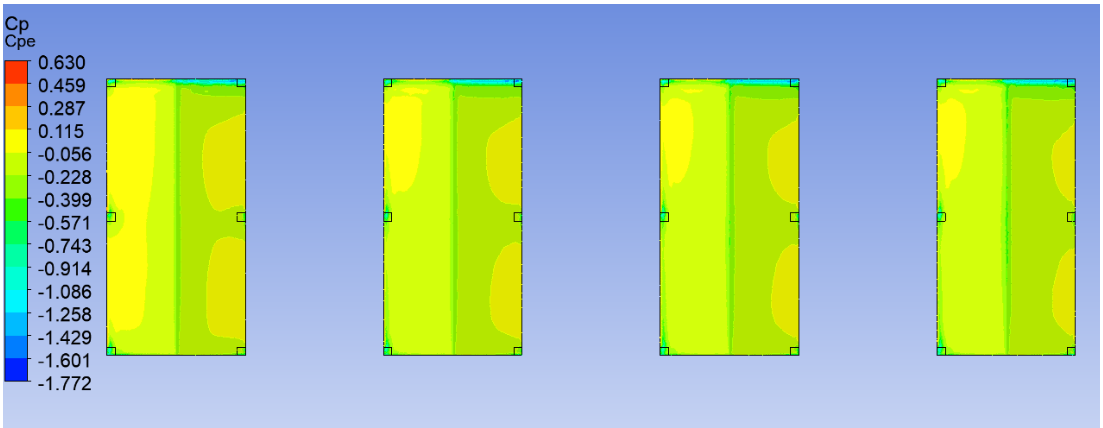

Fig 65 - External Pressure Coefficient at Wind Direction 60^0

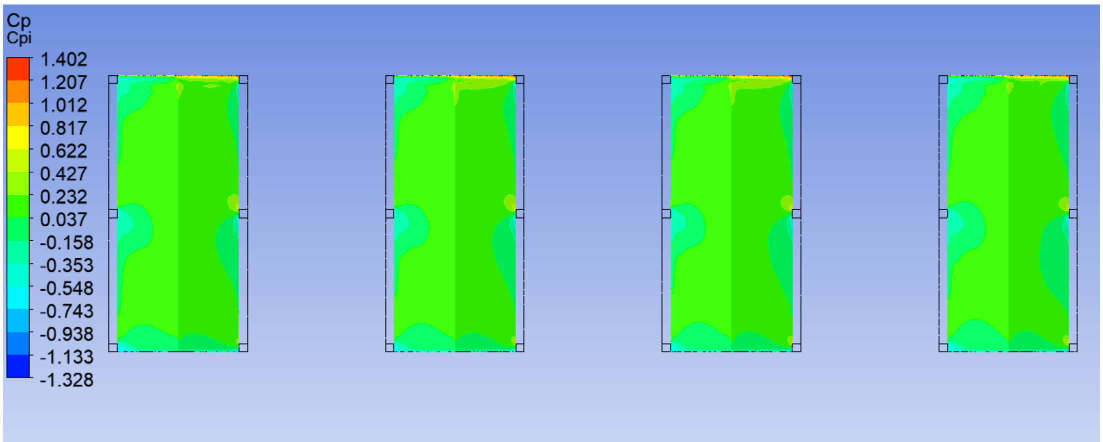

Fig 66 – Internal Pressure Coefficient at Wind Direction 60^0

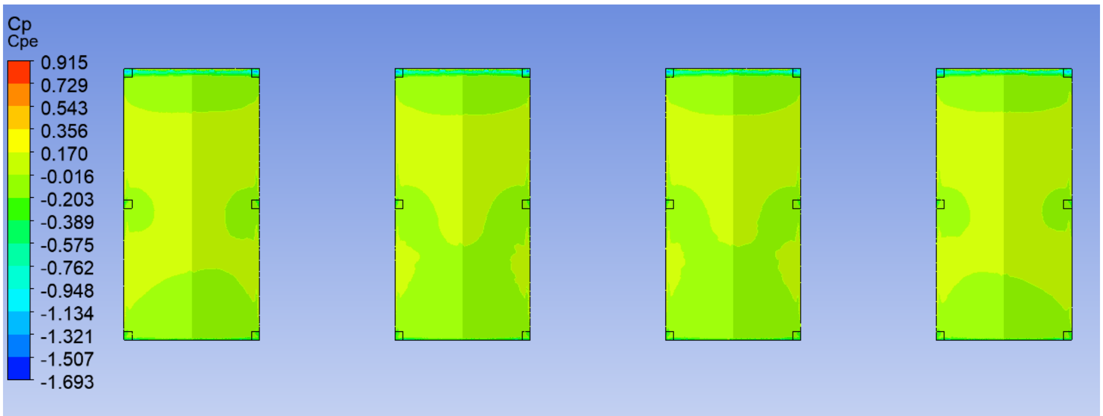

Fig 67 - External Pressure Coefficient at Wind Direction 90^0

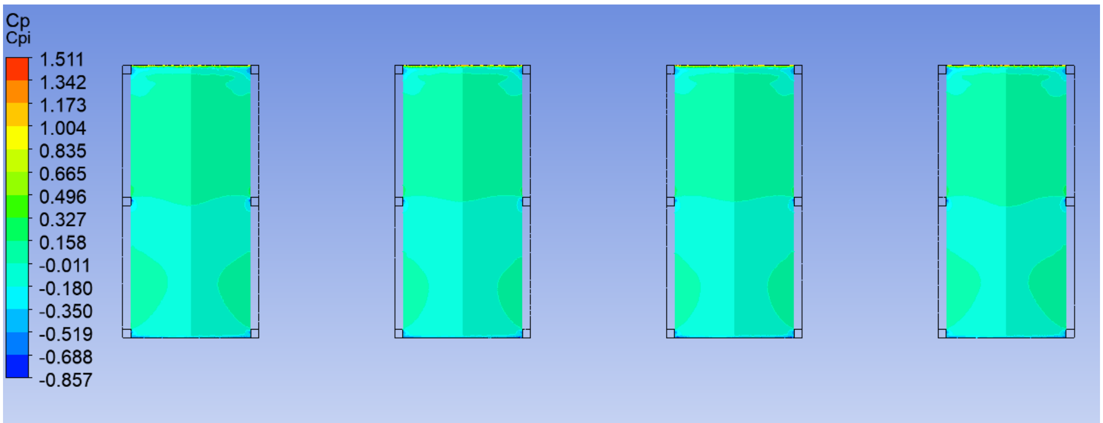

Fig 68 – Internal Pressure Coefficient at Wind Direction 90^0

4.1.4 Pitch Angle 10° and Spacing 3B/2

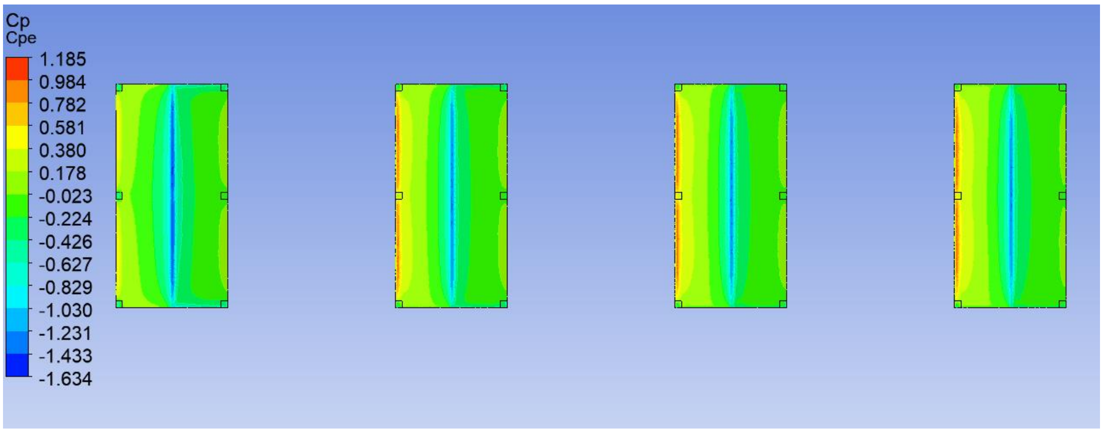

Fig 69 - External Pressure Coefficient at Wind Direction 0^0

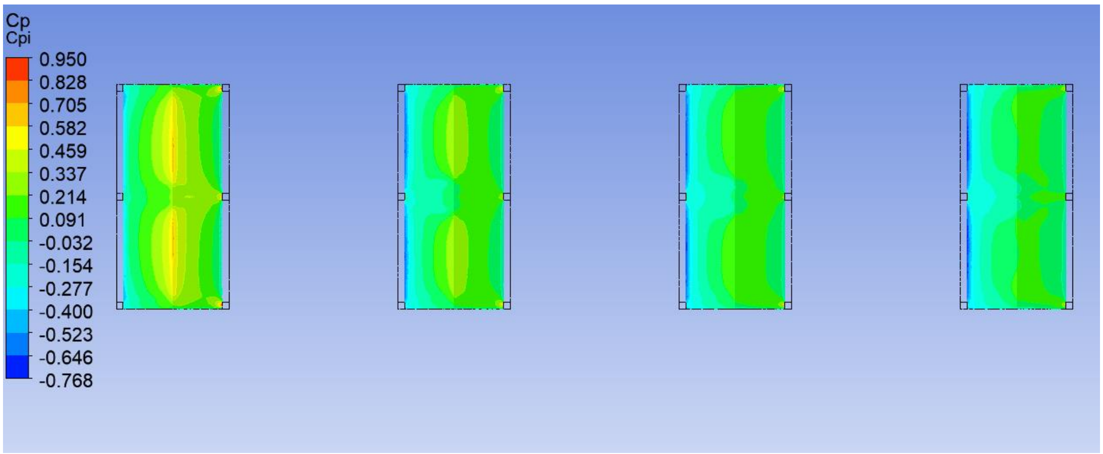

Fig 70 – Internal Pressure Coefficient at Wind Direction 0^0

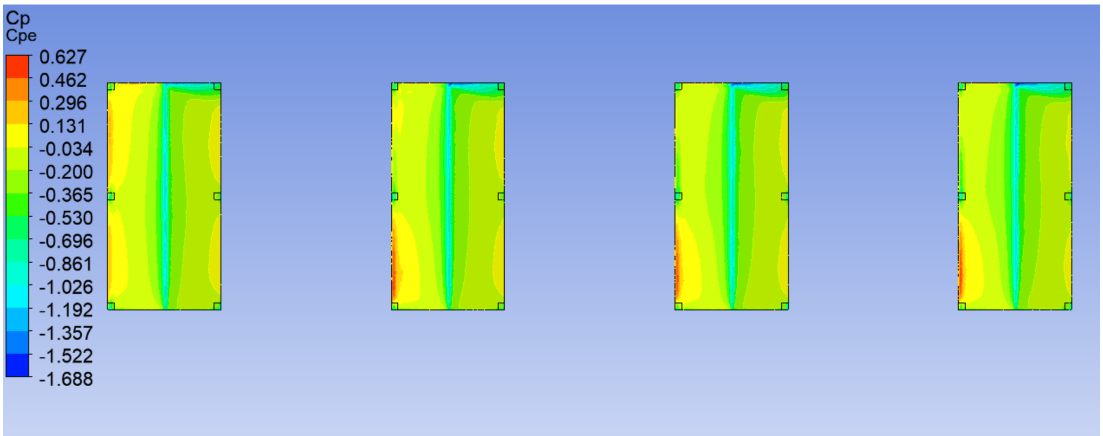

Fig 71 - External Pressure Coefficient at Wind Direction 30^0

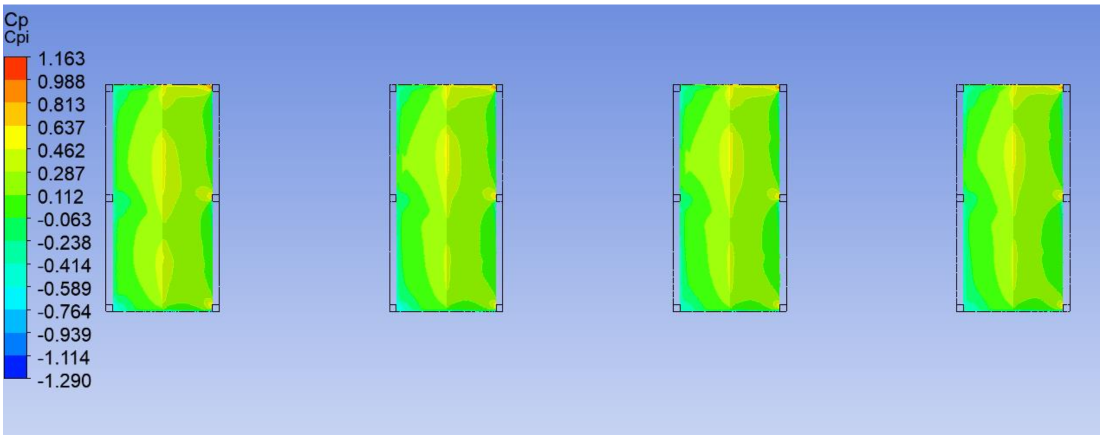

Fig 72 – Internal Pressure Coefficient at Wind Direction 30^0

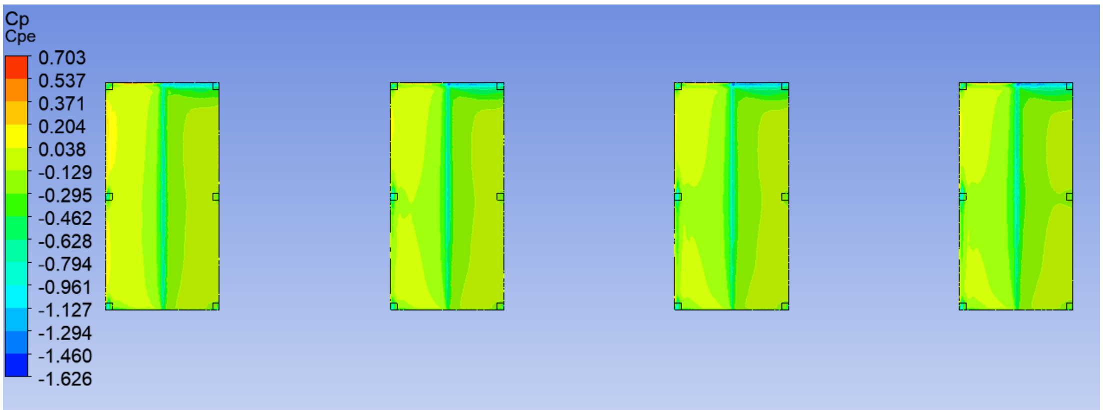

Fig 73 - External Pressure Coefficient at Wind Direction 45^0

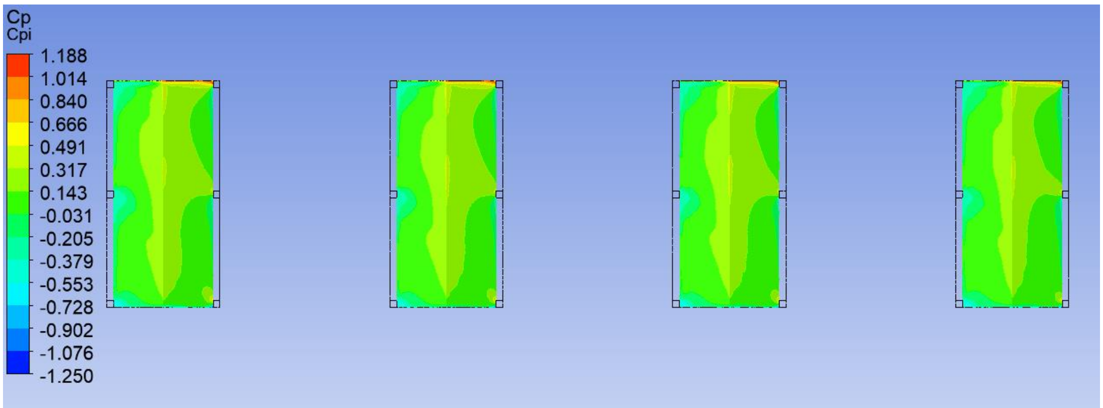

Fig 74 – Internal Pressure Coefficient at Wind Direction 45^0

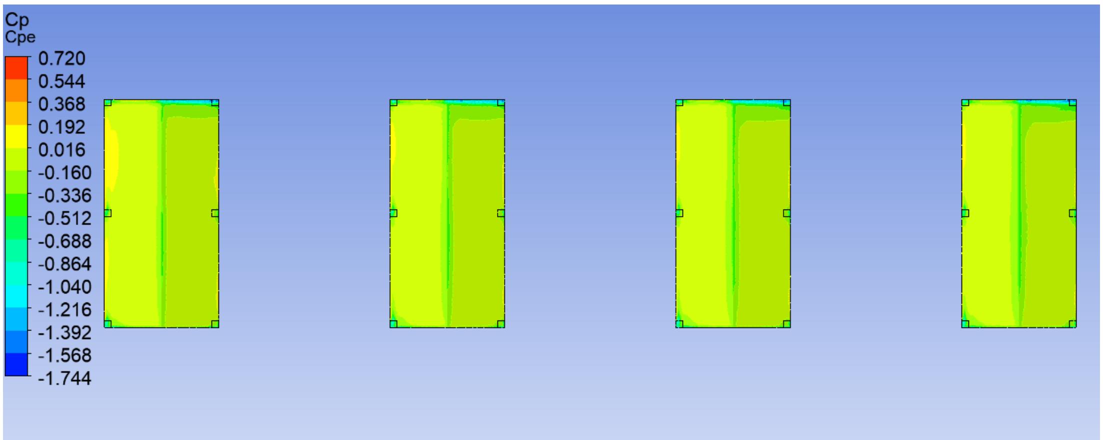

Fig 75 - External Pressure Coefficient at Wind Direction 60^0

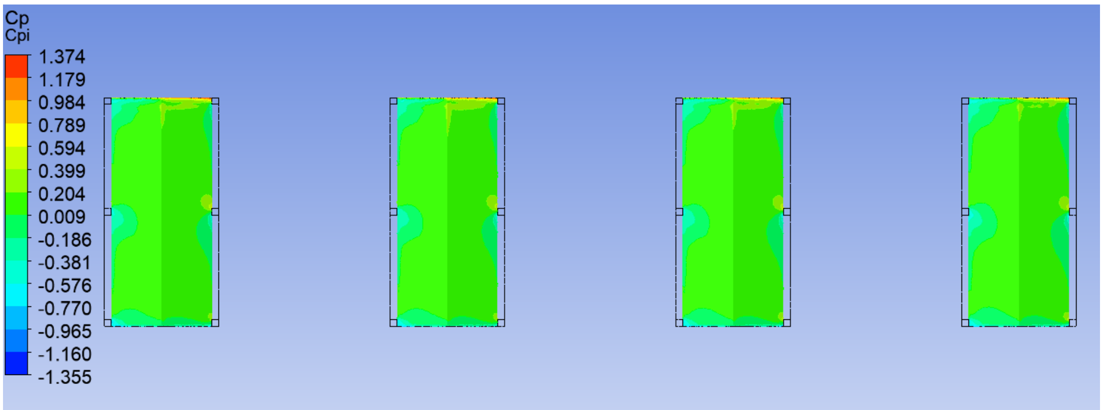

Fig 76 – Internal Pressure Coefficient at Wind Direction 60^0

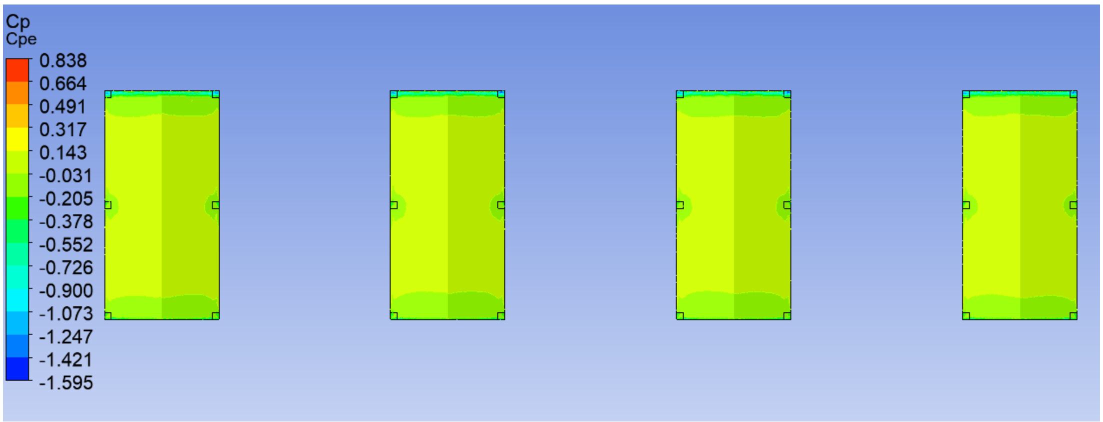

Fig 77 - External Pressure Coefficient at Wind Direction 90^0

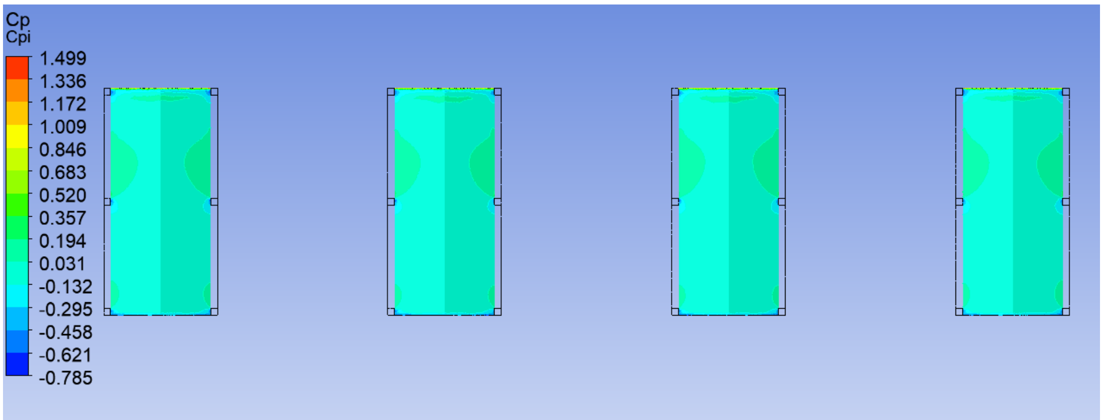

Fig 78– Internal Pressure Coefficient at Wind Direction 90^0

4.1.5 Pitch Angle 10° and Spacing 2B

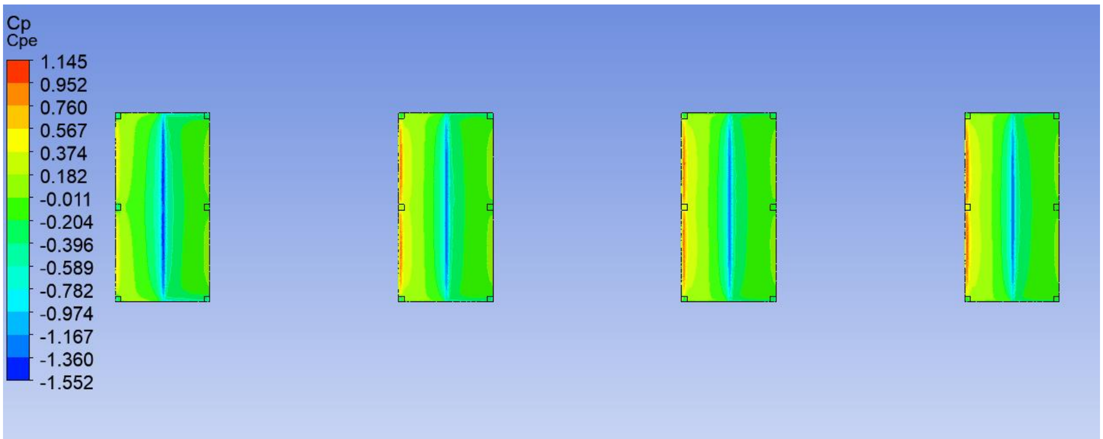

Fig 79 - External Pressure Coefficient at Wind Direction 0^0

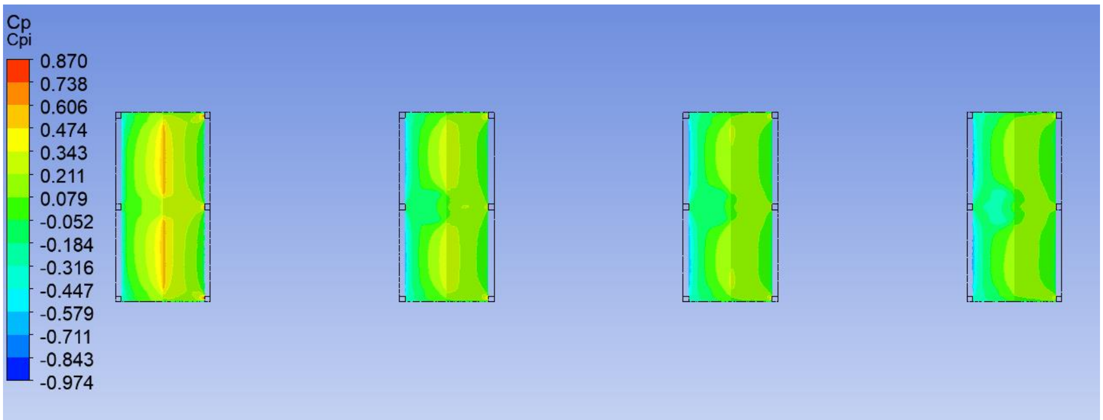

Fig 80 – Internal Pressure Coefficient at Wind Direction 0^0

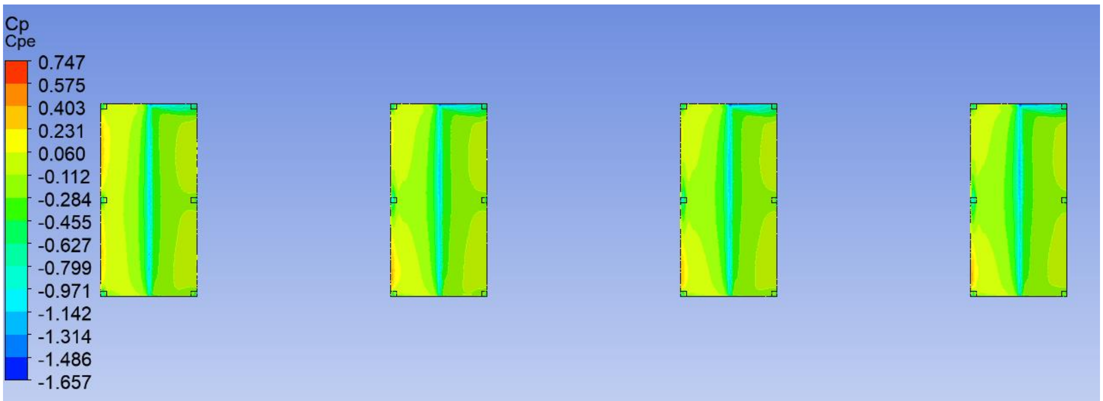

Fig 81 - External Pressure Coefficient at Wind Direction 30^0

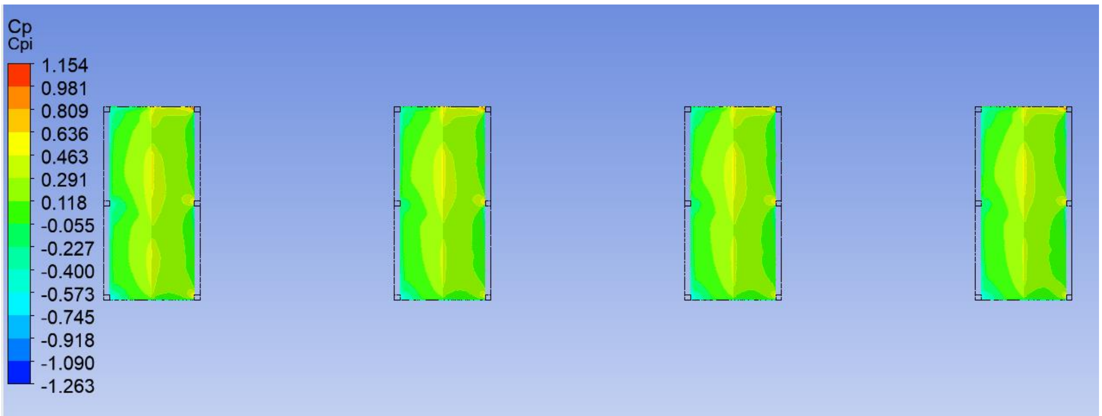

Fig 82 – Internal Pressure Coefficient at Wind Direction 30^0

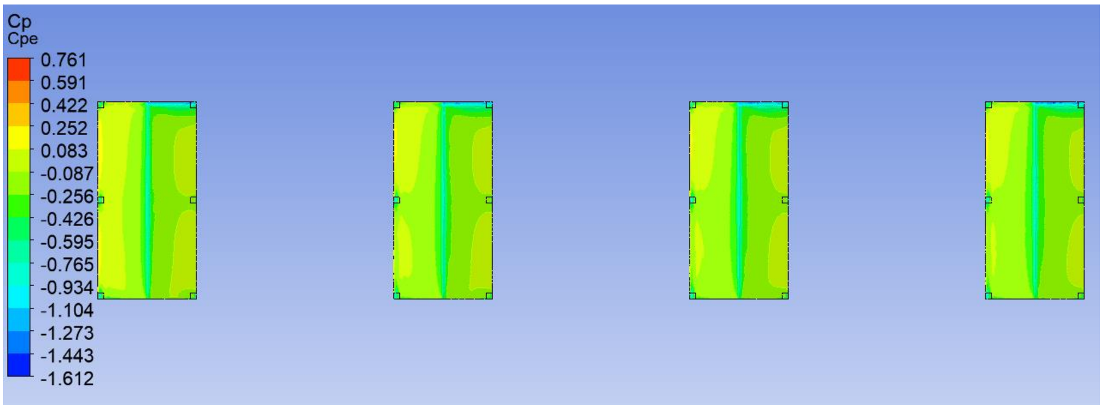

Fig 83 - External Pressure Coefficient at Wind Direction 45^0

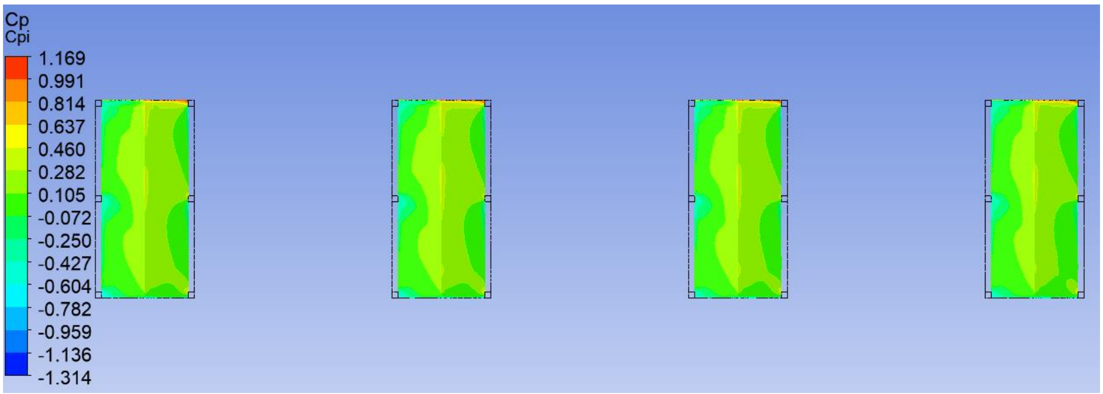

Fig 84 – Internal Pressure Coefficient at Wind Direction 45^0

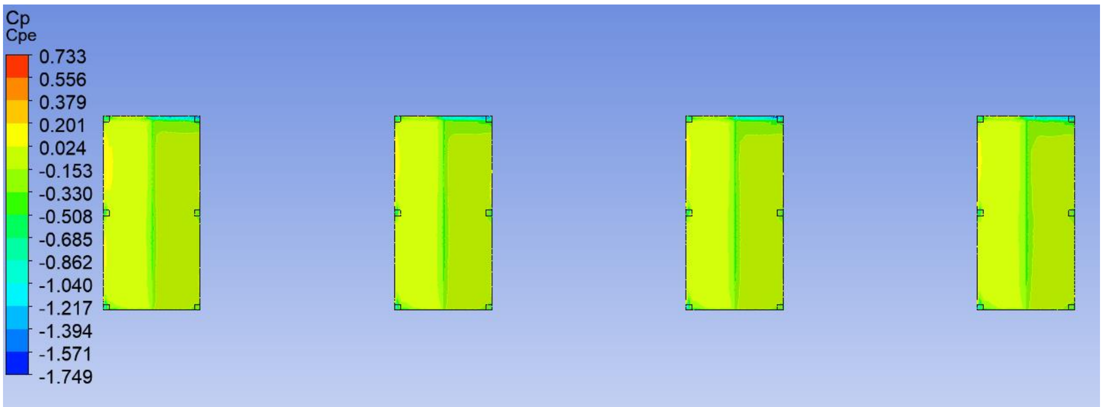

Fig 85 - External Pressure Coefficient at Wind Direction 60^0

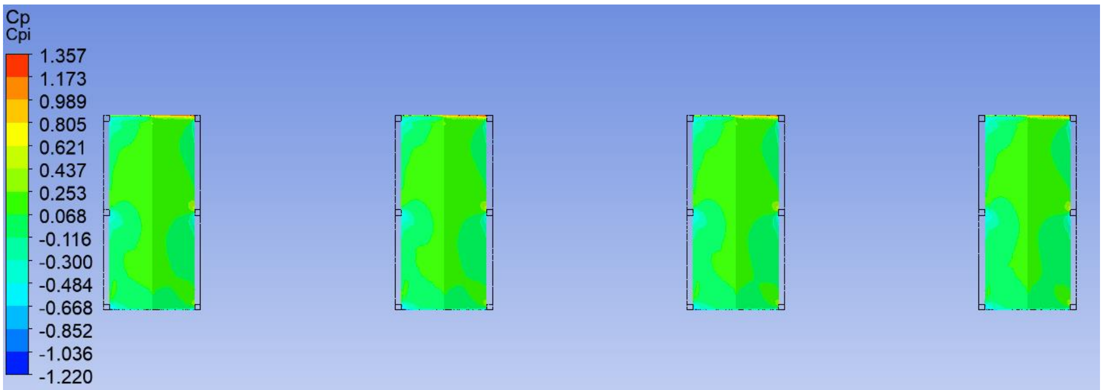

Fig 86– Internal Pressure Coefficient at Wind Direction 60^0

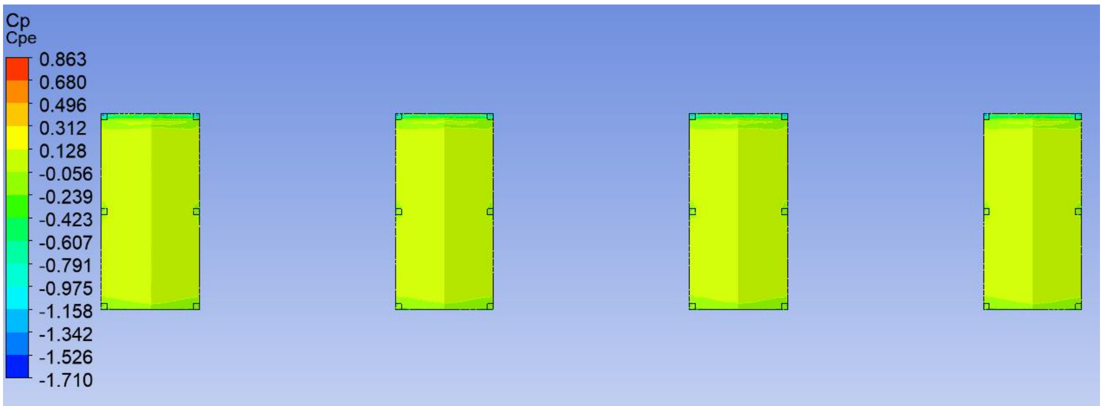

Fig 87 - External Pressure Coefficient at Wind Direction 90^0

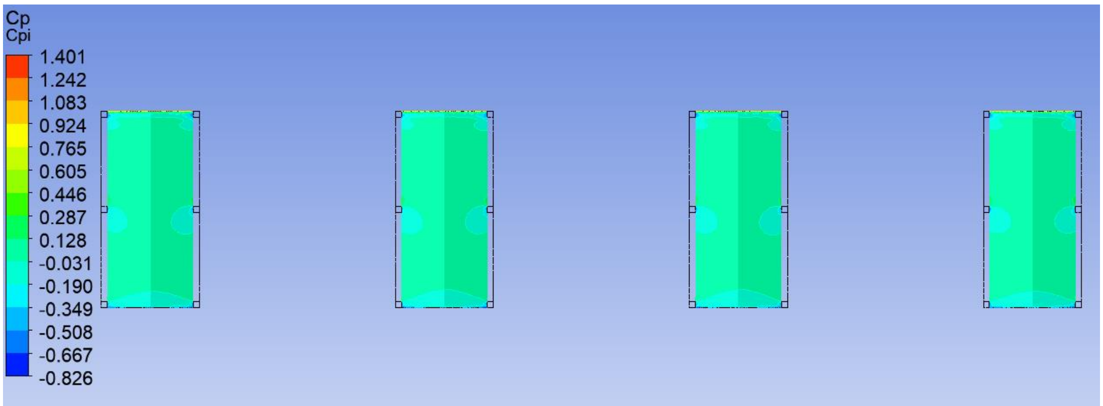

Fig 88 – Internal Pressure Coefficient at Wind Direction 90^0

4.1.6 Pitch Angle 20° and Spacing 0B

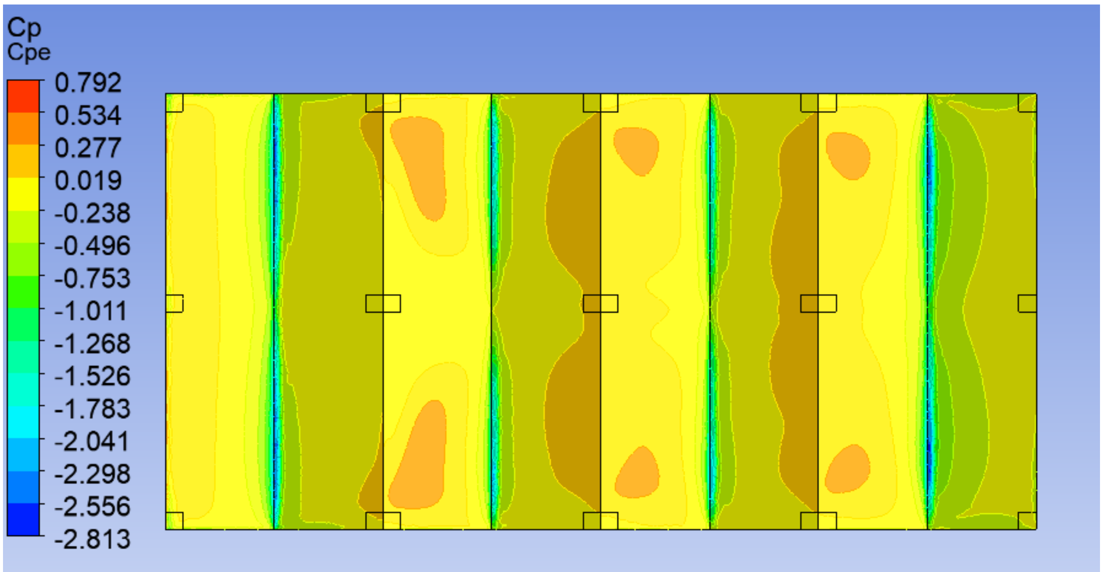

Fig 89 - External Pressure Coefficient at Wind Direction 0^0

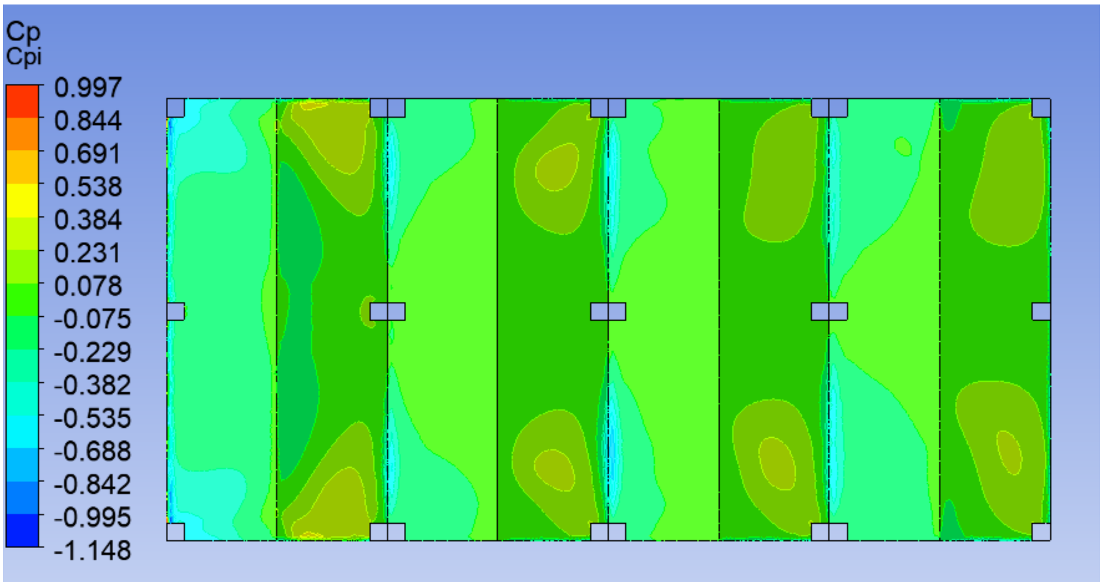

Fig 90 – Internal Pressure Coefficient at Wind Direction 0^0

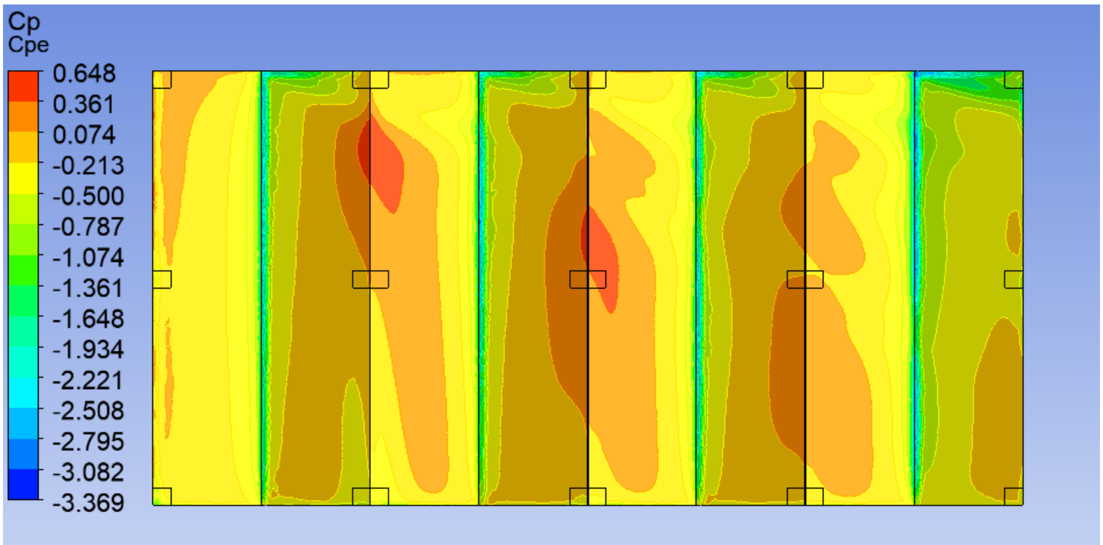

Fig 91 - External Pressure Coefficient at Wind Direction 30^0

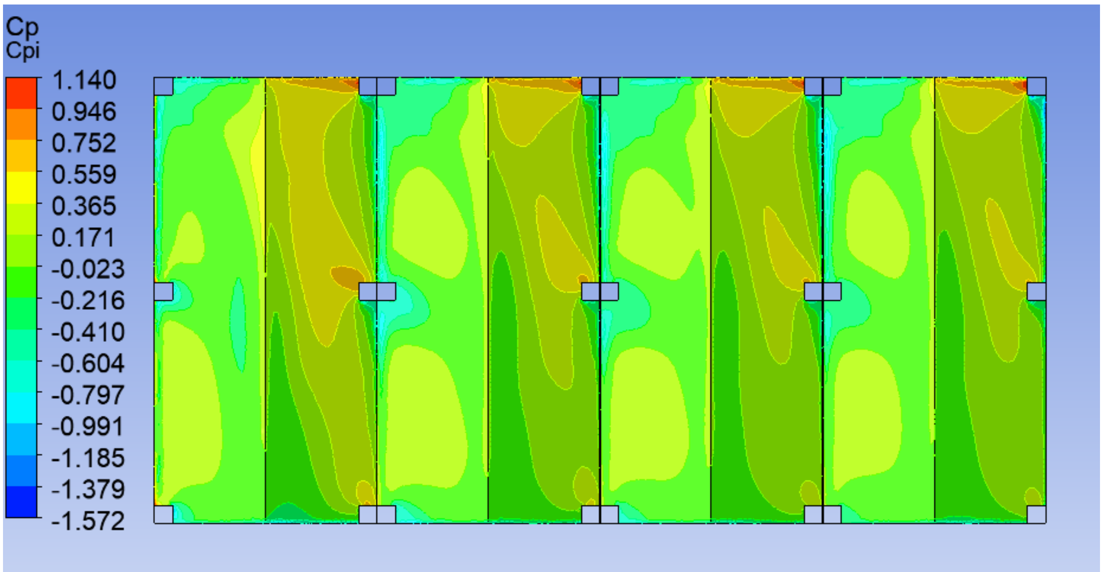

Fig 92 – Internal Pressure Coefficient at Wind Direction 30^0

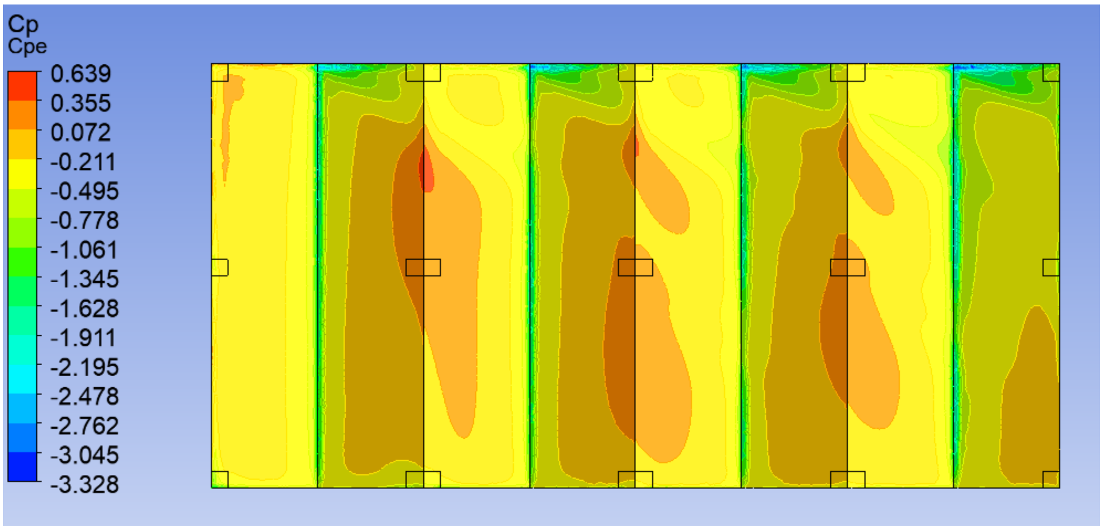

Fig 93 - External Pressure Coefficient at Wind Direction 45^0

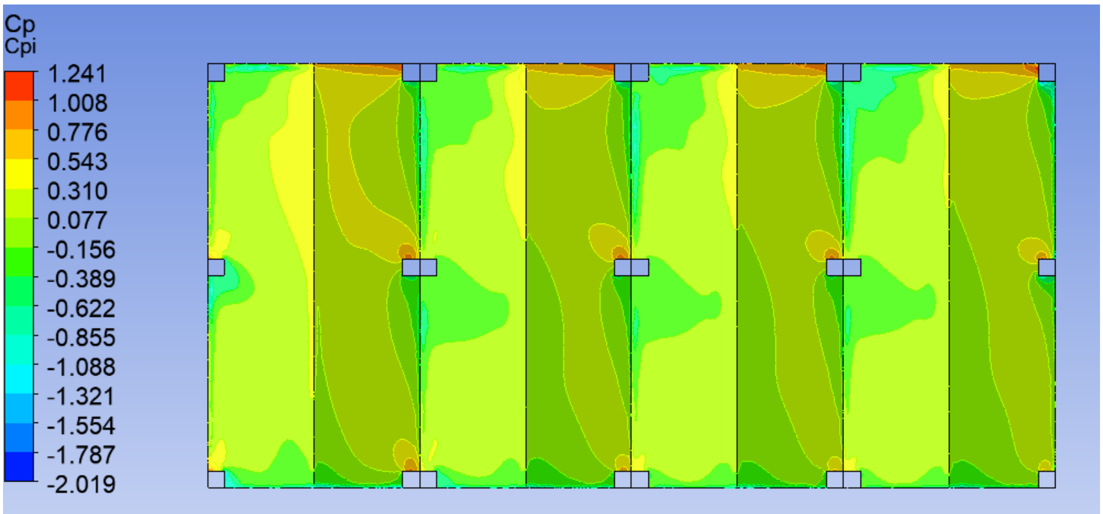

Fig 94 – Internal Pressure Coefficient at Wind Direction 45^0

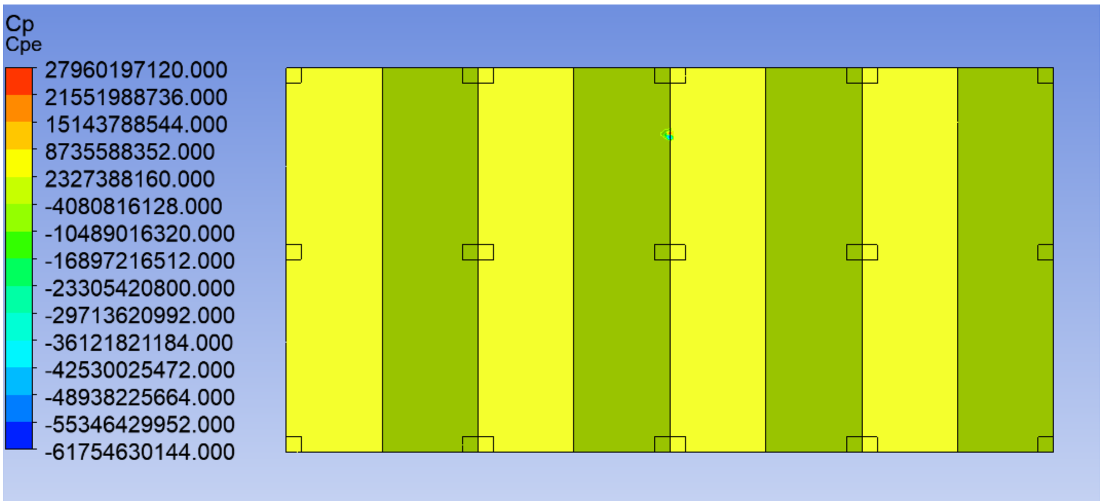

Fig 95 - External Pressure Coefficient at Wind Direction 60^0

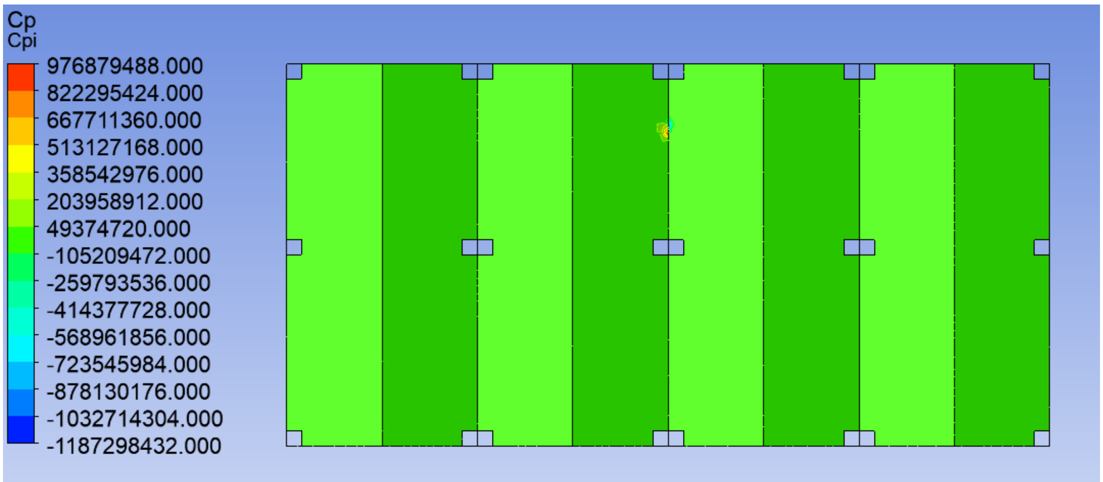

Fig 96 – Internal Pressure Coefficient at Wind Direction 60^0

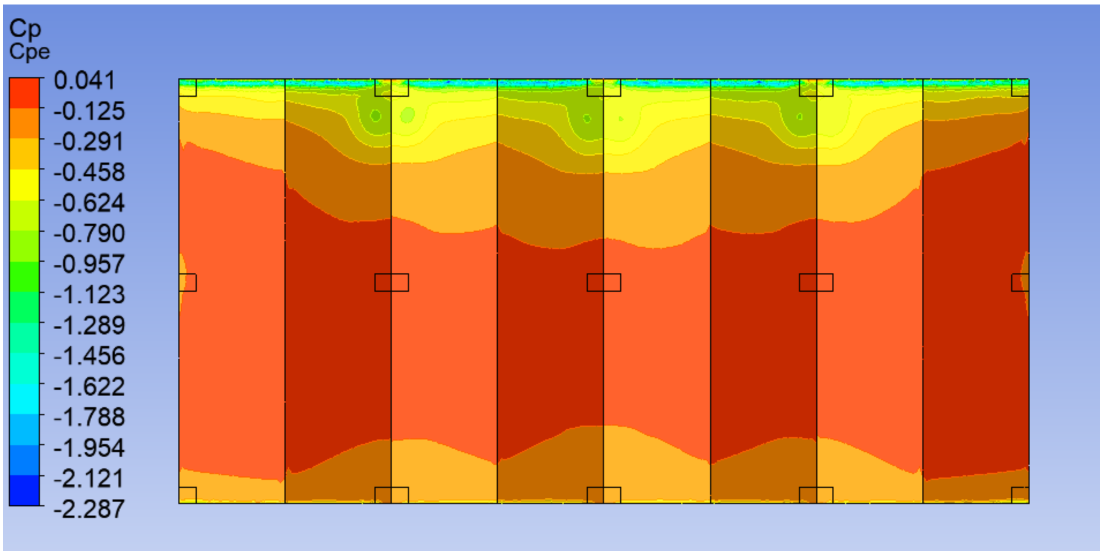

Fig 97 - External Pressure Coefficient at Wind Direction 90^0

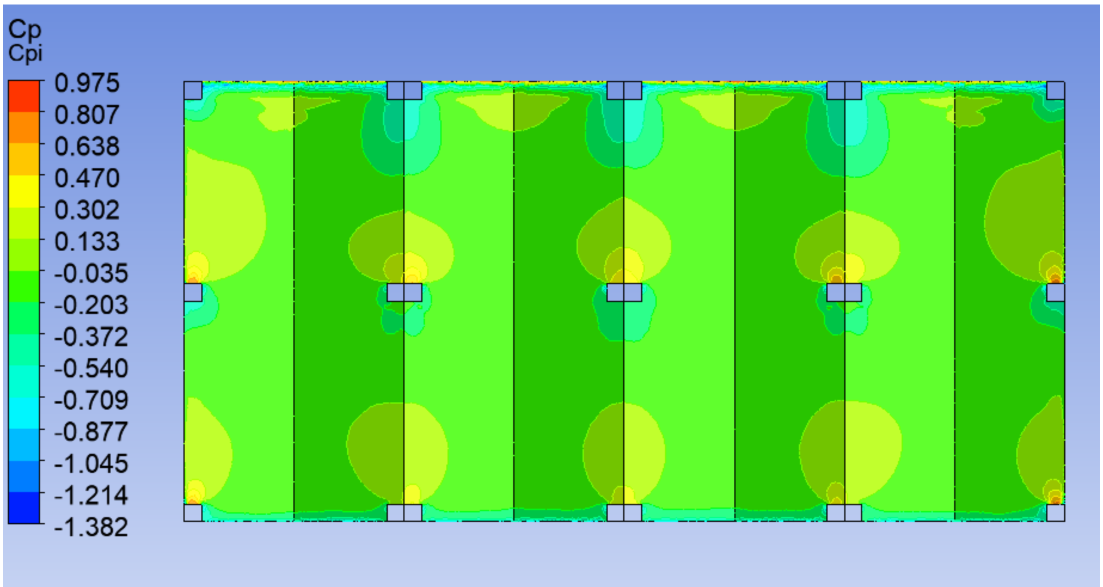

Fig 98 – Internal Pressure Coefficient at Wind Direction 90^0

4.1.7 Pitch Angle 20° and Spacing B/2

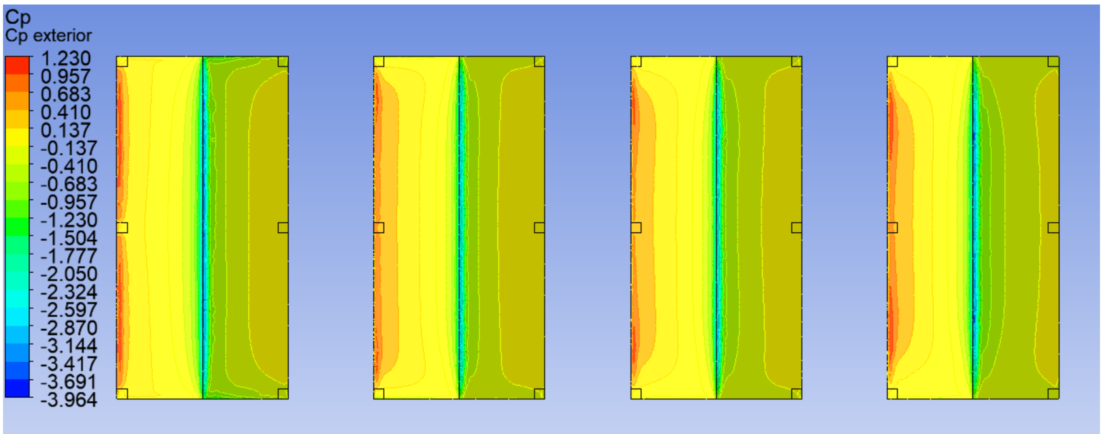

Fig 99 - External Pressure Coefficient at Wind Direction 0^0

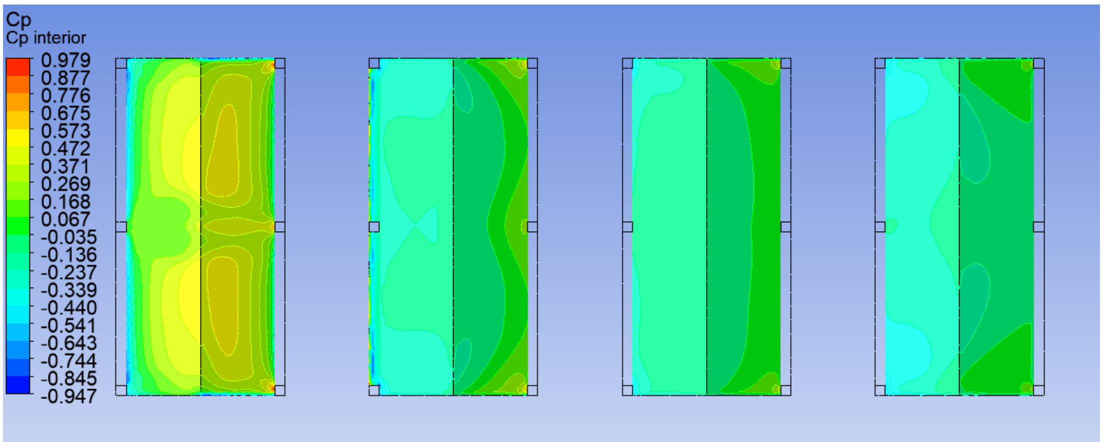

Fig 100 – Internal Pressure Coefficient at Wind Direction 0^0

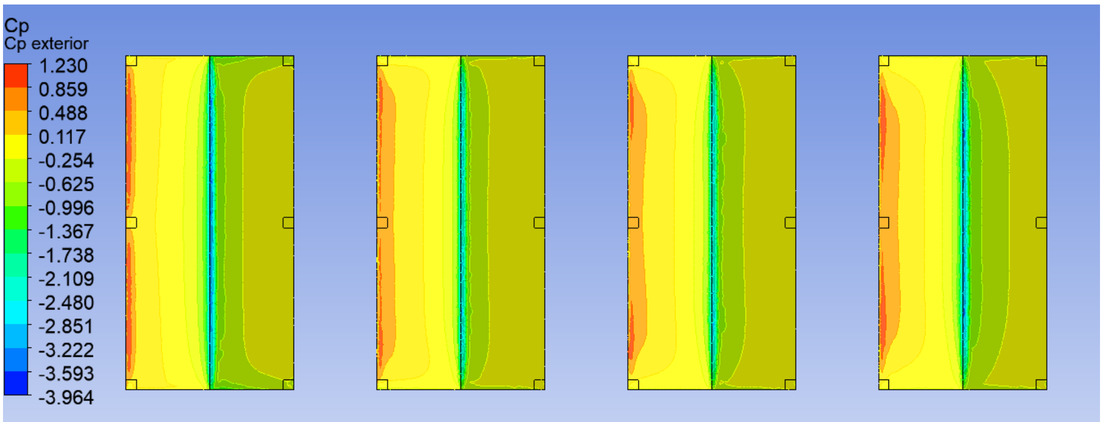

Fig 101 - External Pressure Coefficient at Wind Direction 30^0

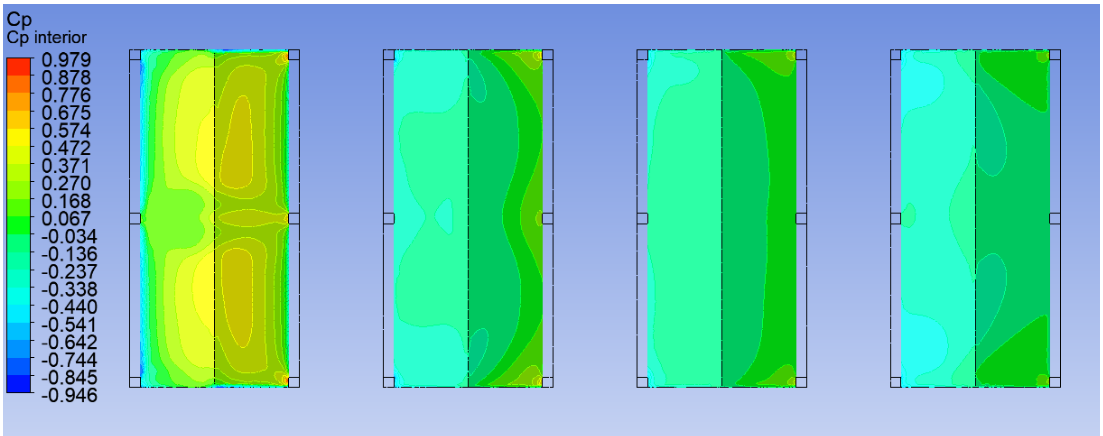

Fig 102 – Internal Pressure Coefficient at Wind Direction 30^0

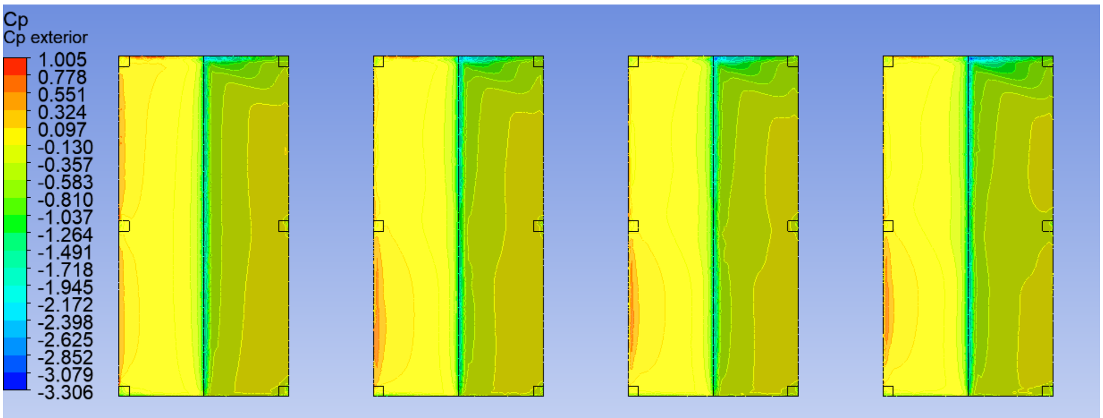

Fig 103 - External Pressure Coefficient at Wind Direction 45^0

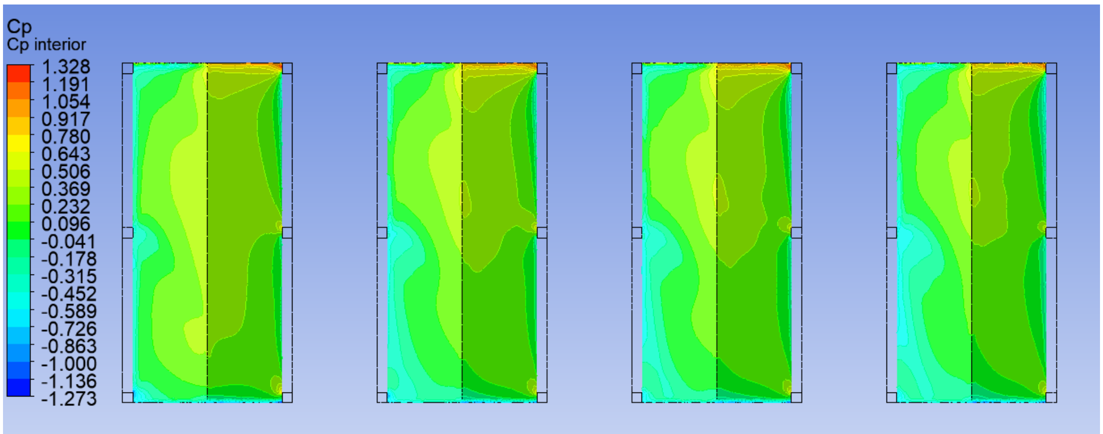

Fig 104 – Internal Pressure Coefficient at Wind Direction 45^0

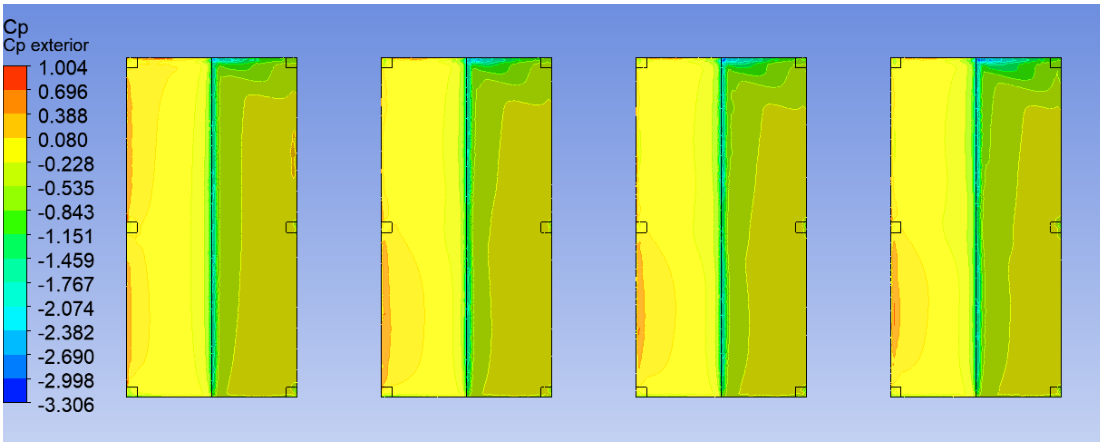

Fig 105 - External Pressure Coefficient at Wind Direction 60^0

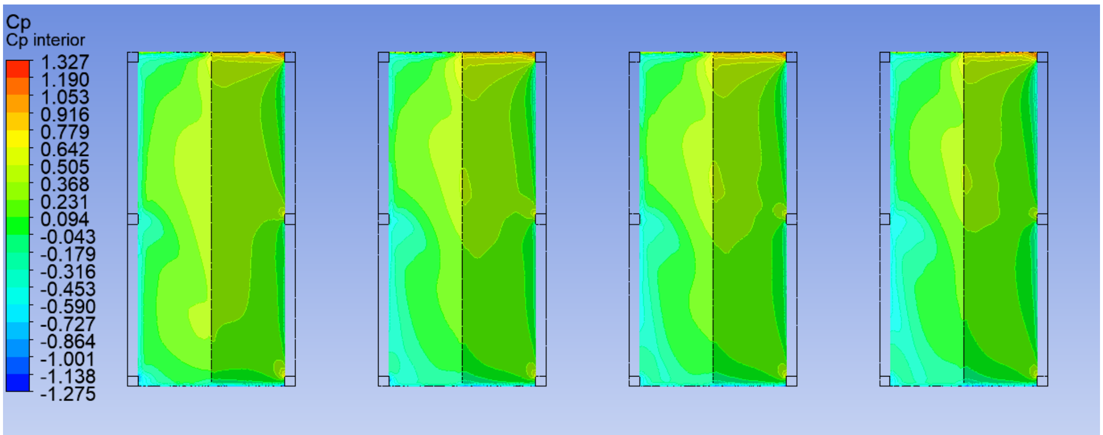

Fig 106 – Internal Pressure Coefficient at Wind Direction 60^0

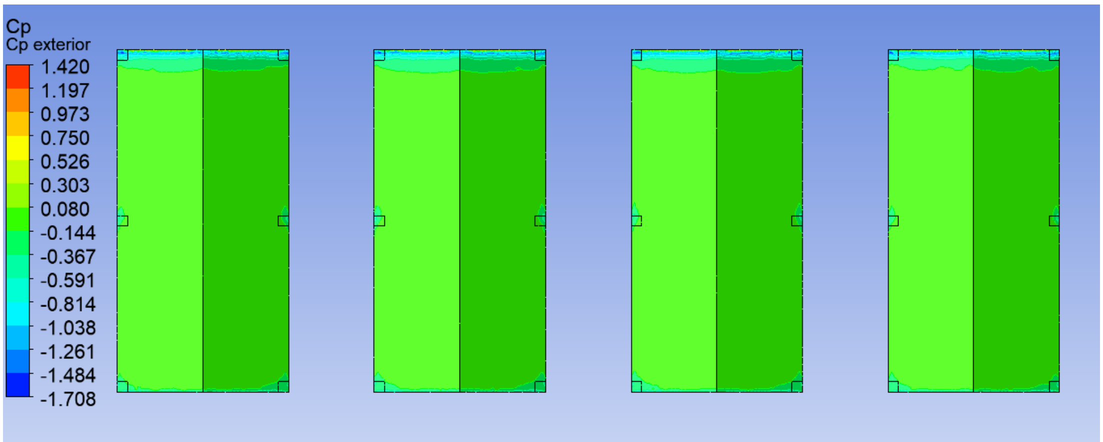

Fig 107 - External Pressure Coefficient at Wind Direction 90^0

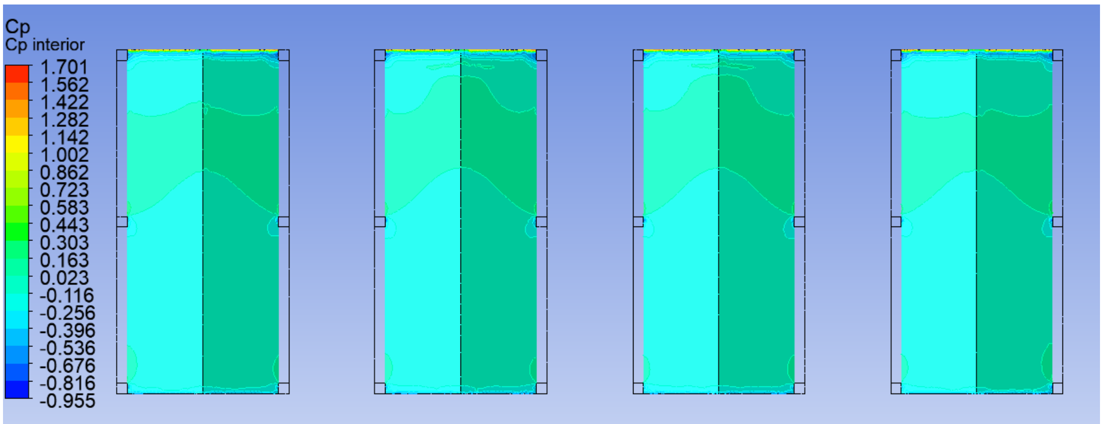

Fig 108 – Internal Pressure Coefficient at Wind Direction 90^0

4.1.8 Pitch Angle 20° and Spacing B

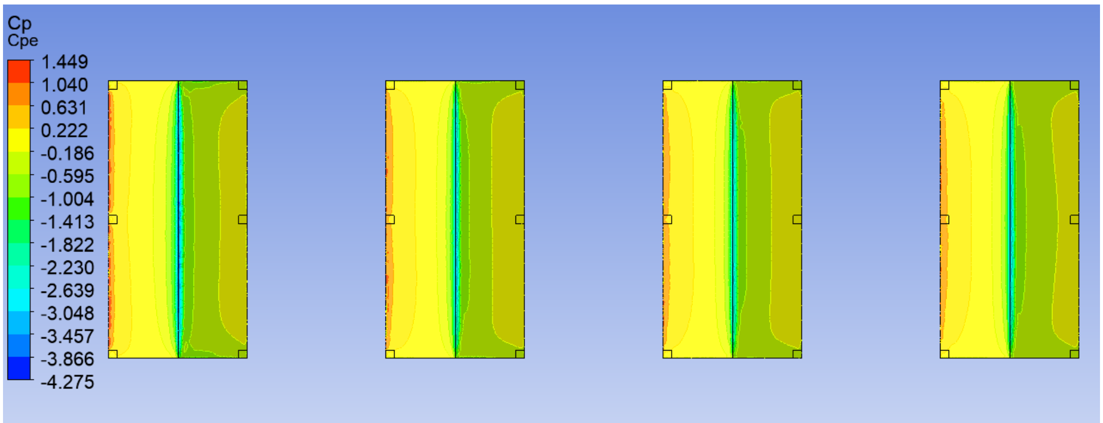

Fig 109 - External Pressure Coefficient at Wind Direction 0^0

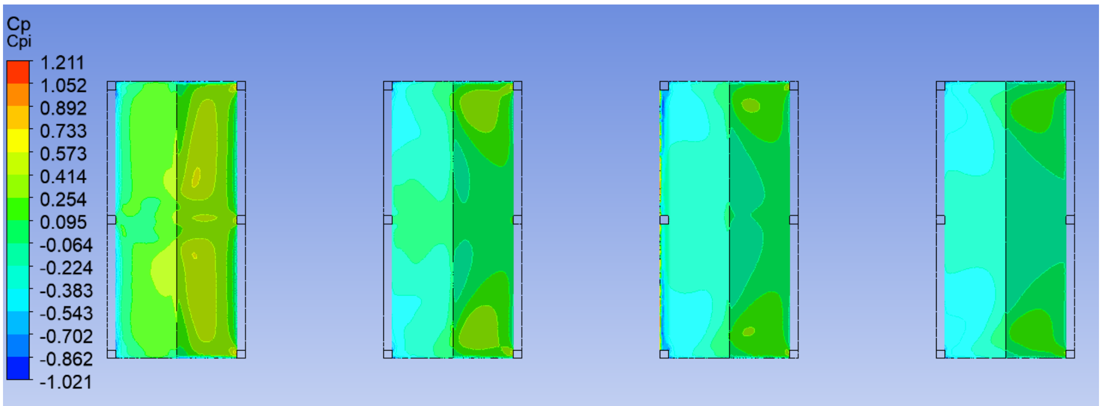

Fig 110 – Internal Pressure Coefficient at Wind Direction 0^0

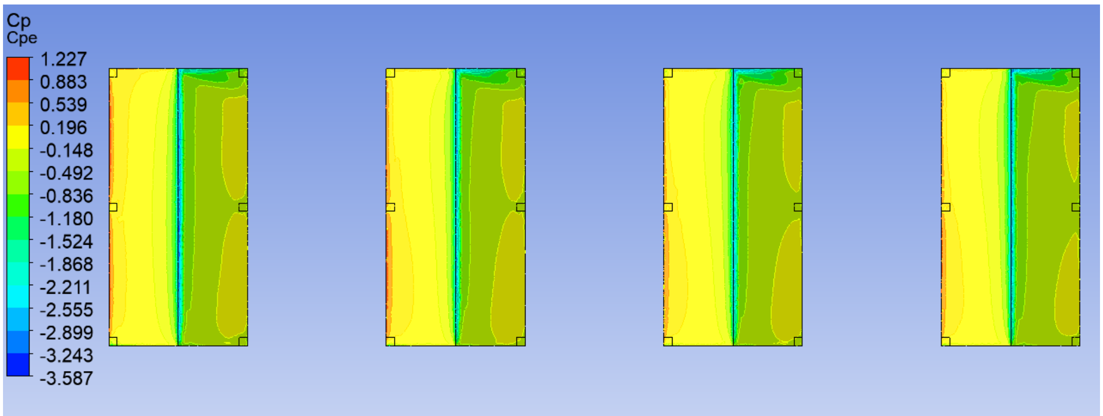

Fig 111 - External Pressure Coefficient at Wind Direction 30^0

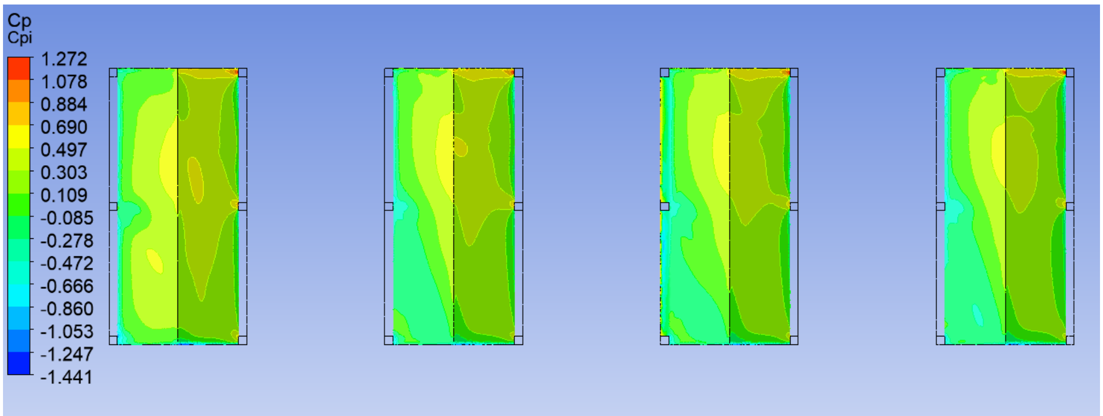

Fig 112 – Internal Pressure Coefficient at Wind Direction 30^0

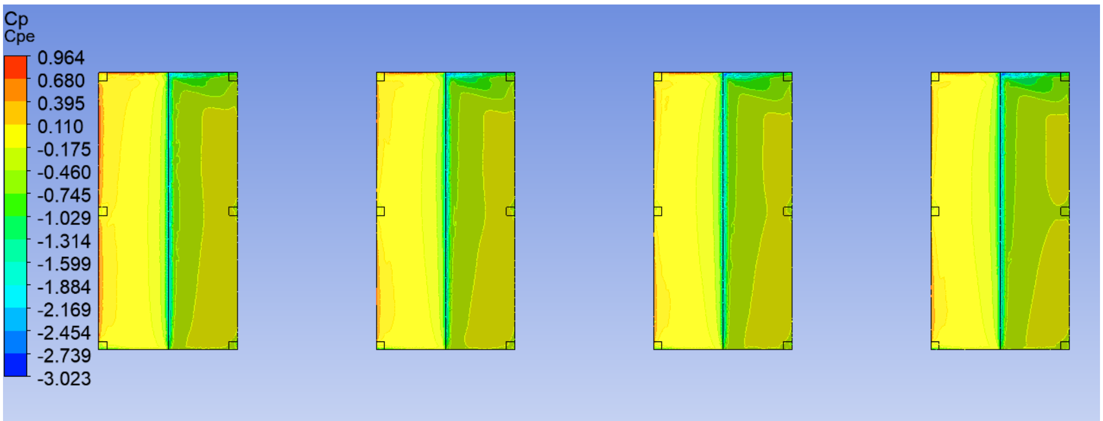

Fig 113- External Pressure Coefficient at Wind Direction 45^0

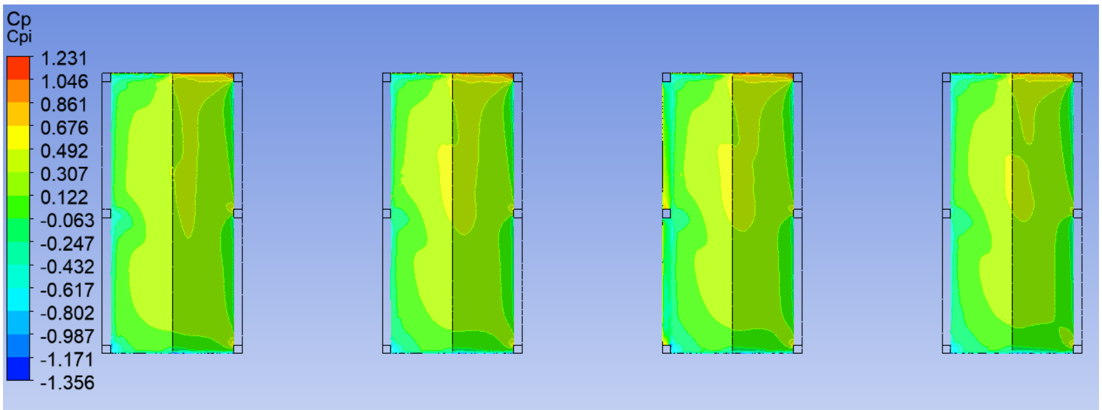

Fig 114 – Internal Pressure Coefficient at Wind Direction 45^0

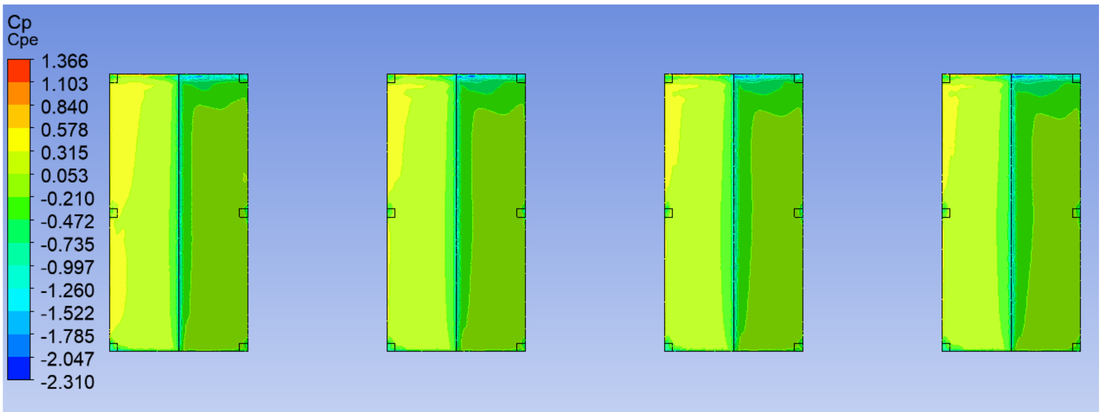

Fig 115 - External Pressure Coefficient at Wind Direction 60^0

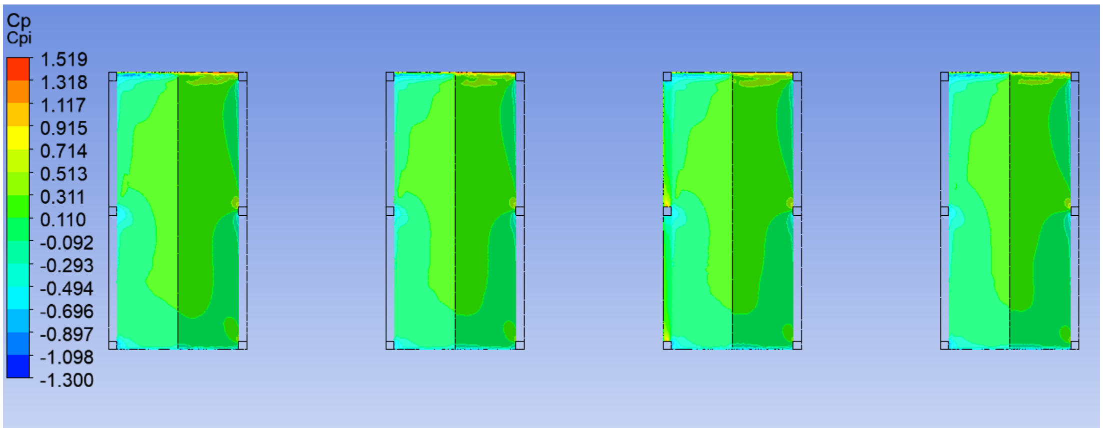

Fig 116 – Internal Pressure Coefficient at Wind Direction 60^0

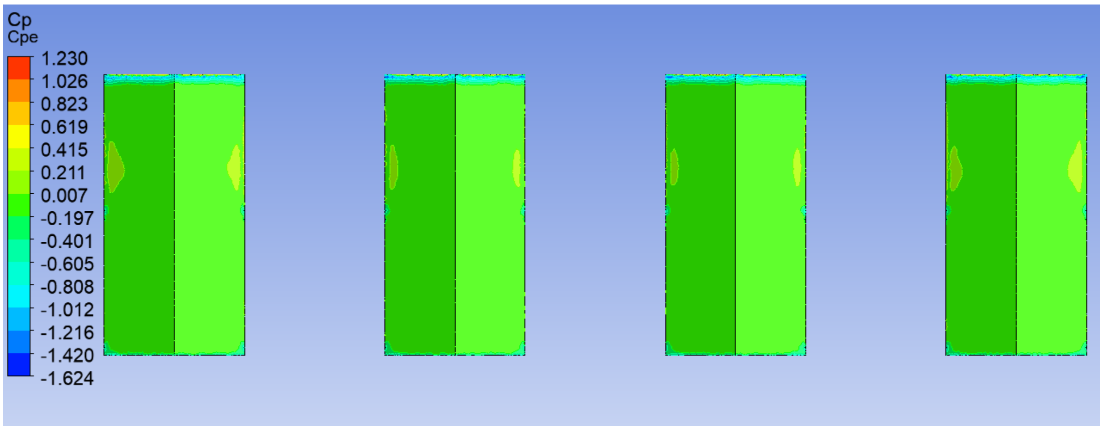

Fig 117 - External Pressure Coefficient at Wind Direction 90^0

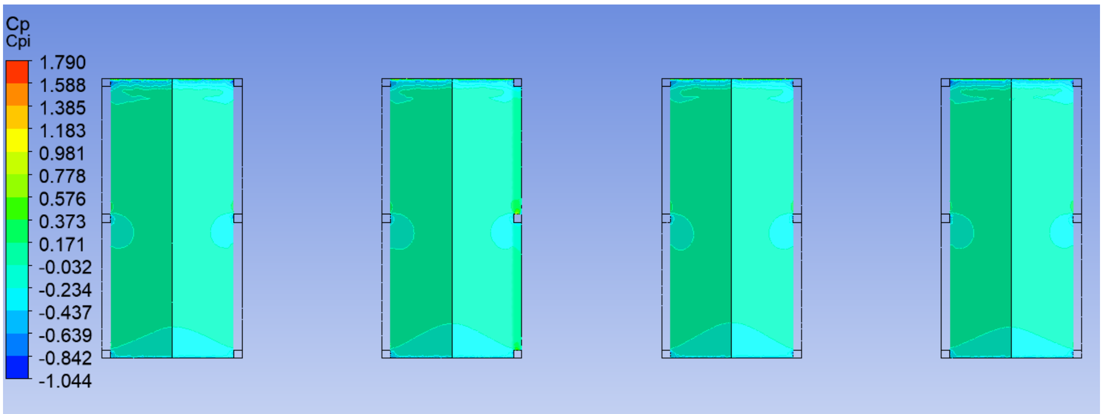

Fig 118 – Internal Pressure Coefficient at Wind Direction 90^0

4.1.9 Pitch Angle 20° and Spacing 3B/2

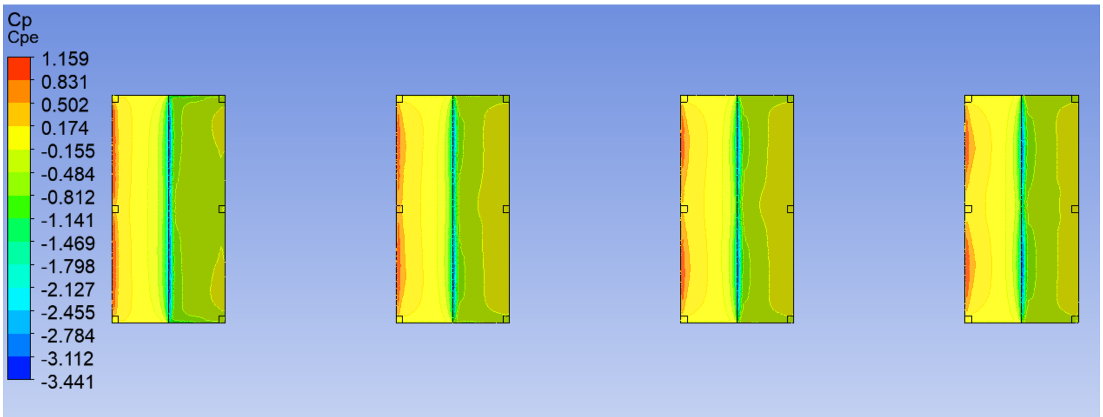

Fig 119 - External Pressure Coefficient at Wind Direction 0^0

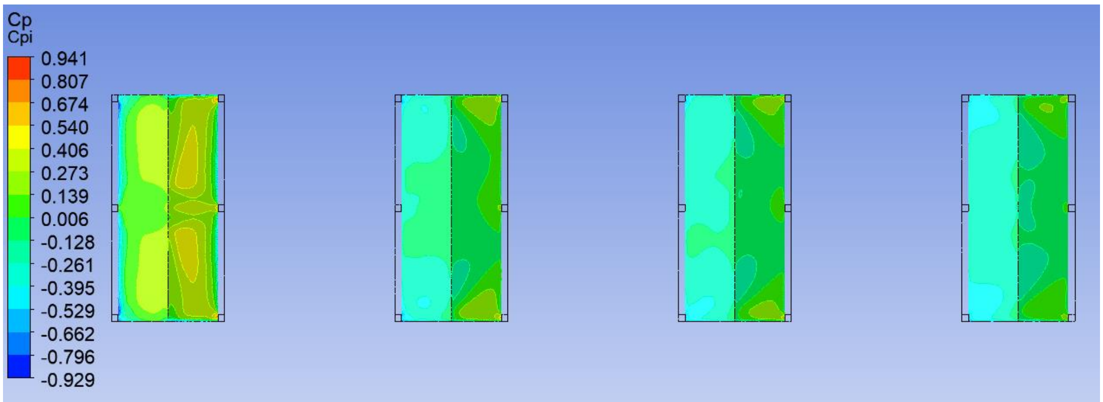

Fig 120 – Internal Pressure Coefficient at Wind Direction 0^0

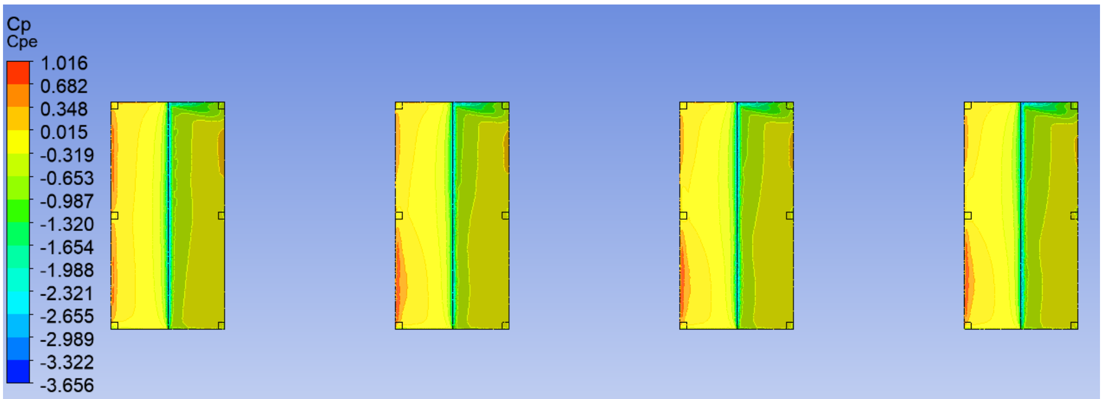

Fig 121 - External Pressure Coefficient at Wind Direction 30^0

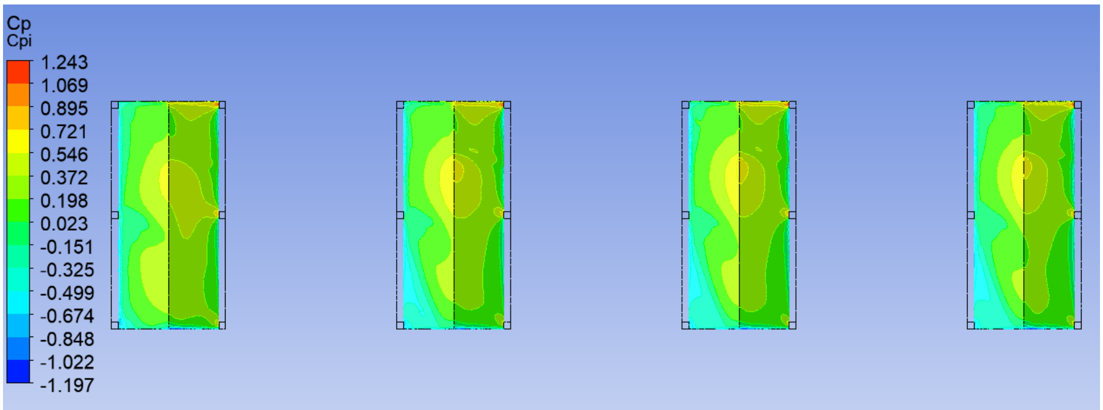

Fig 122 – Internal Pressure Coefficient at Wind Direction 30^0

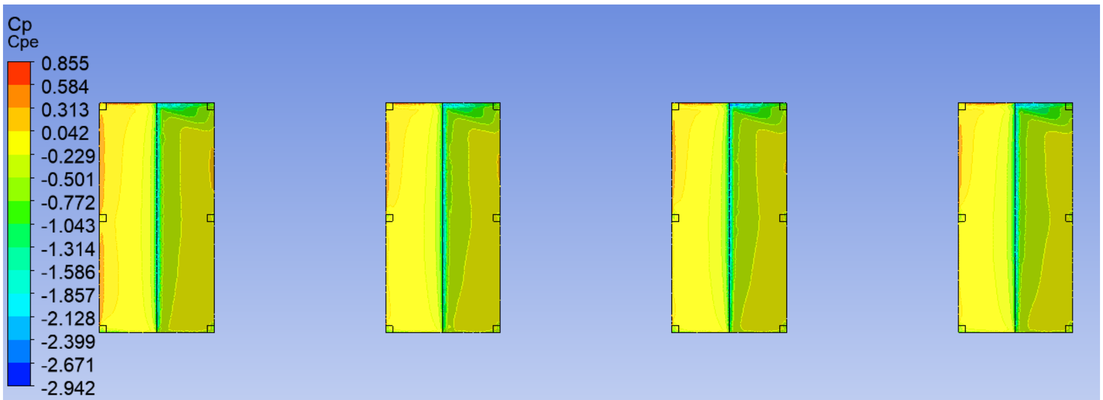

Fig 123 - External Pressure Coefficient at Wind Direction 45^0

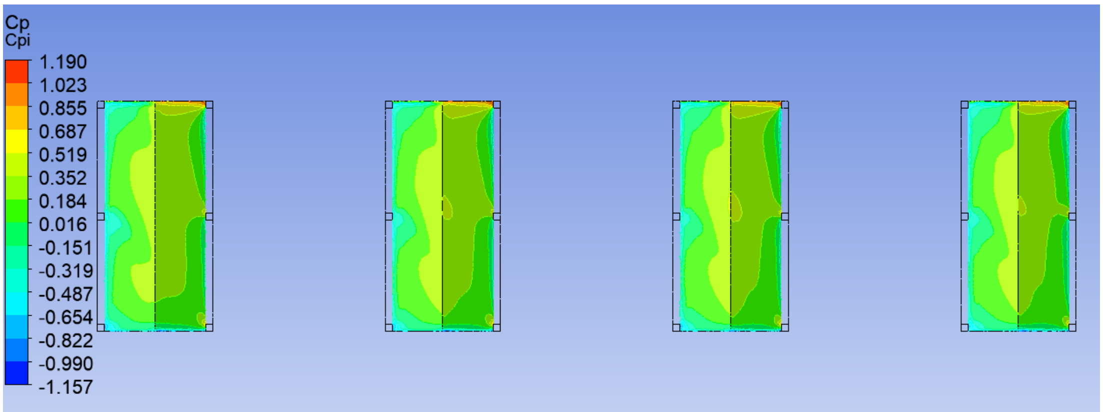

Fig 124 – Internal Pressure Coefficient at Wind Direction 45^0

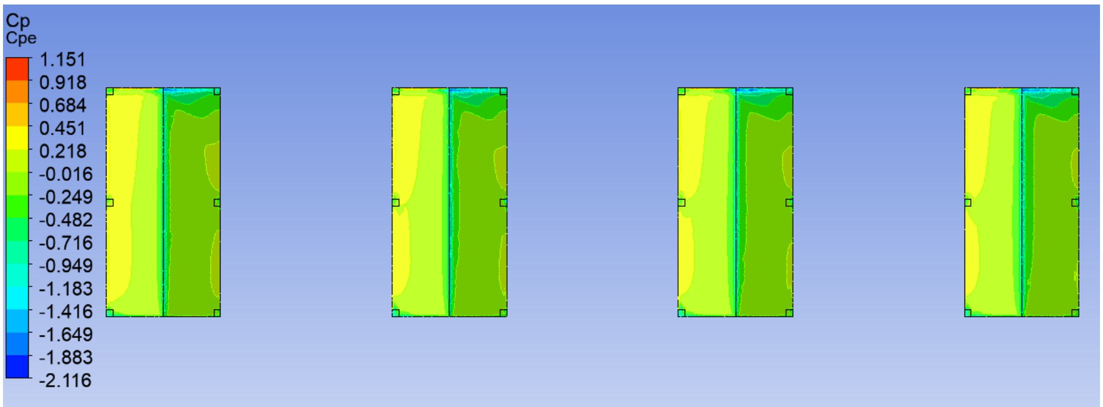

Fig 125 - External Pressure Coefficient at Wind Direction 60^0

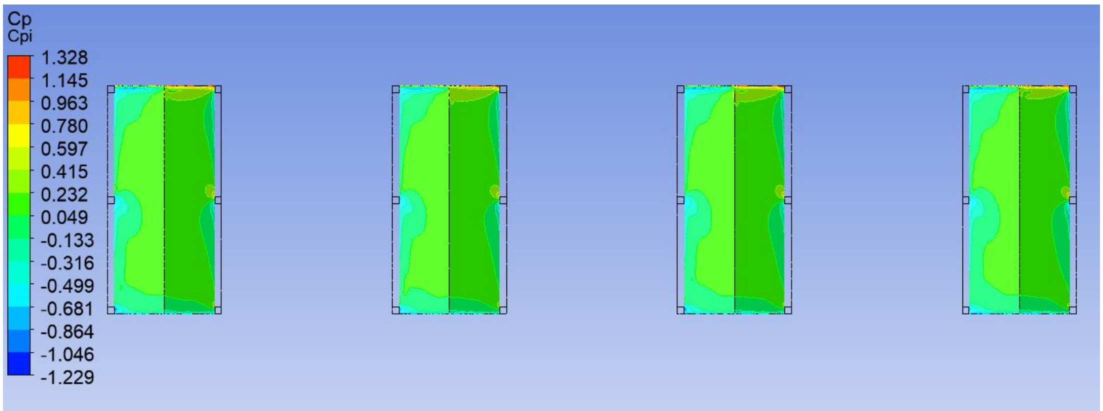

Fig 126 – Internal Pressure Coefficient at Wind Direction 60^0

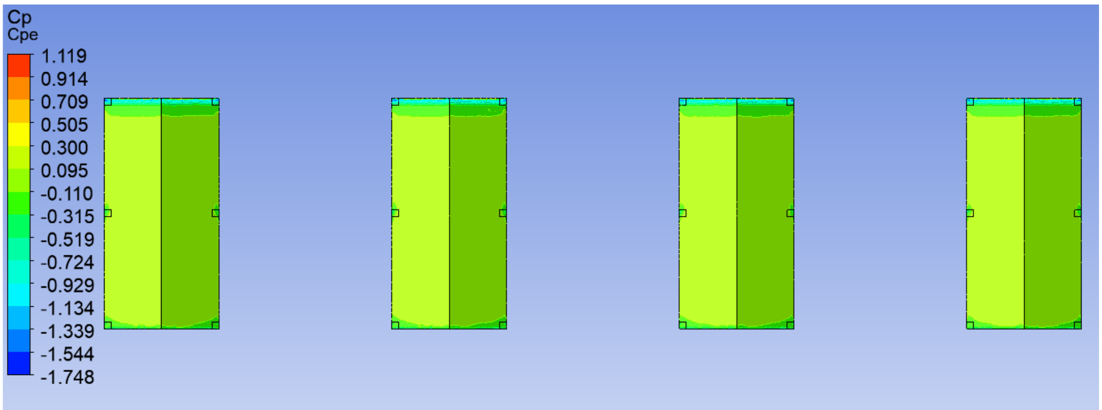

Fig 127 - External Pressure Coefficient at Wind Direction 90^0

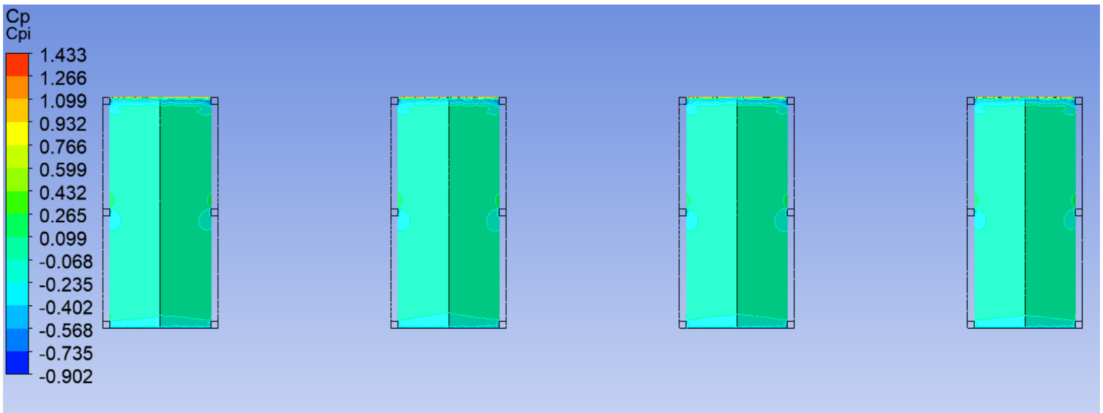

Fig 128 – Internal Pressure Coefficient at Wind Direction 90^0

4.1.10 Pitch Angle 20° and Spacing 2B

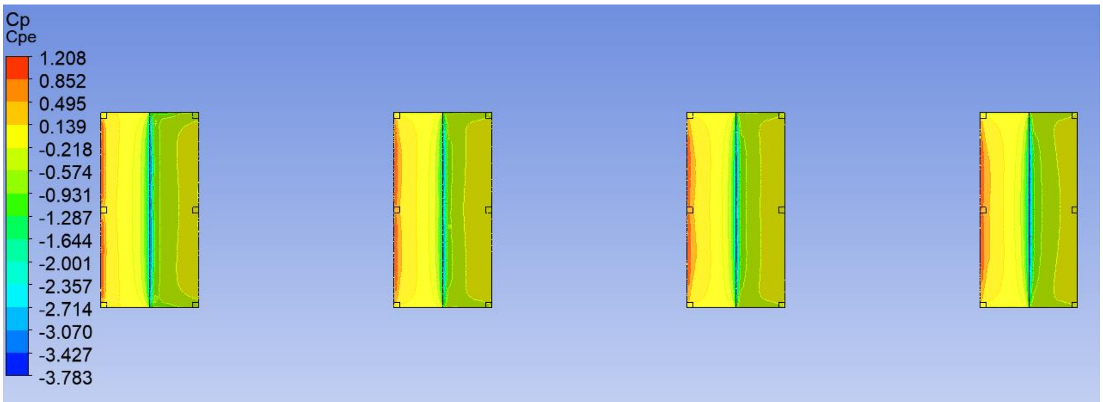

Fig 129 - External Pressure Coefficient at Wind Direction 0^0

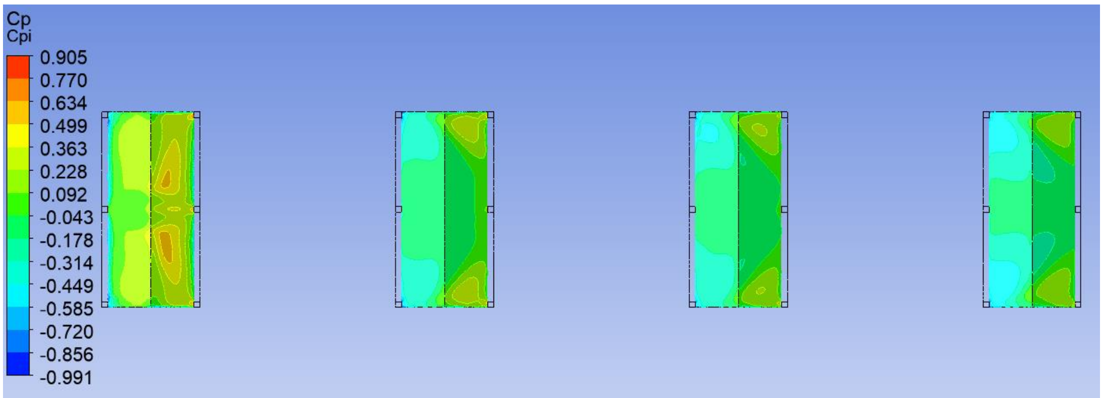

Fig 130 – Internal Pressure Coefficient at Wind Direction 0^0

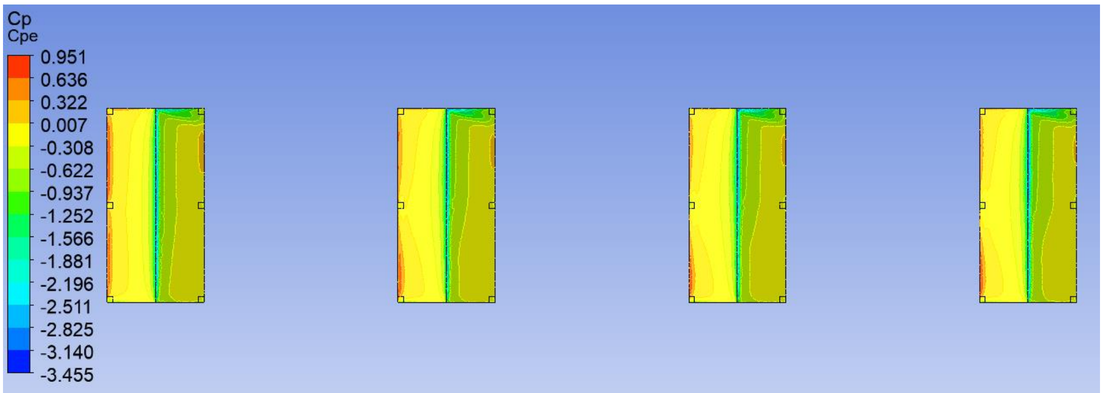

Fig 131 - External Pressure Coefficient at Wind Direction 30^0

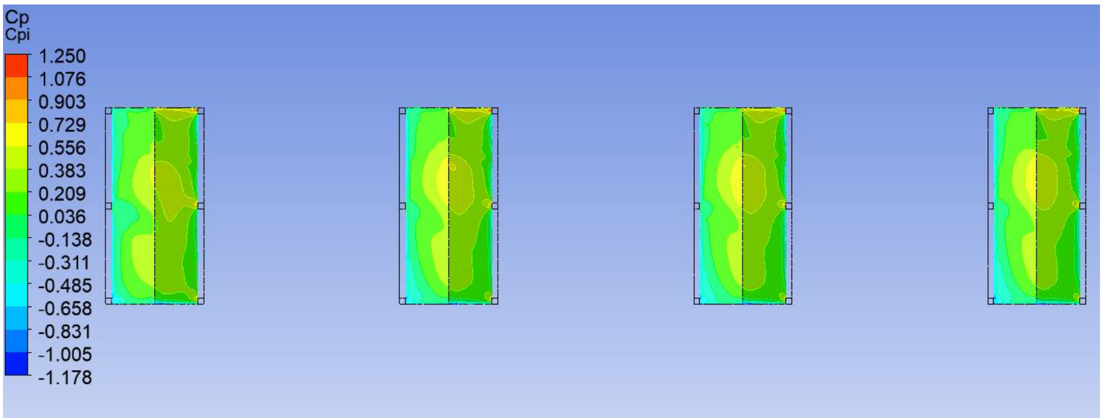

Fig 132 – Internal Pressure Coefficient at Wind Direction 30^0

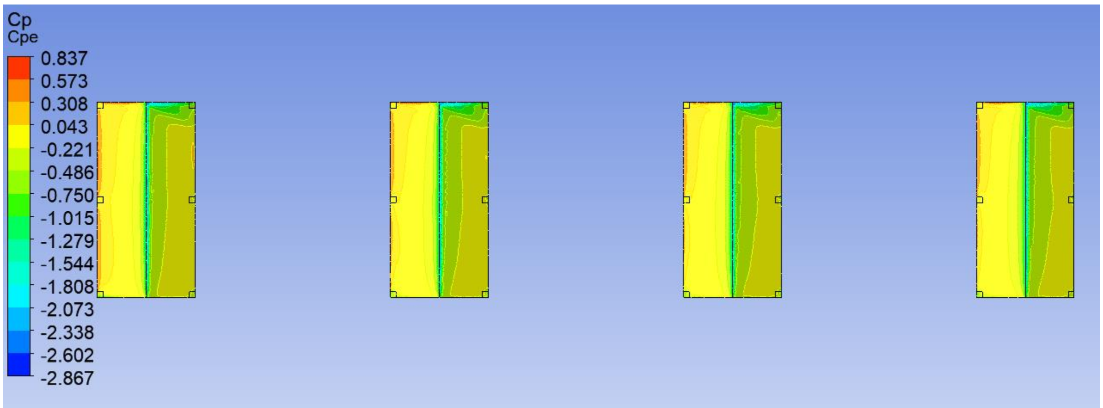

Fig 133 - External Pressure Coefficient at Wind Direction 45^0

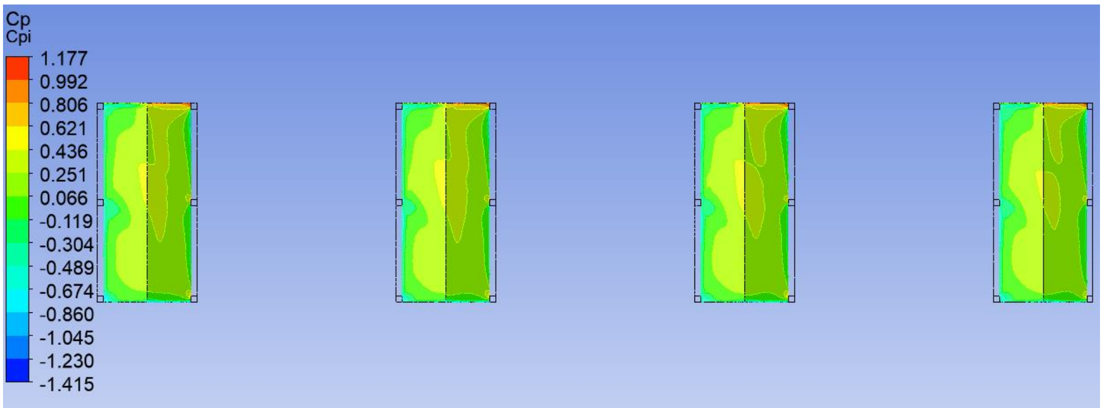

Fig 134– Internal Pressure Coefficient at Wind Direction 45^0

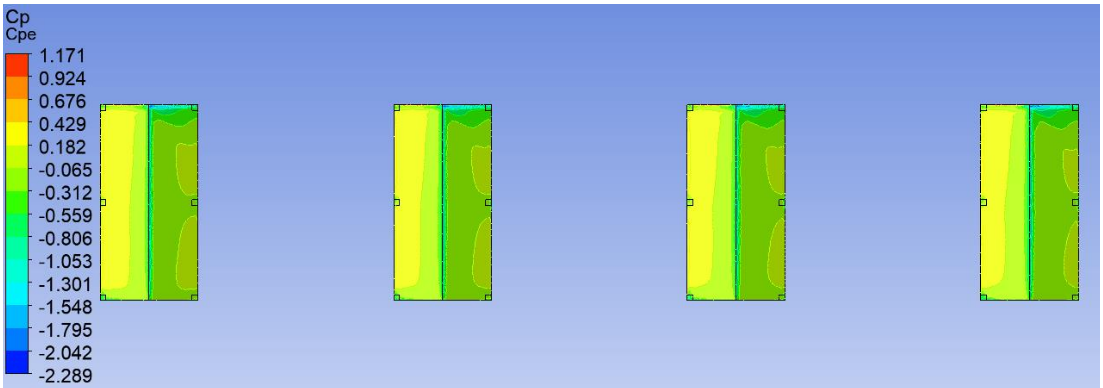

Fig 135 - External Pressure Coefficient at Wind Direction 60^0

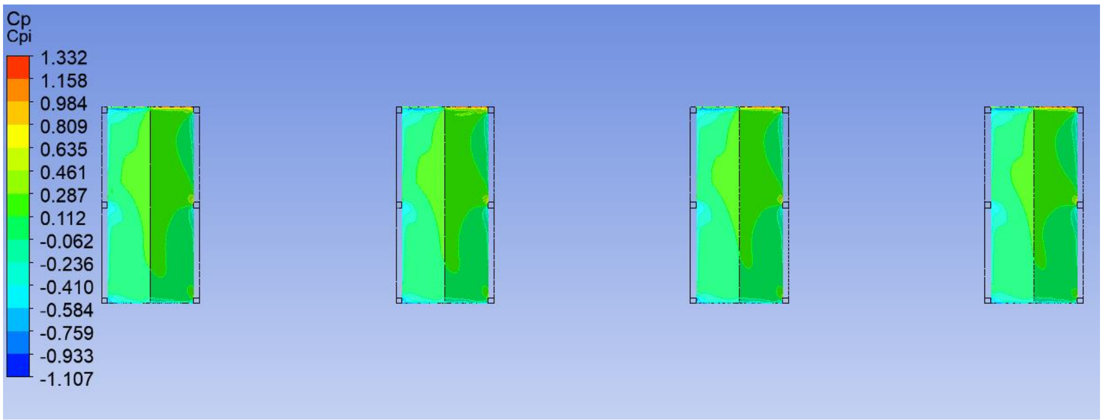

Fig 136 – Internal Pressure Coefficient at Wind Direction 60^0

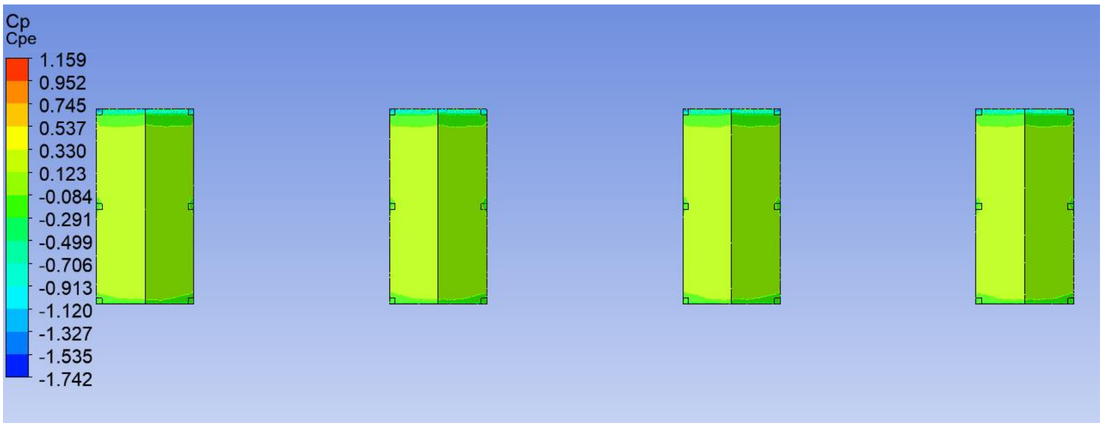

Fig 137 - External Pressure Coefficient at Wind Direction 90^0

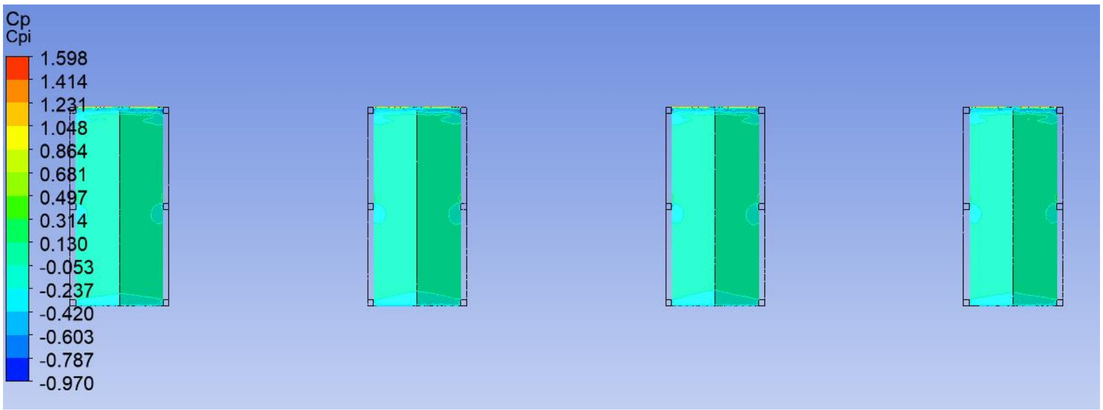

Fig 138 – Internal Pressure Coefficient at Wind Direction 90^0

4.1.11 Pitch Angle 30° and Spacing 0B

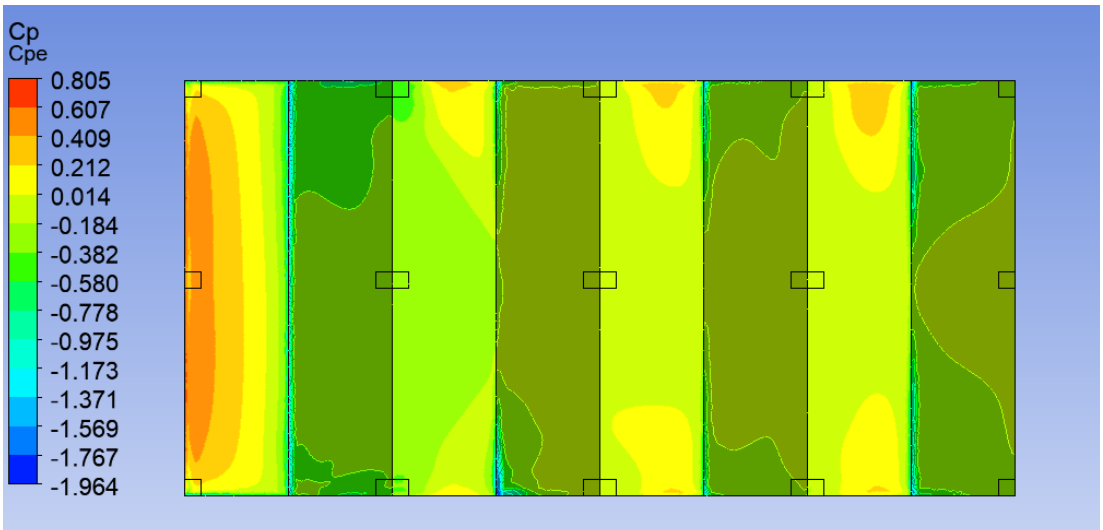

Fig 139 - External Pressure Coefficient at Wind Direction 0^0

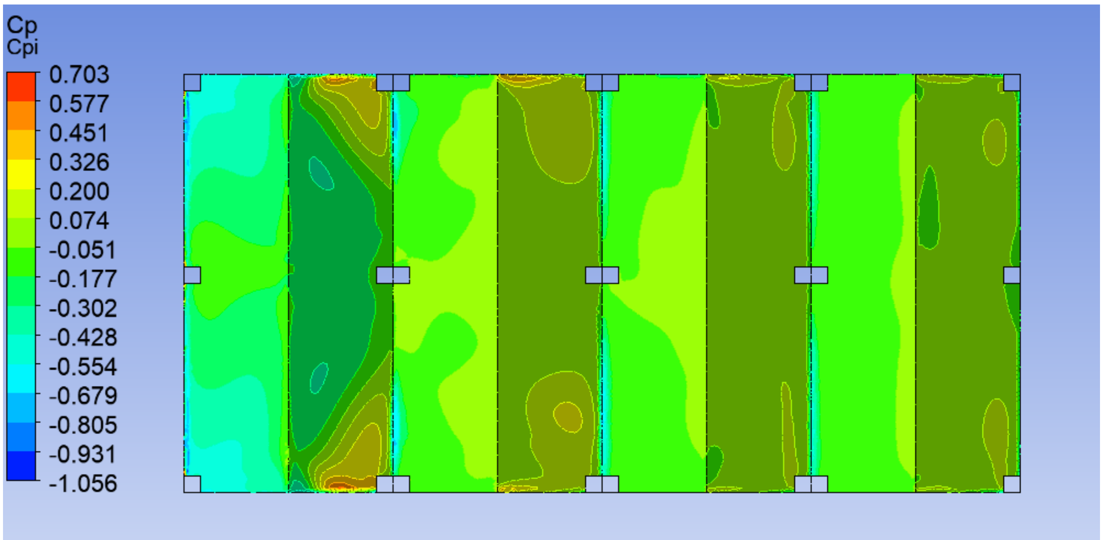

Fig 140 – Internal Pressure Coefficient at Wind Direction 0^0

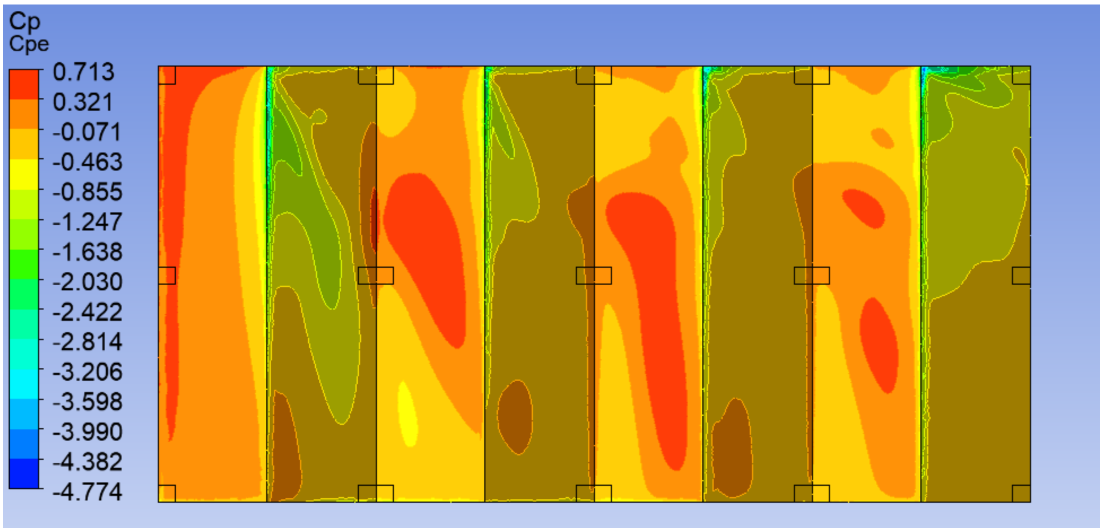

Fig 141 - External Pressure Coefficient at Wind Direction 30^0

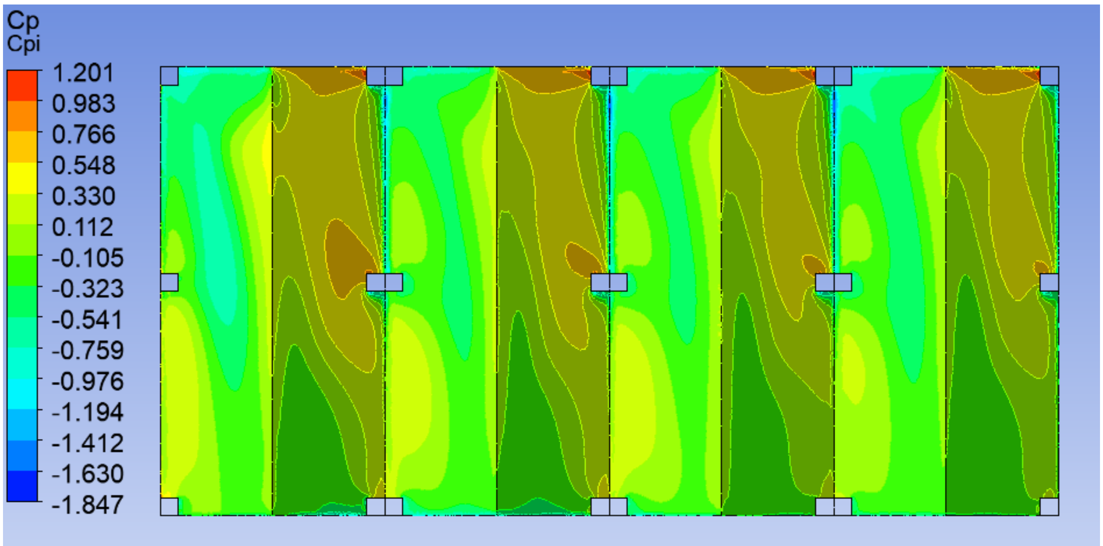

Fig 142 – Internal Pressure Coefficient at Wind Direction 30^0

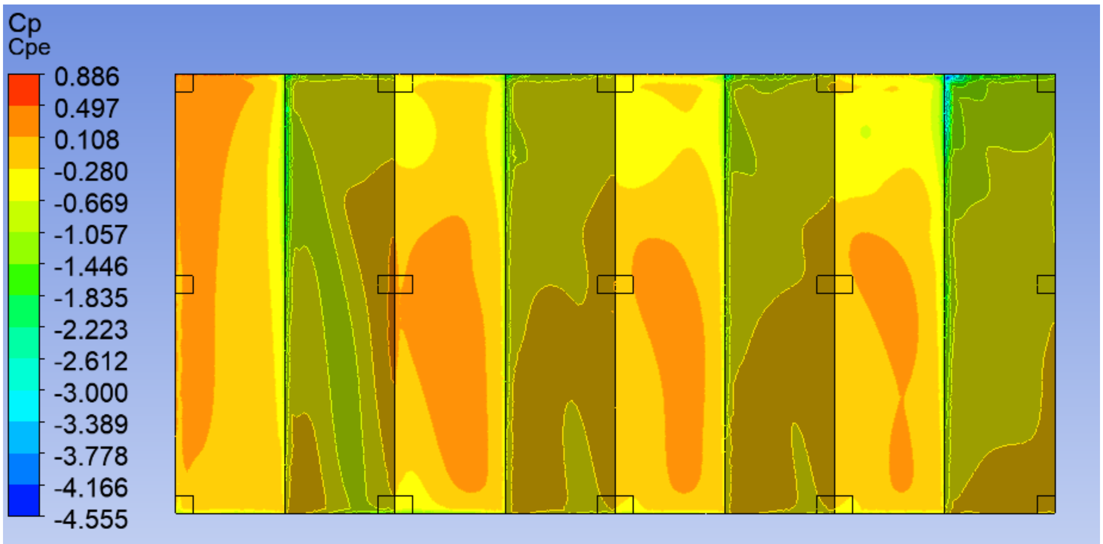

Fig 143 - External Pressure Coefficient at Wind Direction 45^0

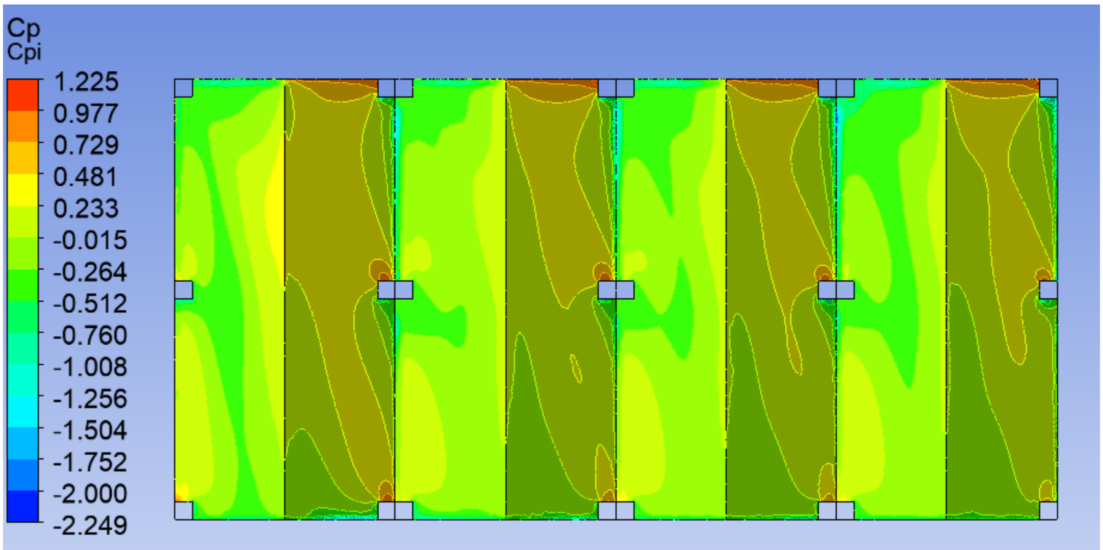

Fig 144 – Internal Pressure Coefficient at Wind Direction 45^0

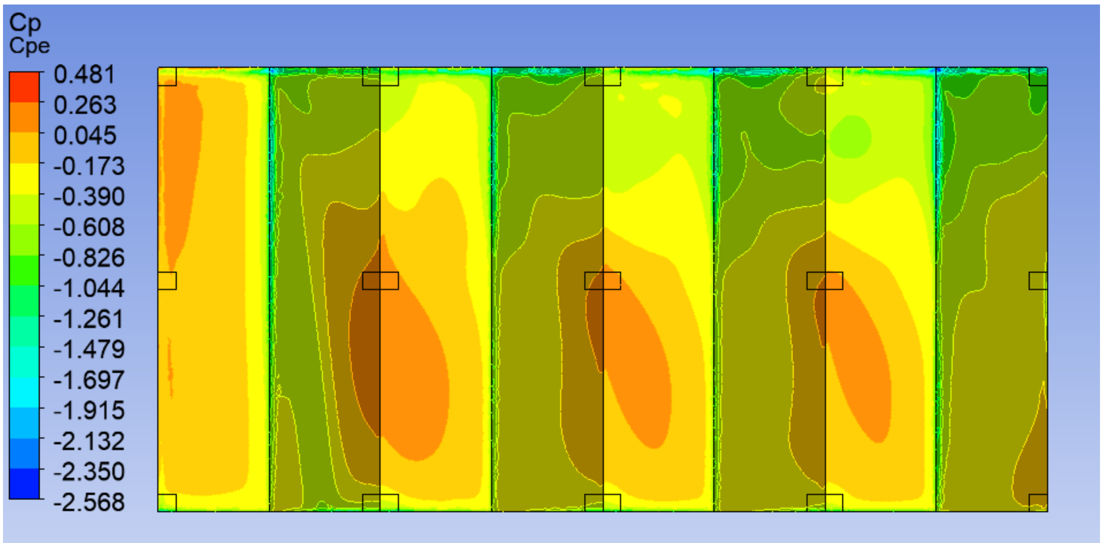

Fig 145- External Pressure Coefficient at Wind Direction 60^0

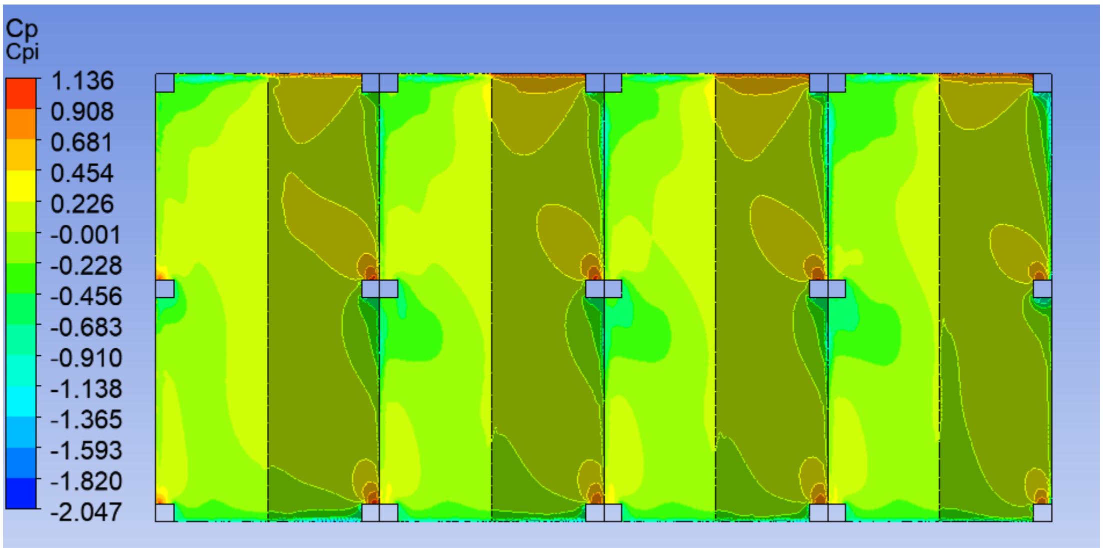

Fig 146 – Internal Pressure Coefficient at Wind Direction 60^0

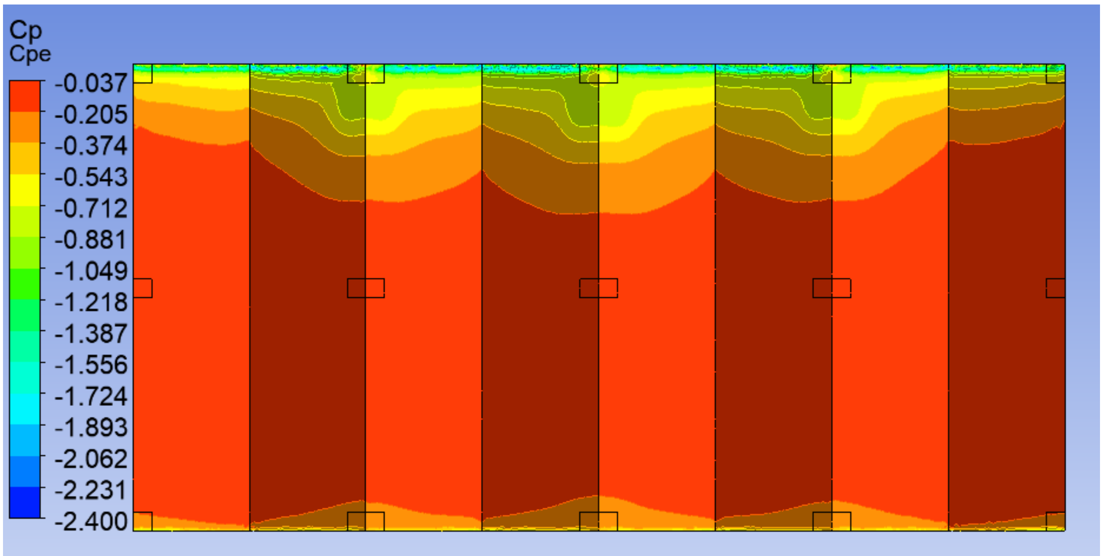

Fig 147 - External Pressure Coefficient at Wind Direction 90^0

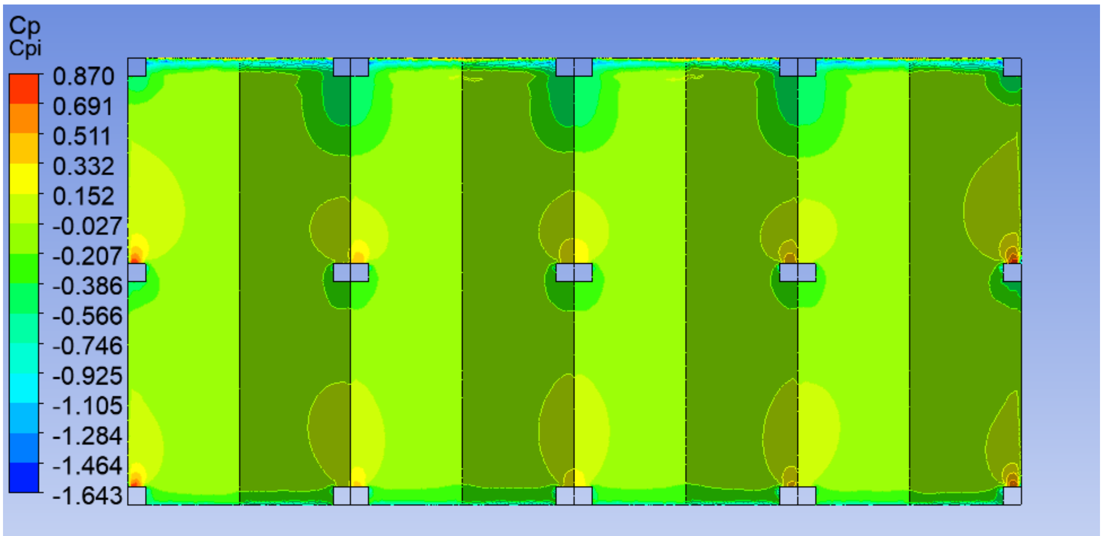

Fig 148 – Internal Pressure Coefficient at Wind Direction 90^0

4.1.12 Pitch Angle 30° and Spacing B/2

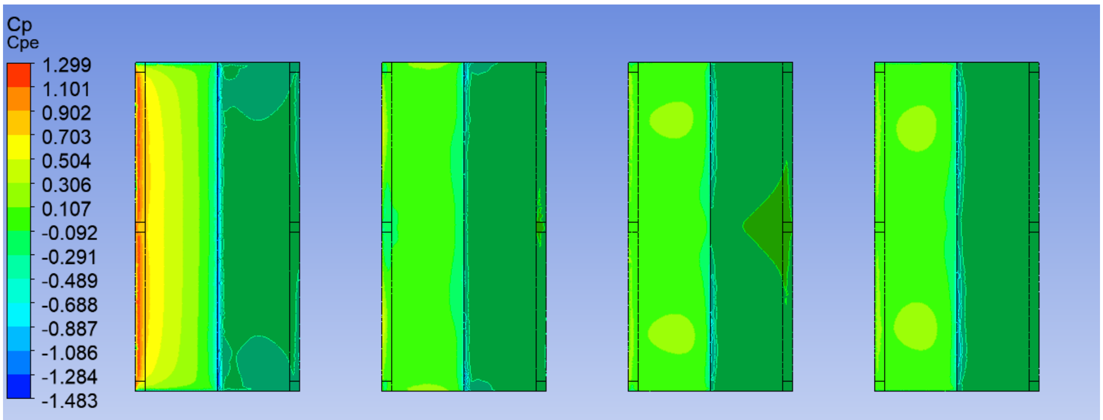

Fig 149 - External Pressure Coefficient at Wind Direction 0^0

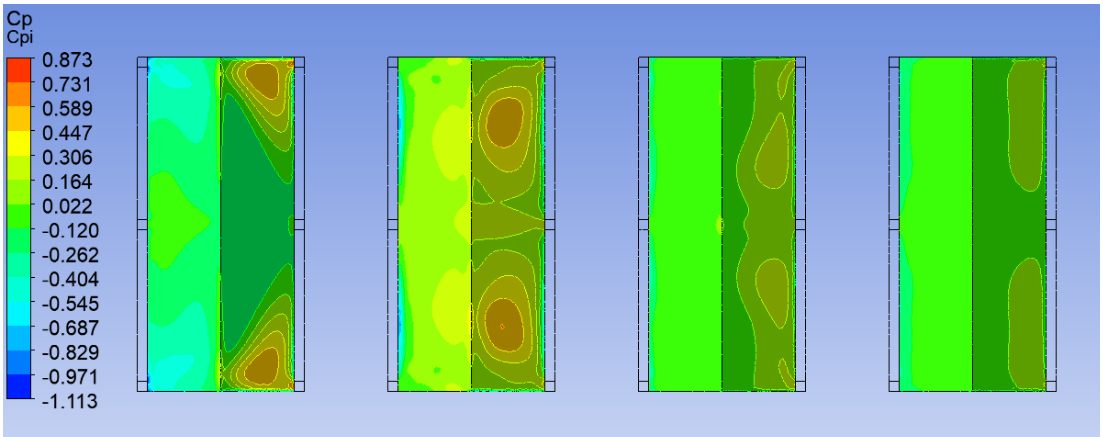

Fig 150 – Internal Pressure Coefficient at Wind Direction 0^0

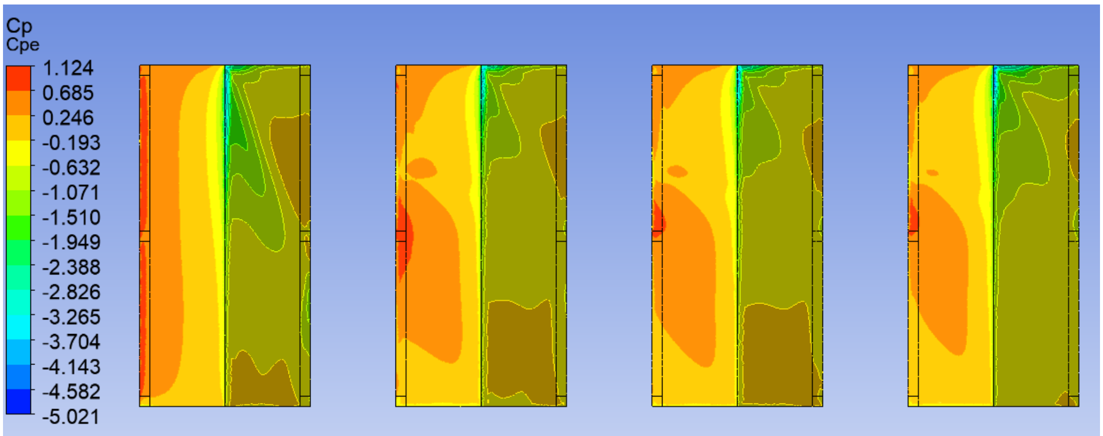

Fig 151 - External Pressure Coefficient at Wind Direction 30^0

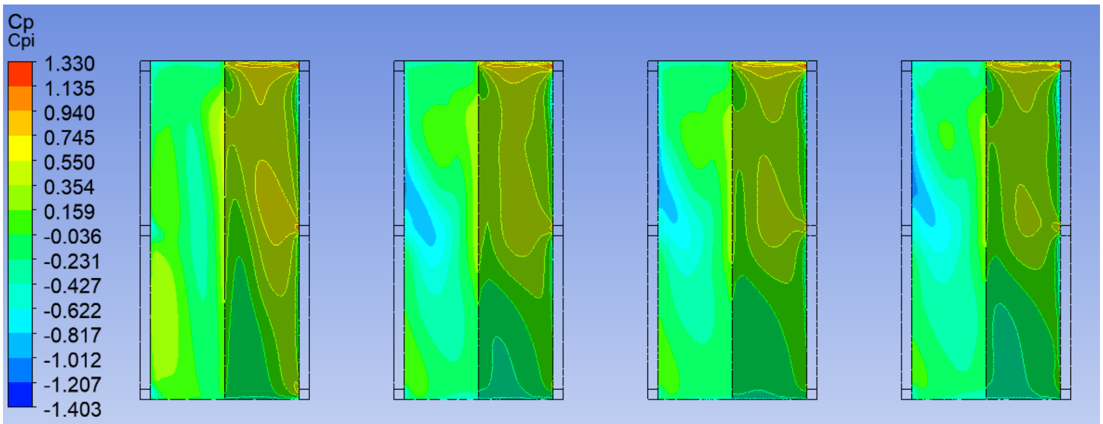

Fig 152 – Internal Pressure Coefficient at Wind Direction 30^0

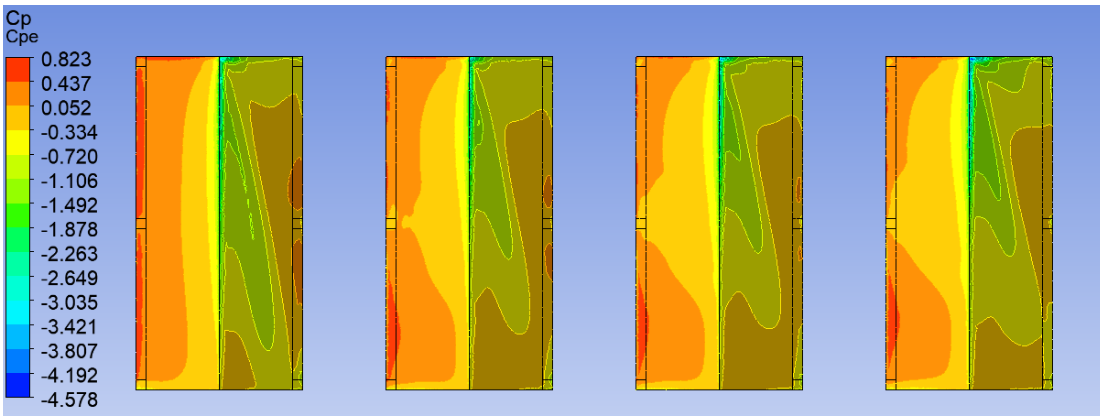

Fig 153 - External Pressure Coefficient at Wind Direction 45^0

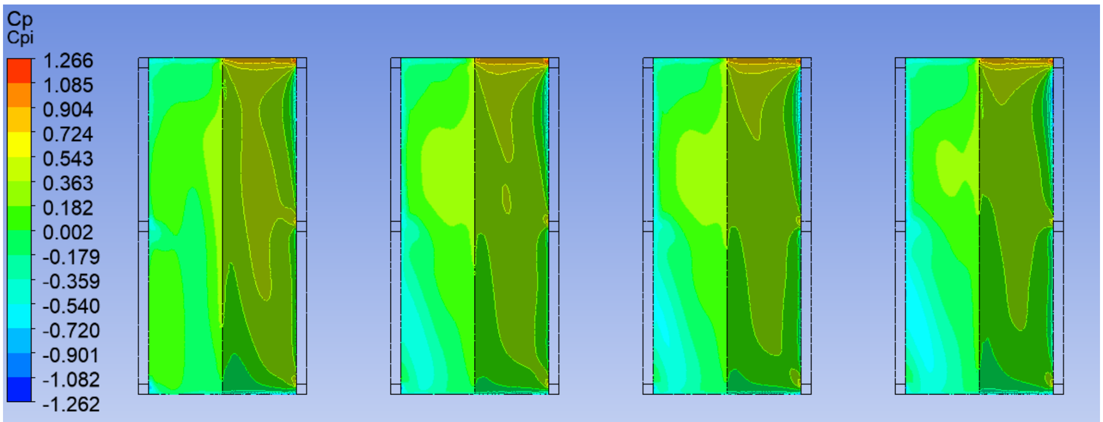

Fig 154 – Internal Pressure Coefficient at Wind Direction 45^0

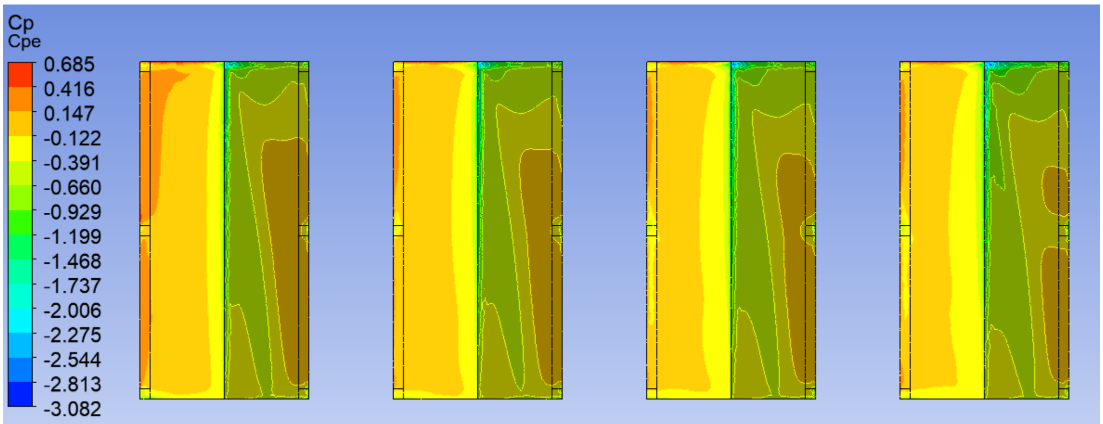

Fig 155 - External Pressure Coefficient at Wind Direction 60^0

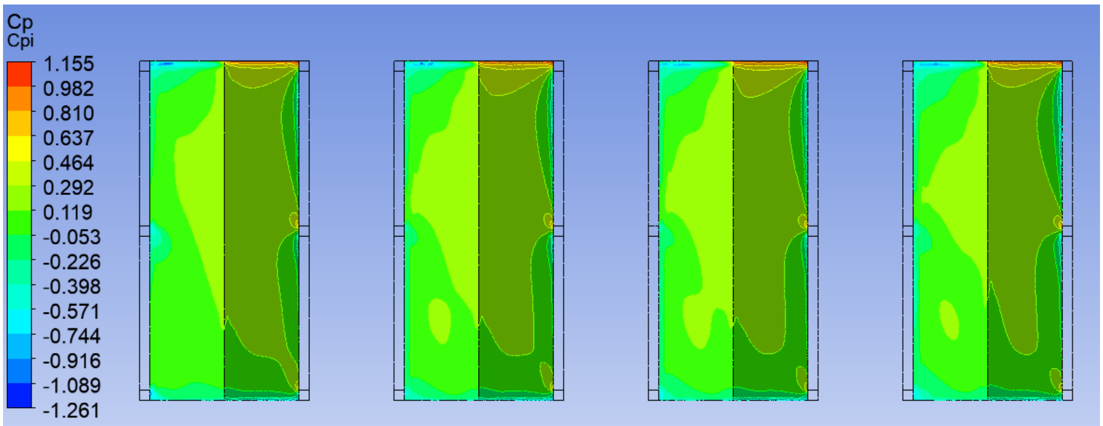

Fig 156 – Internal Pressure Coefficient at Wind Direction 60^0

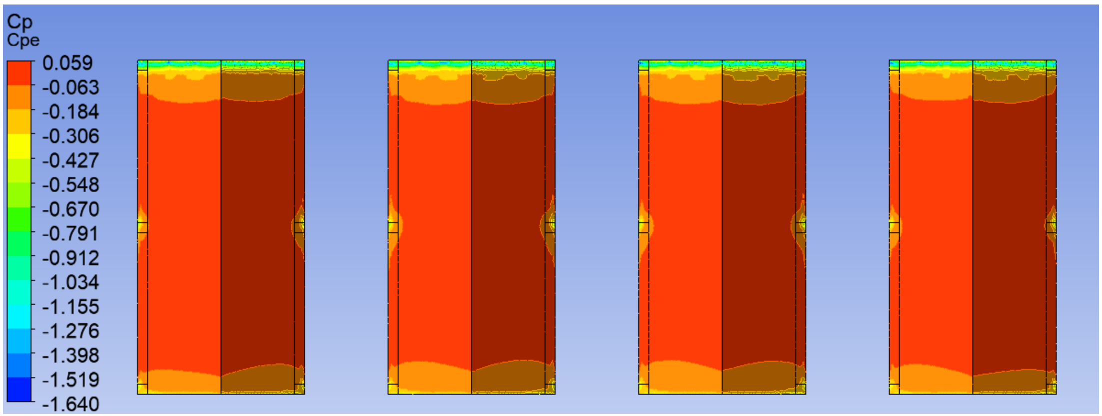

Fig 157- External Pressure Coefficient at Wind Direction 90^0

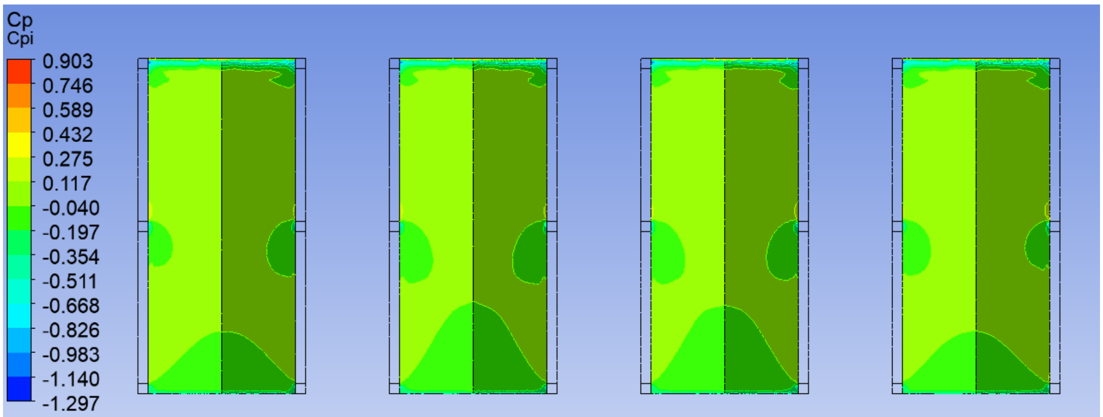

Fig 158– Internal Pressure Coefficient at Wind Direction 90^0

4.1.13 Pitch Angle 30° and Spacing B

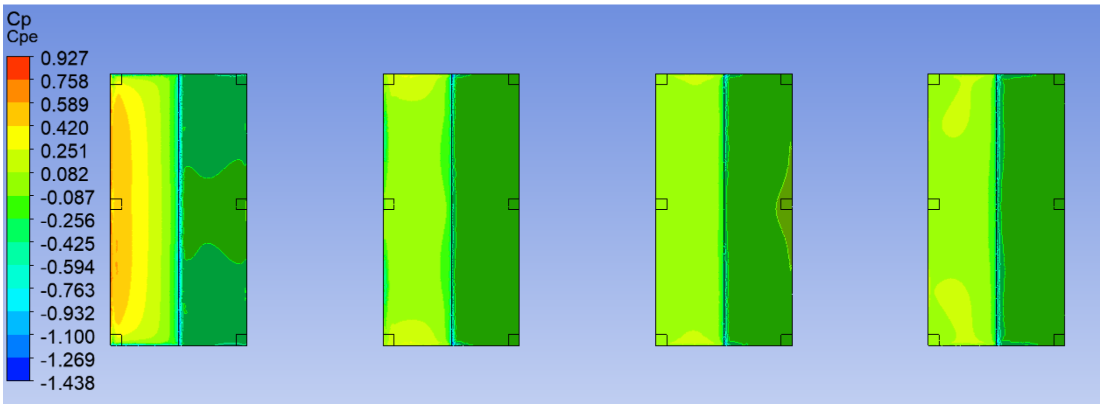

Fig 159 - External Pressure Coefficient at Wind Direction 0^0

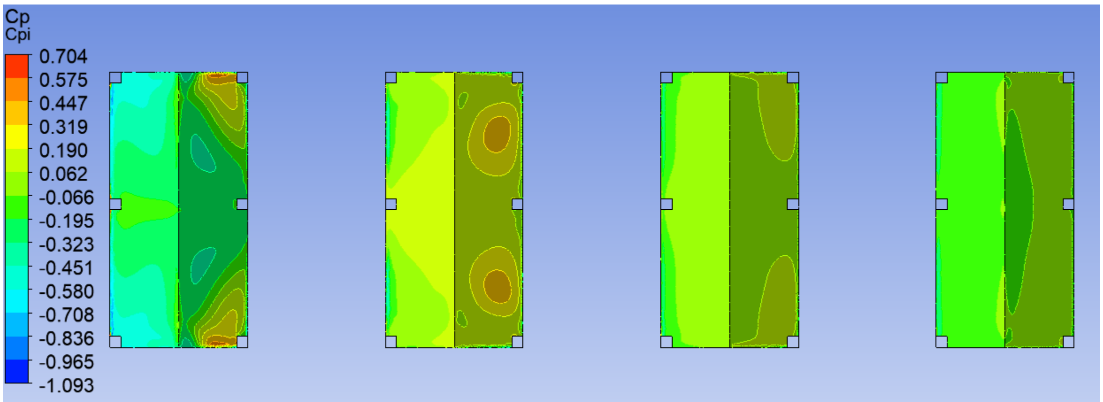

Fig 160 – Internal Pressure Coefficient at Wind Direction 0^0

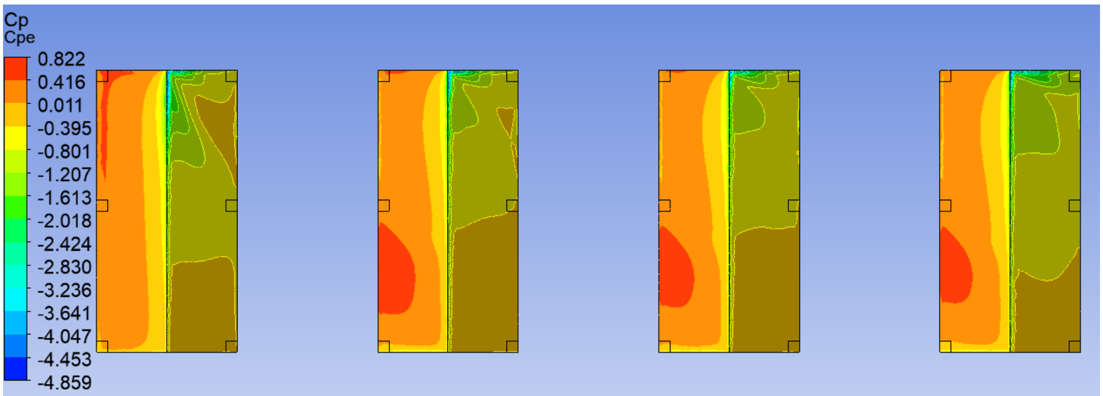

Fig 161 - External Pressure Coefficient at Wind Direction 30^0

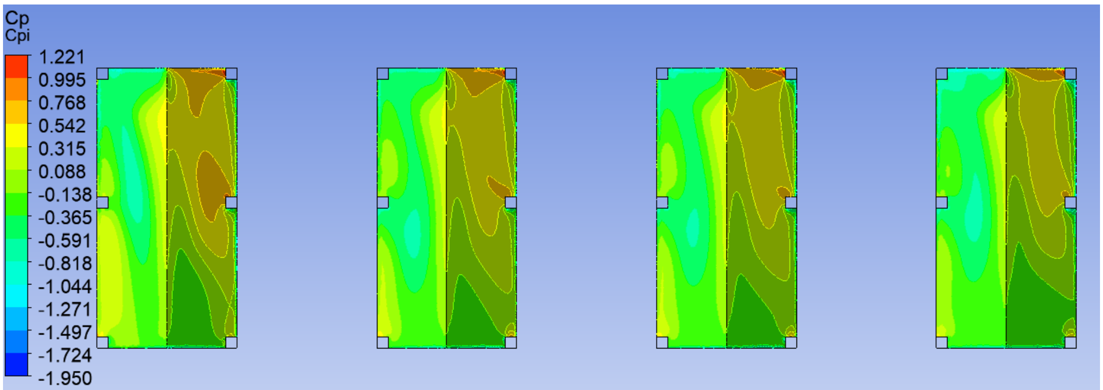

Fig 162 – Internal Pressure Coefficient at Wind Direction 30^0

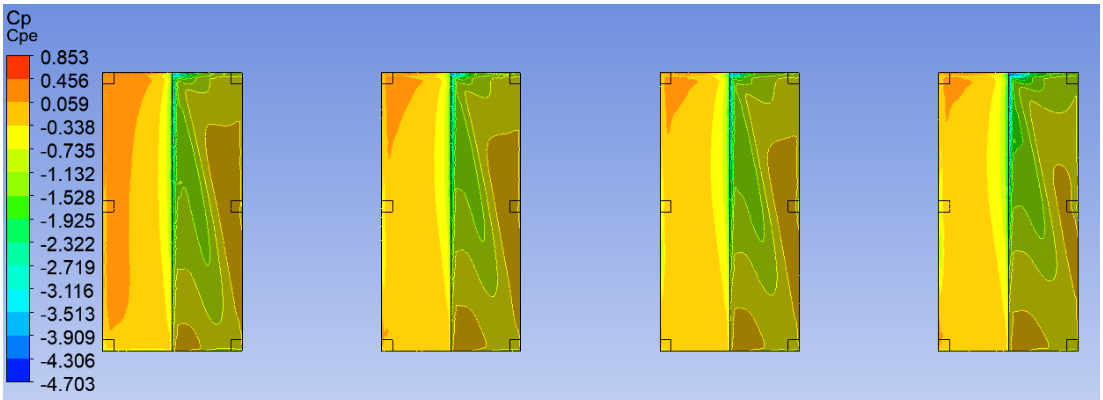

Fig 163 - External Pressure Coefficient at Wind Direction 45^0

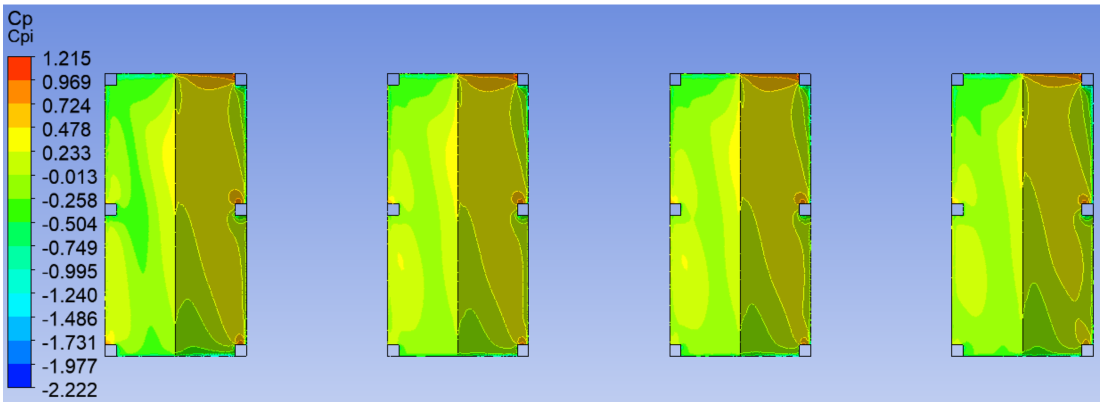

Fig 164– Internal Pressure Coefficient at Wind Direction 45^0

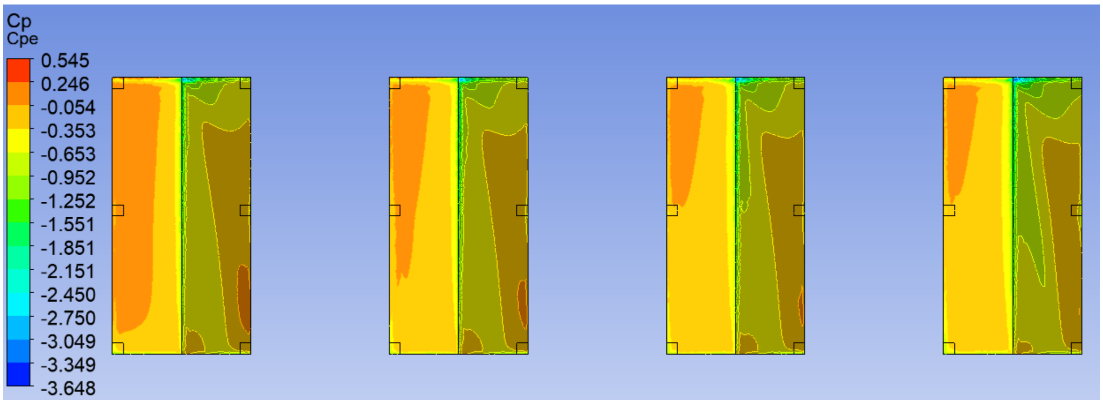

Fig 165 - External Pressure Coefficient at Wind Direction 60^0

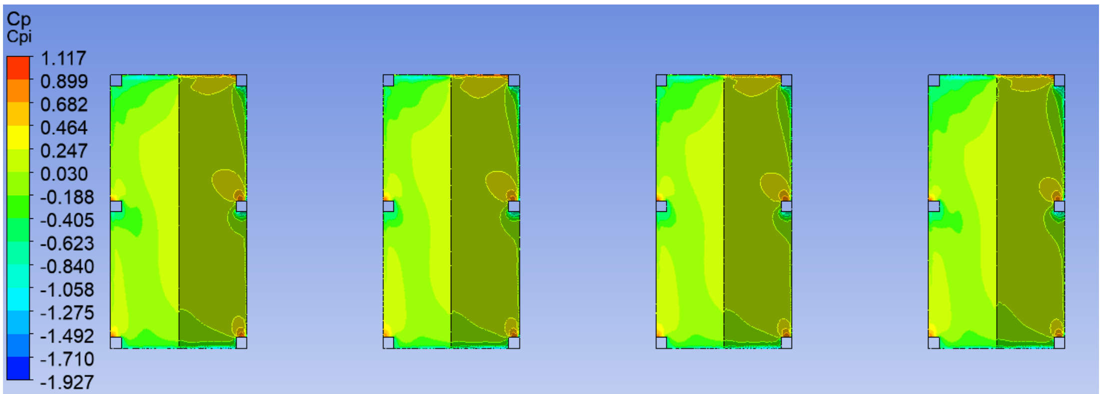

Fig 166 – Internal Pressure Coefficient at Wind Direction 60^0

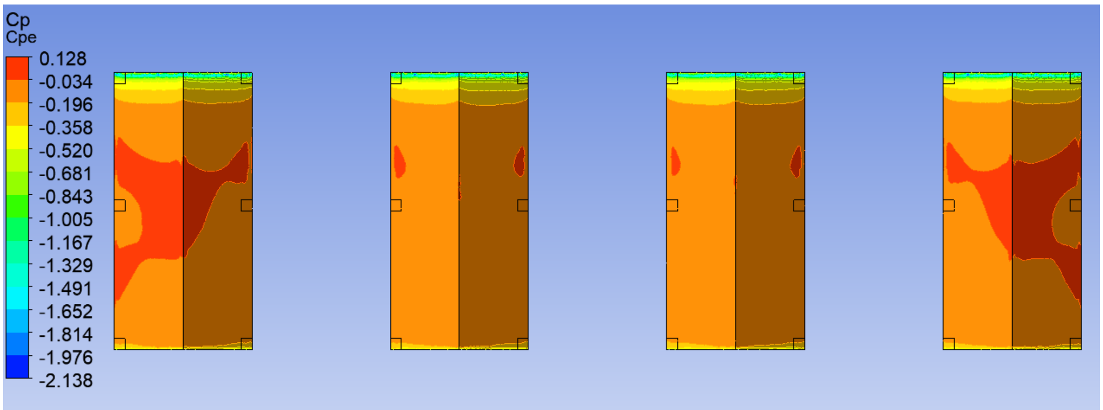

Fig 167- External Pressure Coefficient at Wind Direction 90^0

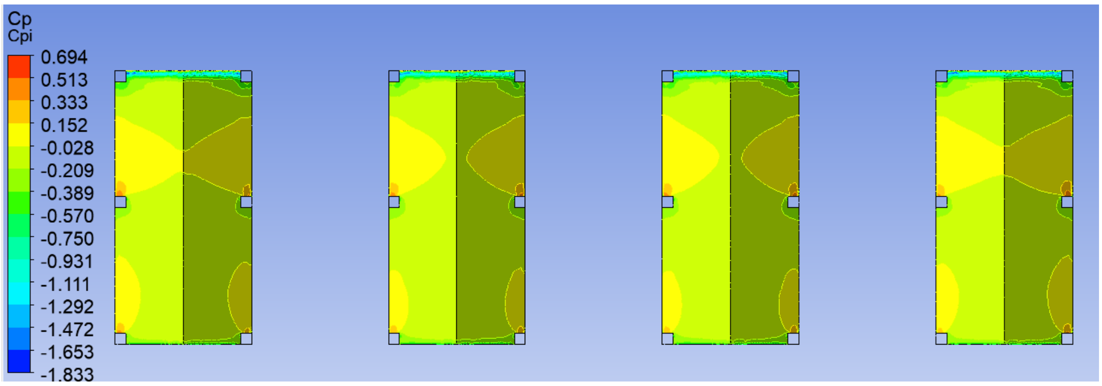

Fig 168 – Internal Pressure Coefficient at Wind Direction 90^0

4.1.14 Pitch Angle 30° and Spacing 3B/2

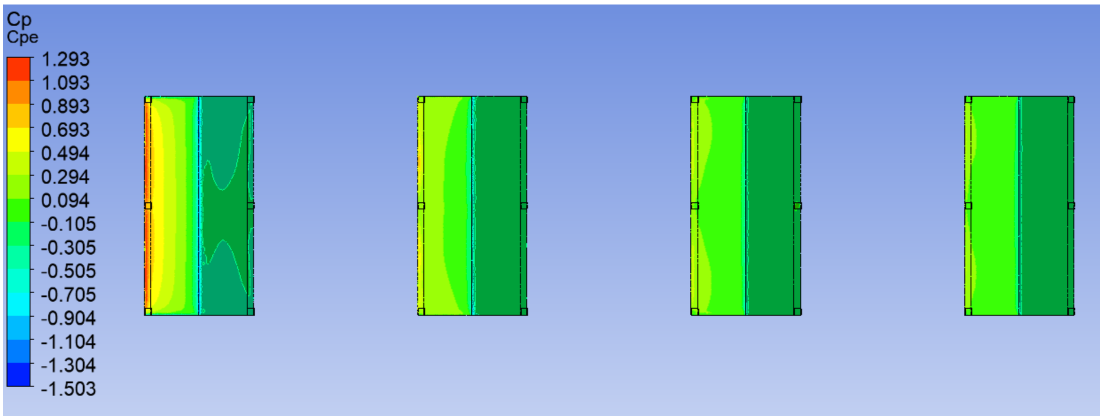

Fig 169 - External Pressure Coefficient at Wind Direction 0^0

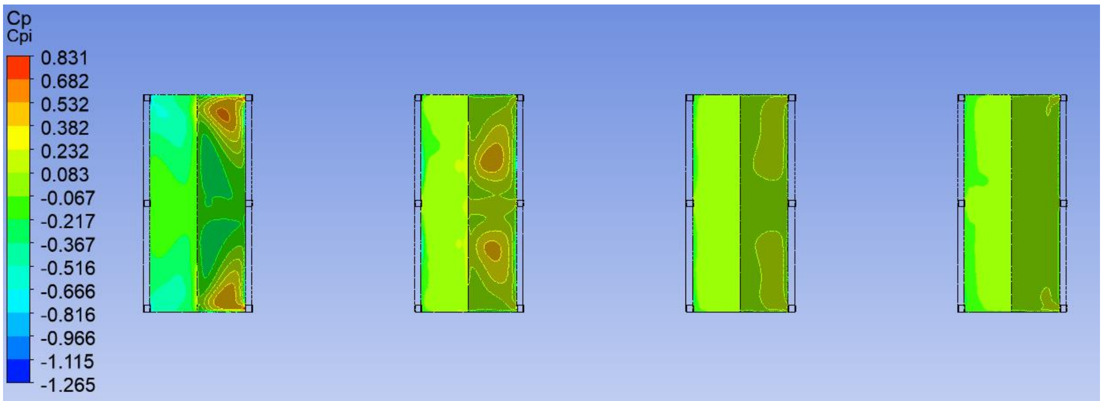

Fig 170– Internal Pressure Coefficient at Wind Direction 0^0

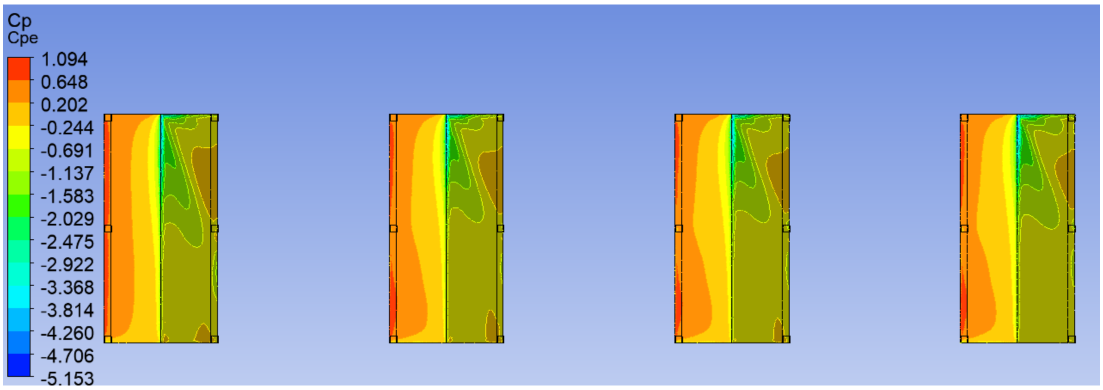

Fig 171 - External Pressure Coefficient at Wind Direction 30^0

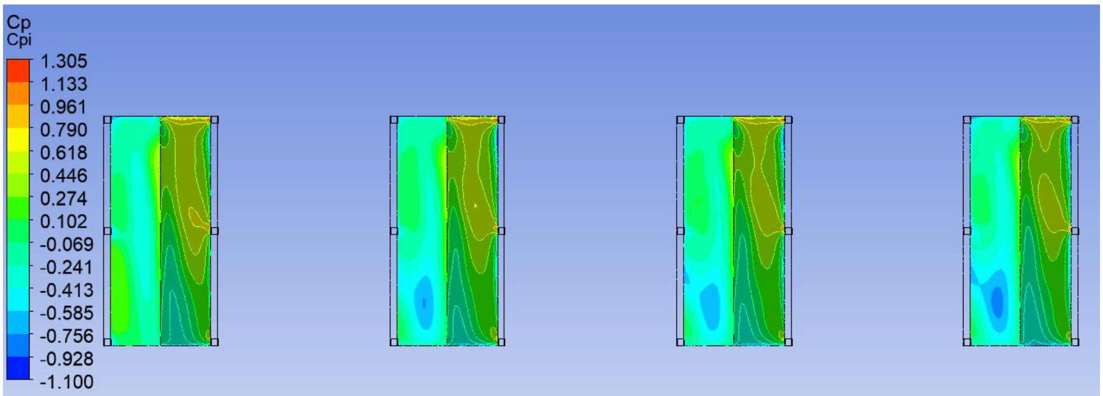

Fig 172– Internal Pressure Coefficient at Wind Direction 30^0

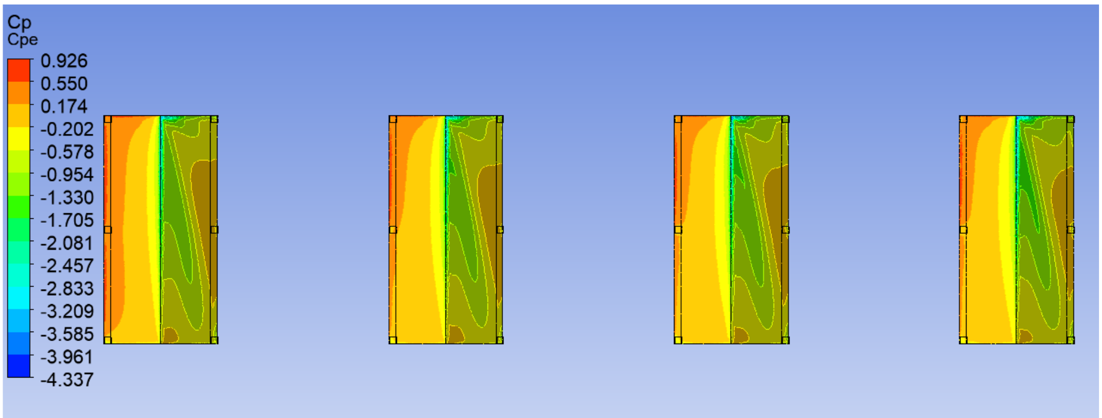

Fig 173 - External Pressure Coefficient at Wind Direction 45^0

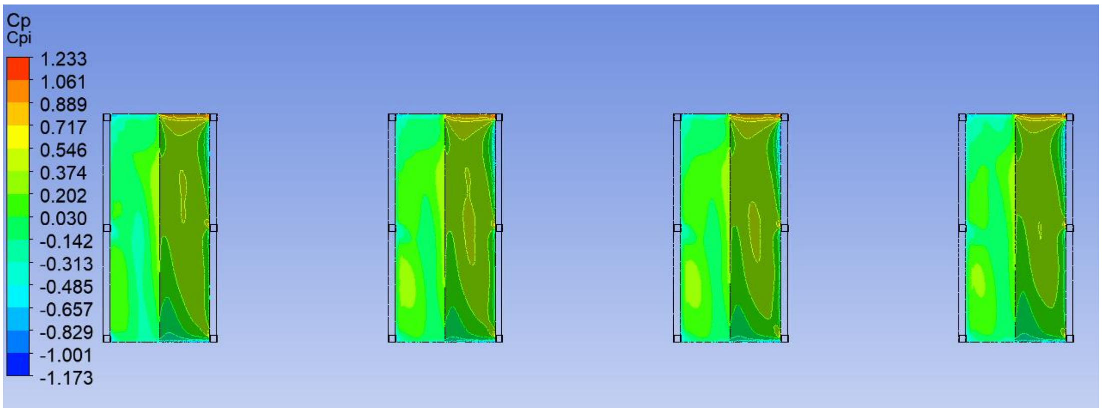

Fig 174– Internal Pressure Coefficient at Wind Direction 45^0

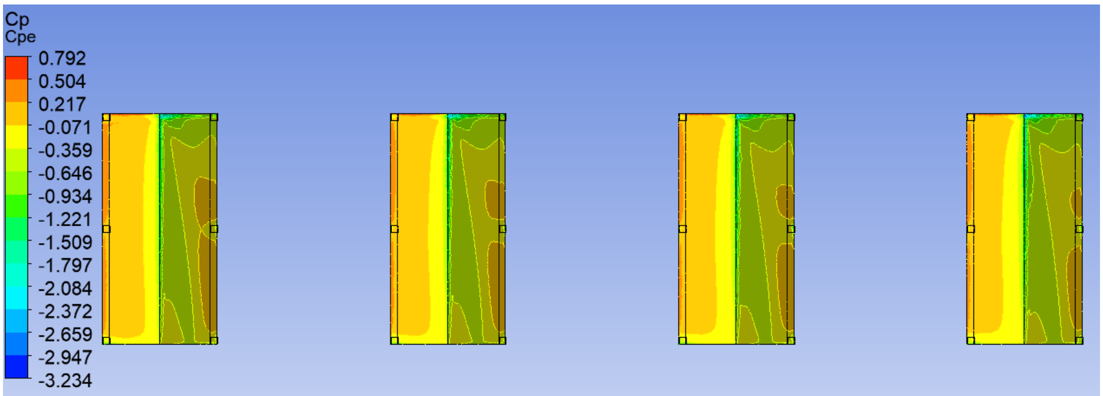

Fig 175 - External Pressure Coefficient at Wind Direction 60^0

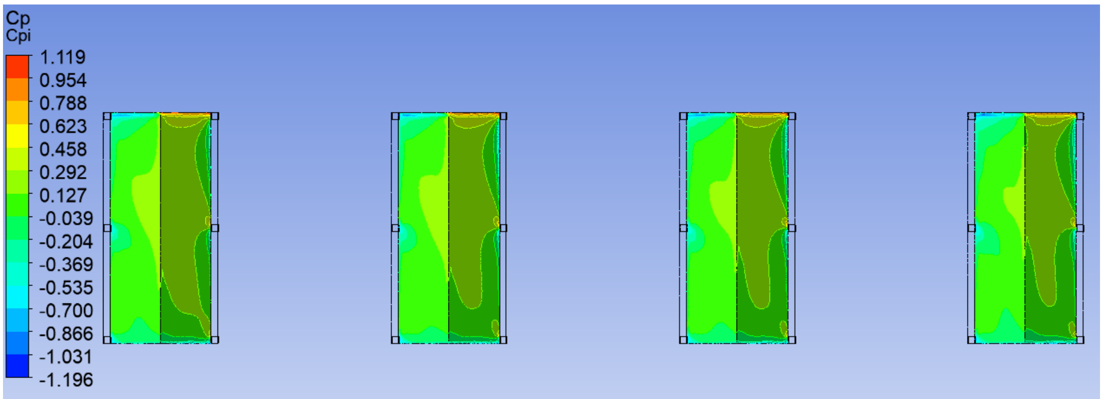

Fig 176– Internal Pressure Coefficient at Wind Direction 60^0

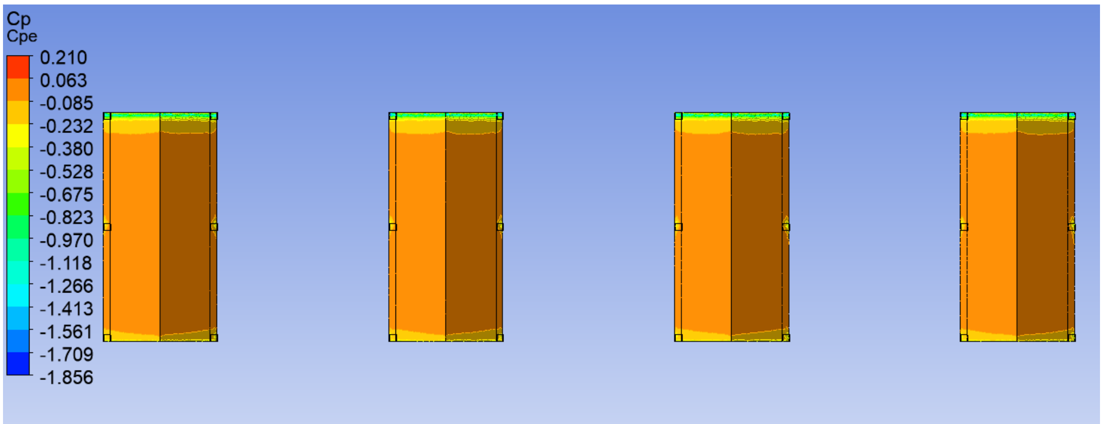

Fig 177 - External Pressure Coefficient at Wind Direction 90^0

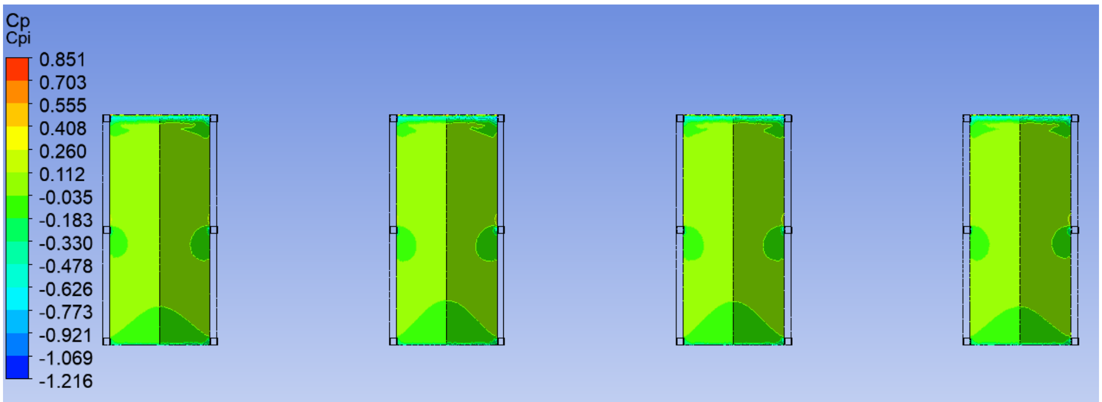

Fig 178– Internal Pressure Coefficient at Wind Direction 90^0

4.1.15 Pitch Angle 30° and Spacing 2B

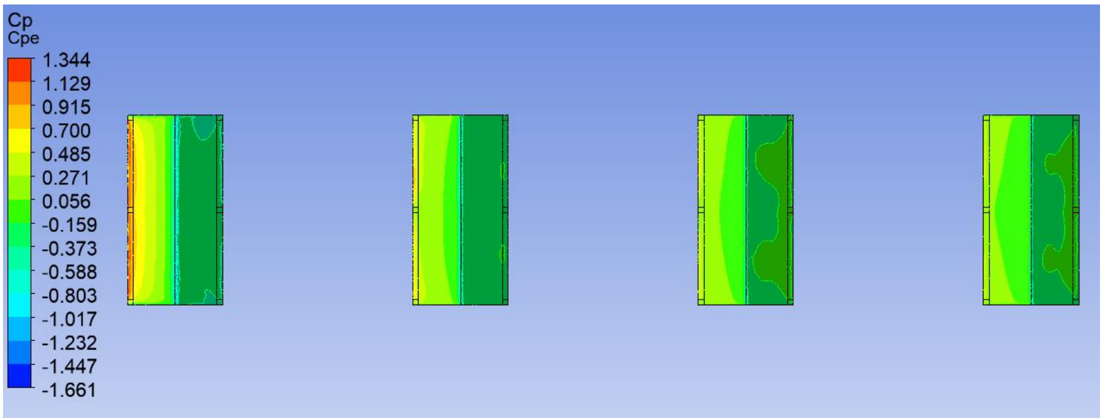

Fig 179 - External Pressure Coefficient at Wind Direction 0^0

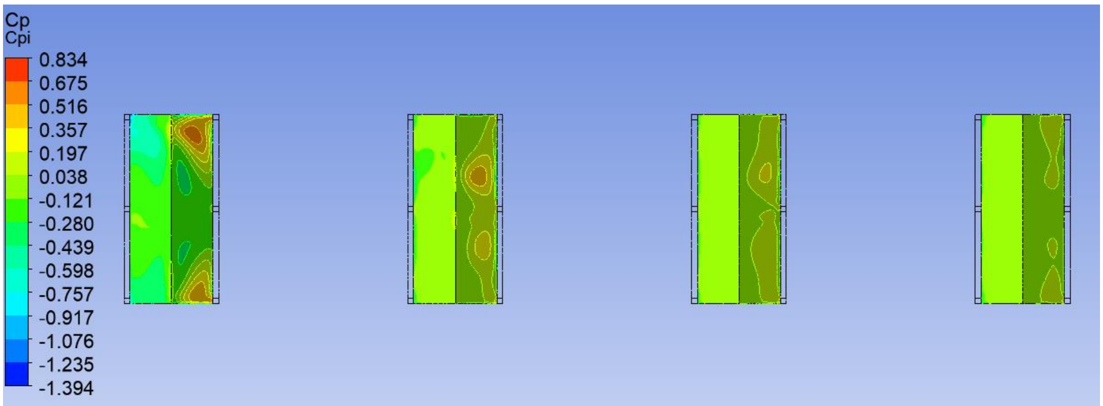

Fig 180– Internal Pressure Coefficient at Wind Direction 0^0

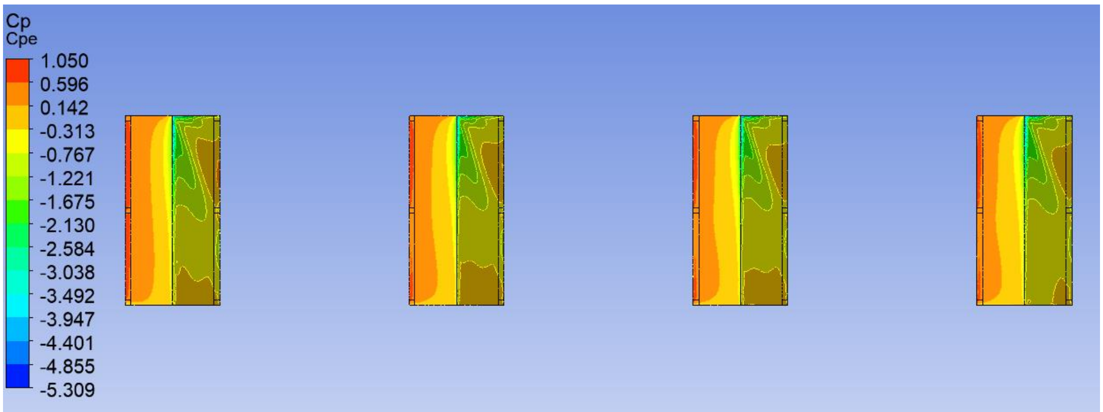

Fig 181 - External Pressure Coefficient at Wind Direction 30^0

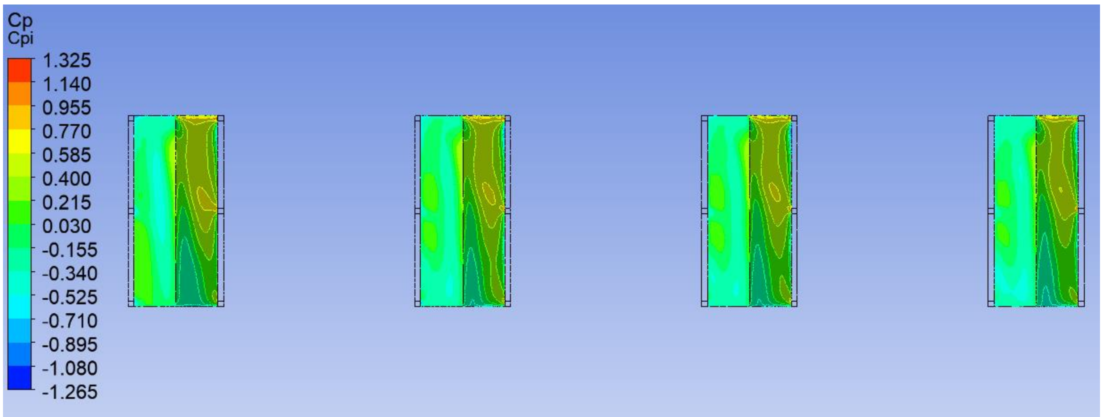

Fig 182– Internal Pressure Coefficient at Wind Direction 30^0

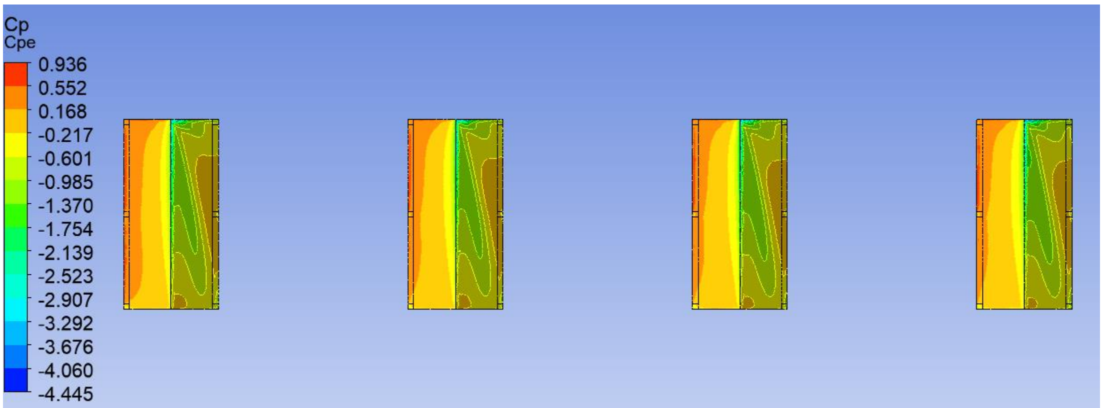

Fig 183 - External Pressure Coefficient at Wind Direction 45^0

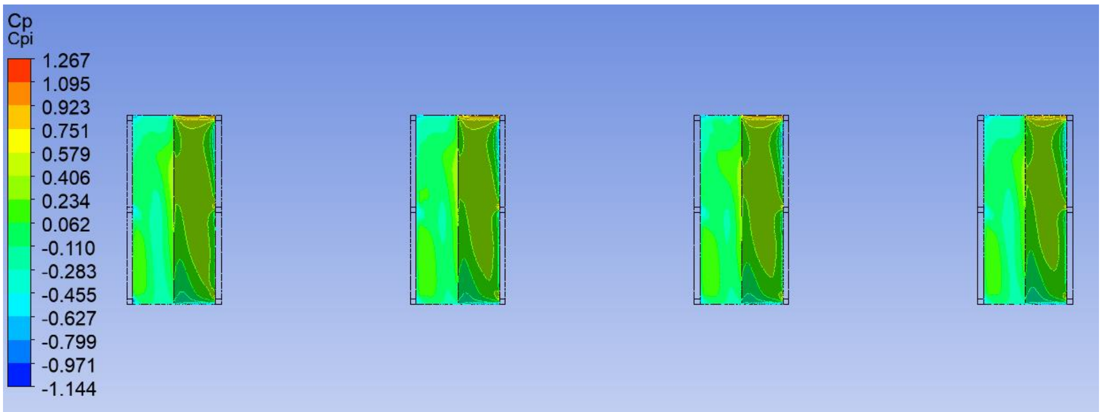

Fig 184– Internal Pressure Coefficient at Wind Direction 45^0

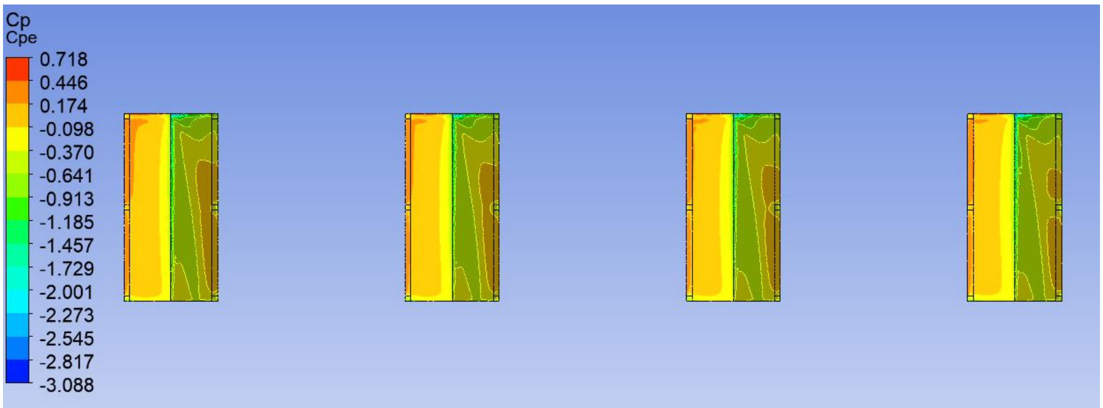

Fig 185 - External Pressure Coefficient at Wind Direction 60^0

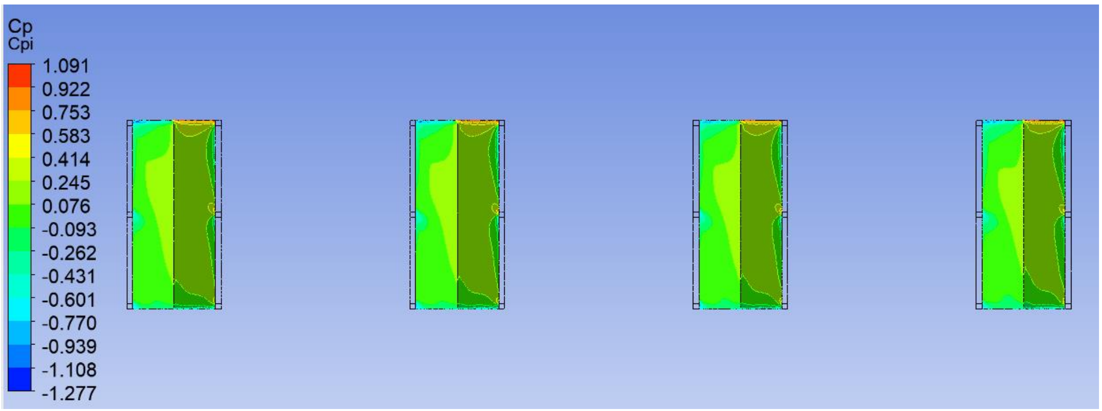

Fig 186– Internal Pressure Coefficient at Wind Direction 60^0

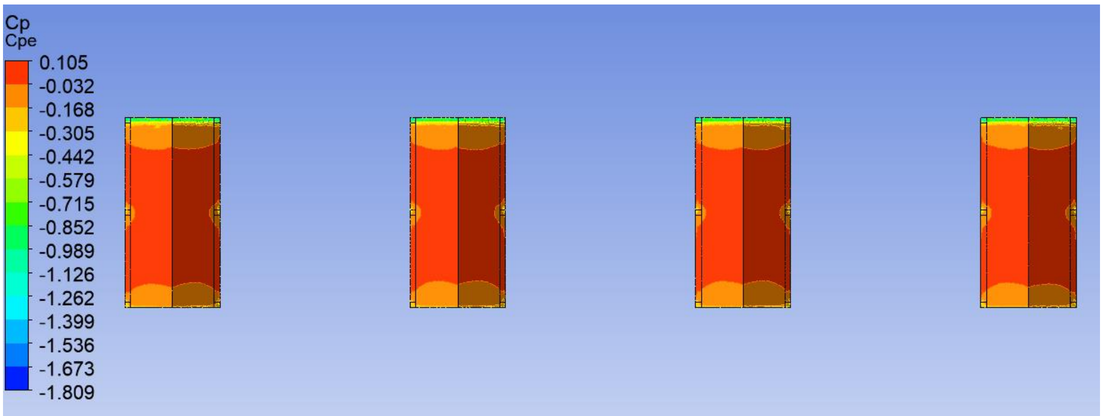

Fig 187- External Pressure Coefficient at Wind Direction 90^0

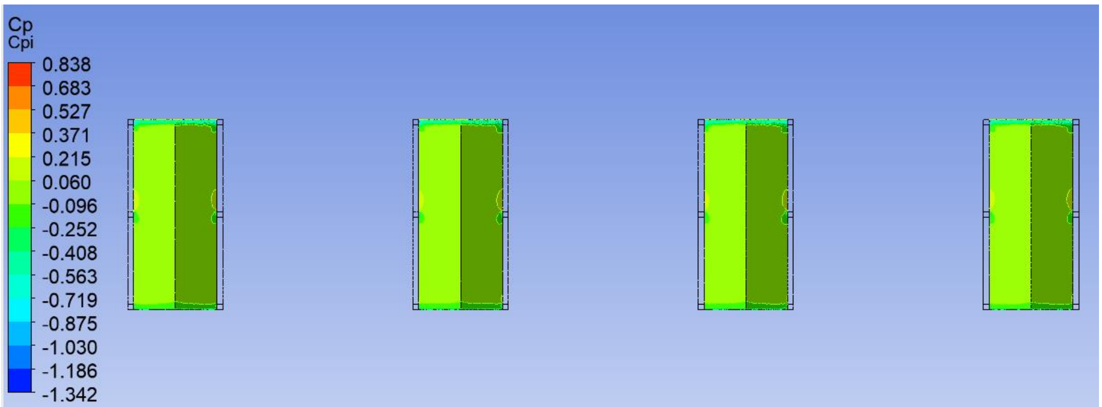

Fig 188– Internal Pressure Coefficient at Wind Direction 90^0

5. INTERFERENCE STUDY RESULTS

The interference is studied between the buildings by varying the orientation of the buildings. This is performed by changing the space between the buildings and rotating the domain with 0° to 90 °. Also , the spacing between the buildings are varied by multiples of the width of the building as 0,0.5b,b,1.5b,2b.

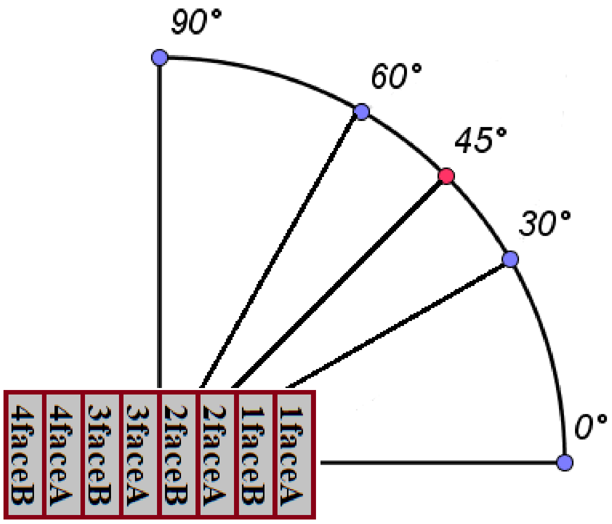

Fig 189 – Direction of wind incidence on the structure

Cpe and Cpi versus wind incidence angle are reported below, the graph are plotted for the same.

Slope Angle = 10°

Table 2 Coefficient of Pressure ($Cpext$) at Slope Angle 10°, Spacing 0

Cpext	**1 Face A**	**1 Face B**	**2 Face A**	**2 Face B**	**3 Face A**	**3 Face B**	**4 Face A**	**4 Face B**
Ɵ =0°	-0.213597	-0.074772	0.0012553	-0.046403	-0.004636	-0.067108	-0.065415	-0.300824
Ɵ=30 °	-0.262211	-0.15076	-0.087714	-0.142991	-0.100411	-0.165836	-0.145357	-0.370036
Ɵ=45 °	-0.262679	-0.19891	-0.155259	-0.211179	-0.167502	-0.228257	-0.192861	-0.339409
Ɵ=60 °	-0.22692	-0.220508	-0.208193	-0.264821	-0.235211	-0.276084	-0.234873	-0.276804
Ɵ=90 °	-0.139299	-0.194897	-0.214531	-0.22644	-0.226535	-0.2143	-0.194843	-0.139405

Table 3 Coefficient of Pressure ($Cpint$) at Slope Angle 10°, Spacing 0

Cpint	**1 Face A**	**1 Face B**	**2 Face A**	**2 Face B**	**3 Face A**	**3 Face B**	**4 Face A**	**4 Face B**
Ɵ =0°	-0.131211	0.0709714	-0.043793	0.0452482	-0.043433	0.0377901	-0.039809	0.0916681
Ɵ=30 °	0.0362359	0.215407	-0.070665	0.158107	-0.074745	0.12405	-0.093934	0.100999
Ɵ=45 °	0.0479619	0.150192	-0.062649	0.0964271	-0.079858	0.0741463	-0.112659	0.0593031
Ɵ =60 °	0.0621345	0.104363	-0.021123	0.10085	-0.028419	0.0969938	-0.065975	0.0609159
Ɵ =90°	-0.058075	-0.078806	-0.079430	-0.081974	-0.081846	-0.07914	-0.078976	-0.058275

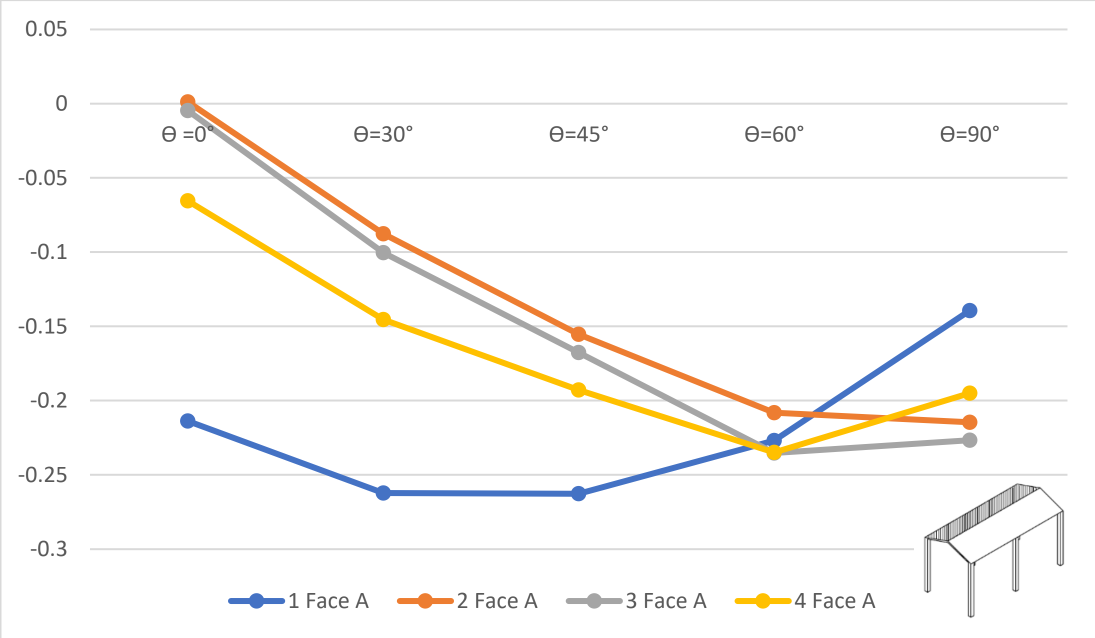

Fig 190 Cpe for roof angle 10° and zero spacing for windward side

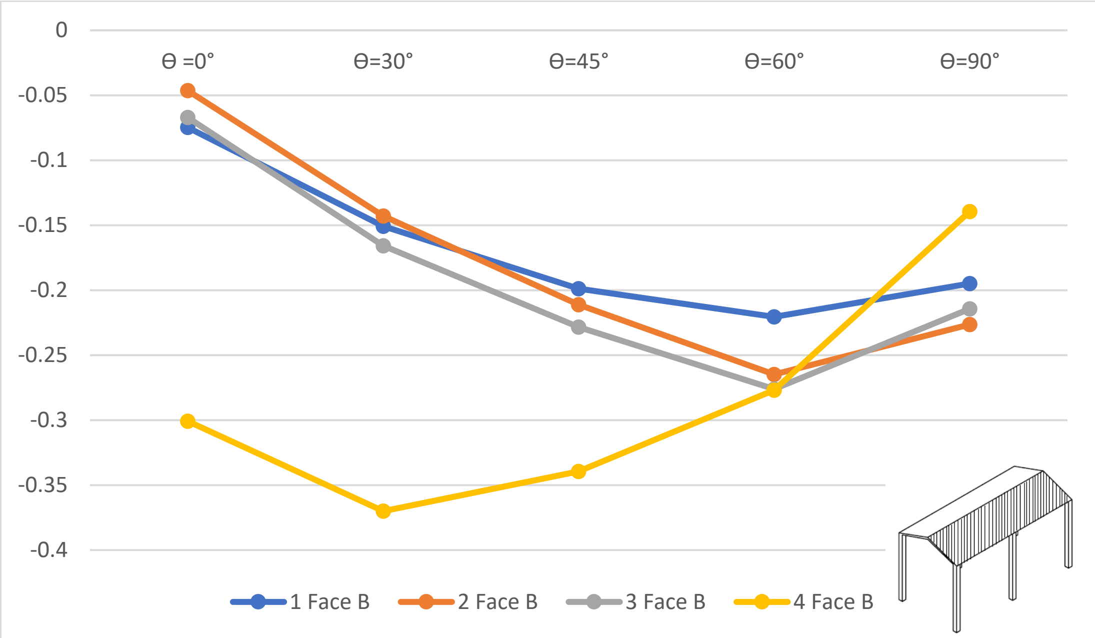

Fig 191 Cpe for roof angle 10° and zero spacing for leeward side

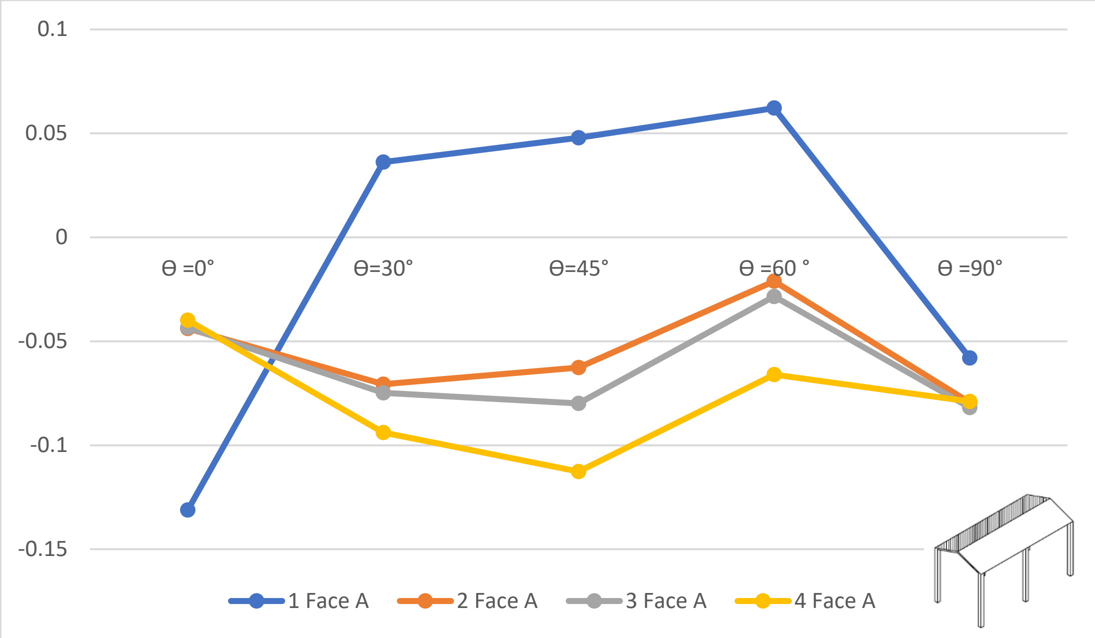

Fig 192 Cpi for roof angle 10° and zero spacing for windward side

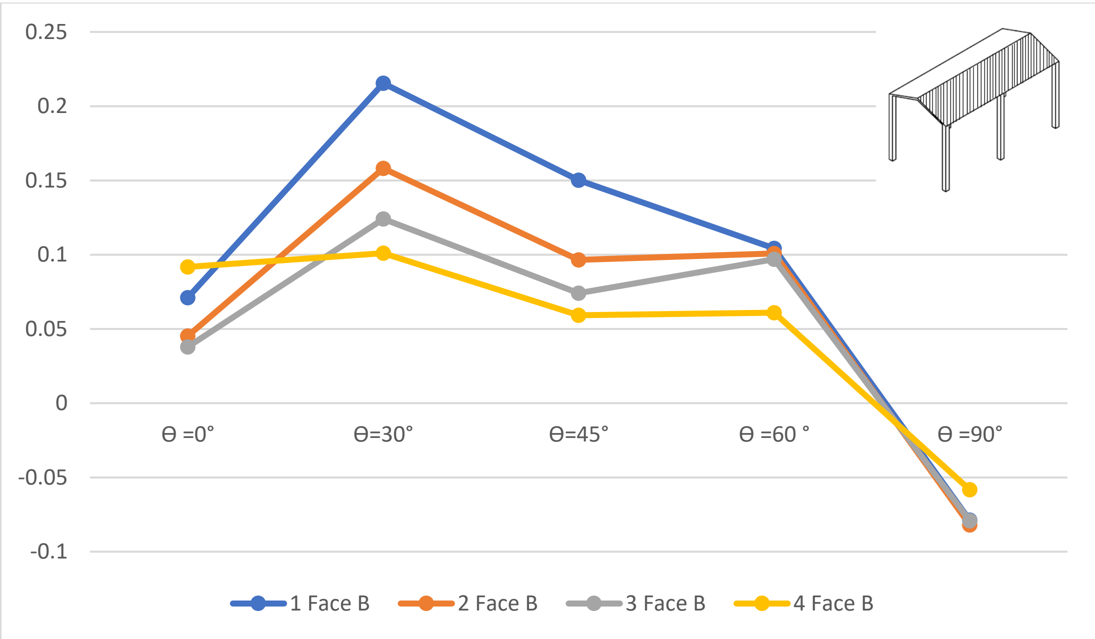

Fig 193 Cpi for roof angle 10° and zero spacing for leeward side

Table 4 Coefficient of Pressure ($Cpext$) at Slope Angle 10°, Spacing 0.5b

Cpext	**1 Face A**	**1 Face B**	**2 Face A**	**2 Face B**	**3 Face A**	**3 Face B**	**4 Face A**	**4 Face B**
Ɵ = 0°	-0.133416	-0.247754	0.0317264	-0.209582	0.038515	-0.214899	0.0280224	-0.245444
Ɵ =30°	-0.151855	-0.220955	-0.090566	-0.223678	-0.109989	-0.24134	-0.124967	-0.272881
Ɵ =45°	-0.124462	-0.170804	-0.129834	-0.189066	-0.160961	-0.210617	-0.168651	-0.234346
Ɵ =60°	-0.083099	-0.114075	-0.131121	-0.135489	-0.153579	-0.149654	-0.153513	-0.160763
Ɵ =90°	-0.038452	-0.042110	-0.047457	-0.048048	-0.048082	-0.047368	-0.042409	-0.038834

Table 5 Coefficient of Pressure ($Cp\text{int}$) at Slope Angle 10°, Spacing 0.5b

Cpint	**1 Face A**	**1 Face B**	**2 Face A**	**2 Face B**	**3 Face A**	**3 Face B**	**4 Face A**	**4 Face B**
Ɵ = 0°	0.145333	0.258081	-0.057136	0.135391	-0.096125	0.0906363	-0.130551	0.0501456
Ɵ =30°	0.126448	0.249977	0.0524117	0.188631	0.0400127	0.166656	0.0020387	0.125346
Ɵ =45°	0.0942887	0.18088	0.070179	0.165733	0.0635527	0.155833	0.0283098	0.122476
Ɵ =60°	0.0647077	0.113038	0.068884	0.113921	0.0656003	0.108911	0.0400436	0.0860015
Ɵ =90°	-0.004518	-0.007023	-0.005924	-0.006411	-0.006168	-0.006042	-0.007360	-0.004715

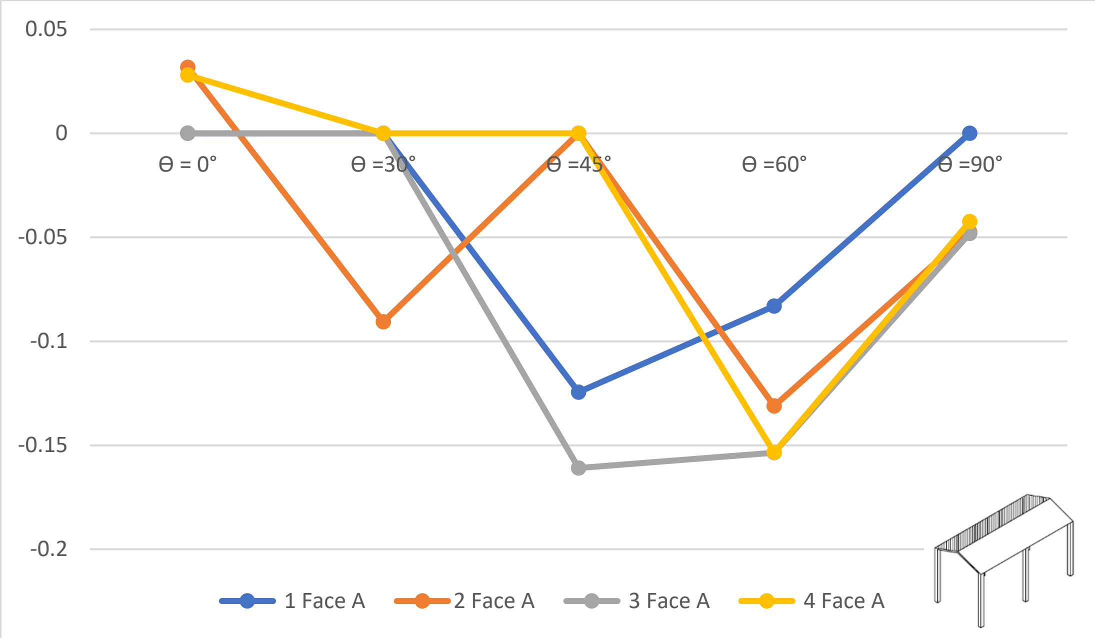

Fig 194 Cpe for roof angle 10° and 0.5b spacing for windward side

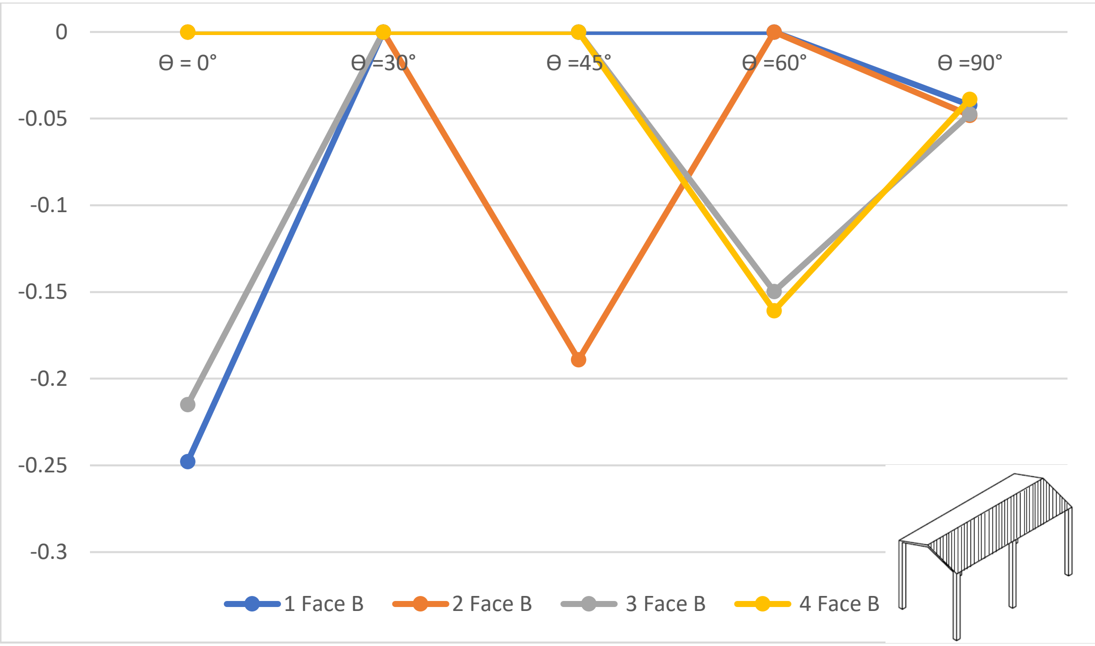

Fig 195 Cpe for roof angle 10° and 0.5b spacing for leeward side

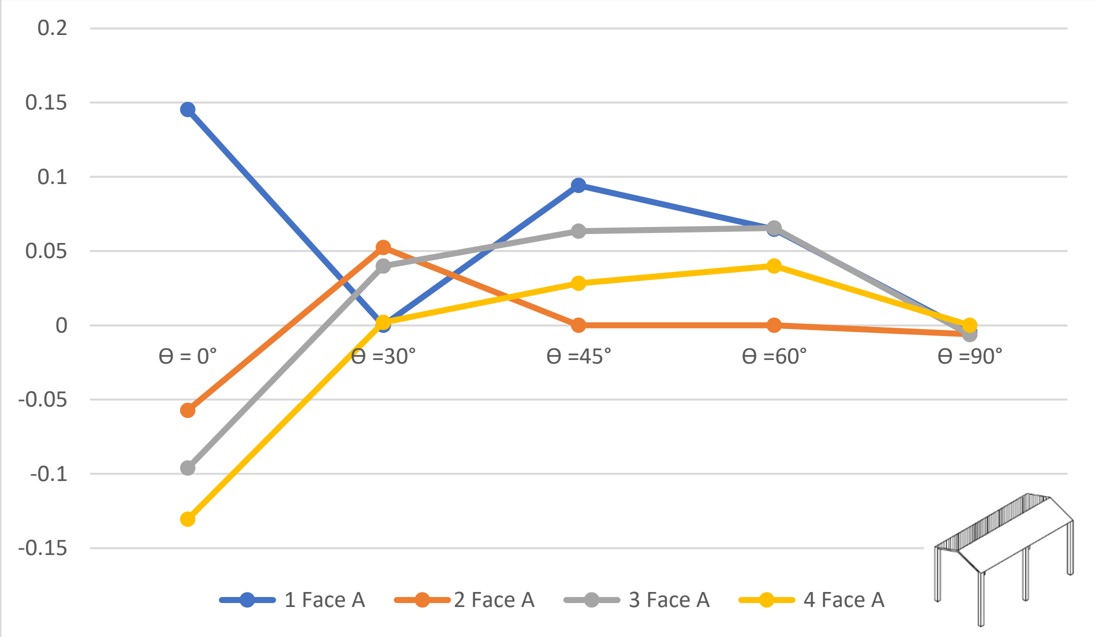

Fig 196 Cpi for roof angle 10° and 0.5b spacing for windward side

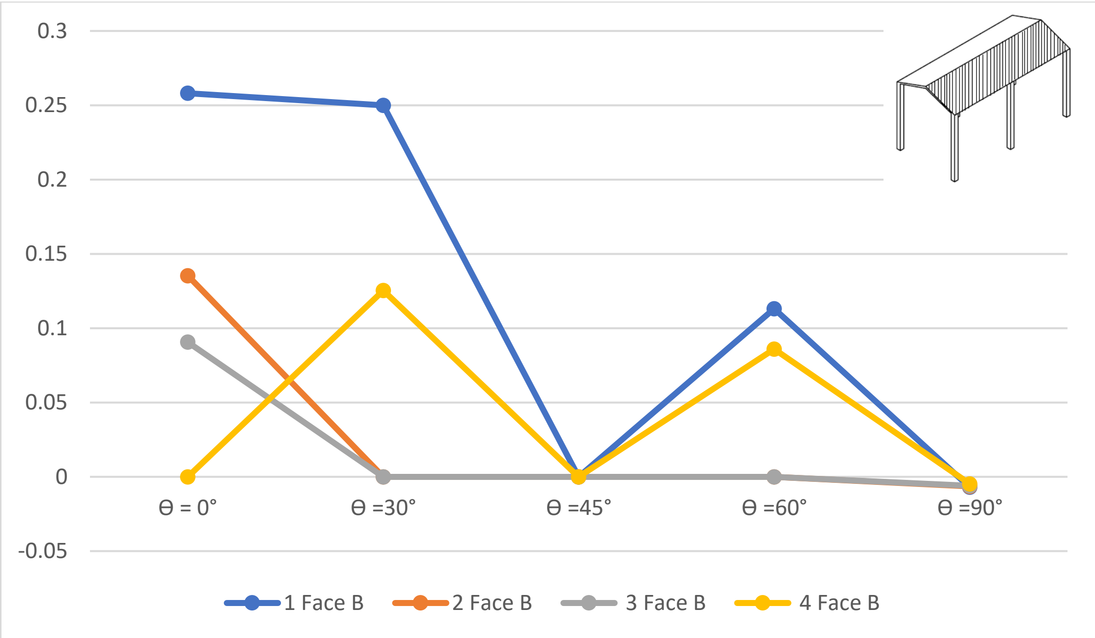

Fig 197 Cpi for roof angle 10° and 0.5b spacing for leeward side

Table 6 Coefficient of Pressure ($Cpext$) at Slope Angle 10°, Spacing b

Cpext	**1 Face A**	**1 Face B**	**2 Face A**	**2 Face B**	**3 Face A**	**3 Face B**	**4 Face A**	**4 Face B**
ϴ = 0°	-0.136035	-0.265751	0.0131868	-0.22571	0.0292859	-0.222973	0.0261534	-0.237758
ϴ =30°	-0.145853	-0.232515	-0.128152	-0.236356	-0.157896	-0.253212	-0.17238	-0.276746
ϴ =45°	-0.117761	-0.180263	-0.154435	-0.195262	-0.176728	-0.208771	-0.183173	-0.226245
ϴ =60°	-0.072739	-0.111312	-0.116138	-0.12876	-0.130604	-0.139457	-0.135465	-0.152099
ϴ =90°	-0.035282	-0.036739	-0.039867	-0.040136	-0.039940	-0.039848	-0.036158	-0.034592

Table 7 Coefficient of Pressure ($Cp\text{int}$) at Slope Angle 10°, Spacing b

Cpint	**1 Face A**	**1 Face B**	**2 Face A**	**2 Face B**	**3 Face A**	**3 Face B**	**4 Face A**	**4 Face B**
ϴ = 0°	0.132055	0.243529	-0.043929	0.139644	-0.094594	0.0967935	-0.129032	0.0590776
ϴ =30°	0.104628	0.229357	0.0673964	0.191754	0.0669139	0.181317	0.040767	0.153403
ϴ =45°	0.0683733	0.157076	0.0743316	0.151188	0.0720207	0.146561	0.0501159	0.12601
ϴ =60°	0.0517688	0.101555	0.0587548	0.103054	0.0565285	0.100015	0.0411118	0.0849894
ϴ =90°	-0.005438	-0.006983	-0.008160	-0.008439	-0.008018	-0.007879	-0.006440	-0.005034

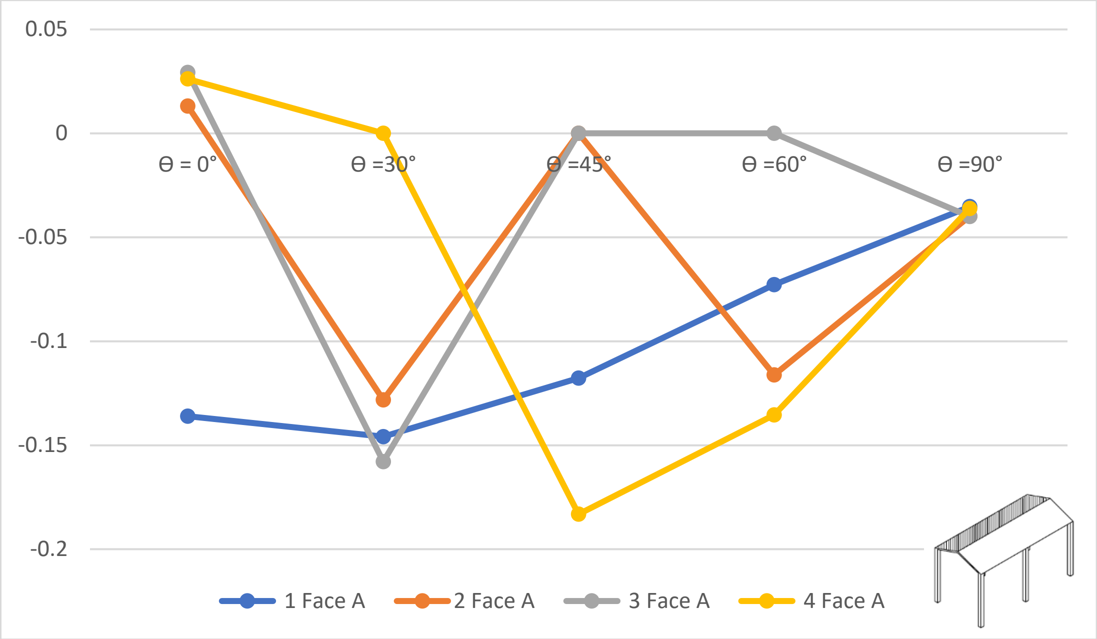

Fig 198 Cpe for roof angle 10° and b spacing for windward side

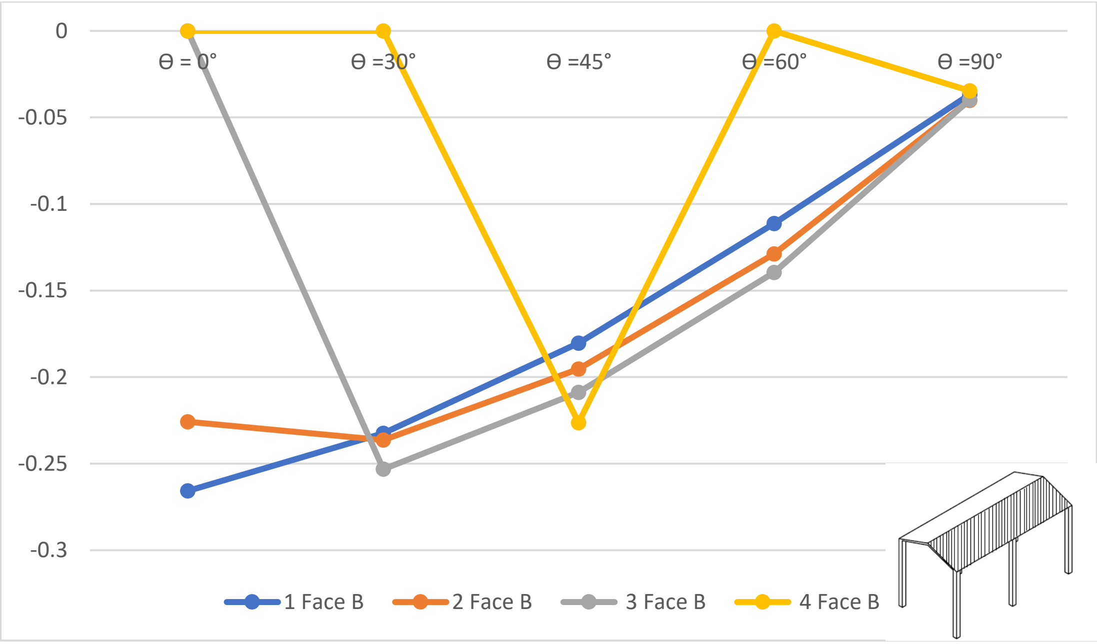

Fig 199 Cpe for roof angle 10° and b spacing for leeward side

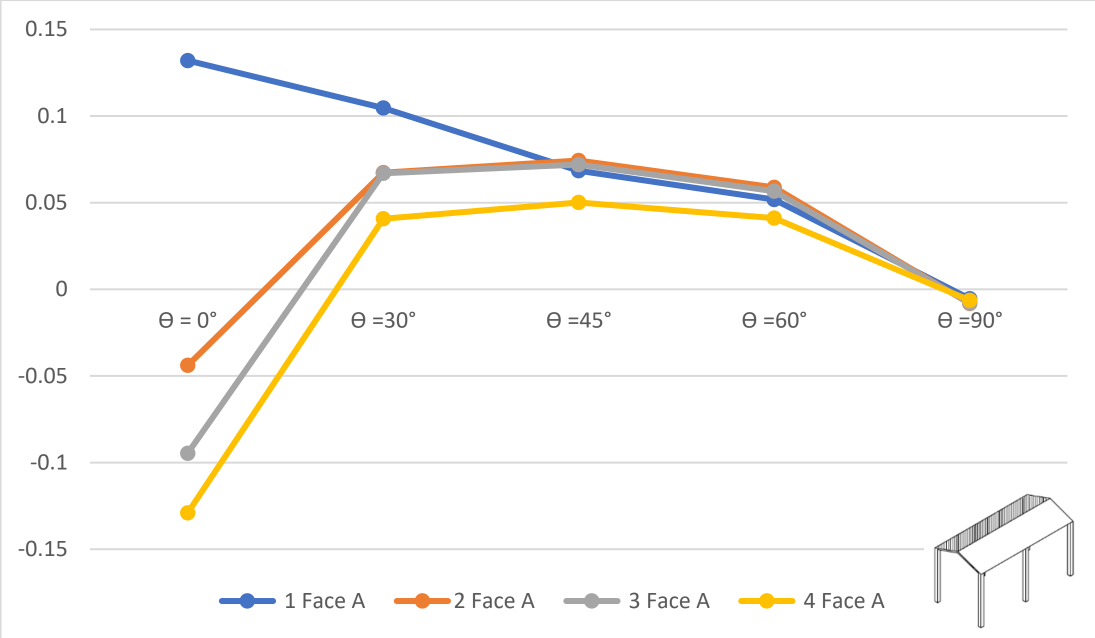

Fig 200 Cpi for roof angle 10° and b spacing for windward side

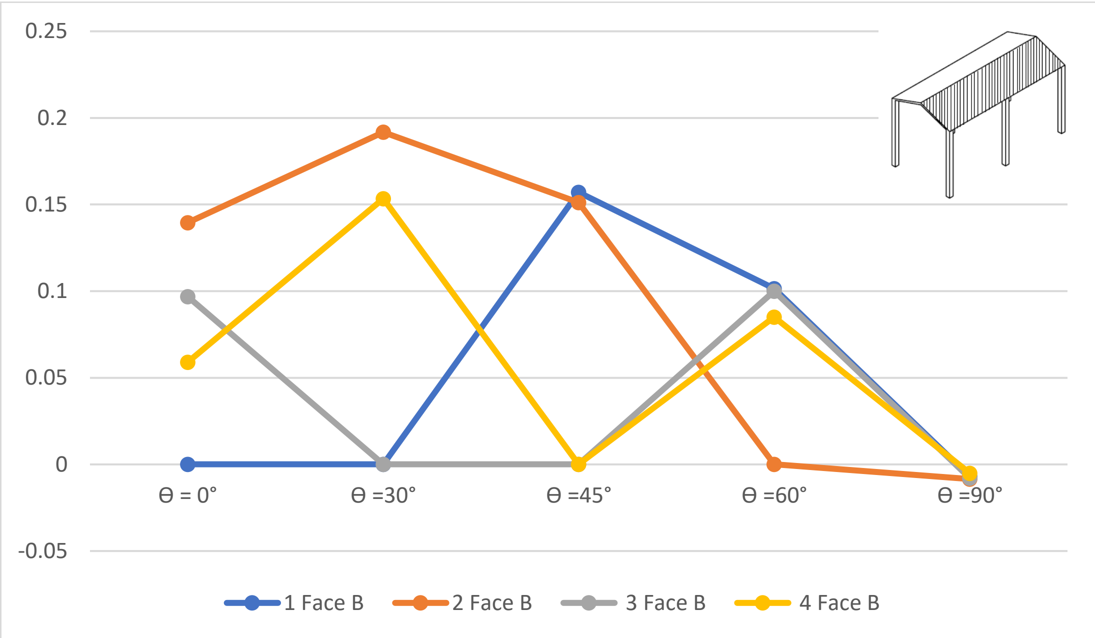

Fig 201 Cpi for roof angle 10° and b spacing for leeward side

Table 8 Coefficient of Pressure ($Cpext$) at Slope Angle 10°, Spacing 1.5

Cpext	1 Face A	1 Face B	2 Face A	2 Face B	3 Face A	3 Face B	4 Face A	4 Face B
ϴ = 0°	-0.13803	-0.274743	0.0007576	-0.235045	0.0225704	-0.227171	0.0232225	-0.235405
ϴ =30°	-0.142942	-0.239589	-0.158195	-0.247512	-0.184321	-0.262672	-0.196299	-0.281784
ϴ =45°	-0.111223	-0.181216	-0.162571	-0.196109	-0.180423	-0.205012	-0.188745	-0.221774
ϴ =60°	-0.069696	-0.113307	-0.095629	-0.126046	-0.103578	-0.133773	-0.107908	-0.144008
ϴ =90°	-0.032826	-0.033409	-0.035653	-0.035655	-0.035753	-0.035697	-0.033300	-0.032624

Table 9 Coefficient of Pressure ($Cp\text{int}$) at Slope Angle 10°, Spacing 1.5b

Cpint	1 Face A	1 Face B	2 Face A	2 Face B	3 Face A	3 Face B	4 Face A	4 Face B
ϴ = 0°	0.124188	0.235043	-0.035363	0.139976	-0.083791	0.100105	-0.119248	0.065826
ϴ =30°	0.0931309	0.218464	0.0869355	0.196164	0.0898457	0.191487	0.0710597	0.172248
ϴ =45°	0.0602797	0.149945	0.076665	0.152031	0.0762052	0.147489	0.059438	0.131182
ϴ =60°	0.043459	0.0950233	0.0449724	0.093754	0.0411107	0.0903336	0.0294884	0.0801632
ϴ =90°	-0.004846	-0.006243	-0.006964	-0.006840	-0.006405	-0.006725	-0.006475	-0.005268

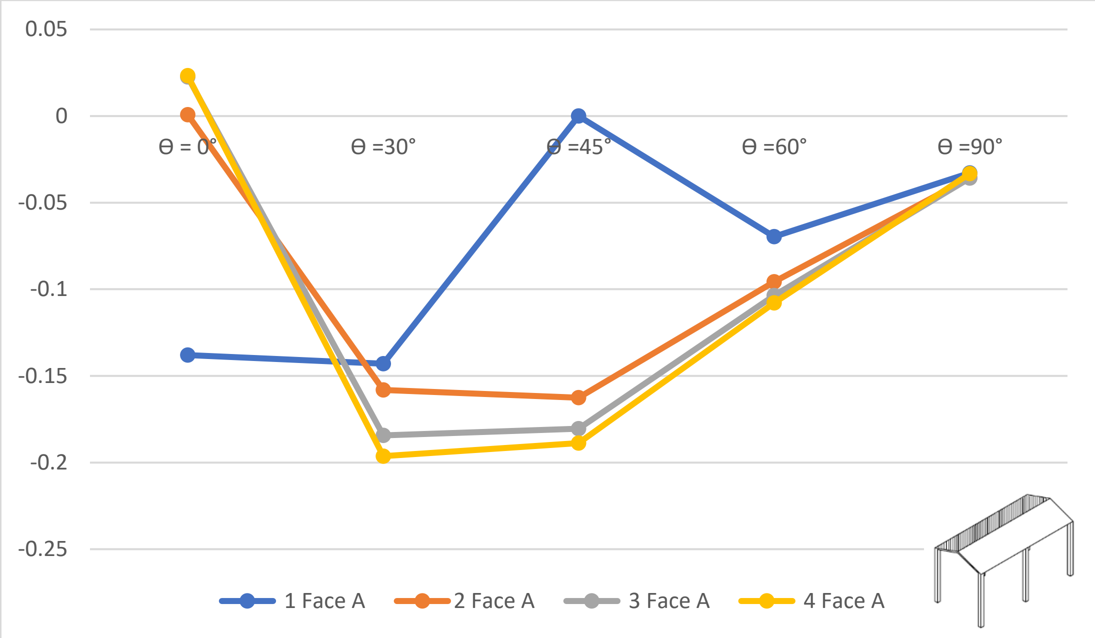

Fig 202 Cpe for roof angle 10° and 1.5b spacing for windward side

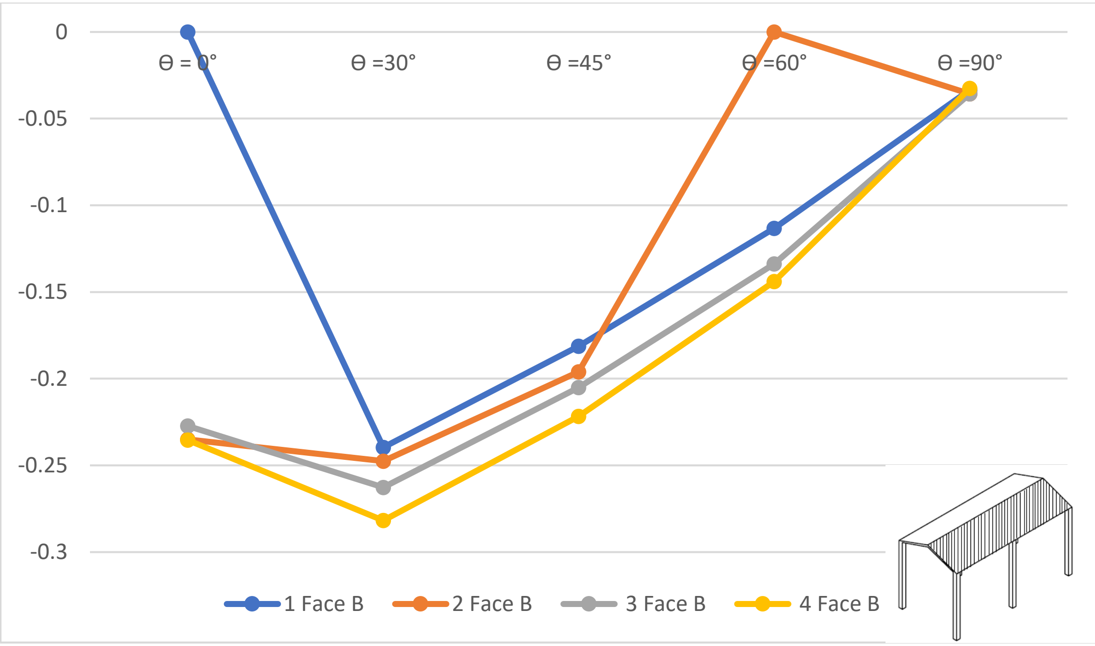

Fig 203 Cpe for roof angle 10° and 1.5b spacing for leeward side

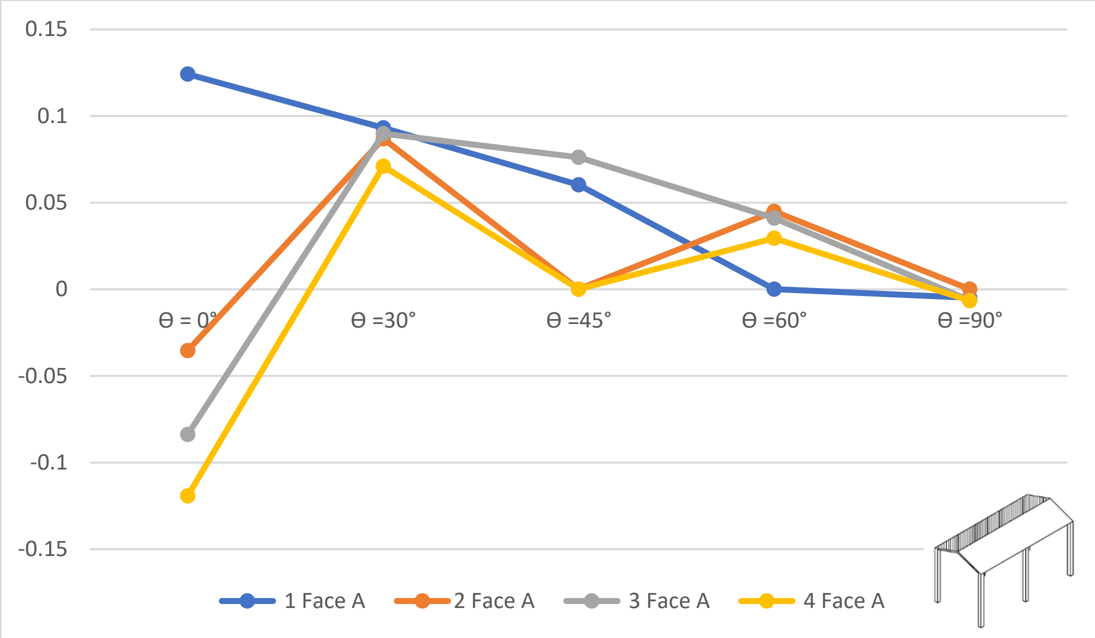

Fig 204 Cpi for roof angle 10° and 1.5b spacing for windward side

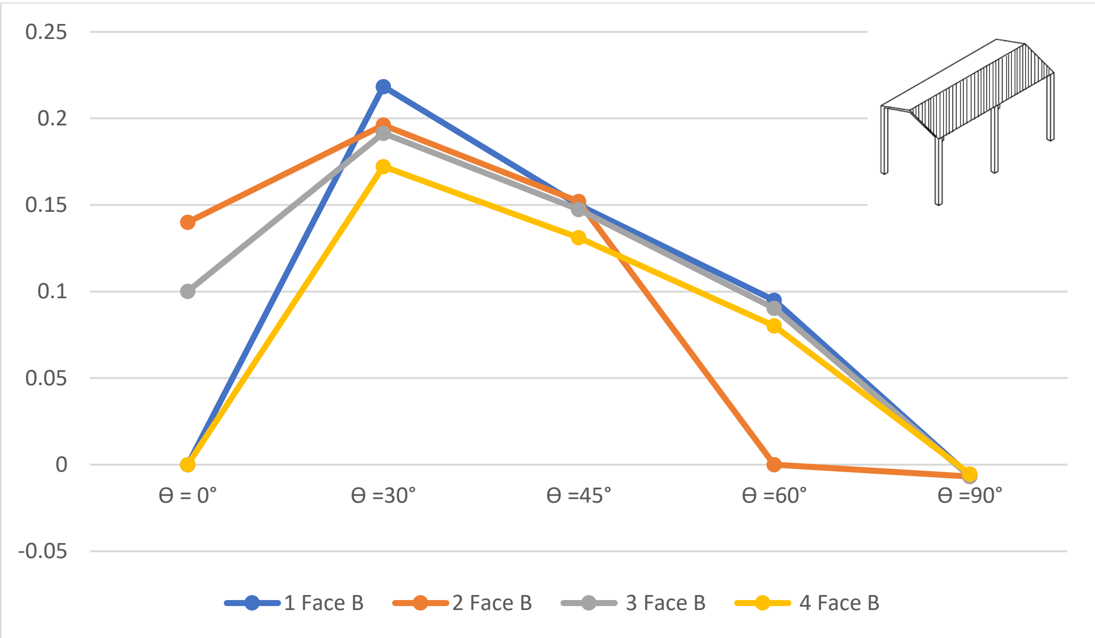

Fig 205 Cpi for roof angle 10° and 1.5b spacing for leeward side

Table 10 Coefficient of Pressure ($Cpext$) at Slope Angle 10°, Spacing 2b

Cpext	1 Face A	1 Face B	2 Face A	2 Face B	3 Face A	3 Face B	4 Face A	4 Face B
Ɵ = 0°	-0.138104	-0.208746	-0.010696	-0.240807	0.0156796	-0.231652	0.0185178	-0.236387
Ɵ =30°	-0.141044	-0.192227	-0.179247	-0.252573	-0.200418	-0.262401	-0.213177	-0.278051
Ɵ =45°	-0.1098	-0.147268	-0.147922	-0.198088	-0.158802	-0.205116	-0.165848	-0.218196
Ɵ =60°	-0.069986	-0.092929	-0.086005	-0.125527	-0.091663	-0.130606	-0.096687	-0.139702
Ɵ =90°	-0.030528	-0.030665	-0.032944	-0.032629	-0.032920	-0.032844	-0.031073	-0.030600

Table 11 Coefficient of Pressure ($Cp\text{int}$) at Slope Angle 10°, Spacing 2b

Cpint	1 Face A	1 Face B	2 Face A	2 Face B	3 Face A	3 Face B	4 Face A	4 Face B
Ɵ = 0°	0.115065	0.228597	-0.032108	0.14338	-0.075682	0.108646	-0.111581	0.0803643
Ɵ =30°	0.0851165	0.212885	0.0966725	0.199789	0.0984326	0.196558	0.0851826	0.179709
Ɵ =45°	0.0519952	0.142775	0.0626627	0.144542	0.0600219	0.139843	0.0474899	0.126777
Ɵ =60°	0.0406973	0.0916573	0.0394096	0.0899137	0.0350174	0.0862737	0.026617	0.0776144
Ɵ =90°	-0.003562	-0.004805	-0.004998	-0.005350	-0.005499	-0.005381	-0.004987	-0.004222

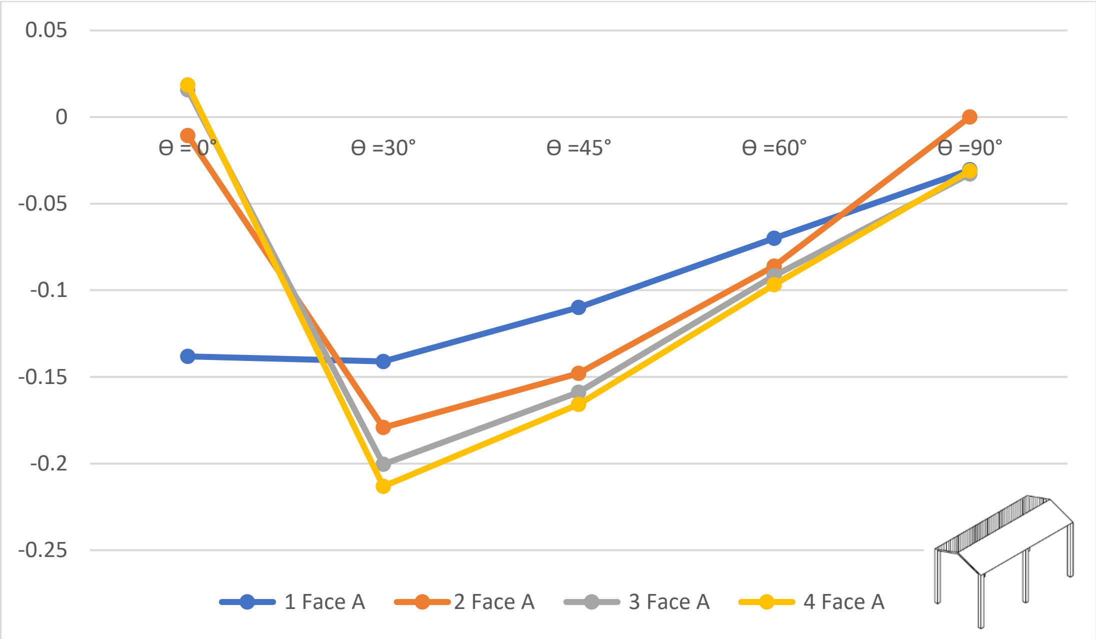

Fig 206 Cpe for roof angle 10° and 2b spacing for leeward side

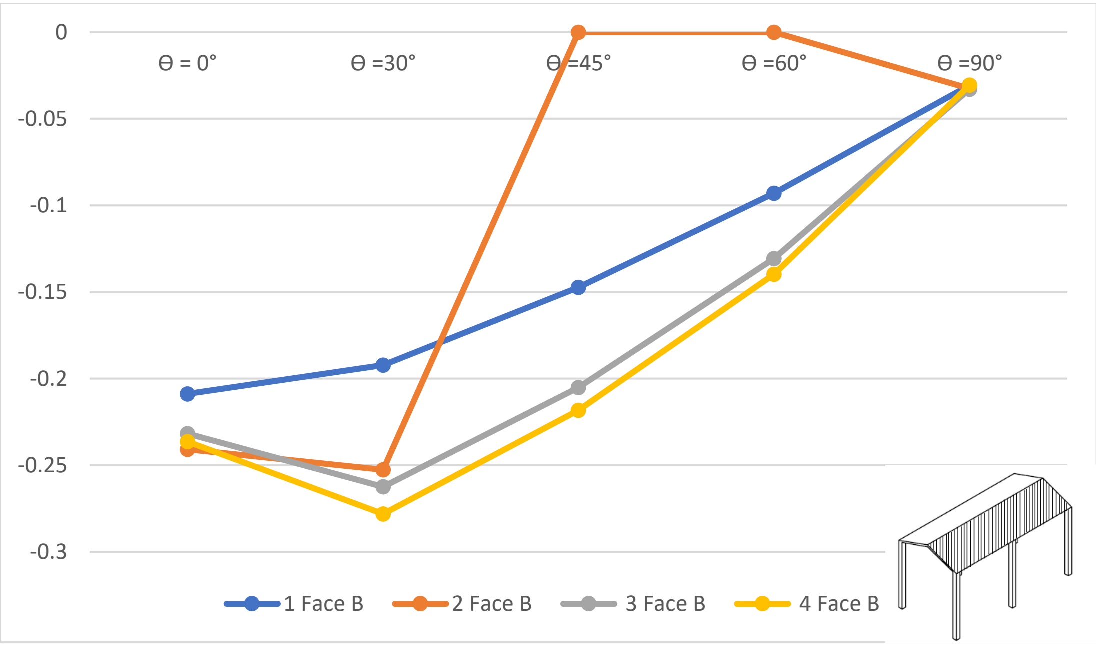

Fig 207 Cpe for roof angle 10° and 2b spacing for leeward side

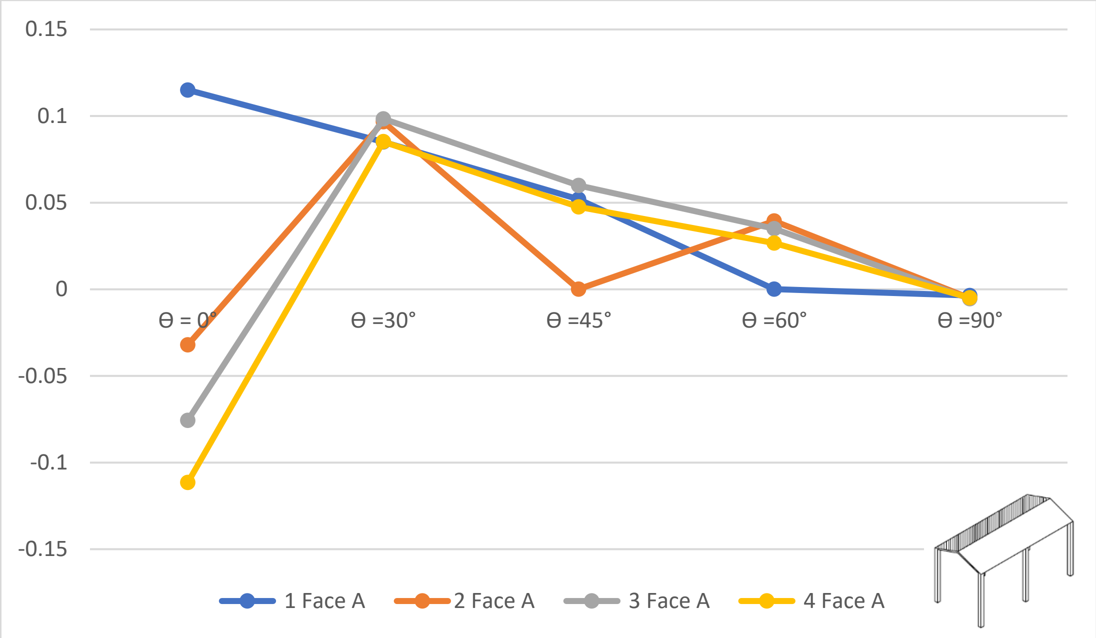

Fig 208 Cpi for roof angle 10° and 2b spacing for windward side

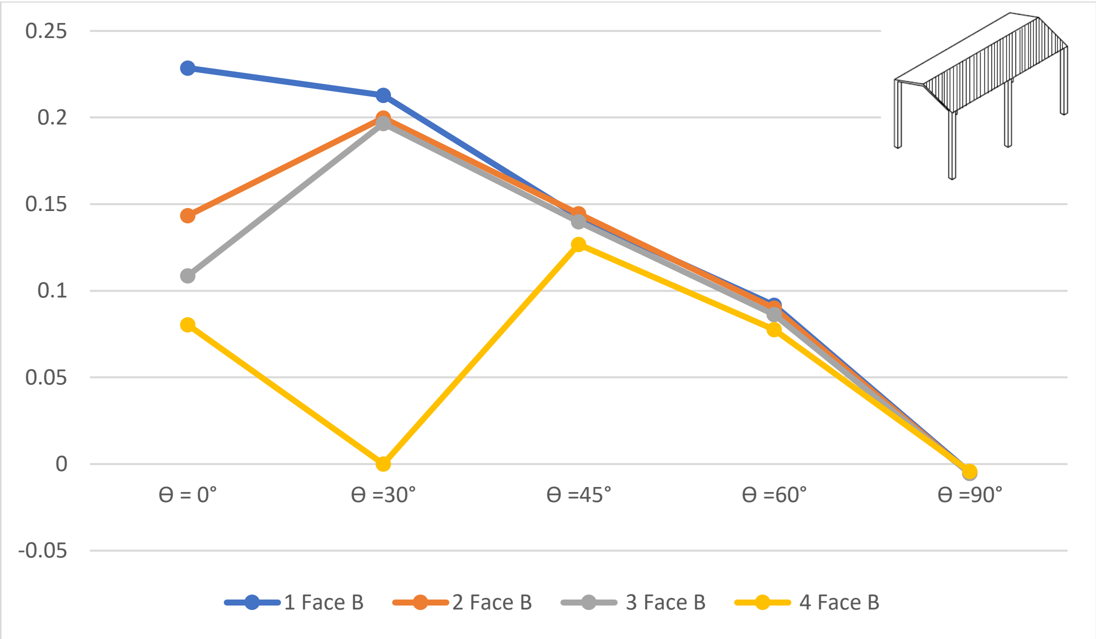

Fig 209 Cpi for roof angle 10° and 2b spacing for leeward side

Slope Angle = 20°

Table 12 Coefficient of Pressure ($Cpext$) at Slope Angle 20°, Spacing 0

Cpext	1 Face A	1 Face B	2 Face A	2 Face B	3 Face A	3 Face B	4 Face A	4 Face B
ϴ = 0°	-0.136512	-0.243456	-0.002040	-0.125988	0.0167814	-0.137571	-0.048550	-0.368098
ϴ =30°	-0.190029	-0.283777	-0.044293	-0.20437	-0.049702	-0.248273	-0.131763	-0.532136
ϴ =45°	-0.198743	-0.264568	-0.113213	-0.258988	-0.130635	-0.283268	-0.191886	-0.482618
ϴ =60°	-0.233701	0.506668	-0.312717	-0.337964	-0.118577	0.202477	-0.38243.4	-0.111215
ϴ =90°	-0.142182	-0.199731	-0.218635	-0.231057	-0.231137	-0.218801	-0.200544	-0.142513

Table 13Coefficient of Pressure ($Cp\text{int}$) at Slope Angle 20°, Spacing 0

Cpint	1 Face A	1 Face B	2 Face A	2 Face B	3 Face A	3 Face B	4 Face A	4 Face B
ϴ = 0°	-0.173819	0.0392802	-0.069823	0.0503973	-0.075869	0.0489498	-0.100904	0.0519373
ϴ =30°	-0.081777	0.199592	-0.080634	0.136327	0.084484	0.12423	-0.096454	0.122157
ϴ =45°	-0.038921	0.17932	-0.098891	0.11509	-0.106479	0.108541	-0.130558	0.0989472
ϴ =60°	-0.101103	-0.27144.1	-0.78126.9	0.1071510	-0.126559	-0.120237	-0.47267.4	-0.25963
ϴ =90°	-0.067982	-0.095874	-0.094681	-0.099430	-0.100236	-0.096269	-0.097179	-0.069506

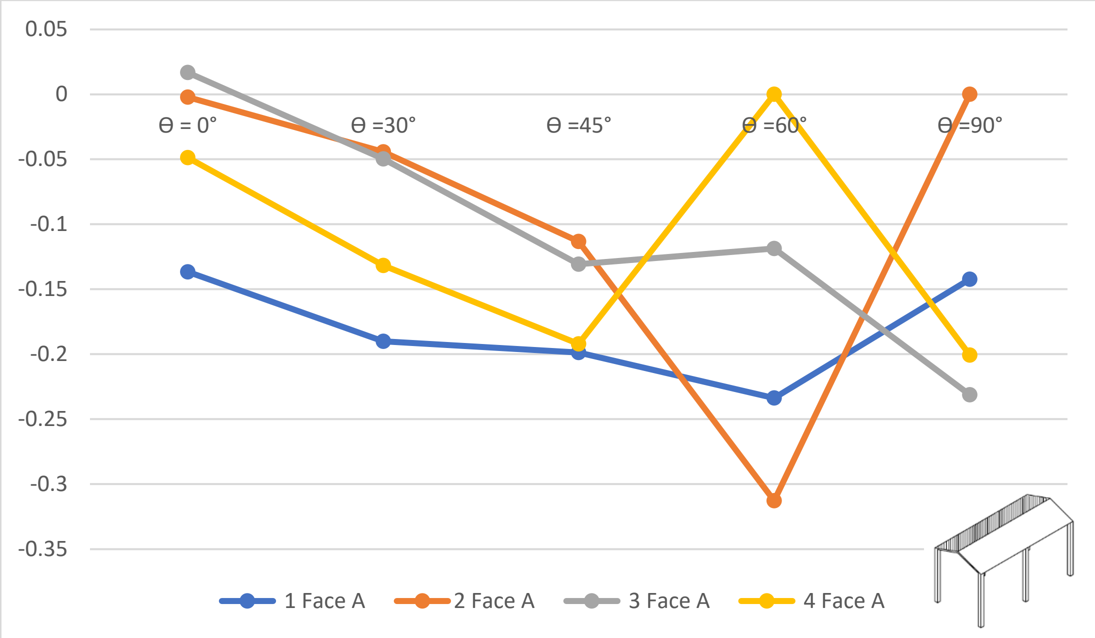

Fig 210 Cpe for roof angle 20° and zero spacing for windward side

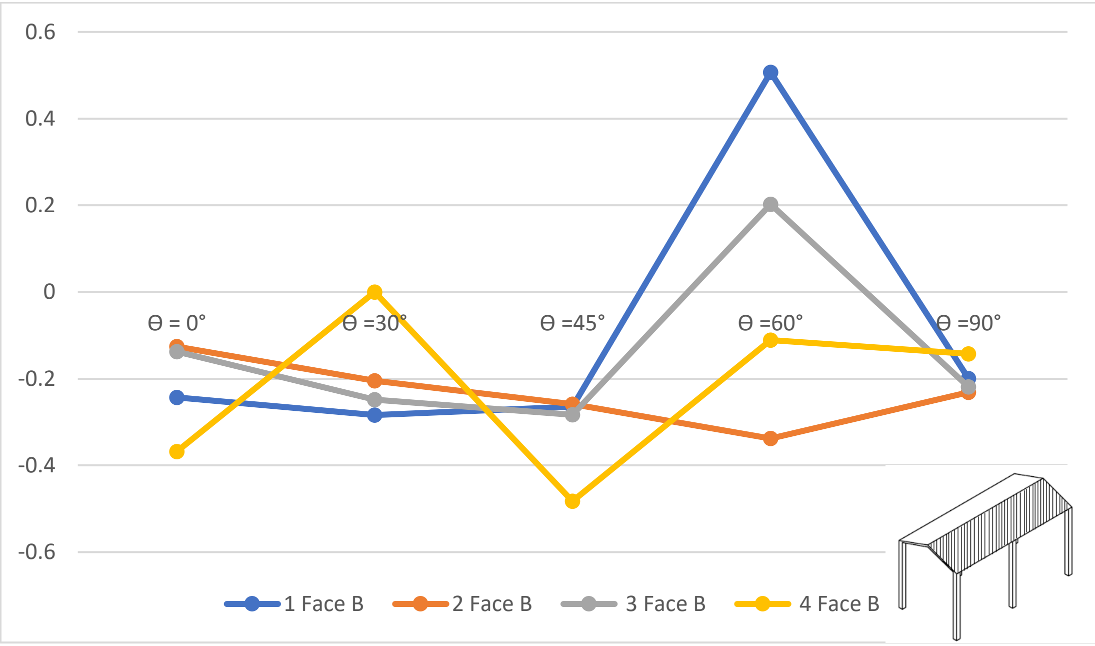

Fig 211 Cpe for roof angle 20° and zero spacing for leeward side

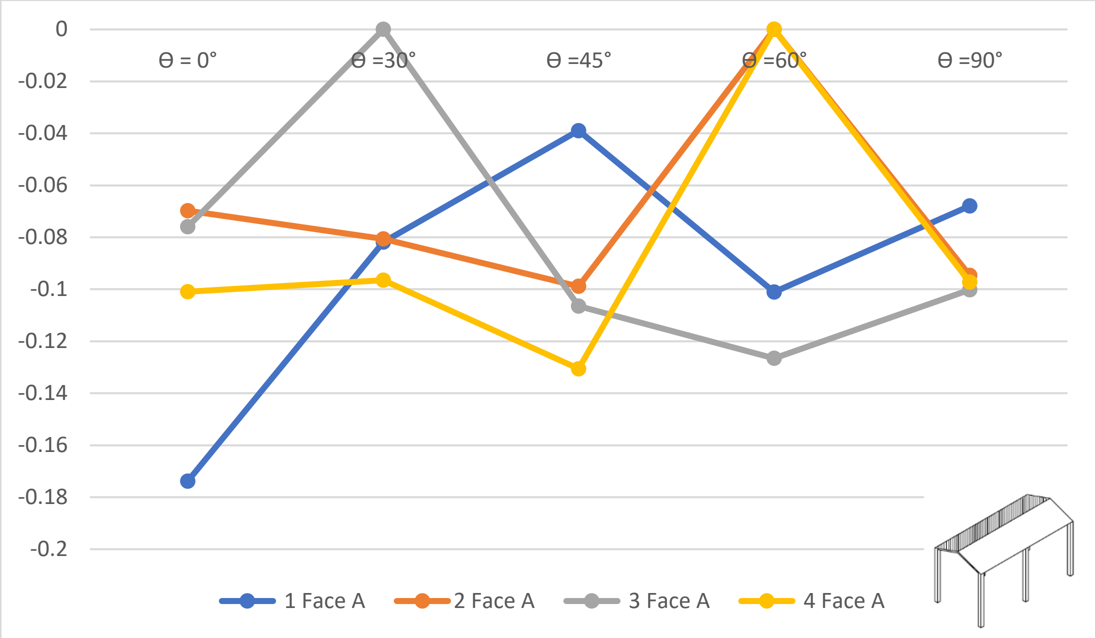

Fig 211 Cpi for roof angle 20° and zero spacing for windward side

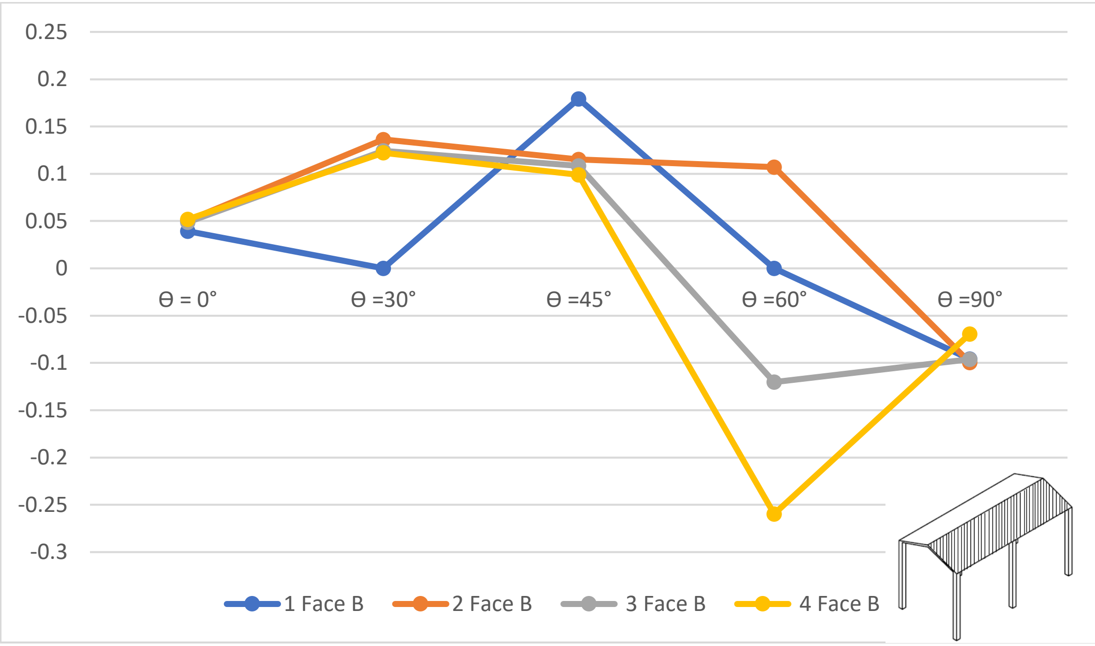

Fig 212 Cpi for roof angle 20° and zero spacing for leeward side

Table 14 Coefficient of Pressure ($Cpext$) at Slope Angle 20°, Spacing 0.5b

Cpext	**1 Face A**	**1 Face B**	**2 Face A**	**2 Face B**	**3 Face A**	**3 Face B**	**4 Face A**	**4 Face B**
ϴ = 0°	-0.088883	-0.41688	0.0617159	-0.297483	0.0433459	-0.342228	0.0167721	-0.451628
ϴ =30°	-0.088646	-0.416626	0.062018	-0.29709	0.0435989	-0.341757	0.0168922	-0.451114
ϴ =45°	-0.0938	-0.295248	-0.095023	-0.299541	-0.137564	-0.332112	-0.160413	-0.38693
ϴ =60°	-0.09486	-0.296358	-0.096086	-0.300775	-0.138597	-0.333252	-0.161371	-0.387914
ϴ =90°	-0.049054	-0.053283	-0.059494	-0.060354	-0.060449	-0.059826	0.052841	-0.049550

Table 15 Coefficient of Pressure ($Cp\text{int}$) at Slope Angle 20°, Spacing 0.5b

Cpint	**1 Face A**	**1 Face B**	**2 Face A**	**2 Face B**	**3 Face A**	**3 Face B**	**4 Face A**	**4 Face B**
ϴ = 0°	0.152988	0.349955	-0.156535	-0.028703	-0.115381	-0.029558	-0.184765	-0.077346
ϴ =30°	0.15324	0.350184	-0.142021	-0.028415	-0.114991	-0.029237	-0.184831	-0.077733
ϴ =45°	0.108603	0.239455	0.0559931	0.21864	0.0510747	0.20655	-0.000638	0.170954
ϴ =60°	0.10751	0.238415	0.0549075	0.217587	0.0496638	0.205512	-0.001600	-0.001600
ϴ =90°	-0.011369	-0.015298	-0.015047	-0.015151	-0.015297	-0.014523	-0.015773	-0.015773

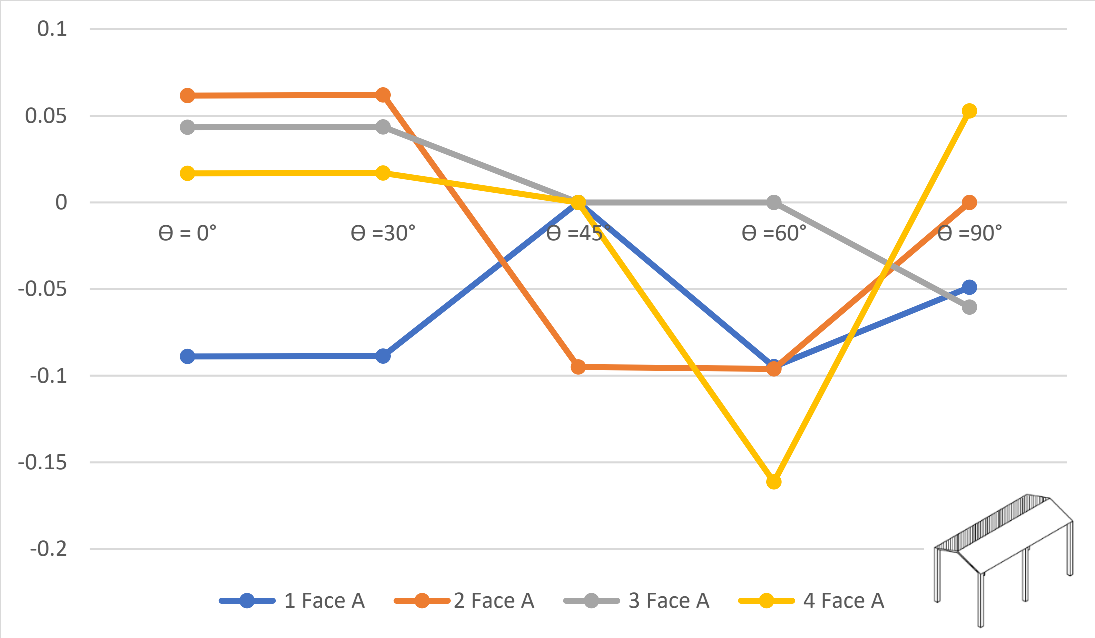

Fig 213Cpi for roof angle 20° and 0.5b spacing for windward side

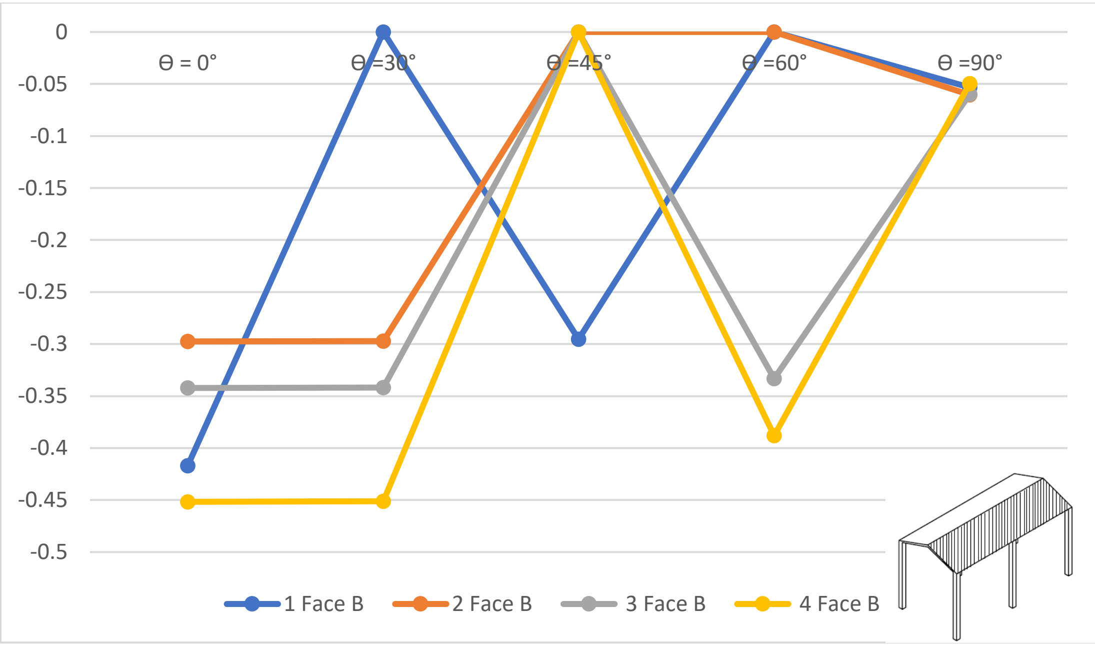

Fig 214 Cpi for roof angle 20° and 0.5b spacing for leeward side

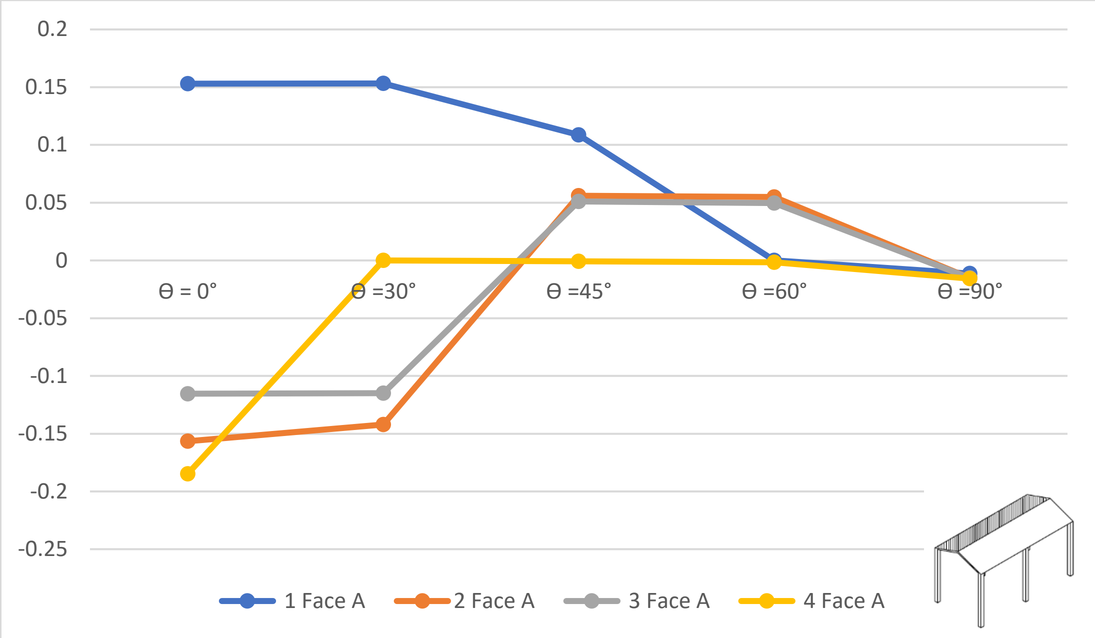

Fig 215 Cpi for roof angle 20° and 0.5b spacing for windward side

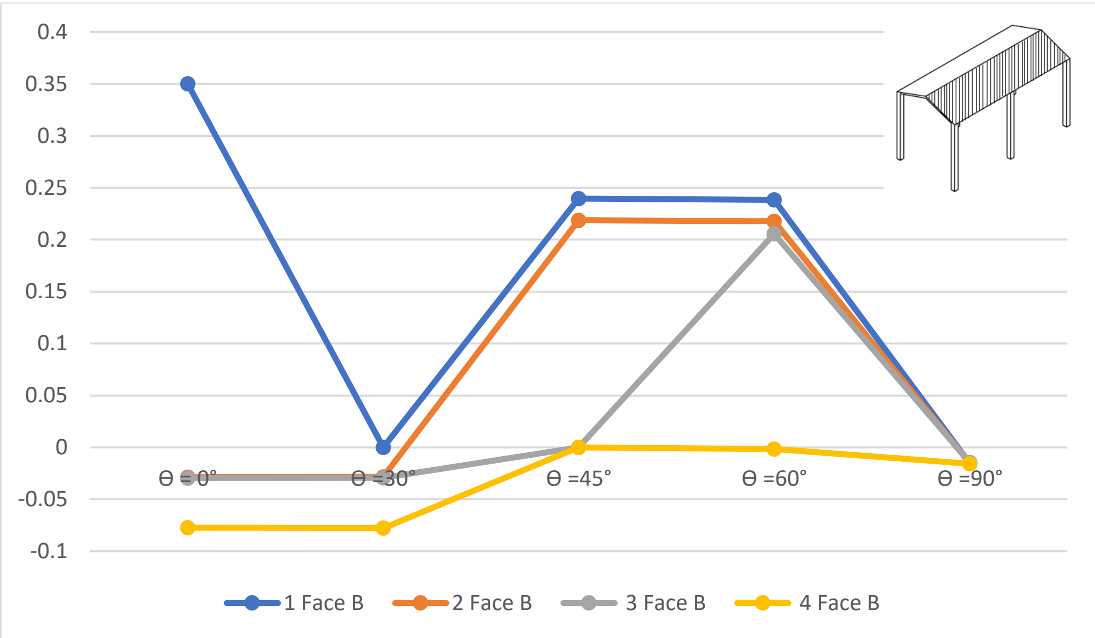

Fig 216 Cpi for roof angle 20° and 0.5b spacing for leeward side

Table 16 Coefficient of Pressure ($Cpext$) at Slope Angle 20°, Spacing b

Cpext	1 Face A	1 Face B	2 Face A	2 Face B	3 Face A	3 Face B	4 Face A	4 Face B
Ɵ = 0°	-0.088507	-0.507378	0.0175217	-0.41155	0.0212104	-0.401351	0.0216318	-0.442277
Ɵ =30°	-0.096043	-0.44038	-0.069476	-0.423974	-0.112345	-0.450098	-0.130175	-0.494773
Ɵ =45°	-0.074023	-0.324942	-0.117129	-0.342653	-0.1471	-0.363016	-0.164102	-0.399271
Ɵ =60°	-0.044784	-0.189731	-0.089719	-0.215149	-0.108245	-0.232685	-0.118382	-0.253229
Ɵ =90°	-0.043663	-0.044269	-0.048239	-0.048611	-0.047706	-0.047950	0.0438436	-0.043457

Table 17 Coefficient of Pressure ($Cp\text{int}$) at Slope Angle 20°, Spacing b

Cpint	1 Face A	1 Face B	2 Face A	2 Face B	3 Face A	3 Face B	4 Face A	4 Face B
Ɵ = 0°	0.147240	0.333273	-0.131033	0.0941997	-0.17907	0.0305532	-0.230032	-0.031219
Ɵ =30°	0.118682	0.304196	0.0147051	0.258604	0.0029398	0.237103	-0.025766	0.207359
Ɵ =45°	0.0938242	0.224166	0.101168	0.219858	0.0843882	0.212483	0.0672441	0.188487
Ɵ =60°	0.0621676	0.140969	0.0699391	0.139419	0.0647918	0.133861	0.0482776	0.118571
Ɵ =90°	-0.008050	-0.008700	-0.007918	-0.006479	-0.002647	-0.006046	-0.008902	-0.006702

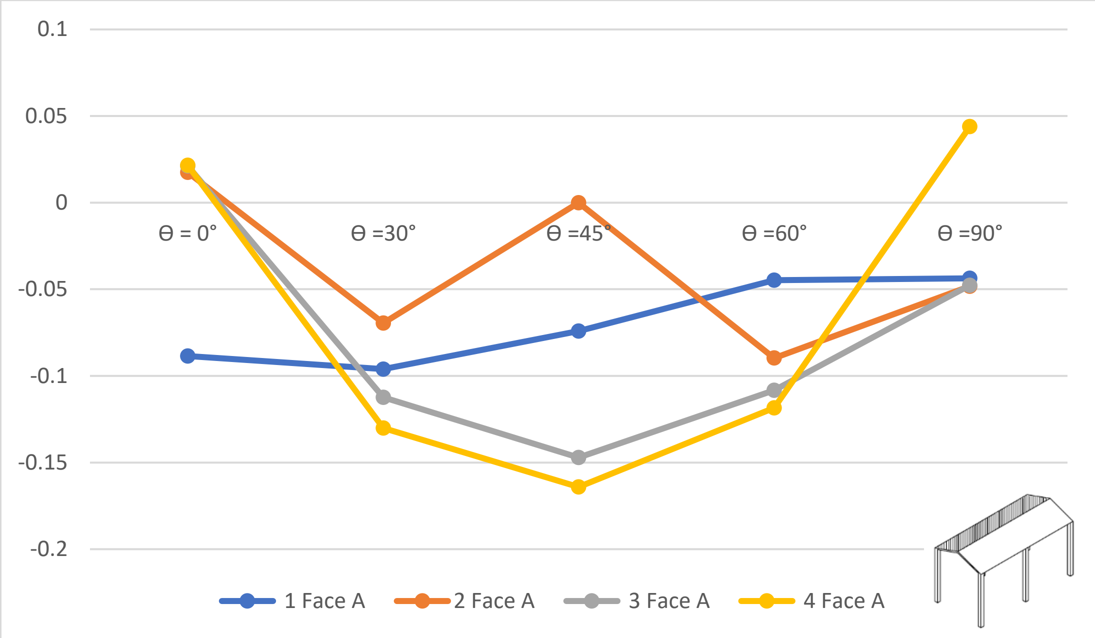

Fig 217 Cpe for roof angle 20° and b spacing for windward side

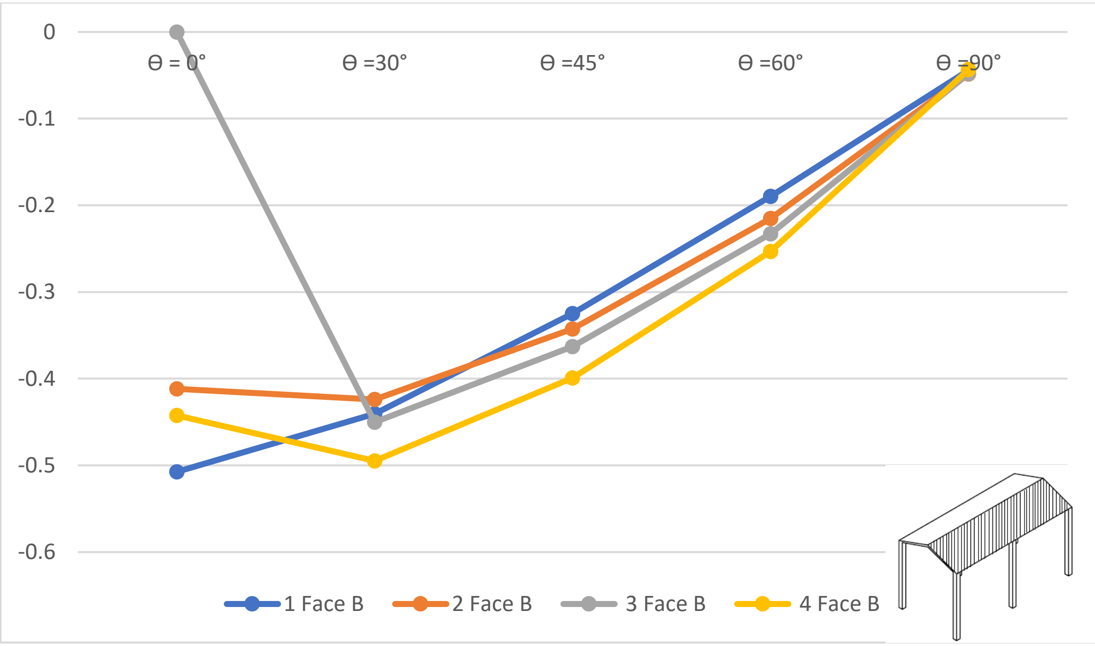

Fig 218 Cpe for roof angle 20° and b spacing for leeward side

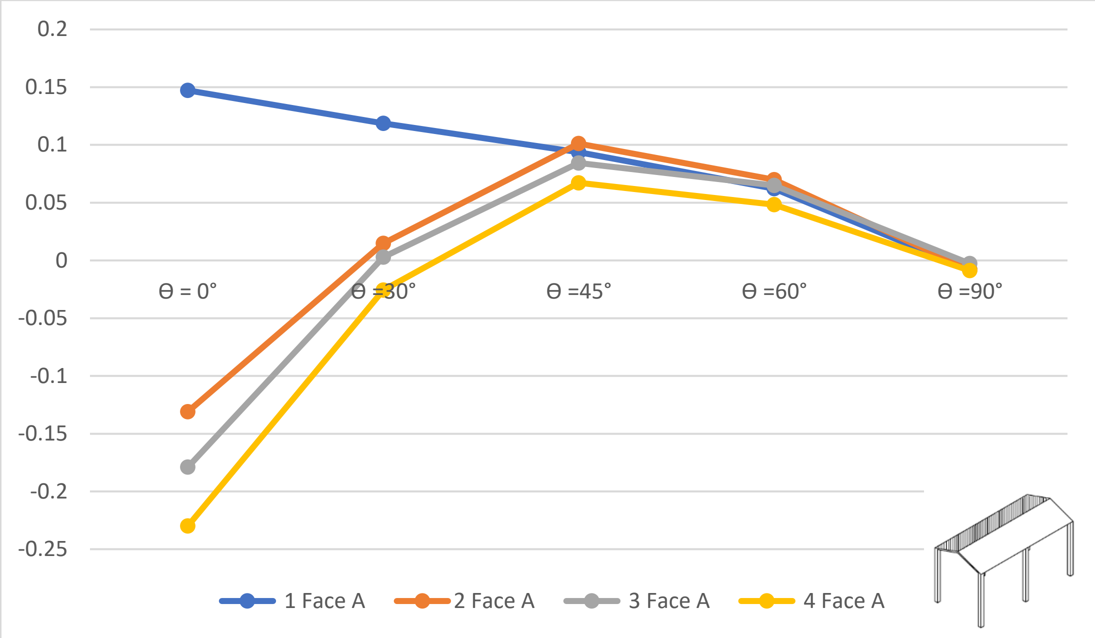

Fig 219 Cpi for roof angle 20° and b spacing for windward side

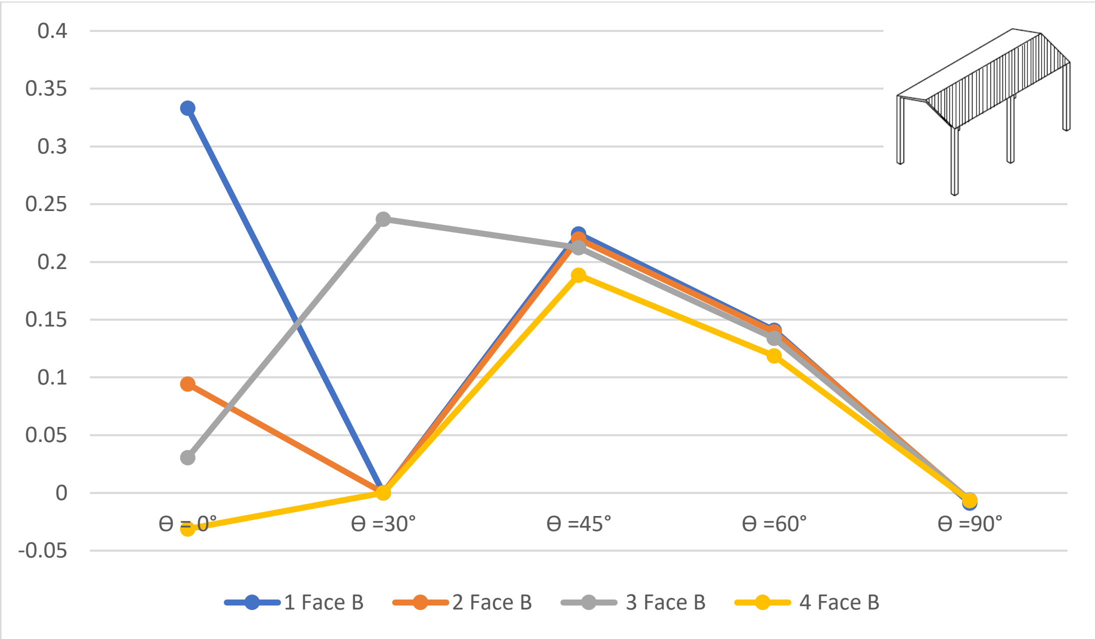

Fig 220 Cpi for roof angle 20° and b spacing for leeward side

Table 18 Coefficient of Pressure ($Cpext$) at Slope Angle 20°, Spacing 1.5b

Cpext	1 Face A	1 Face B	2 Face A	2 Face B	3 Face A	3 Face B	4 Face A	4 Face B
ϴ = 0°	-0.082571	-0.467472	0.0184975	-0.340561	0.0175337	-0.33505	-0.004203	-0.377229
ϴ =30°	-0.142115	-0.454571	-0.142765	-0.445017	-0.173467	-0.466299	-0.195011	-0.502302
ϴ =45°	-0.110177	-0.338931	-0.174159	-0.353898	-0.198494	-0.369581	-0.214162	-0.398032
ϴ =60°	-0.065925	-0.201191	-0.095685	-0.218288	-0.105177	-0.227285	-0.113661	-0.2456
ϴ =90°	-0.046946	-0.047210	-0.050612	-0.050785	-0.050851	-0.050450	-0.047543	-0.046416

Table 19 Coefficient of Pressure ($Cp\text{int}$) at Slope Angle 20°, Spacing 1.5b

Cpint	1 Face A	1 Face B	2 Face A	2 Face B	3 Face A	3 Face B	4 Face A	4 Face B
ϴ = 0°	0.0656561	0.26761	-0.166498	-0.001610	-0.170933	-0.036886	-0.193456	-0.060603
ϴ =30°	0.0920745	0.276719	0.0531459	0.252167	0.051289	0.244707	0.0273359	0.223088
ϴ =45°	0.058563	0.197807	0.0884055	0.204974	0.0884241	0.201239	0.0671066	0.182589
ϴ =60°	0.0399129	0.118479	0.0424225	0.117701	0.0369636	0.112862	0.0223424	0.100718
ϴ =90°	-0.017474	-0.018650	-0.021593	-0.021002	-0.020583	-0.020106	-0.018792	-0.017429

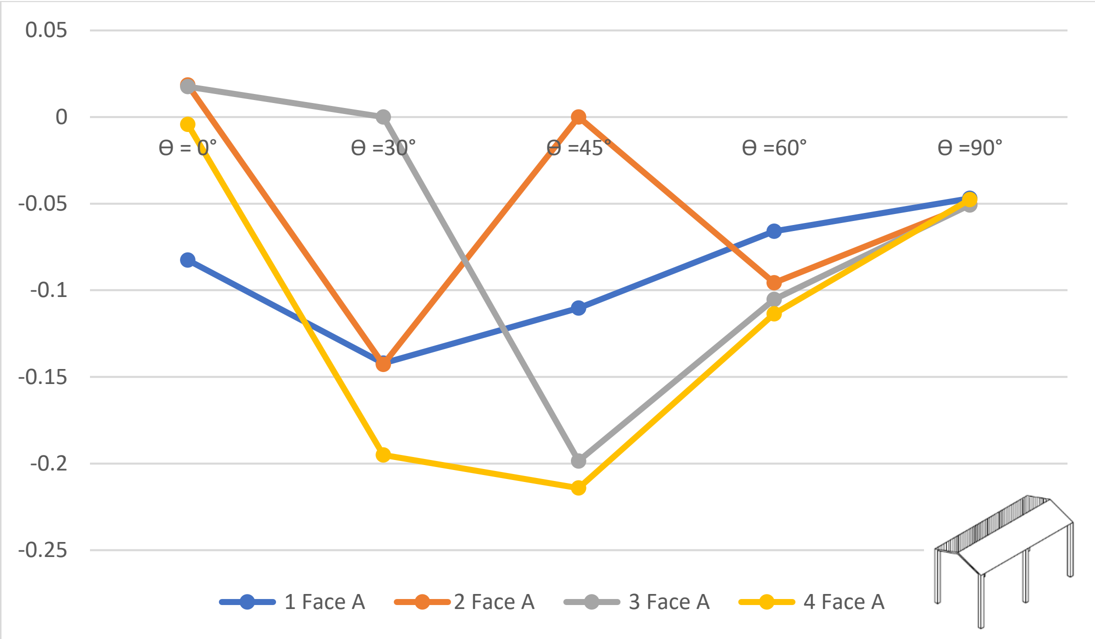

Fig 221 Cpe for roof angle 20° and 1.5b spacing for windward side

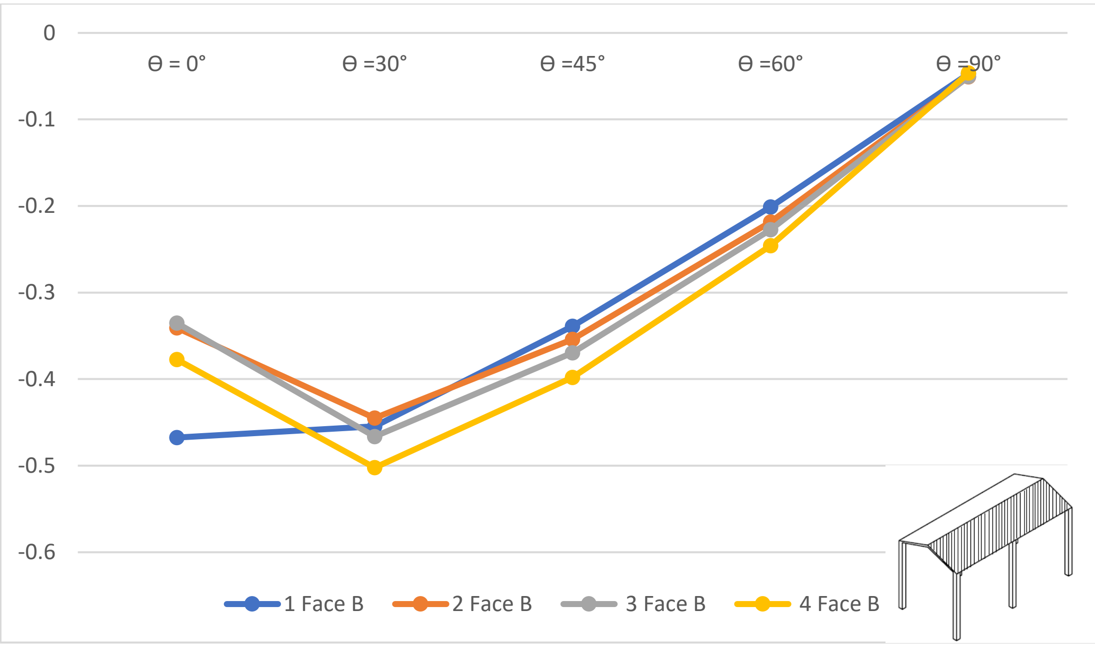

Fig 222 Cpe for roof angle 20° and 1.5b spacing for leeward side

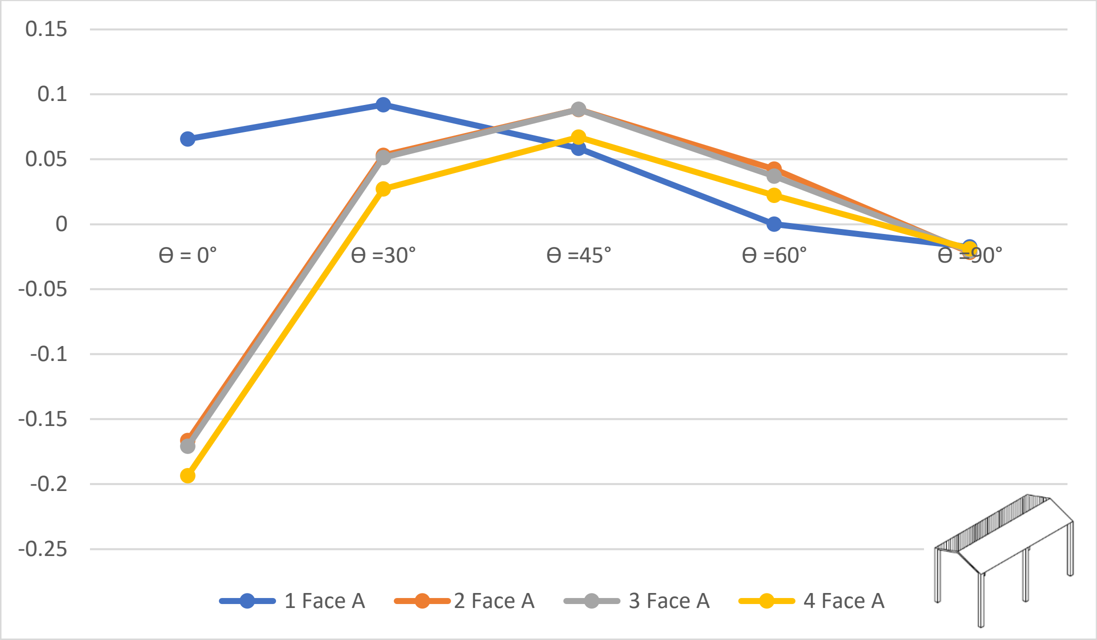

Fig 223 Cpi for roof angle 20° and 1.5b spacing for windward side

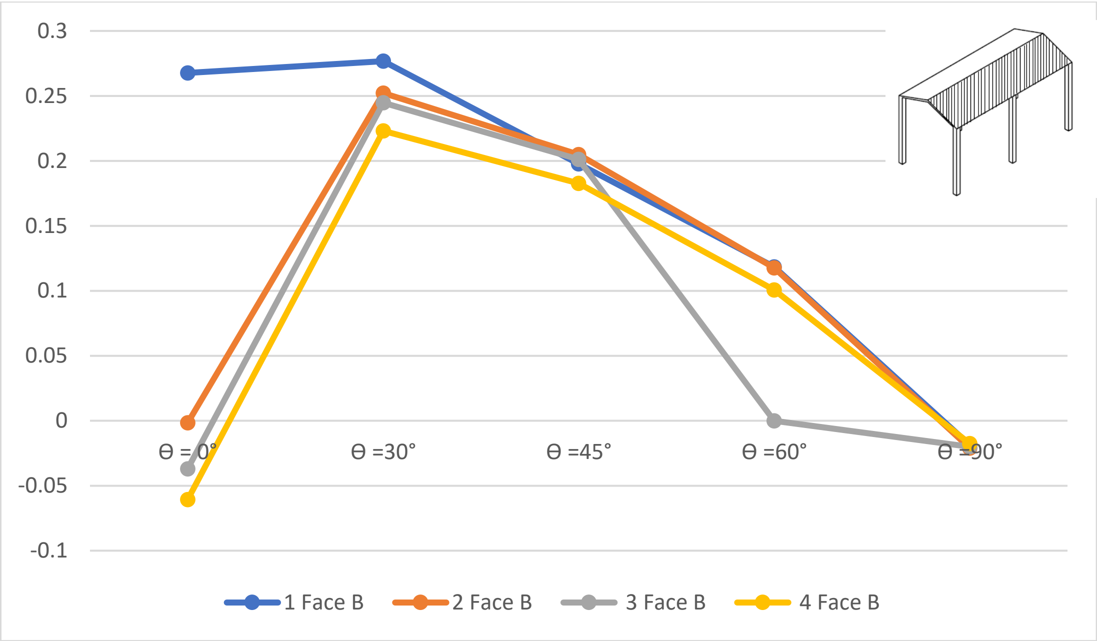

Fig 224 Cpi for roof angle 20° and 1.5b spacing for leeward side

Table 20 Coefficient of Pressure ($Cpext$) at Slope Angle 20°, Spacing 2b

Cpext	1 Face A	1 Face B	2 Face A	2 Face B	3 Face A	3 Face B	4 Face A	4 Face B
ϴ = 0°	-0.119075	-0.490922	-0.018032	-0.398893	-0.013930	-0.417597	-0.022691	-0.46426
ϴ =30°	-0.146532	-0.455469	-0.181371	-0.450716	-0.210271	-0.466674	-0.226475	-0.493074
ϴ =45°	-0.108586	-0.339279	-0.156424	-0.359208	-0.173496	-0.372477	-0.185687	-0.392851
ϴ =60°	-0.067442	-0.202294	-0.086010	-0.215377	-0.093982	-0.223824	-0.101908	-0.238796
ϴ =90°	-0.046329	-0.045958	-0.047358	-0.047958	-0.048016	-0.047636	-0.045999	-0.046255

Table 21 Coefficient of Pressure ($Cp\text{int}$) at Slope Angle 20°, Spacing 2b

Cpint	1 Face A	1 Face B	2 Face A	2 Face B	3 Face A	3 Face B	4 Face A	4 Face B
ϴ = 0°	0.0601425	0.2695	-0.16135	0.0283631	-0.190245	-0.011001	-0.239126	-0.053692
ϴ =30°	0.0833263	0.267895	0.0967579	0.260472	0.0964918	0.252668	0.0781828	0.233055
ϴ =45°	0.0522305	0.190128	0.0717955	0.194114	0.0658631	0.187819	0.0486222	0.171685
ϴ =60°	0.0389553	0.116601	0.0338833	0.112807	0.0286337	0.107705	0.0168836	0.0957746
ϴ =90°	-0.014988	-0.016356	-0.018861	-0.018930	-0.019377	-0.018857	-0.016784	-0.015456

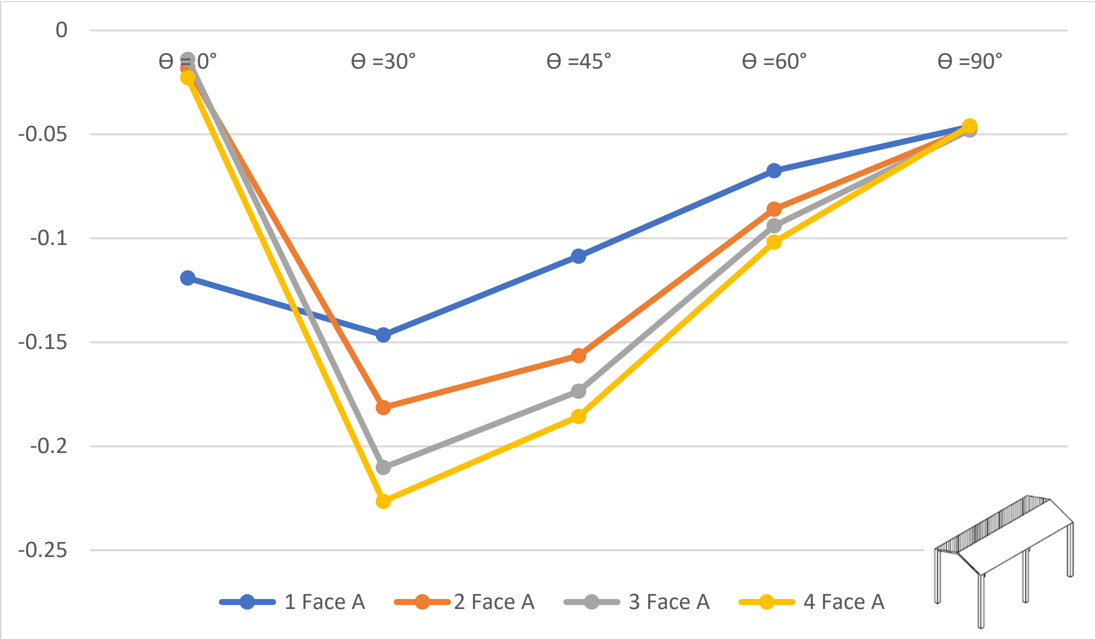

Fig 225 Cpe for roof angle 20° and 2b spacing for windward side

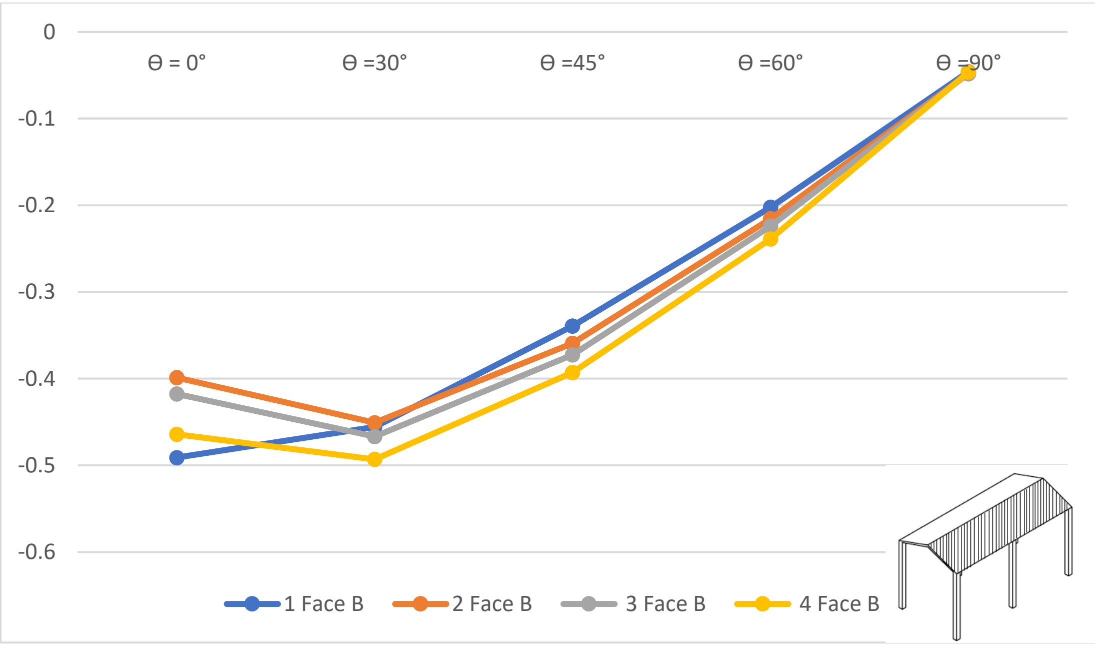

Fig 226 Cpe for roof angle 20° and 2b spacing for leeward side

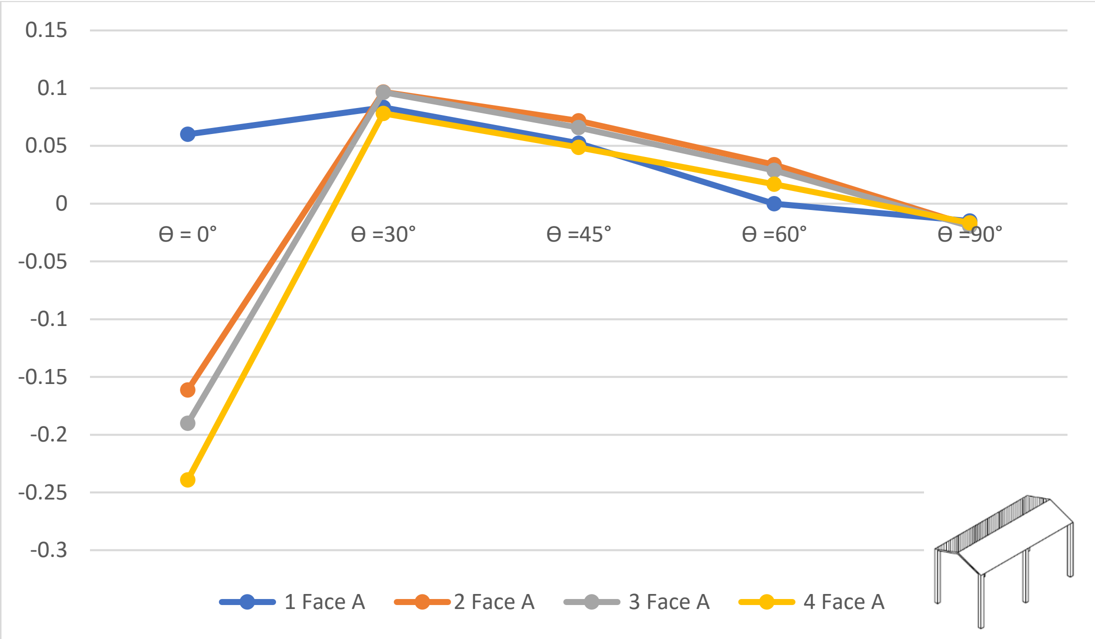

Fig 227 Cpi for roof angle 20° and 2b spacing for windward side

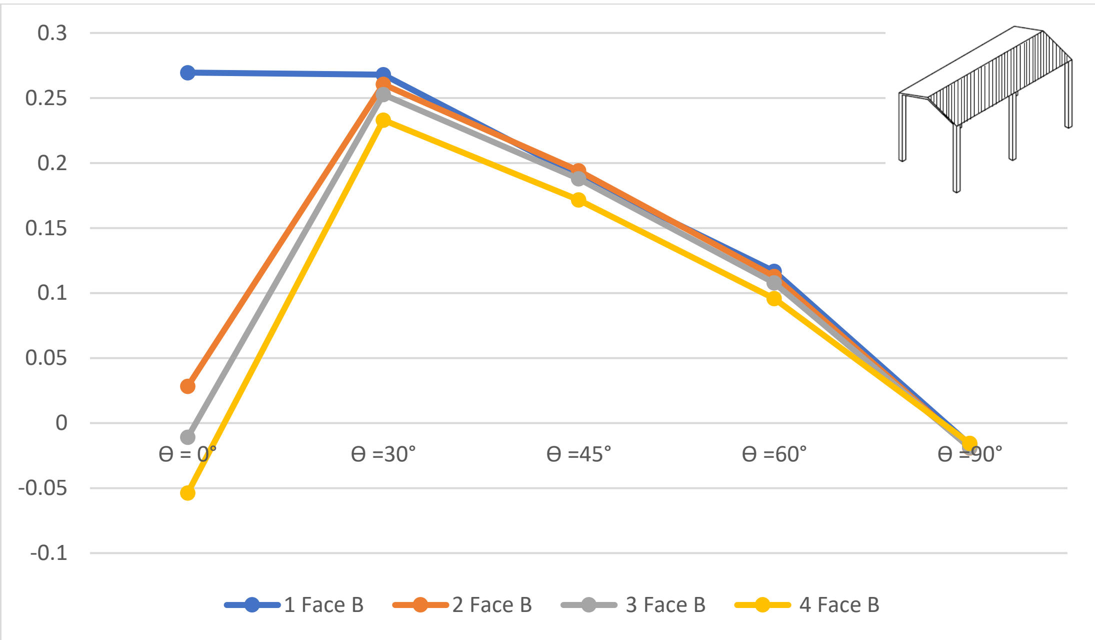

Fig 228 Cpi for roof angle 20° and 2b spacing for leeward side

Slope Angle = 30°

Table 22 Coefficient of Pressure ($Cpext$) at Slope Angle 30°, Spacing 0

Cpext	1 Face A	1 Face B	2 Face A	2 Face B	3 Face A	3 Face B	4 Face A	4 Face B
Ɵ = 0°	0.14053	-0.381143	-0.2181	-0.163257	-0.035905	-0.15732	-0.047915	-0.25161
Ɵ =30°	0.0693672	-0.497329	-0.022457	-0.325394	0.0394617	-0.310811	-0.043662	-0.524055
Ɵ =45°	-0.027737	-0.488896	-0.037639	-0.352646	-0.100804	-0.38044	-0.17324	-0.563329
Ɵ =60°	-0.120857	-0.360094	-0.159883	-0.358242	-0.212153	-0.385768	-0.248686	-0.463928
Ɵ =90°	-0.163756	-0.231702	-0.250072	-0.264331	-0.264276	-0.250279	-0.23169	-0.163403

Table 23 Coefficient of Pressure ($Cp\mathrm{int}$) at Slope Angle 30°, Spacing 0

Cpint	1 Face A	1 Face B	2 Face A	2 Face B	3 Face A	3 Face B	4 Face A	4 Face B
Ɵ = 0°	-0.292299	-0.112574	-0.074401	0.0384506	-0.089674	-0.003507	-0.086983	-0.007935
Ɵ =30°	-0.190927	0.18909	-0.15735	0.149436	-0.153367	0.127058	-0.217746	0.0923169
Ɵ =45°	-0.117222	0.199067	-0.137771	0.131614	-0.158203	0.117894	-0.195456	0.0971604
Ɵ =60°	-0.024384	0.117003	-0.080663	0.108975	-0.092025	0.114891	-0.135498	0.0949251
Ɵ =90°	-0.088815	-0.120366	-0.117445	-0.121595	-0.121421	-0.117181	-0.120664	-0.088966

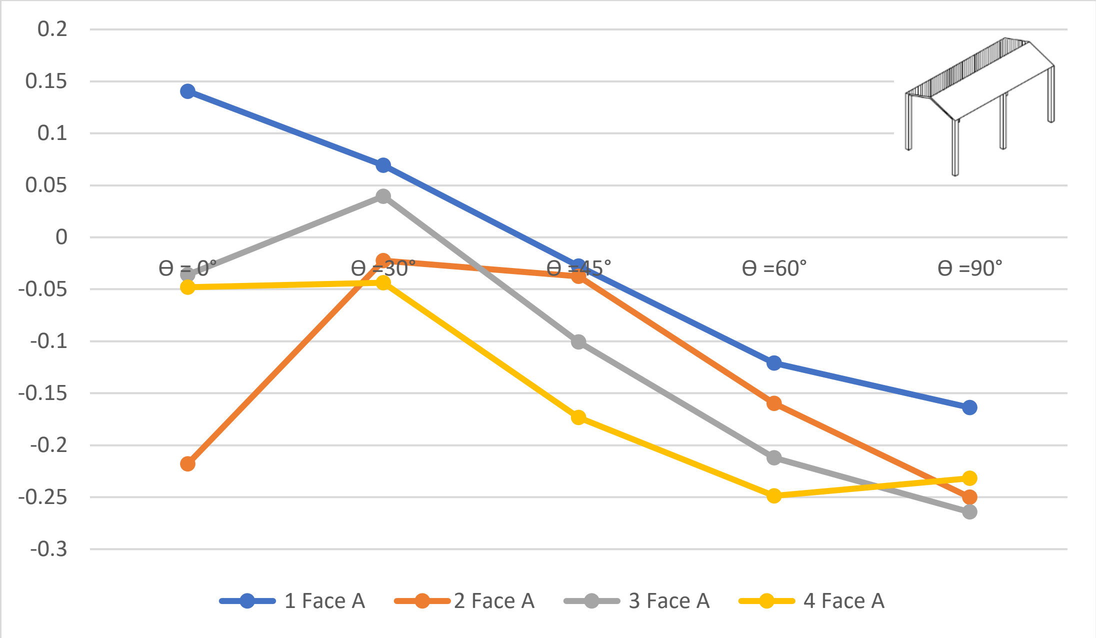

Fig 229 Cpi for roof angle 30° and zero spacing for windward side

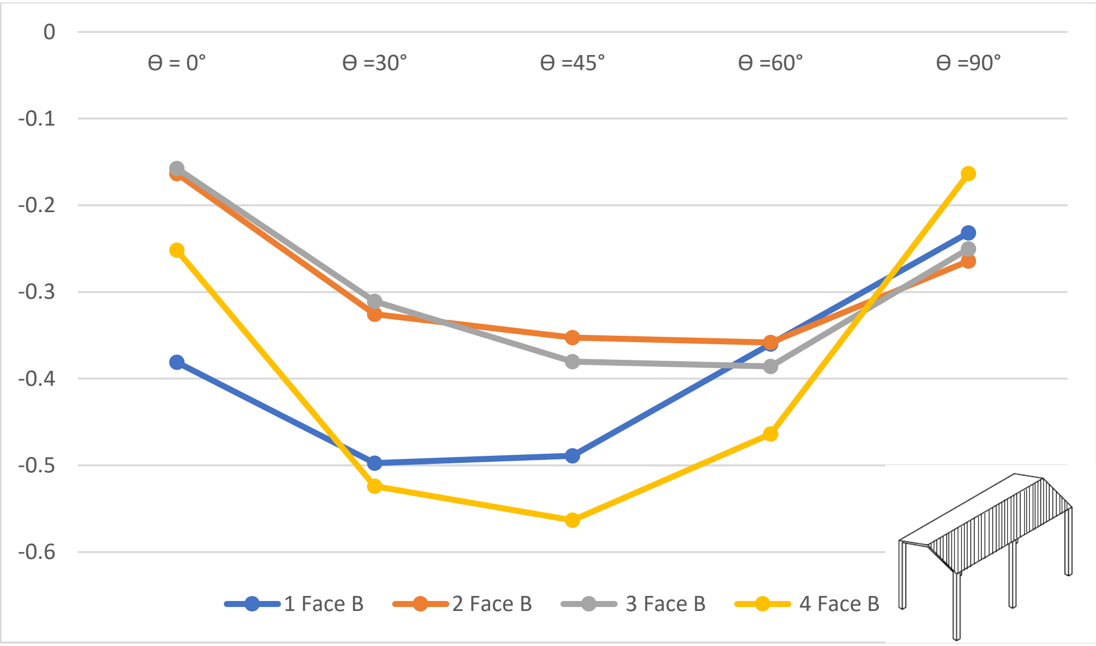

Fig 230 Cpi for roof angle 30° and zero spacing for leeward side

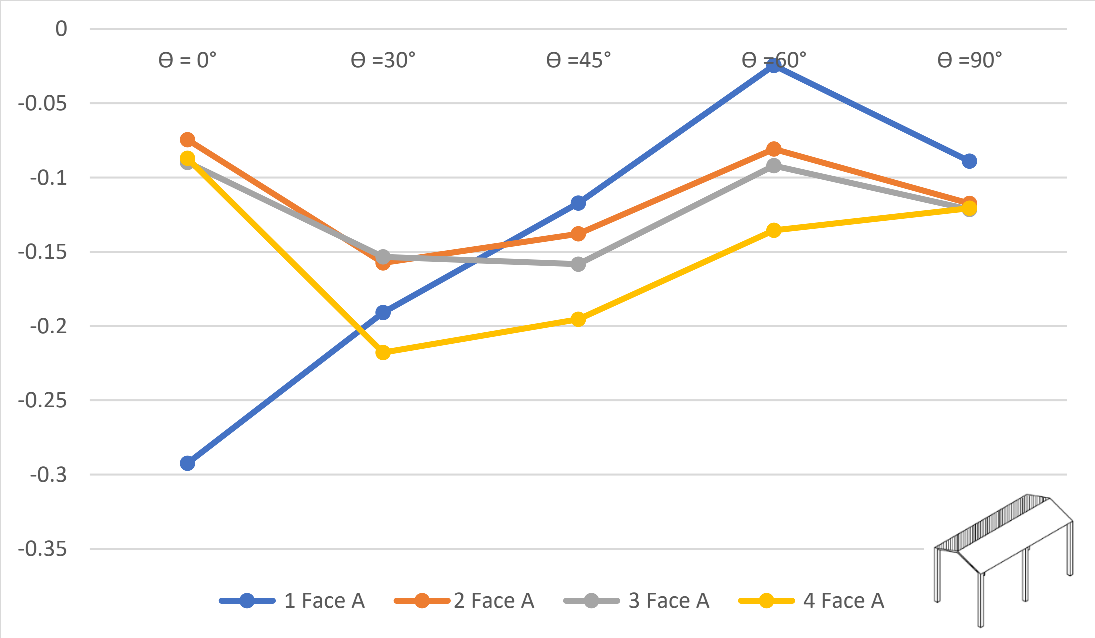

Fig 231 Cpi for roof angle 30° and zero spacing for windward side

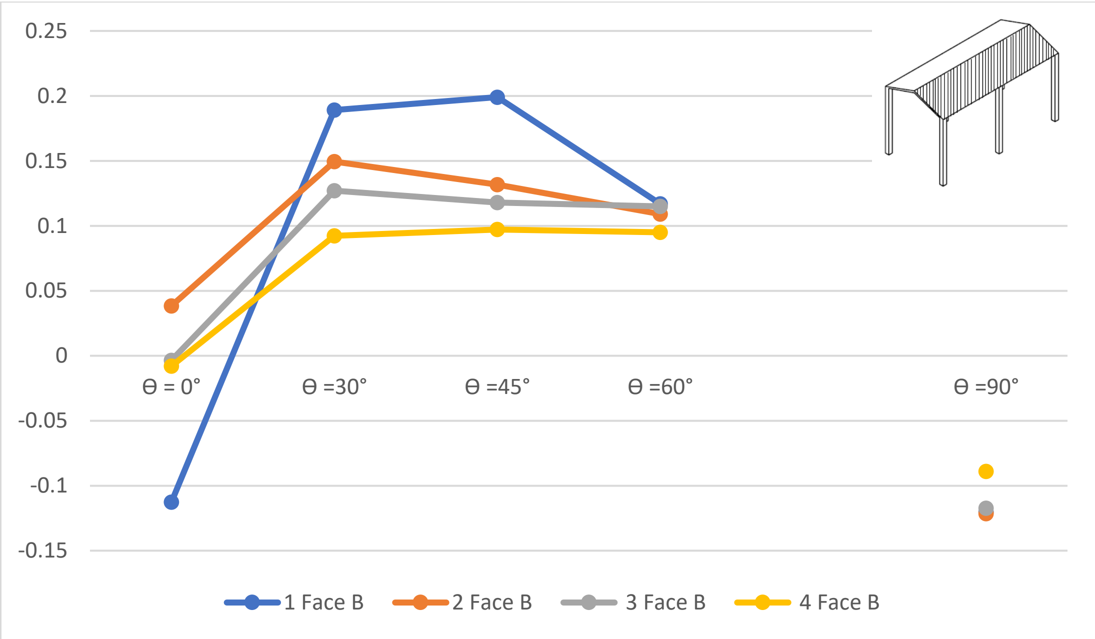

Fig 232 Cpi for roof angle 30° and zero spacing for leeward side

Table 24 Coefficient of Pressure ($Cpext$) at Slope Angle 30°, Spacing 0.5b

Cpext	1 Face A	1 Face B	2 Face A	2 Face B	3 Face A	3 Face B	4 Face A	4 Face B
ϴ = 0°	0.31214	-0.296548	-0.032135	-0.182249	0.0092404	-0.156955	0.0142492	-0.219205
ϴ =30°	0.154586	-0.524726	0.172422	-0.401896	0.14293	-0.416757	0.0928454	-0.567365
ϴ =45°	0.0322647	-0.5368	0.0081238	-0.453344	-0.024096	-0.481513	-0.05488	-0.579569
ϴ =60°	-0.018125	-0.31363	-0.099249	-0.336434	-0.129907	-0.364464	-0.144682	-0.414445
ϴ =90°	-0.060963	-0.063249	-0.070693	-0.070237	-0.070307	-0.070507	-0.063354	-0.060634

Table 25 Coefficient of Pressure ($Cp\text{int}$) at Slope Angle 30°, Spacing 0.5b

Cpint	1 Face A	1 Face B	2 Face A	2 Face B	3 Face A	3 Face B	4 Face A	4 Face B
ϴ = 0°	-0.22653	-0.006498	0.0830023	0.234973	-0.056241	0.0659357	-0.09376	-0.004160
ϴ =30°	-0.025451	0.260808	-0.213521	0.166087	-0.206238	0.136868	-0.273992	0.0775528
ϴ =45°	0.0296308	0.264801	-0.008178	0.237321	-0.034095	0.217657	-0.109212	0.168987
ϴ =60°	0.040191	0.153385	0.0676114	0.158697	0.0651402	0.155012	0.0343387	0.13319
ϴ =90°	-0.024400	-0.028693	-0.028191	-0.029231	-0.029097	-0.028097	-0.029024	-0.024526

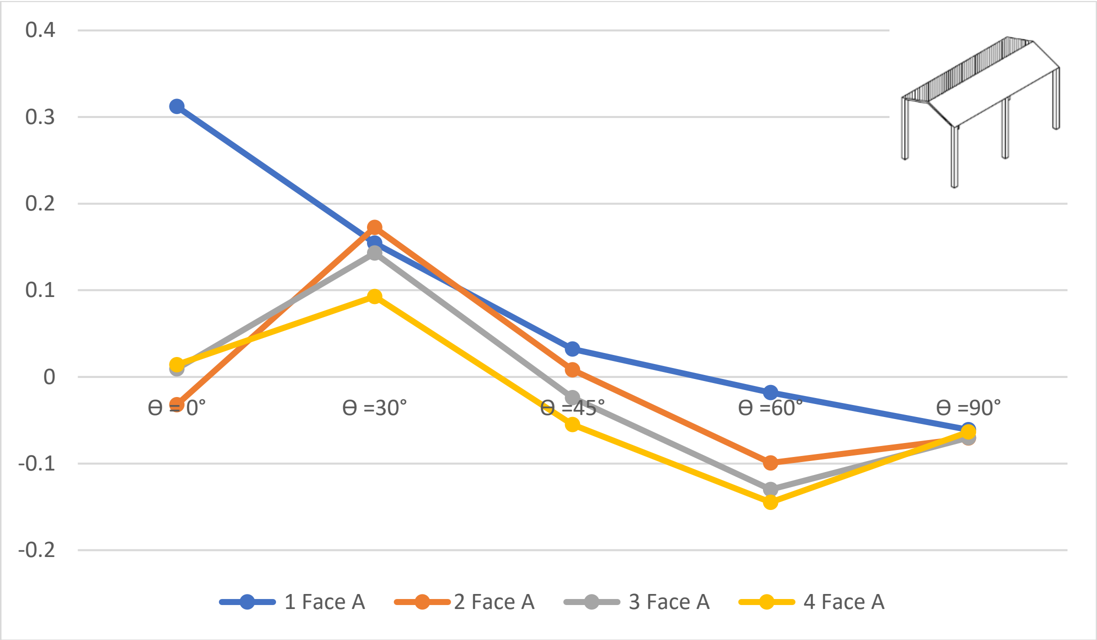

Fig 233 Cpe for roof angle 30° and 0.5b spacing for windward side

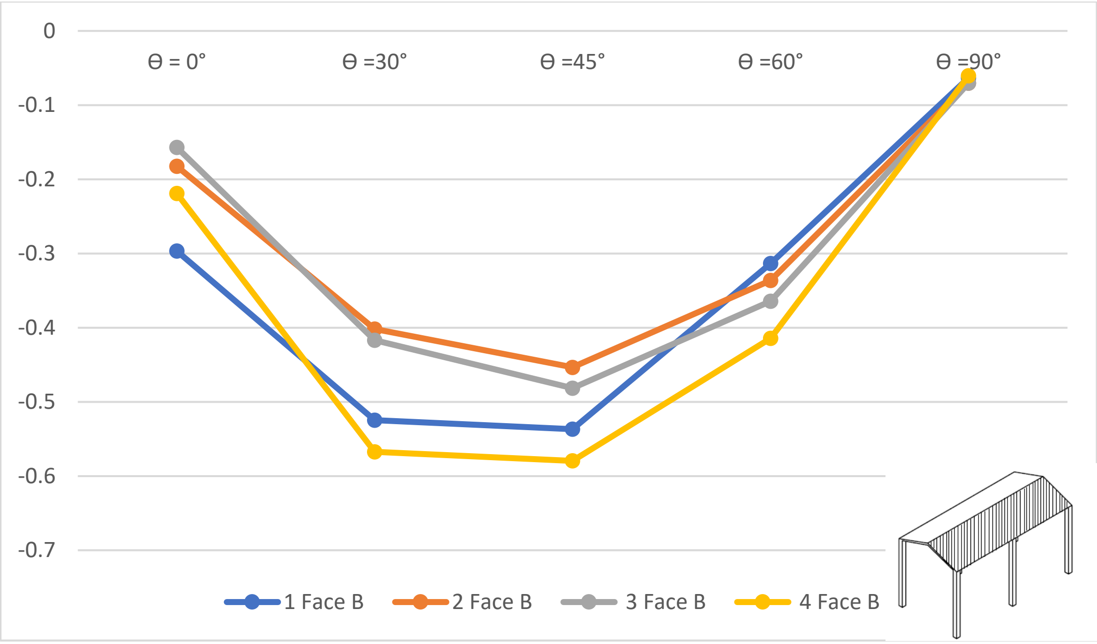

Fig 234 Cpe for roof angle 30° and 0.5b spacing for leeward side

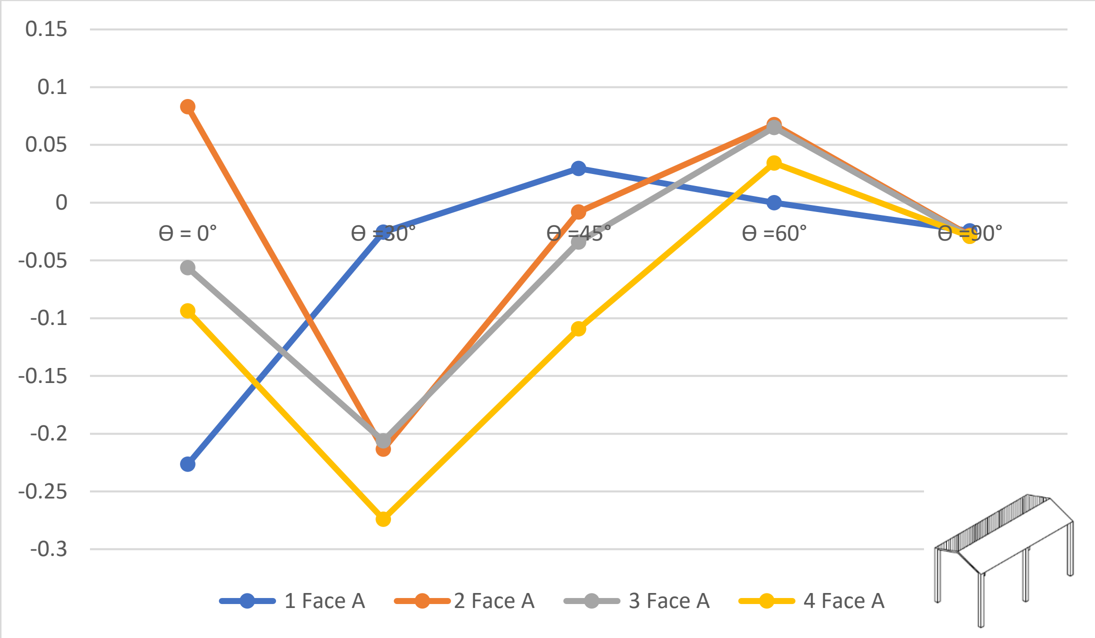

Fig 235 Cpi for roof angle 30° and 0.5b spacing for windward side

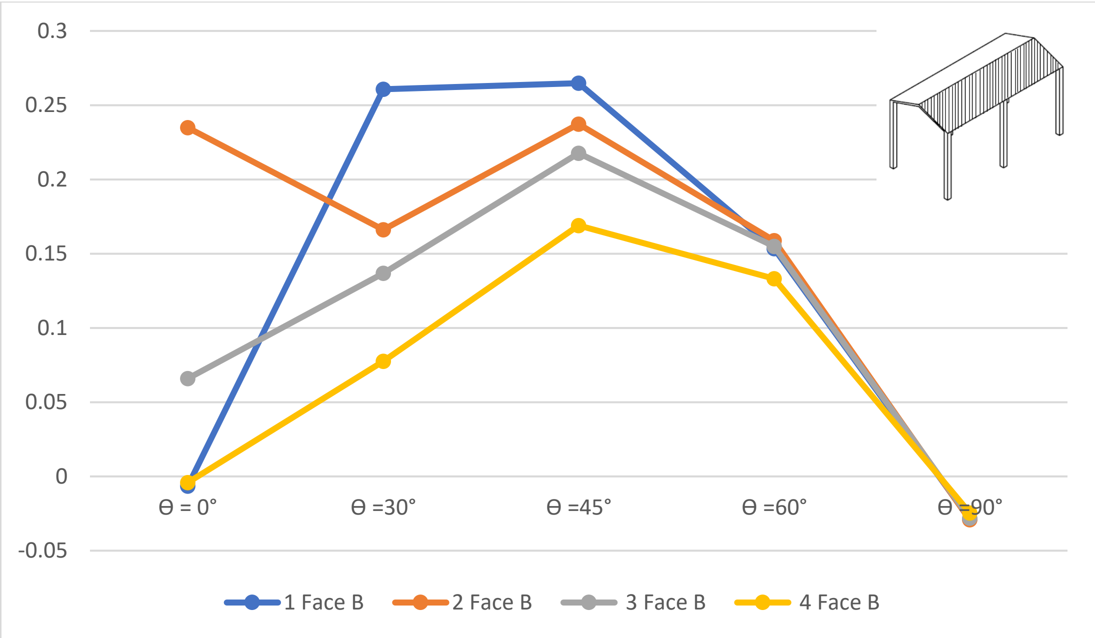

Fig 236 Cpi for roof angle 30° and 0.5b spacing for leeward side

Table 26 Coefficient of Pressure ($Cpext$) at Slope Angle 30°, Spacing b

Cpext	**1 Face A**	**1 Face B**	**2 Face A**	**2 Face B**	**3 Face A**	**3 Face B**	**4 Face A**	**4 Face B**
Ɵ = 0°	0.184975	-0.293559	-0.020125	-0.185691	0.0081613	-0.151308	0.0180174	-0.208058
Ɵ =30°	0.0500059	-0.572087	0.119389	-0.504406	0.098475	-0.53356	0.060566	-0.654422
Ɵ =45°	-0.112016	-0.708082	-0.19663	-0.675601	-0.240763	-0.70938	-0.270307	-0.786094
Ɵ =60°	-0.104146	-0.419566	-0.174016	-0.442261	-0.199575	-0.476607	-0.224929	-0.547783
Ɵ =90°	-0.108117	-0.111558	-0.117875	-0.11865	-0.119133	-0.118407	-0.111741	-0.107946

Table 27 Coefficient of Pressure ($Cpint$) at Slope Angle 30°, Spacing b

Cpint	**1 Face A**	**1 Face B**	**2 Face A**	**2 Face B**	**3 Face A**	**3 Face B**	**4 Face A**	**4 Face B**
Ɵ = 0°	-0.329923	-0.138946	0.0348878	0.156593	-0.046554	0.0339036	-0.103884	-0.035716
Ɵ =30°	-0.182879	0.210551	-0.236835	0.179918	-0.249639	0.156091	-0.31533	0.0810159
Ɵ =45°	-0.103339	0.229103	-0.022928	0.2384	-0.022507	0.227665	-0.086969	0.182361
Ɵ =60°	-0.056280	0.129175	-0.030420	0.128992	-0.040565	0.124037	-0.076754	0.100724
Ɵ =90°	-0.076980	-0.082144	-0.085137	-0.085766	-0.086264	-0.085996	-0.081240	-0.076491

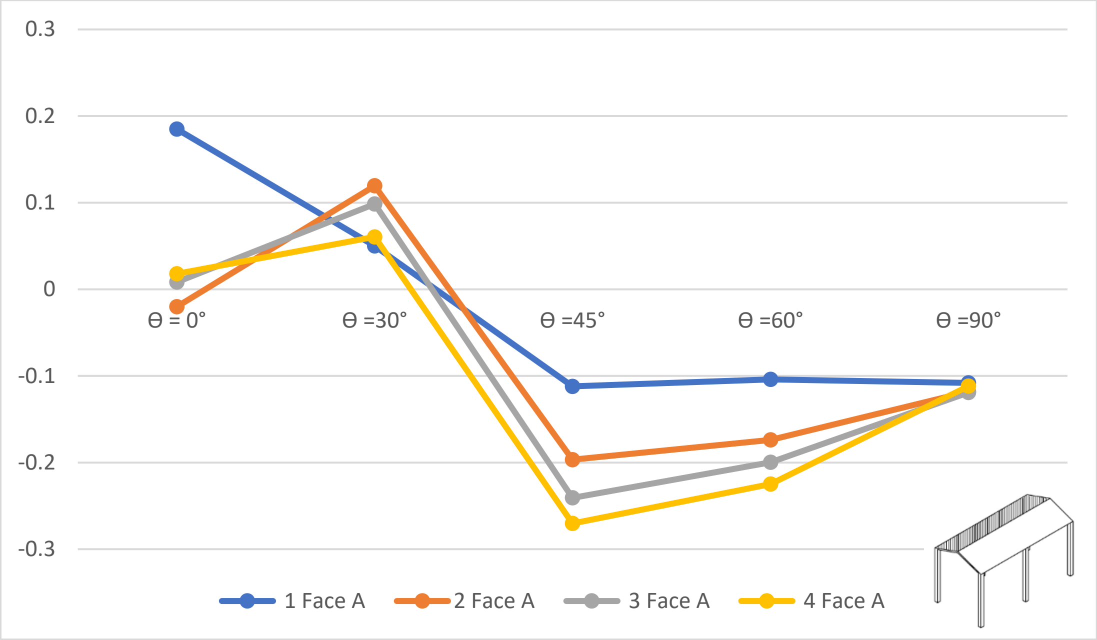

Fig 237 Cpe for roof angle 30° and b spacing for windward side

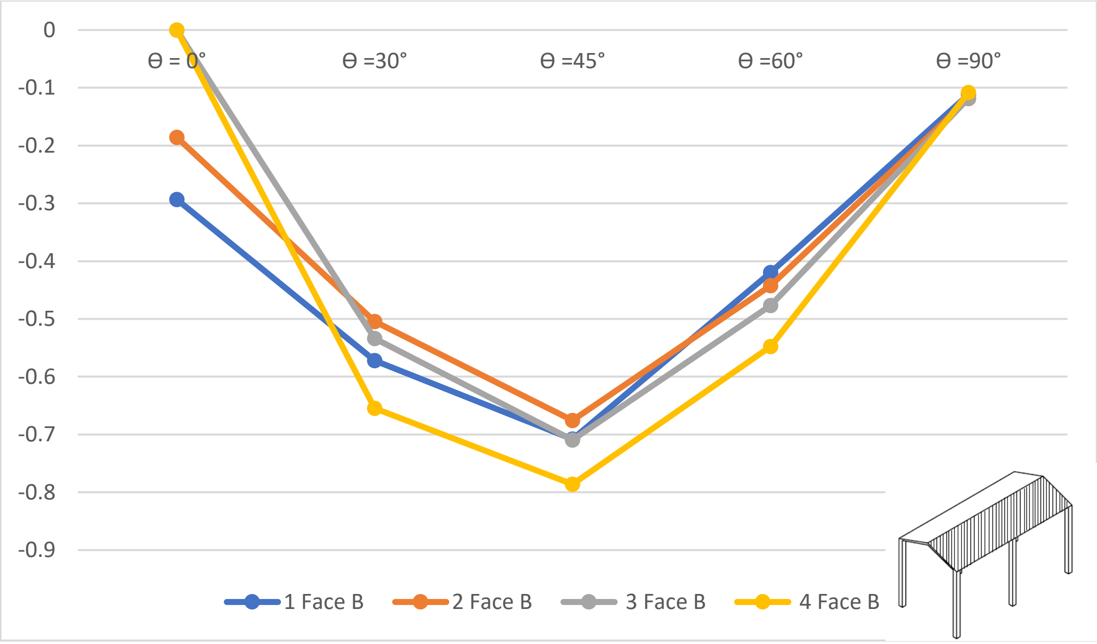

Fig 238 Cpe for roof angle 30° and b spacing for leeward side

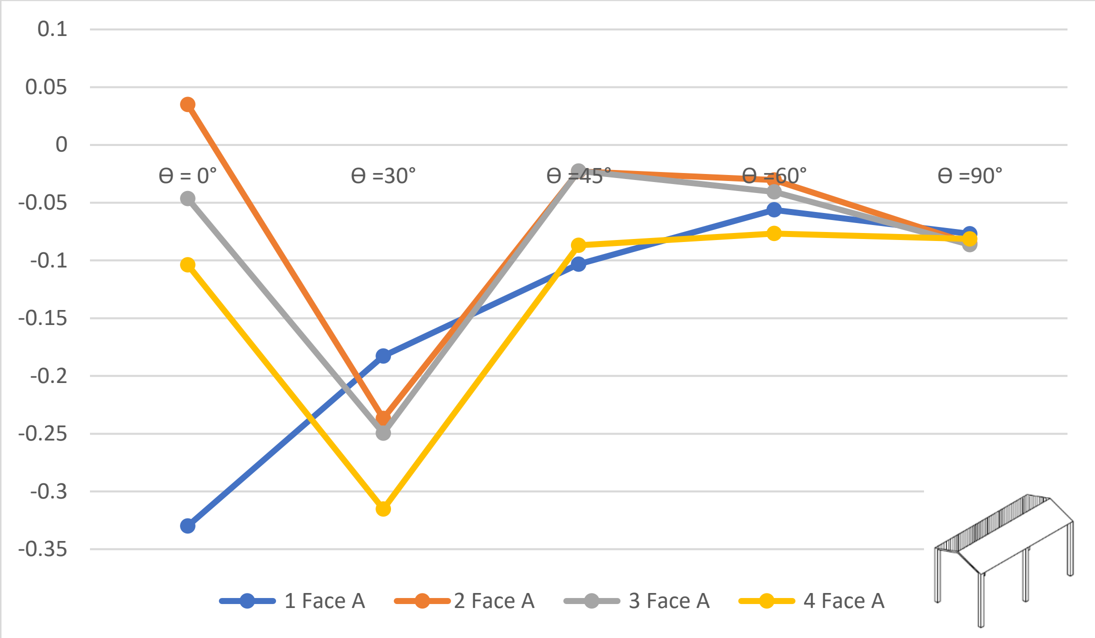

Fig 239 Cpi for roof angle 30° and b spacing for windward side

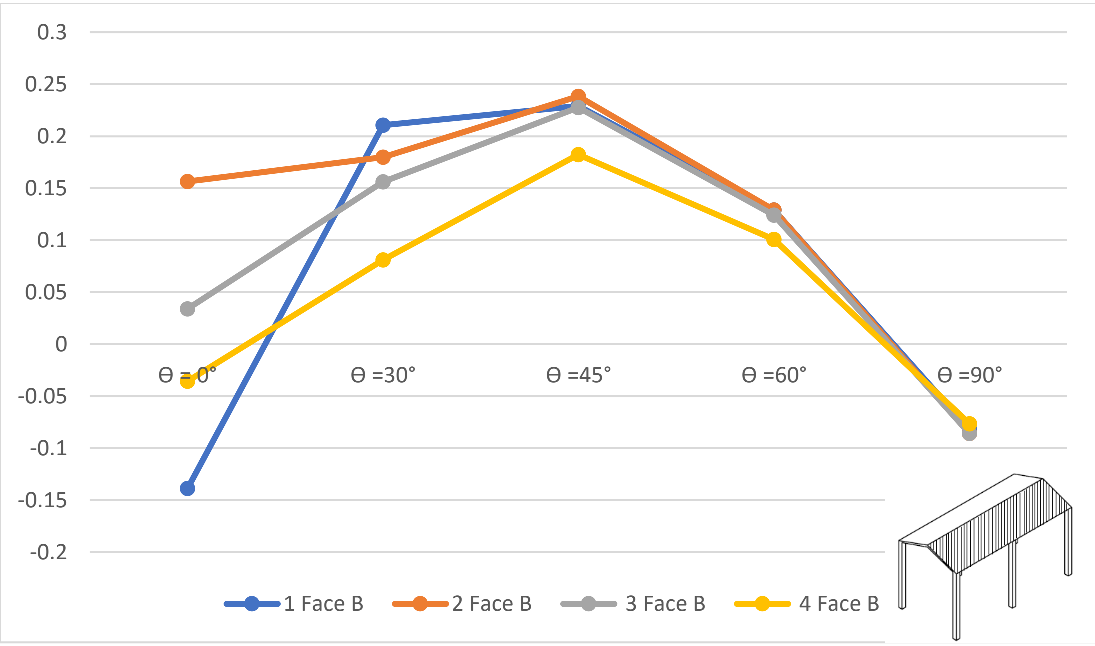

Fig 240 Cpi for roof angle 30° and b spacing for leeward side

Table 28 Coefficient of Pressure ($Cpext$) at Slope Angle 30°, Spacing 1.5b

Cpext	**1 Face A**	**1 Face B**	**2 Face A**	**2 Face B**	**3 Face A**	**3 Face B**	**4 Face A**	**4 Face B**
ϴ = 0°	0.308349	-0.342752	0.0940123	-0.214647	0.0450252	-0.164173	0.0206292	-0.174506
ϴ =30°	0.126554	-0.639605	0.115287	-0.580216	0.0896983	-0.602104	0.0680639	-0.669048
ϴ =45°	0.0222092	-0.60309	-0.050072	-0.619062	-0.075961	-0.643545	-0.095012	-0.692817
ϴ =60°	-0.01236	-0.335933	-0.041524	-0.35553	-0.054188	-0.373022	-0.065599	-0.40351
ϴ =90°	-0.052955	-0.053269	-0.056018	-0.055818	-0.055879	-0.055732	-0.052781	-0.052499

Table 29 Coefficient of Pressure ($Cp\text{int}$) at Slope Angle 30°, Spacing 1.5b

Cpint	**1 Face A**	**1 Face B**	**2 Face A**	**2 Face B**	**3 Face A**	**3 Face B**	**4 Face A**	**4 Face B**
ϴ = 0°	-0.266106	-0.030280	-0.007801	0.141958	-0.024480	0.0600451	-0.064775	-0.001585
ϴ =30°	-0.086595	0.221252	-0.205215	0.21394	-0.206918	0.189994	-0.276321	0.151531
ϴ =45°	-0.023856	0.231755	0.0425888	0.238508	0.0399402	0.230293	0.0064449	0.201604
ϴ =60°	0.0132341	0.142241	0.0205933	0.136183	0.0087823	0.129094	-0.015969	0.117147
ϴ =90°	-0.025611	-0.027294	-0.028731	-0.029047	-0.028966	-0.028172	-0.027614	-0.025661

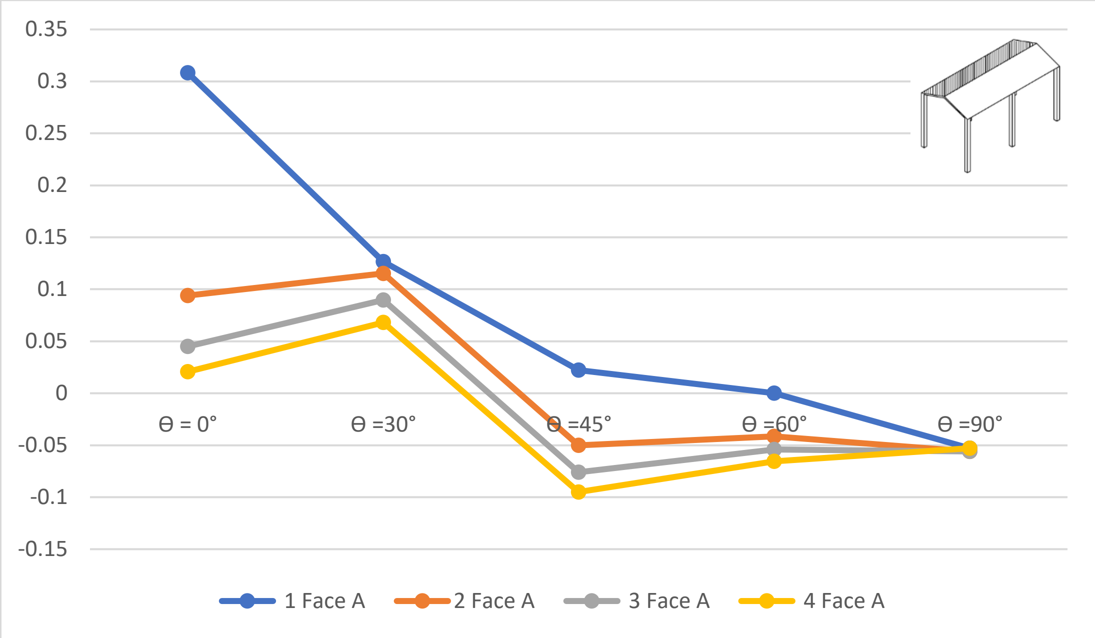

Fig 241 Cpe for roof angle 30° and 1.5b spacing for windward side

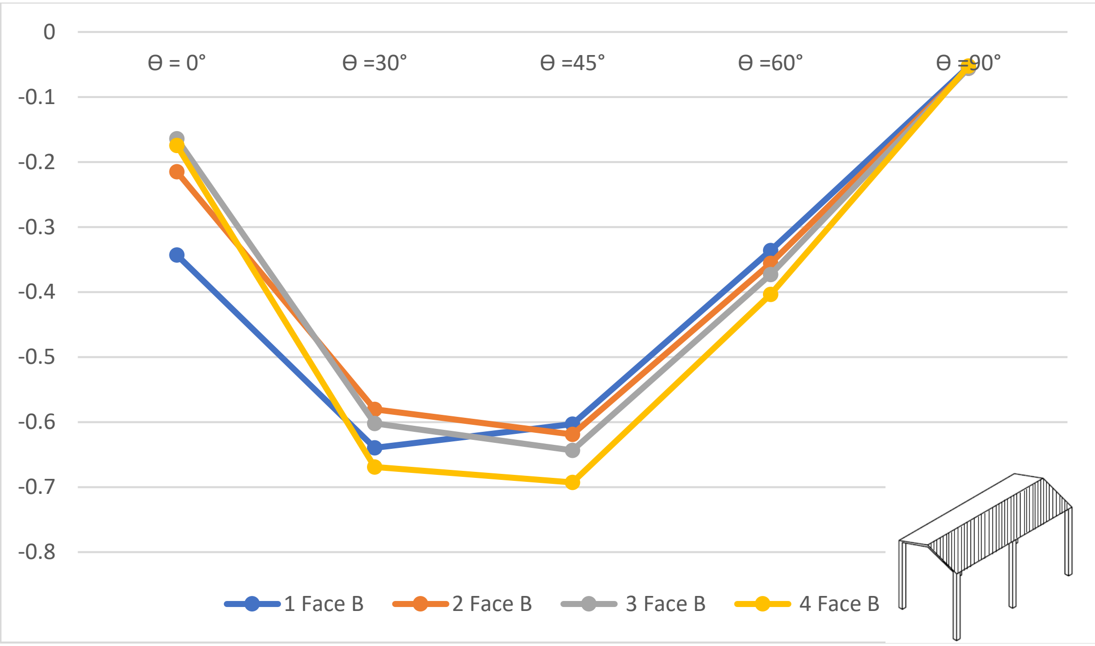

Fig 242 Cpe for roof angle 30° and 1.5b spacing for leeward side

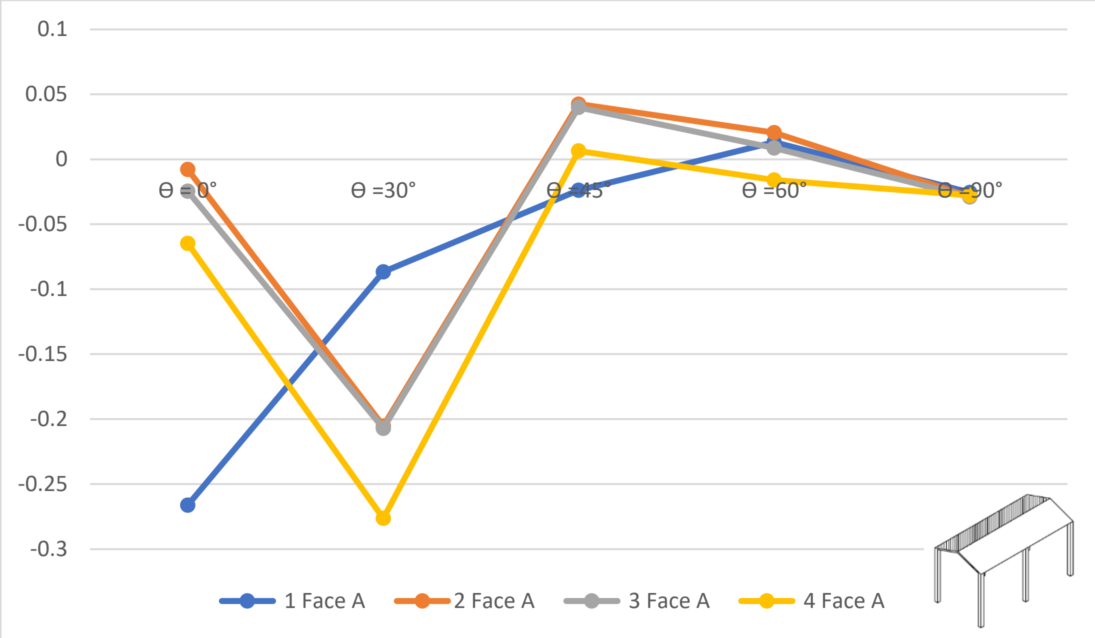

Fig 243 Cpi for roof angle 30° and 1.5b spacing for windward side

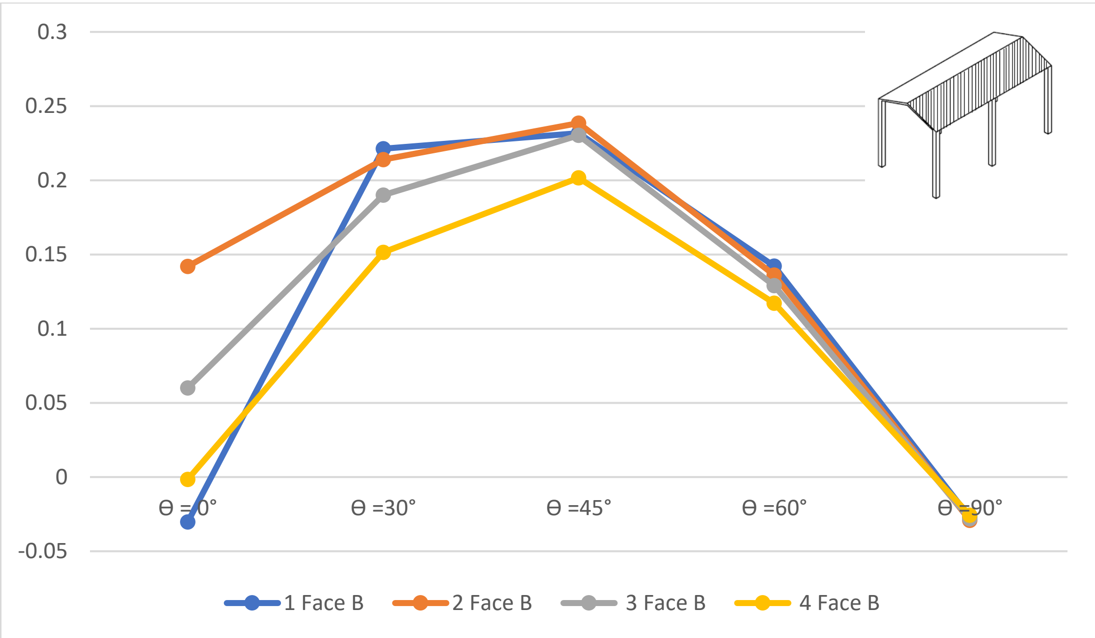

Fig 244 Cpi for roof angle 30° and 1.5b spacing for leeward side

Table 30 Coefficient of Pressure ($Cpext$) at Slope Angle 30°, Spacing 2b

Cpext	**1 Face A**	**1 Face B**	**2 Face A**	**2 Face B**	**3 Face A**	**3 Face B**	**4 Face A**	**4 Face B**
ϴ = 0°	0.300838	-0.370284	0.123761	-0.221382	0.0611798	-0.17294	0.0283344	-0.173586
ϴ =30°	0.11876	-0.664093	0.069859	-0.629528	0.0475599	-0.647057	0.0256454	-0.691151
ϴ =45°	0.0225485	-0.616142	-0.026852	-0.638977	-0.041999	-0.659389	-0.059935	-0.697401
ϴ =60°	-0.013198	-0.342552	-0.033535	-0.361648	-0.042689	-0.374875	-0.054977	-0.400355
ϴ =90°	-0.051419	-0.051557	-0.053314	-0.053415	-0.052871	-0.053315	-0.051631	-0.051067

Table 31 Coefficient of *Pressure* ($Cp\mathrm{int}$) at Slope Angle 30°, Spacing 2b

Cpint	**1 Face A**	**1 Face B**	**2 Face A**	**2 Face B**	**3 Face A**	**3 Face B**	**4 Face A**	**4 Face B**
ϴ = 0°	-0.278614	-0.042009	-0.059847	0.0625712	-0.031571	0.0451014	-0.055178	-0.000835
ϴ =30°	-0.107574	0.205961	-0.11104	0.213693	-0.119615	0.199754	-0.161309	0.164403
ϴ =45°	-0.033500	0.226731	0.0000871	0.224874	-0.004164	0.215177	-0.04188	0.191264
ϴ =60°	0.0104958	0.137746	0.0066531	0.131807	-0.003067	0.124864	-0.021898	0.110316
ϴ =90°	-0.024582	-0.025346	-0.027323	-0.027121	-0.027983	-0.027836	-0.024920	-0.023966

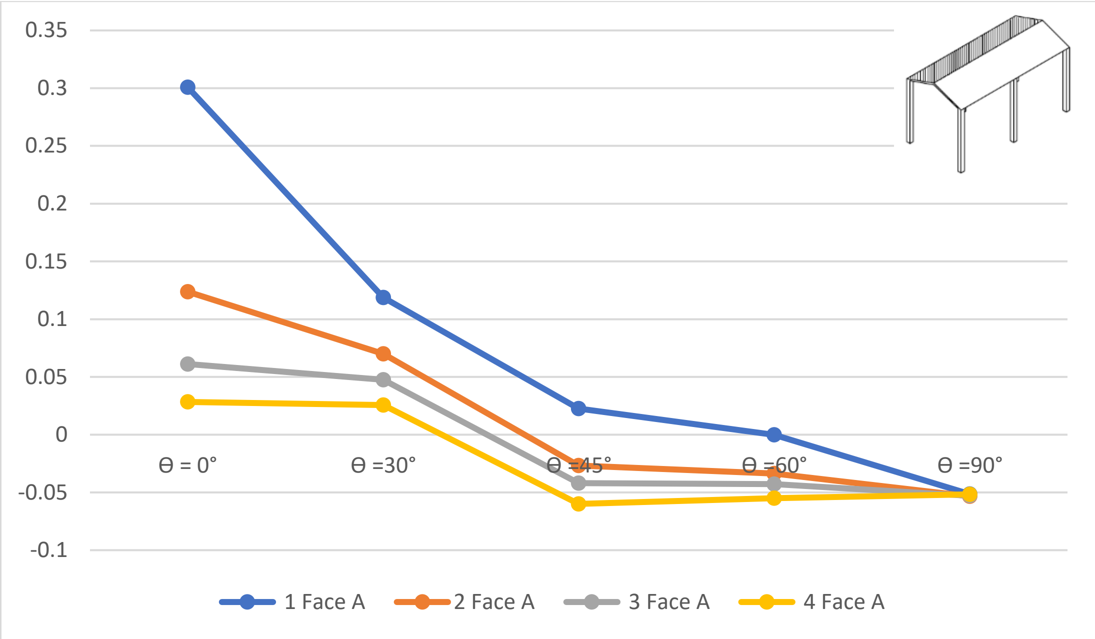

Fig 245 Cpe for roof angle 30° and 2b spacing for windward side

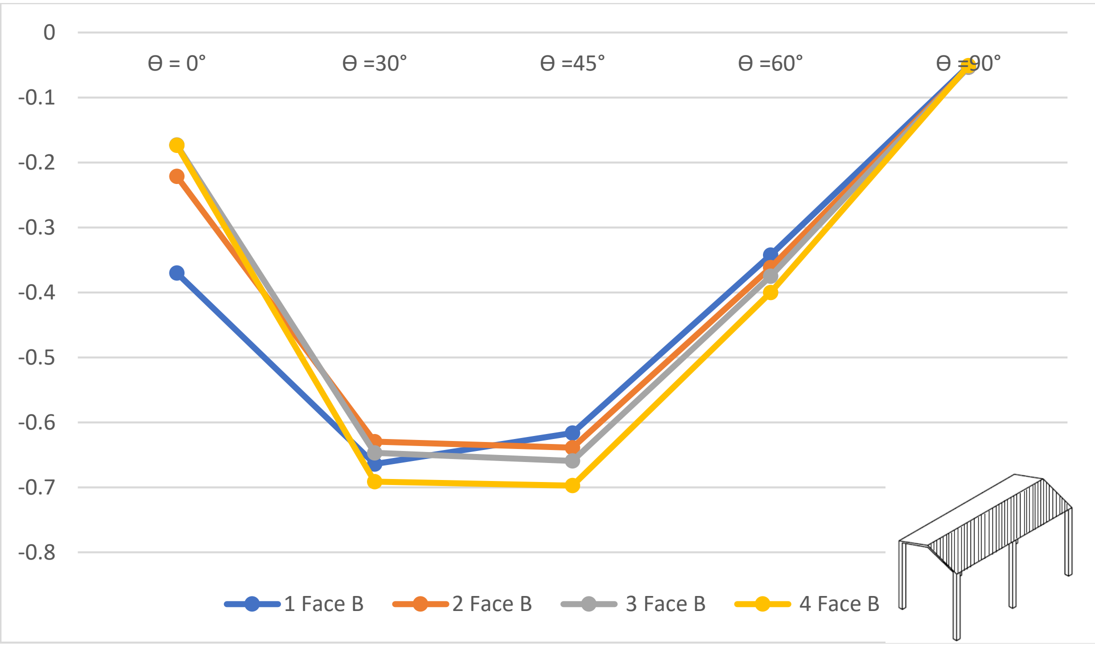

Fig 246 Cpi for roof angle 30° and 2b spacing for leeward side

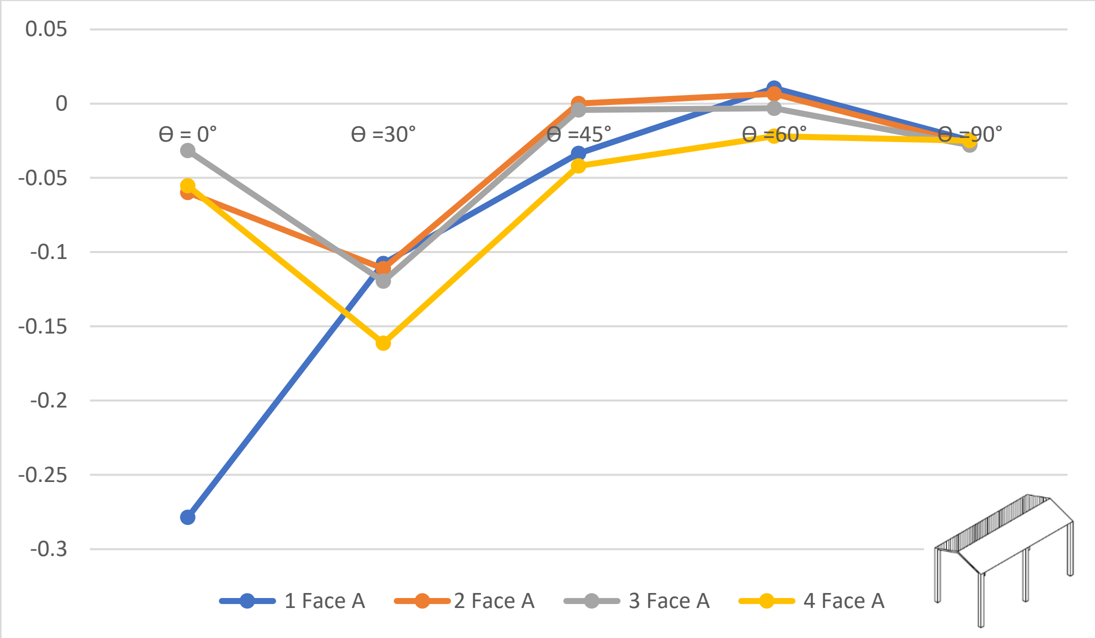

Fig 247 Cpi for roof angle 30° and 2b spacing for windward side

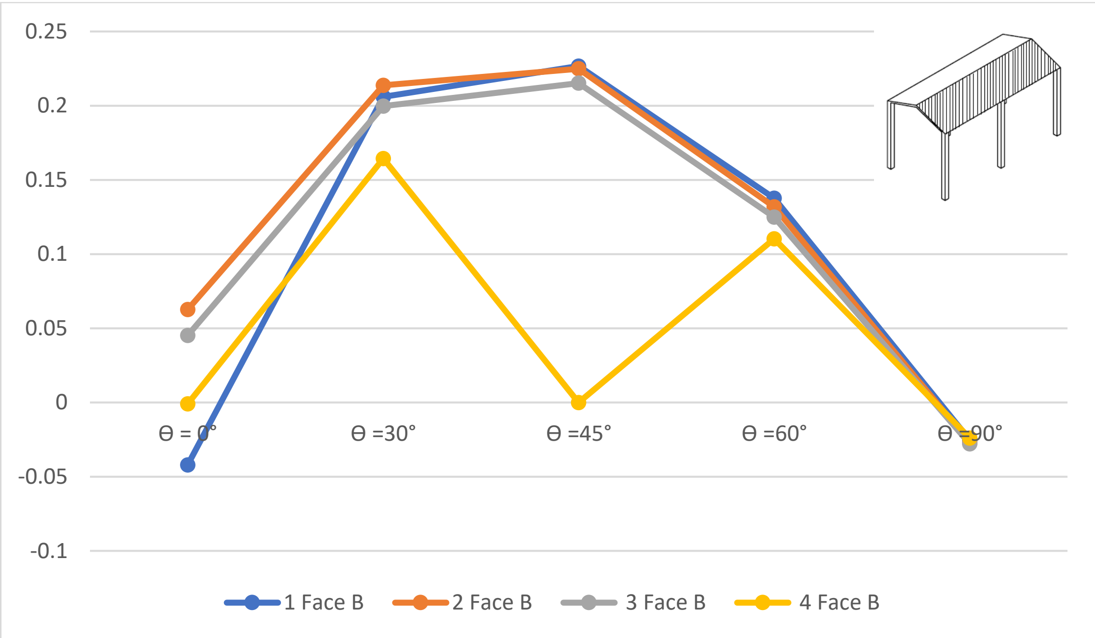

Fig 248 Cpi for roof angle 30° and 2b spacing for leeward side

6.CONCLUSION

Through this study, the wind load variation on the pitched roof due to the change of spacing configurations and several rotations conditions is explored. Five spacing configurations, between the interfering model and the instrumented model, based on the width of structures, were simulated to study the effects on the coefficients of pressure for the instrumented building and then compared with isolated wind flow conditions.

The key findings of the study can be described in the following points:

- The $C_{pe(avg)}$ and $C_{pi(avg)}$ values of both roof faces A & B show similar variation for all the interfering conditions and the isolated case. The external sides exhibit suction pressure whereas the internal sides experience positive pressure with larger
- Extremely smaller values of C_{pi} were observed for smaller angles of rotation irrespective of the pitch angle and spacing between the buildings.
- As the spacing between the structures is increased, a lesser shielding effect is highlighted among the adjacent bodies.
- Closely spaced buildings let to stagnation of the wind between the structures, and as the spacing increases, wind velocity is slightly increased in the zone between the structures, hence giving a more natural ventilation and a negligible increase in suction on external surfaces.

The results and conclusions established in this study would have direct implications for similar studies on the other roof types. This comparative study provides key insight into the difference created by the shape and curvature of the roof on the pressure coefficients which could be extended to other families of roofs. This would prove to be beneficial in the study of the structural soundness of the roof types under wind load conditions, accompanied by an economic design. This study could also be beneficial in adjusting to high-speed wind conditions.

REFERENCES

[1] A.F. Akon, G.A. Kopp, “Turbulence structure and similarity in the separated flow above a low building in the 675 atmospheric boundary layer”, J. Wind Eng. Ind. Aerodyne. 2018; 182 87-100.

[2] B. Chen, L. Shang, M. Qin, X. Chen, Q. Yang, “Wind interference effects of high-rise building on low-rise building with 673 flat roof”, J. Wind Eng. Ind. Aerodyne. 2018; 183 88-113. 674

[3] N.M. Guirguisa, A.A. Abd El-Aziz, M.M. Nassief, “Study of wind effects on different buildings of pitched roofs”, 640 Desalination 2007; 209 (1-3): 190-198. 641

[4] P. Huang, X. Peng, M. Gu, “Aerodynamic devices to mitigate rooftop suctions on a gable roof building”, J. Wind Eng. Ind. 643 Aerodyne. 2014; 135 90-104.

[5] P. Richards, S. Norris,” LES modelling of unsteady flow around the Silsoe cube,” J. Wind Eng. Ind. Aerodyne. 2015; 144 671 70-78. 672

[6] Roy A.K., Aziz A. and Singh J., “Wind Effect on Canopy Roof of Low Rise Buildings”, lnternational Conference Emerging Trends in Engineering lnnovations and Technology Management, 2, 365– 371 (2017)

[7] Singh J and Roy AK (2021) “Wind loads on roof of low-rise buildings”. Disaster Advances, 14(5): 83-98

[8] Singh J. and Kumar A., CFD simulation of the wind field around pyramidal roofed single - story buildings, SN Applied Science, 1, 1–10 (2019) 111.

[9] T. Van Hooff, B. Blocken, On the effect of wind direction and urban surroundings on natural ventilation of a large 655 semi-enclosed stadium, Compute Fluids 2010; 39 (7): 1146-1155. 656

[10] X.Shen, R. Su, G.K. Ntinas, G. Zhang, Influence of sidewall openings on air change rate and airflow conditions inside 659 and outside low-rise naturally ventilated buildings, Energ Buildings. 2016; 130 453-464

[11] Y. Tominaga, B. Blocken, Wind tunnel experiments on cross-ventilation flow of a generic building with contaminant 657 dispersion in unsheltered and sheltered conditions, Build. Environ. 2015; 92 452-461. 658

[12] Zahrai S.M., Table Size Effect on Wind Resistance of ModBit Roofing Systems, Asian Journal of Civil Engineering, 15(5), 705–20 (2014) 110.

[13] Y.L. Xu, G.F. Reardon, Variations of wind pressure on hip roofs with roof pitch, Journal of Wind Engineering and Industrial Aerodynamics 73 (1998) 267-284

[14] J.D. Ginger, J.D. Holmes, Effect of building length on wind loads on low – rise buildings with a steep roof pitch, Journal of Wind Engineering and Industrial Aerodynamics 91 (2003) 1377 – 1400

[15] P. A. Blackmore, “Load reduction on flat roofs - the effect of edge profile,” Journal of Wind Engineering and Industrial Aerodynamics 29 (1988)89–98

[16] J. Singh and A. K. Roy, “Effects of roof slope and wind direction on wind pressure distribution on the roof of a square plan pyramidal low-rise building using CFD simulation,” International Journal of Advanced Structural Engineering, vol. 11, no. 2, pp. 231–254, Jun. 2019,

[17] S. Ahmad and K. Kumar, “Interference effects on wind loads on low-rise hip roof buildings,” Engineering Structures, vol. 23, no. 12, pp. 1577–1589, 2001.

[18] P. Sanyal and S. K. Dalui, “Effects of side ratio for ‘Y’ plan shaped tall building under wind load,” Building Simulation, vol. 14, no. 4, pp. 1221–1236, Aug. 2021

[19] Y. Ozmen, E. Baydar, J.P.A.J. van Beeck, "Wind flow over the low-rise building models with gabled roofs having different pitch angles", Building and Environment, Volume 95,2016,pp 63-74

[20] Hoxey, R.P., Robertson, A.P., Basara, B., and Younis, B.A. (1993). "Geometric parameters that affect wind loads on low-rise buildings: full-scale and CFD experiments." Journal of Wind Engineering and Industrial Aerodynamics, 50: 243-252.

[21] Verma, A., and Ahuja, A.K. (2015). "Wind Pressure Distribution on Rectangular Plan Buildings with Multiple Domes." International Journal of Engineering and Technical Research, 3(7): 129-133.

[22] Rani, N., and Ahuja, A.K. (2017). "Wind Loads on Multi-Span Mono-Slope Canopy Roof". Urbanization Challenges in Emerging Economies, ASCE India Conference, December 12–14, 2017, New Delhi, India.

[23] Krishna, P. (1995). "Wind loads on low rise buildings". Journal of Wind Engineering and Industrial Aerodynamics, 54-55: 383-396.

[24] M. Mallick, A. Kumar, and K. C. Patra, "Experimental Investigation on the Wind-Induced Pressures on C-Shaped Buildings," KSCE Journal of Civil Engineering, vol. 23, no. 8, pp. 3535–3546, 2019.

[25] A. S. Tecle, G. T. Bitsuamlak, and A. G. Chowdhury, "Opening and Compartmentalization Effects of Internal Pressure in Low-Rise Buildings with Gable and Hip Roofs," Journal of Architectural Engineering, vol. 21, no. 1, p. 04014002, Mar. 2015

[26] T. Stathopoulos, D. Chiovitti, and L. Dodaro, "Wind shielding effects of trees on low buildings," Building and Environment, vol. 29, no. 2, pp. 141–150, 1994.

[27] Juliya Mironova (2020). "Wind impact on low-rise buildings when placing high-rises into the existing development". Materials Scienceand Engineering 890 (2020) 012055.

[28] Sanyal, P., and Dalui, S.K. (2020). “Effects of side ratio for ‘Y’ planshaped tall building under wind load.” Wind and Structures An International Journal 30(3):145-160